Université du Québec
Institut national de la recherche scientifique
Centre Énergie, Matériaux et Télécommunications

INTERFERENCE AND RESOURCE MANAGEMENT TECHNIQUES FOR WIRELESS NETWORKS

Par

NGUYEN MINH TRI

Thèse présentée pour l'obtention du grade de
Doctorat en philosophie, Ph.D.
en télécommunications

Jury d'évaluation

Examinateur externe	Prof. Mohamed E. Bedeer, *University of Saskatchewan*
	Dr. Khoa T. Phan *La Trobe University*
Examinateur interne	Prof. André Girard *INRS-ÉMT*
Directeur de recherche	Prof. Long Bao Le *INRS-ÉMT*

Acknowledgments

First, I would like to express my sincere gratitude to my supervisor, Professor Long Bao Le for his advises to me on the way of pursuing my doctoral study at INRS-ÉMT, University of Québec. His remarkable technical knowledge and passion for research have inspired and motivated me since the beginning of my PhD endeavor. Thanks to his invaluable support and guidance, my Ph.D is fruitful not only in terms of results but also in terms of the skills that I have gained during my study. I would like to gratefully acknowledge other members of my Ph.D. committee – Professor André Girard of INRS-ÉMT who has thoroughly reviewed and provided constructively comments on my dissertation. I would also like to thank Professor Ebrahim Mohamed, University of Saskatchewan and Doctor Khoa Phan, La Trobe University for serving as the external examiners to my Ph.D. dissertation and for giving constructive feedback that helped me improve the technical quality of this dissertation. I would like to express gratitude to my colleagues at the Networks and Cyber Physical Systems Lab (NECPHY-Lab), INRS-ÉMT, University of Québec, as well as my friends in Montreal: Vu Ha, Tuong Hoang, Thinh Tran, Ti Nguyen, Dung Le, Hoang Vu, Tung Phan, Dat Nguyen for their recommendations in research and for the memorable life moments during my time at INRS.

Lastly, I devote my sincere love and gratitude to my family members: Mom, Dad, and my sister, who always support me in my life endeavors and encourage me to maintain my persistence during tough moments. Specially thanks to my wife who has been with me and embraced me every time I felt down. My Ph.D. study would not be completed without their constant and unconditional support. I thank you all and I hope that my accomplishments will make you proud.

Abstract

Global wireless communication demands have seen dramatic growth over the past decade along the rapid increase in the numbers of human and machine based connections. Moreover, next-generation wireless networks and technologies must be developed to support diverse requirements in terms of data rate, latency, reliability for different vertical applications such as e-health, smart factories, and smart cities. To meet these requirements given limited spectrum resource, it becomes critical to leverage under-utilized usable frequency bands and to enhance the spectrum efficiency. To this end, one must address great challenges in engineering hardware components such as antennas and radio frequency circuits to effectively exploit higher frequency bands while improvement of spectrum efficiency requires more sophisticated communications techniques and novel interference and resource management strategies.

There has been growing interests in leveraging different aerial platforms including low-altitude unmanned aerial vehicles (UAVs), high-altitude UAVs, balloons, dense low-orbit satellites in recent years for providing reliable, ubiquitous, and economical wireless services. Among them, UAVs-based communications platforms can provide low-cost solutions for various communications scenarios (e.g., wireless areas with limited infrastructure or high traffic demand) and the UAV-based wireless networks offer extra degrees of freedom to optimize the underlying wireless network to enhance the coverage, throughput, and energy efficiency thanks to unique UAV's attributes such as mobility, flexibility, and controllable altitude. UAV communications can also be leveraged to enhance the communications quality of wireless cellular networks and to support various Internet of Thing (IoT) applications such as data dissemination or data collection. The overall objective of this PhD research is to develop interference and resource management strategies for next generation wireless networks where UAV communications are leveraged to effectively support different applications with diverse quality of service (QoS) requirements. Specifically, our research has resulted in three major contributions as summarized in the following.

First, we propose the joint interference cancellation, channel estimation, and data symbol detection for a general interference setting where the interfering source and interfered receiver are un-synchronized and occupy overlapping channels of different bandwidths. We construct a two-phase framework where the interference and desired channel coefficients are estimated by using the joint maximum likelihood-maximum a posteriori probability (JML-MAP) criteria in the first phase; and the MAP based symbol detection is performed in the second phase. We propose an iterative algorithm for interference cancellation, channel estimation and data detection based on the proposed two-phase framework. We then conduct analysis of channel estimation error, residual interference, symbol error rate, and optimize the pilot density to achieve the maximum throughput.

Second, we study the resource allocation and trajectory optimization problem for multi-UAV based wireless networks to maximize the number of admitted users while satisfying their data transmission demands. To tackle the formulated mixed integer non-linear programming (MINLP) problem, we first introduce soft admission variables and solve the corresponding optimization problem by an iterative algorithm. Each iteration comprises two steps, namely soft admission maximization and user removal. The proposed method guarantees to increase the number of admitted users over iterations and therefore, converge to a stable solution.

Finally, we study the joint optimization of multi-UAV's trajectories, transmit power, user-UAV association, and user pairing for multi-UAV based wireless networks employing the non-orthogonal multiple access (NOMA) for uplink communications. The design aims to minimize the total user's energy consumption while guaranteeing to successfully transmit their required data to the UAV-mounted base stations. To tackle the underlying problem, we derive the optimal power allocation as a function of other variables, which is used to transform the optimization problem into an equivalent form. We then propose an iterative algorithm to solve the obtained optimization problem by using Block Coordinate Descent method where three sub-problems are solved in each iteration. Specifically, given the UAVs' trajectories and data rates, we solve the NOMA user pairing and user-UAV association sub-problem optimally by exploiting its special structure. Then, we optimize the users' data rates and UAVs' trajectories in the second and third sub-problems, respectively, by using the successive convex approximation method.

For all proposed designs and algorithms, we provide extensive analytical and numerical studies which illustrate their achievable performances as the values of different key parameters vary. The numerical studies also demonstrate the efficacy of our proposed algorithms and their significant performance gains versus the state-of-the-art designs.

Contents

List of Figures

List of Algorithms

Chapter 1

Extended Summary

1.1 Background and Motivations

Global wireless communication demands have seen dramatic growth over the past decade along the rapid increase in the numbers of human and machine based connections. In fact, it is predicted by Ericsson that total mobile traffic volume can reach 131 exabytes per month by the end of 2024 [1]. Moreover, recent forecast shows that billions of wireless devices, from low-cost internet of things (IoT) devices, wearables, to virtual/augmented/mixed reality devices, and smart vehicles will be connected with wireless networks over the next few years [2, 3]. Furthermore, next-generation wireless networks and technologies must be developed to support diverse requirements in terms of data rate, latency, reliability for different vertical applications such as e-health, smart factories, and smart cities. To meet these requirements given limited spectrum resource, it becomes critical to leverage under-utilized usable frequency bands and to enhance the spectrum efficiency. In general, one must address great challenges in engineering hardware components such as antennas and radio frequency circuits to effectively exploit higher frequency bands while improvement of spectrum efficiency requires more sophisticated communications techniques and resource allocation such as novel interference and resource management strategies.

Exploiting different frequency bands and improving the spectrum efficiency are two critical directions to fundamentally enhance the wireless network capacity and performance. In particular, several under-explored frequency bands such as those above 6Ghz have been under study for 5G wireless networks recently. Note that the minimum guard-bands defined in [4] are larger than those defined in LTE [5] for the same values of channel bandwidth. This is to mitigate the negative effects of unwanted out-of-band emissions, or adjacent channel interference. However, from the spectrum efficiency perspective, it is desirable to squeeze the guard-bands, or even allow simultaneous data transmission/reception on overlapping bands, and apply advanced interference cancellation techniques to manage the interference such as in the case of Full Duplex (FD) radios [6]. Furthermore, future wireless networks must support different applications with diverse requirements in terms of data rates; therefore, communication signals generated by different applications can require different communication bandwidths. In general, developing advanced interference management techniques for concurrent communications over adjacent and overlapping frequency bands is challenging and it requires much further research [7].

Another promising approach to enhance the spectrum efficiency is to employ advanced Non-Orthogonal Multiple Access (NOMA) strategies [8]. Specifically, NOMA enables wireless networks to serve multiple users using the same resource in time, frequency, or space. In fact, NOMA has shown to have various advantages from the information theory perspective [9]. Moreover, NOMA is also more energy efficient than the conventional Orthogonal Multiple Access (OMA) [10] under various settings. To realize NOMA, successive interference cancellation (SIC) is typically employed to decode the intended messages while effectively mitigating the interference [11]. However, the SIC process increases the complexity of receivers. Moreover, one must perform user grouping to determine users using the same resource and optimize the resource allocation to further optimize the network performance. Therefore, much further research for NOMA is needed before the technology is ready for practical deployment.

There has been growing interests in leveraging different aerial platforms including low-altitude unmanned aerial vehicles (UAVs), high-altitude UAVs, balloons, dense low-orbit satellite constellations in recent years for providing reliable, ubiquitous, and economical wireless services [12, 13]. Among them, UAVs-based communications platforms can provide low-cost solutions for various communications scenarios (e.g., wireless areas with limited infrastructure or high traffic demand) and the UAV-based wireless networks (called UWNs hereafter) offer extra degrees of freedom to optimize the underlying wireless network to enhance the coverage, throughput, and energy efficiency thanks to unique UAV's attributes such as mobility, flexibility, and controllable altitude. With appropriate deployment, UAV-based communications can provide favorable Line-of-Sight (LoS) communications channels [14] for ground users. UAV communications can also be leveraged to enhance the communications quality of wireless cellular networks and to support various Internet of Thing (IoT) applications such as data dissemination or data collection [15]. Therefore, UWNs are expected to play an important role in 5G and beyond-5G wireless systems [16].

In this dissertation, our main objective is to develop interference and resource management strategies for next generation wireless networks where many aerial components are involved to support different applications that demand diverse quality of services. Specifically, the research contributions of this dissertation are summarized in the next sections.

1.2 Research Contributions

In this PhD research, our main objective is to develop interference and resource management strategies for next generation wireless networks which employ aerial (UAVs) components to support different applications having diverse qualities of services. In particular, our works focus on two aspects. The first aspect is interference cancellation in a general setting where the interfering and interfered communication's signals have different bandwidths. In the second aspect, we study resource allocation problems in UWNs where our designs focus on two important objectives: admission maximization in the downlink direction, and user energy consumption minimization in the uplink direction. The following sections describe the main contributions of this dissertation.

1.2.1 Interference Cancellation, Channel Estimation, and Symbol Detection for Communications on Overlapping Channels

In this contribution, we propose the joint interference cancellation, fast fading channel estimation, and data symbol detection for a general interference setting where transmit signal of the interfering communication and received signal of the interfered (desired) communication occupy overlapping channels of different bandwidths. Existing works in literature have not considered joint channel estimation, interference cancellation, and symbol detection for the scenario in which two un-synchronized mutual interfering signals have different bandwidths in the fast fading environment. Our work aims to fill this gap in the literature where we make the following contributions.

- First, we propose a two-phase framework for joint interference cancellation, channel estimation, and symbol detection. In the first phase, we estimate the interference coefficients and then subtract the estimated interference. After that, fast-fading channel coefficients at pilot positions are estimated. In the second phase, we derive the *a posteriori probabilities* for both series and individual symbols, given the channel coefficients at pilot positions, from which we propose corresponding detection methods that offer a trade off between precision and complexity. We further develop an iterative algorithm for interference cancellation, channel estimation, and data detection based on the proposed two-phase framework.

- Second, we provide several analysis about the performances of the proposed non-iterative technique in terms of the residual interference and the overall symbol error rate. The analysis shows that the residual interference has bounded power as the interference power tends to infinity. However, the effect of the fast fading channel to the residual interference is irreducible no matter how large the SNR is. Therefore there are fundamental floors for the channel estimation and symbol detection performances due to fast fading.

- Finally, we discuss and show numerically that there exists an optimal frame structure (i.e., optimal pilot density) to achieve the maximum system throughput.

In this section, $\mathbf{I}_N$ represents the $N \times N$ identity matrix, $\mathbf{1}_{M,N}$ is the $M \times N$ all-one matrix, $\mathbf{A}^H$ is the *Hermitian transpose* of matrix $\mathbf{A}$, x^* is the *conjugate* of complex value x, $(\star)$ denotes the convolution operation and $(\propto)$ denotes '*proportional to*'. Since this is a summary version, theorems and propositions are stated without following proofs. Please refer to Chapter 5 for the full version where the proofs of every theorem and proposition are presented.

1.2.1.1 System Model and Problem Statement

The considered setting is illustrated in Fig. 1.1. In the scenario, two communication links denoted by $\mathbb{S}^{\mathsf{d}}$ (desired link) and $\mathbb{S}^{\mathsf{i}}$ (interfering link) operate on *arbitrarily* overlapping frequency bands. The transmitted signal from $\mathbb{S}^{\mathsf{i}}$ interferes with the received signal of $\mathbb{S}^{\mathsf{d}}$ in a general scenario where their bandwidth ratio is an integer[1]. The interfering channel from the interfering source to the

[1]We consider arbitrarily overlapping bands, hence the studied setting covers both adjacent-band and in-band interferences. These two types of interference correspond to the practical scenarios in satellite communications [17,18] and terrestrial communications [19,20].

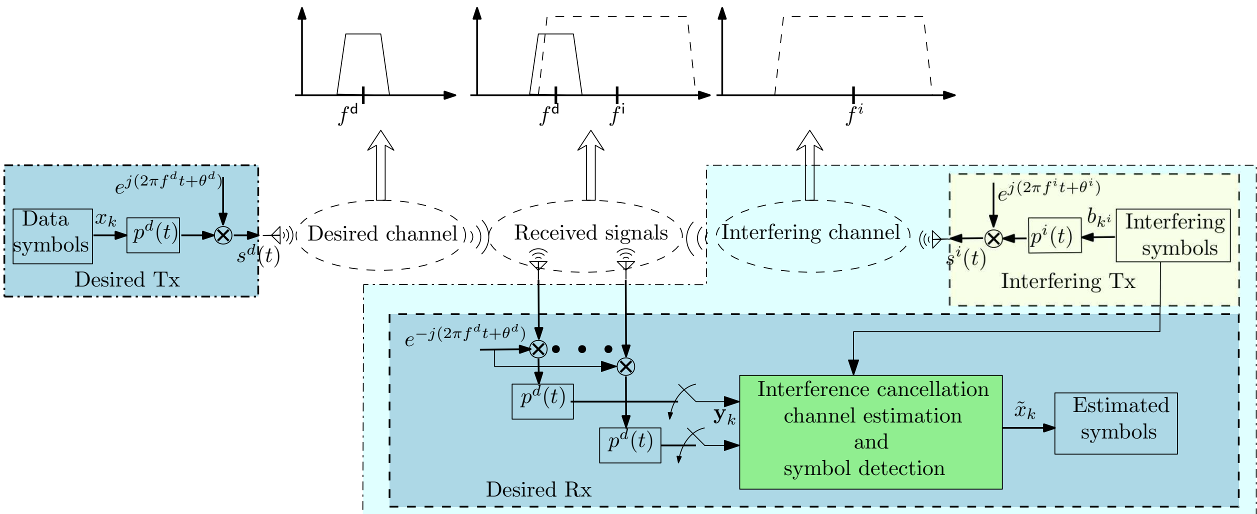

Figure 1.1: Considered interference scenario

antennas of the desired receiver is assumed to be line of sight. The desired communication channel experiences the fast fading where the channel coefficient changes from symbol to symbol according to the first order Markov process [21, 22]. The studied interference scenario occurs in practice when the interfering Tx and the desired Rx are located close to each other and the desired Rx has access to the interfering symbols (e.g., via a dedicated connection) as in the full-duplex relay [19, 20]. The transmitted signal of the desired communication with the carrier frequency f^{d} can be written as

$$s^{\mathsf{d}}(t) = \sum_{k=-\infty}^{\infty} x_k p^{\mathsf{d}}\left(t - kT^{\mathsf{d}} + \epsilon^{\mathsf{d}}\right) e^{j\left(2\pi f^{\mathsf{d}} t + \theta^{\mathsf{d}}\right)}, \tag{1.1}$$

where x_k is the kth transmitted symbol. The pulse shaping function $p^{\mathsf{d}}(t)$ has unity gain; T^{d}, ϵ^{d} and θ^{d} represent the symbol duration, time and phase offsets, respectively. The signal from the interfering source can be expressed similarly as follows:

$$s^{\mathsf{i}}(t) = \sum_{k^{\mathsf{i}}=-\infty}^{\infty} b_{k^{\mathsf{i}}} p^{\mathsf{i}}\left(t - k^{\mathsf{i}}T^{\mathsf{i}} - t^{\mathsf{i}}\right) e^{j\left(2\pi f^{\mathsf{i}} t + \theta^{\mathsf{i}}\right)}, \tag{1.2}$$

where $p^{\mathsf{i}}(t)$ denotes the pulse shaping filter with unity gain, the interfering signal has the center frequency $f^{\mathsf{i}} = f^{\mathsf{d}} - \Delta f$, the k^{i}th symbol is $b_{k^{\mathsf{i}}}$; t^{i} and θ^{i} account for the time/phase difference of the two systems and transmission time delay from the interfering transmitter to the interfered receiver, respectively. Assume that there are N_{r} receiver antennas for $\mathbb{S}^{\mathsf{d}}$, then the received signal is

$$\mathbf{y}(t) = \mathbf{h}^{\mathsf{d}}(t) \star s^{\mathsf{d}}(t) + \mathbf{h}^{\mathsf{i}}(t) \star s^{\mathsf{i}}(t) + \mathbf{w}(t), \tag{1.3}$$

where $\mathbf{w}(t)$ is the thermal noise, $\mathbf{h}^{\mathsf{d}}(t)$, $\mathbf{h}^{\mathsf{i}}(t)$ denote $N_{\mathsf{r}}\times 1$ vectors of desired and interfering channel impulse responses. At the receiver of $\mathbb{S}^{\mathsf{d}}$, the signals are down-converted to baseband and then passes through a matched filter with the impulse response $p^{\mathsf{d}}(t)$. The filtered continuous signals are sampled at $\left(kT^{\mathsf{d}}+\epsilon^{\mathsf{d}}\right)$ to yield the discrete time signal $\mathbf{y}_k = \mathbf{h}^{\mathsf{d}}_k x_k + \mathcal{I}_k + \mathbf{w}_k$, where $\mathbf{w}_k$ represents the vector of noise having complex Gaussian distribution with covariance matrix $\sigma^2\mathbf{I}_{N_{\mathsf{r}}}$ ($\mathbf{w}_k$ is called AWGN hereafter); $\mathcal{I}_k$ denotes the equivalent baseband, discrete time interfering signal which will be derived shortly. Firstly, we express the interference terms in the continuous time domain as follows:

$$\mathcal{I}(t) = \left\{\left(\mathbf{h}^{\mathsf{i}}(t)\star s^{\mathsf{i}}(t)\right)e^{-j(2\pi f^{\mathsf{d}}t+\theta^{\mathsf{d}})}\right\}\star p^{\mathsf{d}}(t). \tag{1.4}$$

Substituting $s^{\mathsf{i}}(t)$ from (1.2) into (1.4), we obtain the equivalent baseband interference signal whose sampled signal at time $(kT^{\mathsf{d}}+\epsilon^{\mathsf{d}})$ is $\mathcal{I}_k = \mathcal{I}(t)|_{t=kT^{\mathsf{d}}+\epsilon^{\mathsf{d}}} = \mathbf{h}^{\mathsf{i}}_k \sum_{k^{\mathsf{i}}} b_{k^{\mathsf{i}}} c_{k,k^{\mathsf{i}}}$, where $c_{k,k^{\mathsf{i}}}$ represents the EIC which is defined by the following equation.

$$c_{k,k^{\mathsf{i}}} = \int_{-\infty}^{\infty} p^{\mathsf{d}}(kT^{\mathsf{d}}+\epsilon^{\mathsf{d}}-\tau)p^{\mathsf{i}}(\tau-k^{\mathsf{i}}T^{\mathsf{i}}-t^{\mathsf{i}})e^{j\left(2\pi(f^{\mathsf{i}}-f^{\mathsf{d}})\tau+\theta^{\mathsf{i}}+\theta^{\mathsf{d}}\right)}d\tau. \tag{1.5}$$

In this studied scenario, the bandwidth of the interfering signal is M times larger than that of the desired signal. And there are L symbols of $b_{k^{\mathsf{i}}}$'s interfering to each desired symbol x_k where L should be a multiple of the bandwidth ratio M to account for the interference in the filter span of the desired signal. Since the bandwidth ratio is an integer, $c_{k,k^{\mathsf{i}}}$ in (1.5) depends only on the relative difference of k, k^{i}. So we denote them as $\mathbf{c} = [c_1, c_2, ..., c_L]^T$ in the sequel for brevity.

The desired communication link is assumed to have fast fading where the channels have the first-order Markovian property as follows [21]:

$$\mathbf{h}^{\mathsf{d}}_{k+1} = \alpha\mathbf{h}^{\mathsf{d}}_k + \sqrt{1-\alpha^2}\boldsymbol{\Delta}_k, \tag{1.6}$$

where $\boldsymbol{\Delta}_k$ denotes a vector of Circular Symmetric Complex Gaussian (CSCG) noise with zero means and covariance matrix $\sigma^2_{\mathsf{h}}\mathbf{I}_{N_{\mathsf{r}}}$. The additive noise term in (1.6) is called channel evolutionary noise and α is the channel correlation coefficient. The average Signal to Noise Ratio (SNR) is $\rho = \sigma^2_{\mathsf{h}}/\sigma^2$ Without loss of generality, we let $\sigma^2_{\mathsf{h}} = 1$. However, σ^2_{h} may appear occasionally in several expressions whenever needed. From the above equations, we can rewrite the received signal $\mathbf{y}_k$ in the matrix form as follows:

$$\mathbf{y}_k = \mathbf{h}_k^{\mathsf{d}} x_k + \mathbf{B}_k \mathbf{c} + \mathbf{w}_k, \tag{1.7}$$

where $\mathbf{b}_{k,l} = \mathbf{h}_k^{\mathsf{i}} b_{Mk+l}$, $\mathbf{B}_k$ is the $N_{\mathsf{r}} \times L$ matrix whose lth column is $\mathbf{b}_{k,l}$. We will call $\mathbf{B}_k$ the interference matrix hereafter. Recall that $\mathbf{b}_{Mk+l}$ and $\mathbf{h}_k^{\mathsf{i}}$ are given[2], so $\mathbf{B}_k$ is known by the desired receiver. In this work, $\mathbf{y}_k$ is called *received signal* or *observation* interchangeably. Since the interfering channels are known and captured in the interference matrix $\mathbf{B}_k$, we omit the superscript d in the desired channel notation, i.e., $\mathbf{h}_k^{\mathsf{d}}$ becomes $\mathbf{h}_k$. And hereafter *channels* means desired channels discussed in the previous sections. Channel estimation and symbol detection are performed in each frame. We consider the scattered pilot frame structure in the time domain with N_{d} data symbols between two consecutive pilot symbols, and there are N_{p} pilot symbols in a frame [23, 24]. Typical symbol arrangement in a frame is expressed as $[x_1^{\mathsf{p}}, x_{1,1}^{\mathsf{d}}, ..., x_{1,N_{\mathsf{d}}}^{\mathsf{d}}, x_2^{\mathsf{p}}, x_{1,2}^{\mathsf{d}}, ..., x_{2,N_{\mathsf{d}}}^{\mathsf{d}}, ..., x_{N_{\mathsf{p}}-1,N_{\mathsf{d}}}^{\mathsf{d}}, x_{N_{\mathsf{p}}}^{\mathsf{p}}]$, where x_i^{p} denotes the ith pilot symbol, and $[x_{1,i}^{\mathsf{d}}, ..., x_{i,N_{\mathsf{d}}}^{\mathsf{d}}]$ denotes data symbols between the ith and $(i+1)$th pilot symbols.

This work addresses the following questions:

1) Given the interference matrix $\mathbf{B}_k$, the observations $\mathbf{y}_k$ and the pilot symbols, how can one cancel the interference and detect data symbols reliably?

2) What are the effects of fast fading channel evolutionary noise to the overall system performances (EIC estimation, interference cancellation, channel estimation, and symbol detection)?

3) Is there an optimal frame design (i.e., optimal pilot density) that maximizes the throughput in the presence of fast fading and interference?

1.2.1.2 Proposed Algorithm

a) Estimation of Interference and Channel Coefficients

In the first phase, we estimate $\mathbf{c}$ and $\mathbf{h}_n^{\mathsf{p}}, n = 1, ..., N_{\mathsf{p}}$ given the observations $\mathbf{y}_{1:N_{\mathsf{p}}}^{\mathsf{p}}$. For brevity, the superscript p is omitted in this section, i.e., x_i^{p} becomes x_i. We denote $\mathbf{Y} = [\mathbf{y}_{1:n-1}, \mathbf{y}_n, \mathbf{y}_{n+1:N_{\mathsf{p}}}]$.

[2] We assume that the receiver has perfect information about the interfering channel gains $\mathbf{h}_k^{\mathsf{i}}$ which correspond to the line of sight link in this work. Therefore, the interfering channel gains vary slowly over time and they can be estimated accurately.

The estimation criteria for $\mathbf{c}$ and $\mathbf{h}_n$ is expressed as follows: [3]

$$\left\{\tilde{\mathbf{c}}_n, \tilde{\mathbf{h}}_n\right\} = \operatorname{argmax} \quad p(\mathbf{h}_n, \mathbf{Y}|\mathbf{c}). \tag{1.8}$$

In order to estimate $\mathbf{h}_n$ and $\mathbf{c}$ according to (1.8), we need to find $p(\mathbf{h}_n, \mathbf{Y})$[4] whose logarithm is expressed in the following Theorem.

Theorem 1.1. *The log likelihood of the received signals and channel coefficients at pilot position n is*

$$\mathcal{L}_{\mathbf{h}_n,\mathbf{Y}} = \log(p(\mathbf{h}_n, \mathbf{Y})) = -\sum_{i=1}^{N_\mathsf{p}} \left(\mathbf{y}_i - \boldsymbol{\mu}_{i,n}\right)^H \boldsymbol{\Sigma}_{i,n}^{-1} \left(\mathbf{y}_i - \boldsymbol{\mu}_{i,n}\right) - \mathbf{h}_n^H \mathbf{h}_n + const.. \tag{1.9}$$

The related parameters $(\boldsymbol{\mu}_{i,n}, \boldsymbol{\Sigma}_{i,n})$ can be found in Appendix 5.A. Furthermore, the first terms in the right hand side of (1.9) can be decomposed into two quadratic terms where one term contains $\mathbf{h}_n$ and the other contains only $\mathbf{c}$. Since there are two variables to be optimized (i.e., $\mathbf{h}_n$ and $\mathbf{c}$), we first derive the optimal $\mathbf{h}_n$ with respect to $\mathbf{c}$ then we derive the optimal $\mathbf{c}$ by maximizing the corresponding objective function achieved with the optimal $\mathbf{h}_n$.

★ *Step 1-Derivation of the optimal* $\mathbf{h}_n$ *for a given* $\mathbf{c}$: The sum of quadratic terms in (1.9) can be re-written as

$$\tilde{\mathcal{L}}_{\mathbf{h}_n,\mathbf{Y}} = -(\mathbf{h}_n - \tilde{\mathbf{h}}_n)^H \mathbf{A}_n (\mathbf{h}_n - \tilde{\mathbf{h}}_n) - \mathcal{C}_n, \tag{1.10}$$

where $\mathbf{A}_n, \tilde{\mathbf{h}}_n$ and $\mathcal{C}_n$ are defined as

$$\begin{aligned} &\mathbf{A}_n = \mathbf{I}_{N_\mathsf{r}} + \sum_{i=1}^{N_\mathsf{p}} \omega_{i,n}^2 \boldsymbol{\Sigma}_{i,n}^{-1}, \qquad \tilde{\mathbf{h}}_n = \mathbf{A}_n^{-1} \left(\sum_{i=1}^{N_\mathsf{p}} x_{i,n}^* \boldsymbol{\Sigma}_{i,n}^{-1} (\mathbf{y}_{i,n} - \mathbf{B}_{i,n}\mathbf{c}) \right), \\ &\mathcal{C}_n = -\tilde{\mathbf{h}}_n^H \mathbf{A}_n \tilde{\mathbf{h}}_n + \sum_{i=1}^{N_\mathsf{p}} (\mathbf{y}_{i,n} - \mathbf{B}_{i,n}\mathbf{c})^H \boldsymbol{\Sigma}_{i,n}^{-1} (\mathbf{y}_{i,n} - \mathbf{B}_{i,n}\mathbf{c}), \end{aligned} \tag{1.11}$$

[3] We use the MAP criteria to estimate $\mathbf{h}_n$. Note that either $p(\mathbf{h}_n|\mathbf{Y})$ or $p(\mathbf{h}_n, \mathbf{Y})$ can be used, since $p(\mathbf{h}_n, \mathbf{Y}) = p(\mathbf{h}_n|\mathbf{Y})p(\mathbf{Y})$ and $p(\mathbf{Y})$ is independent of the parameter of interest $\mathbf{h}_n$. And The EICs $\mathbf{c}$ are unknown, deterministic parameters within a frame.

[4] For simplicity, we omit $\mathbf{c}$ in the following distributions, i.e., $p(\mathbf{h}_n, \mathbf{Y}|\mathbf{c})$ is simply written as $p(\mathbf{h}_n, \mathbf{Y})$.

where $\omega_{i,n}, x_{i,n}, \mathbf{y}_{i,n}, \mathbf{B}_{i,n}$ and the related parameters are defined in the following equations[5].

$$x_{i,n} = \omega_{i,n} x_i, \quad \mathbf{y}_{i,n} = \mathbf{y}_i - \beta_{i,n}\mathbf{y}_{i+j_{i,n}}, \quad \mathbf{B}_{i,n} = \mathbf{B}_i - \beta_{i,n}\mathbf{B}_{i+j_{i,n}}, \tag{1.12a}$$

$$\omega_{i,n} = \begin{cases} \frac{\alpha_{\mathsf{p}}^{|n-i|}}{1+\rho(1-\alpha_{\mathsf{p}}^{2(|n-i|-1)})}, & i \neq n \\ 1, & i = n \end{cases}, \qquad \beta_{i,n} = \begin{cases} \frac{x_i x^*_{i+j_{i,n}} \rho\alpha_{\mathsf{p}}\left(1-\alpha_{\mathsf{p}}^{2(|n-i|-1)}\right)}{1+\rho\left(1-\alpha_{\mathsf{p}}^{2(|n-i|-1)}\right)}, & i \neq n \\ 0, & i = n \end{cases}. \tag{1.12b}$$

Since $\mathbf{A}_n$ is positive definite, the optimal $\mathbf{h}_n$ that maximizes $\tilde{\mathcal{L}}_{\mathbf{h}_n,\mathbf{Y}}$ in (1.10) is $\tilde{\mathbf{h}}_n$.

★ *Step 2- Derivation of the optimal* $\mathbf{c}$*:* When $\mathbf{h}_n = \tilde{\mathbf{h}}_n$, the function in (1.10) is equal to $-\mathcal{C}_n$ which only depends on $\mathbf{c}$ where

$$\mathcal{C}_n = (\mathbf{c} - \tilde{\mathbf{c}}_n)^H \mathbf{D}_n \left(\mathbf{c} - \tilde{\mathbf{h}}_n\right) + const., \tag{1.13}$$

where $\mathbf{D}_n$ and $\tilde{\mathbf{c}}_n$ are defined in the following equations.

$$\mathbf{D}_n = \sum_{i=1}^{N_{\mathsf{p}}} \mathbf{B}_{i,n}^H \boldsymbol{\Sigma}_{i,n}^{-1} \mathbf{B}_{i,n} - \left(\sum_{i=1}^{N_{\mathsf{p}}} x^*_{i,n} \boldsymbol{\Sigma}_{i,n}^{-1} \mathbf{B}_{i,n}\right)^H \mathbf{A}_n^{-1} \left(\sum_{i=1}^{N_{\mathsf{p}}} x^*_{i,n} \boldsymbol{\Sigma}_{i,n}^{-1} \mathbf{B}_{i,n}\right), \tag{1.14a}$$

$$\tilde{\mathbf{c}}_n = \mathbf{D}_n^{-1} \left\{ \sum_{i=1}^{N_{\mathsf{p}}} \mathbf{B}_{i,n}^H \boldsymbol{\Sigma}_{i,n}^{-1} \mathbf{y}_{i,n} - \left(\sum_{i=1}^{N_{\mathsf{p}}} x^*_{i,n} \boldsymbol{\Sigma}_{i,n}^{-1} \mathbf{B}_{i,n}\right)^H \mathbf{A}_n^{-1} \left(\sum_{i=1}^{N_{\mathsf{p}}} x^*_{i,n} \boldsymbol{\Sigma}_{i,n}^{-1} \mathbf{y}_{i,n}\right) \right\}. \tag{1.14b}$$

It can be verified that $\mathbf{D}_n$ is positive definite by using the *Cauchy-Schwarz* inequality. Then the optimal $\mathbf{c}$ that maximizes $\tilde{\mathcal{L}}_{\mathbf{h}_n,\mathbf{Y}}$ in (1.10) is $\tilde{\mathbf{c}}_n$. We take the average over all $\tilde{\mathbf{c}}_n, n = 1, ..., N_{\mathsf{p}}$ to yield a reduced-variance estimate of $\mathbf{c}$ as follows:

$$\tilde{\mathbf{c}} = \frac{1}{N_{\mathsf{p}}} \sum_{n=1}^{N_{\mathsf{p}}} \tilde{\mathbf{c}}_n. \tag{1.15}$$

In summary, the joint interference estimation, cancellation and channel estimation algorithm is described in Algorithm 1.1.

b) Symbol Detection

[5]We denote the 'sign indicator' $j_{i,n} = -1$ for $i > n$, $j_{i,n} = 1$ for $i < n$ and $j_{i,n} = 0$ for $i = n$.

Algorithm 1.1. Estimation of EICs, Desired Channel Coefficients, and Interference Cancellation

for $n = 1 : N_{\mathsf{p}}$ **do**
  for $i = 1 : N_{\mathsf{p}}$ **do**
    Compute $x_{i,n}, \mathbf{y}_{i,n}, \mathbf{B}_{i,n}, \boldsymbol{\Sigma}_{i,n}$ in (1.11), (1.12a).
  end for
  Compute $\mathbf{A}_n, \mathbf{D}_n$, and then $\tilde{\mathbf{c}}_n$ in (1.11), (1.14a), (1.14b).
end for
Compute $\tilde{\mathbf{c}}$ in (1.15) and subtract the interference.
for $n = 1 : N_{\mathsf{p}}$ **do**
  Estimate $\mathbf{h}_n$ as $\tilde{\mathbf{h}}_n$ in (1.11).
end for
End of algorithm.

With the estimated $\tilde{\mathbf{c}}$, we can subtract the interference. Then the channel coefficients at pilot positions are estimated as $\tilde{\mathbf{h}}_n$ given in (1.11) with $\mathbf{c}$ substituted by $\tilde{\mathbf{c}}$ in (1.15). The estimated channel coefficients at pilot positions will be used for the symbol detection as described in the following. We will describe the symbol detection for the interval $\left[x_i^{\mathsf{p}}, x_{i,1}^{\mathsf{d}}, x_{i,2}^{\mathsf{d}}, ..., x_{i,N_{\mathsf{d}}}^{\mathsf{d}}, x_{i+1}^{\mathsf{p}}\right]$. The method can be applied and repeated for other intervals. For simplicity, we omit the pilot index i and superscript (d) in this section, i.e., the channel coefficients are denoted as $[\mathbf{h}_h, \mathbf{h}_{1:N_{\mathsf{d}}}, \mathbf{h}_t]$, where $\mathbf{h}_h$ and $\mathbf{h}_t$ represent the known channel coefficient at the pilot symbol right before and right after the considered interval, respectively. We provide two different symbol detection methods in the followings.

★ *Series Symbol MAP Detection (S-MAP):* The symbols in an interval are detected as

$$\tilde{\mathbf{x}}_{1:N_{\mathsf{d}}} = \operatorname{argmax} \quad p\left(\mathbf{x}_{1:N_{\mathsf{d}}} | \mathbf{h}_h, \mathbf{h}_t, \mathbf{y}_{1:N_{\mathsf{d}}}\right). \tag{1.16}$$

We now characterize the log likelihood function in the following theorem.

Theorem 1.2. *The log likelihood of data symbols conditioned on the received signals and the channel coefficients at pilot positions right after and before the interval can be expressed in a sum of quadratic functions of data symbols* $\mathbf{x}$ *as*

$$\log\left(p\left(\mathbf{x}_{1:N_{\mathsf{d}}} | \mathbf{h}_h, \mathbf{h}_t, \mathbf{y}_{1:N_{\mathsf{d}}}\right)\right) = const. + \\ \sum_{i=1}^{N_{\mathsf{d}}} \left(\tau_2 \boldsymbol{\Gamma}_{i,1} \mathbf{h}_h + \mathbb{1}_{i=N_{\mathsf{d}}} \tau_2 \mathbf{h}_t + \sum_{j=1}^{i} \frac{x_j^*}{\sigma^2} \boldsymbol{\Gamma}_{i,j} \mathbf{y}_j\right)^H \mathbf{S}_i \left(\tau_2 \boldsymbol{\Gamma}_{i,1} \mathbf{h}_h + \mathbb{1}_{i=N_{\mathsf{d}}} \tau_2 \mathbf{h}_t + \sum_{j=1}^{i} \frac{x_j^*}{\sigma^2} \boldsymbol{\Gamma}_{i,j} \mathbf{y}_j\right), \tag{1.17}$$

where the related parameters are defined in (1.18) and Appendix 5.C.

$$\mathbf{S}_i^{-1} = \left(\frac{1}{\sigma^2} + (1+\alpha^2)\tau_1\right)\mathbf{I}_{N_\mathsf{r}} - \mathbb{1}_{i>1}\tau_2^2\mathbf{S}_{i-1}, \tag{1.18a}$$

$$\bar{\mathbf{h}}_i = \begin{cases} \mathbf{S}_i\left(\tau_2\boldsymbol{\Gamma}_{i,1}\mathbf{h}_h + \tau_2\mathbf{h}_{i+1} + \sum_{j=1}^{i}\frac{x_j^*}{\sigma^2}\boldsymbol{\Gamma}_{i,j}\mathbf{y}_j\right), & i < N_\mathsf{d} \\ \mathbf{S}_i\left(\tau_2\boldsymbol{\Gamma}_{i,1}\mathbf{h}_h + \tau_2\mathbf{h}_t + \sum_{j=1}^{i}\frac{x_j^*}{\sigma^2}\boldsymbol{\Gamma}_{i,j}\mathbf{y}_j\right), & i = N_\mathsf{d} \end{cases}. \tag{1.18b}$$

By computing values of $\log\left(p\left(\mathbf{x}_{1:N_\mathsf{d}}|\mathbf{h}_h, \mathbf{h}_t, \mathbf{y}_{1:N_\mathsf{d}}\right)\right)$ of all possible vectors $\mathbf{x} = [x_1, ..., x_{N_\mathsf{d}}]$ from the constellation points, we obtain the optimally detected symbols by (1.16).

★ *Individual Symbol MAP Detection (I-MAP):* We propose to estimate x_i individually as

$$\tilde{x}_i = \operatorname{argmax} \quad p\left(x_i|\mathbf{h}_h, \mathbf{h}_t, \mathbf{y}_i\right). \tag{1.19}$$

Using similar derivations as those used to obtain the results in Theorem 1.2, we have

$$\tilde{x}_i = \frac{\breve{\mathbf{h}}_i^H\mathbf{y}_i}{\|\breve{\mathbf{h}}_i^H\mathbf{y}_i\|}, \qquad \breve{\mathbf{h}}_i = \frac{\alpha^i}{1-\alpha^{2i}}\mathbf{h}_h + \frac{\alpha^{N_\mathsf{d}+1-i}}{1-\alpha^{2(N_\mathsf{d}+1-i)}}\mathbf{h}_t, \quad \text{for} \quad i = 1, ..., N_\mathsf{d}. \tag{1.20}$$

Then, the detected symbols can be found by mapping $\tilde{x}_i$ to the closest point on the constellation. We summarize the proposed joint channel estimation and symbol detection in Algorithm 1.2.

Algorithm 1.2. Individual Symbol MAP Detection Over Fast Fading Channel (I-MAP)

```
for n = 1 : N_p do
    for i = 1 : N_d do
        Estimate x̃^d_{i,n} from (1.20) and assign x̃^d_{i,n} to the closest point in the constellation.
    end for
end for
End of algorithm.
```

c) Iterative Algorithm for Interference Cancellation, Channel Estimation and Symbol Detection

The joint channel estimation, interference cancellation, and data detection are often performed iteratively where detected data symbols can act as pilot symbols to support the interference cancellation and channel estimation. We propose an iterative approach for interference cancellation, channel estimation, and symbol detection based on the previous two-phase method. We now denote the desired symbols in the frame as $x_n, n = 1, ..., (N_\mathsf{p} - 1)(N_\mathsf{d} + 1) + 1$, where $x_n, n = 1, 1 + N_\mathsf{d} + 1, 1 + 2(N_\mathsf{d} + 1), ...$ are pilot symbols in the previous notations.

In the first phase, the interference estimation, interference cancellation, and channel estimation are performed as presented previously. Except that the number of newly considered pilot symbols[6] is now $\hat{N}_\mathsf{p} = (N_\mathsf{d} + 1)(N_\mathsf{p} - 1) + 1$ (symbols in the whole frame) and the correlation coefficient of channel gains at two consecutive pilot positions is $\hat{\alpha}_\mathsf{p} = \alpha$.

In the second phase, let the estimated channel gains at position n be $\breve{\mathbf{h}}_n$. In order to detect the symbol x_n, we now use the knowledge of $\breve{\mathbf{h}}_{n+1}$ and $\breve{\mathbf{h}}_{n-1}$ as if $n+1$ and $n-1$ are two pilot positions. Apply the I-MAP technique[7] in (1.20), we have

$$\begin{aligned} \tilde{x}_n &= \frac{\hat{\mathbf{h}}_n^H \mathbf{y}_n}{\|\hat{\mathbf{h}}_n^H \mathbf{y}_n\|}, n = 2, ..., (N_\mathsf{p} - 1)(N_\mathsf{d} + 1), \\ \hat{\mathbf{h}}_i &= \frac{\alpha}{1 - \alpha^2} \left(\breve{\mathbf{h}}_{n-1} + \breve{\mathbf{h}}_{n+1} \right). \end{aligned} \tag{1.21}$$

After $\tilde{x}_n$ are detected, in the next iterations, interference cancellation, channel estimation and data detection are performed until convergence is reached. The algorithm converges when there is no change in the detected data symbols. We summarize this iterative approach in Algorithm 1.3.

Algorithm 1.3. Iterative Algorithm for Channel Estimation, Interference Cancellation and Data Detection

Perform Algorithm 1.1 for interference cancellation and channel estimation.
Perform Algorithm 1.2 for I-MAP symbol detection.
while (true) **do**
    Perform Algorithm 1.1 for interference cancellation and channel estimation with $\hat{\alpha}_\mathsf{p} = \alpha$ and $\hat{N}_\mathsf{p} = (N_\mathsf{d} + 1)(N_\mathsf{p} - 1) + 1$.
    Perform Algorithm 1.2 for I-MAP symbol detection with $\hat{N}_\mathsf{d} = 1$. The detected data symbols are denoted as $\bar{\mathbf{x}}^\mathsf{i}$.
    if $\bar{\mathbf{x}}^\mathsf{i} == \bar{\mathbf{x}}^{(\mathsf{i}-1)}$ **then**
        Break the loop (Convergence is reached).
    else
        Increase i and go to the next iteration.
    end if
end while
End of algorithm.

[6]Since all symbols x_n are known (at pilot positions) or detected (at data positions), they are all treated as pilot symbols.

[7]Now as there is only one data symbol between two pilot symbols, S-MAP and I-MAP produce identical results.

1.2.1.3 Performance Analysis

In this section, we conduct performance analysis for the proposed design framework[8] and present key insights from the analysis. Specifically, we show *first*, the characteristics of the channel estimation error and the residual interference, *second*, the achievable SER of our proposed detection methods, and *finally*, the throughput analysis.

In the following analysis, we investigate the residual interference (denoted as $\boldsymbol{\upsilon}_n$) and the channel estimation error (CEE, denoted as $\boldsymbol{\nu}_n$) which are defined as follows.

$$\begin{aligned} \boldsymbol{\upsilon}_n &= \mathbf{B}_n \left(\mathbf{c} - \tilde{\mathbf{c}} \right), \\ \boldsymbol{\nu}_n &= \mathbf{h}_n - \tilde{\mathbf{h}}_n. \end{aligned} \tag{1.22}$$

a) Characteristics of Channel Estimation Error and Residual Interference

First, we provide the following remark about the channel estimation error in case of interference-free.

Remark 1.1. *In case of no interference, the channel estimation error $\boldsymbol{\nu}_n$ has Gaussian distribution with zero mean. Moreover, the effect of channel evolutionary noise to the channel estimation error is negligible as the SNR tends to infinity.*

The fact that the effect of channel evolutionary noise diminishes as SNR goes to infinity suggests that the error floor in channel estimation reported in [25] comes from the residual interference. Therefore, we perform analysis and characterize the interference estimation $\tilde{\mathbf{c}}$ and the residual interference in the following remarks.

Remark 1.2. *The EIC estimation $\tilde{\mathbf{c}}$ is unbiased and the residual interference follows the Gaussian distribution with zero mean. Moreover, the residual interference is independent of $\mathbf{c}$ and has bounded power as the interference power goes to infinity.*

Remark 1.3. *The residual interference power cannot be eradicated completely even with very high SNR. Specifically, when the SNR tends to infinity, there is a floor for the residual interference power.*

[8] Due to the stochastic nature of the channel model and the design, analysis of the iterative algorithm is very involved, which is beyond the scope of this work. Nevertheless, the analysis of the proposed non-iterative two-phase design provides many insights that help explain the behaviors of the iterative algorithm.

b) SER Analysis

The unnormalized $\tilde{x}_i$ in (1.20) is $\breve{\mathbf{h}}_i^H(\mathbf{h}_i x_i + \tilde{\mathbf{w}}_i)$, where $\tilde{\mathbf{w}}_i$ is the sum of the additive Gaussian noise and residual interference[9]. Conditioned on $\mathbf{h}_h$ and $\mathbf{h}_t$, the equivalent SNR for symbol detection of x_i can be expressed as

$$\rho_i^{\mathsf{e}} = \frac{\alpha^{2i}\left|\|\mathbf{h}_h\|^2 \frac{\alpha^i}{1-\alpha^{2i}} + \mathbf{h}_h^H \mathbf{h}_t \frac{\alpha^j}{1-\alpha^{2j}}\right|^2}{(\sigma^2 + \sigma_{\mathsf{i}}^2 + 1 - \alpha^{2i})\left|\mathbf{h}_h^H \mathbf{1}_{N_{\mathsf{r}}} \frac{\alpha^i}{1-\alpha^{2i}} + \mathbf{h}_t^H \mathbf{1}_{N_{\mathsf{r}}} \frac{\alpha^j}{1-\alpha^{2j}}\right|^2}, \tag{1.23}$$

where $j = N_{\mathsf{d}} + 1 - i$. The SER at symbol position i can be calculated as

$$P_i^{\mathsf{e}} = \int p(\mathbf{h}_h, \mathbf{h}_t) f_{\mathsf{e}}(\rho_i^{\mathsf{e}}) d\mathbf{h}_h d\mathbf{h}_t, \tag{1.24}$$

where $f_{\mathsf{e}}(\rho)$ is the error rate corresponding to instantaneous ρ. The closed-form expression for P_i^{e} in (1.24) is difficult to derive. However, P_i^{e} can be computed accurately by using numerical integration or by Monte Carlo simulation. Finally, the overall average SER can be expressed as

$$P^{\mathsf{e}} = \frac{1}{N_{\mathsf{d}}} \sum_{i=1}^{N_{\mathsf{d}}} P_i^{\mathsf{e}}. \tag{1.25}$$

c) Throughput Analysis

The throughput is defined as the average number of successfully transmitted data symbol per symbol period, which is averaged over the frame interval. Note that there are N_{d} transmitted data symbols between two consecutive pilot symbols and the frame consists of N_{p} pilot symbols. Considering the average SER P^{e} in (1.25), the throughput can be calculated as

$$\mathsf{TP} = (1 - P^{\mathsf{e}}) \frac{N_{\mathsf{d}}(N_{\mathsf{p}} - 1)}{(N_{\mathsf{d}} + 1)(N_{\mathsf{p}} - 1) + 1}, \tag{1.26}$$

The pilot density is defined as $1/(N_{\mathsf{d}} + 1)$. It can be verified that when we increase the pilot density (i.e., N_{d} is decreased), P_{e} decreases; thus the first term in (1.26) increases. However, the increasing pilot density leads to higher pilot overhead which reduces the second term in (1.26) and vice versa. Therefore, there is a trade-off between transmission reliability and throughput, which suggests that there exists an optimal value of the pilot density that achieves the maximum throughput. Though

[9] In case of no interference, the covariance matrix is $\sigma^2 \mathbf{I}_{N_{\mathsf{r}}}$. And if there is interference, the covariance matrix is $(\sigma^2 + \sigma_{\mathsf{i}}^2)\mathbf{I}_{N_{\mathsf{r}}}$, where σ_{i}^2 is the power of the residual interference which can be computed from (5.49)

it is difficult to express the closed form of P^{e} in (1.25), the optimal pilot density for given α and ρ can be found effectively by using numerical search methods.

1.2.1.4 Numerical Results

We consider the simulation setting in which the desired receiver has $N_{\mathsf{r}} = 2$ antennas, the coefficient α is chosen in the set $\{0.95, 0.97, 0.99, 0.995, 0.999\}$[10]. The bandwidth of the interfering signal is two times of the bandwidth of the desired signal, which are $30kHz$ and $15kHz$, respectively. The frequency spacing Δ_f between interfering and desired signals will be normalized as $\Delta_f T^{\mathsf{d}}$ where T^{d} denotes the symbol time of the desired signal. We assume that the QPSK modulation is employed; both interfering and interfered signals use the root-raised-cosine pulse shaping function. Moreover, the pulse shaping functions $p^{\mathsf{d}}(t)$ and $p^{\mathsf{i}}(t)$ are assumed to have the roll-off factor equal to 0.25. The interference power is set as strong as the power of the desired signal and the frequency spacing $\Delta_f = 1/T^{\mathsf{d}}$ unless stated otherwise. The number of pilot symbols is set equal to 51. Moreover, the pilot density is chosen in the set $\{25\%, 10\%\}$ corresponding to $\{3, 9\}$ data symbols between two pilot symbols, respectively. Furthermore, for throughput simulation results, we show the throughputs obtained for various pilot densities ranging from 50% to 6.25%. The results presented in this section are obtained by averaging over 10^4 random realizations.

a) Performance of the Proposed Channel Estimation Technique

For the interference-free scenario, we investigate the effect of different parameters to the channel estimation errors. We note that the performance of the channel estimation technique presented in this section depends mainly on N_{d} and α. Specifically, the performance depends on α_{p} which is the correlation coefficient of channel gains at two consecutive pilot positions. Different values of N_{d} (different pilot densities) have the corresponding values of α_{p}. We will show the numerical channel estimation mean squared error (CMSE) which is calculated as

$$\mathsf{CMSE} = \frac{1}{N_{\mathsf{p}} N_{\mathsf{r}}} \sum_{n=1}^{N_{\mathsf{p}}} \mathbf{tr}\left(\mathbb{E}\left[\left(\mathbf{h}_n - \tilde{\mathbf{h}}_n\right)\left(\mathbf{h}_n - \tilde{\mathbf{h}}_n\right)^H\right]\right). \tag{1.27}$$

[10]In Clarke's mode, $\alpha = J_0(2\pi f_D T^{\mathsf{d}})$, where f_D is the maximum Doppler spread [26] (recall that T^{d} is the symbol period of the desired signal). Specifically, $\alpha = 0.999$ corresponds to 150 Hz of Doppler spread with symbol rate of 15 Kbps. If the desired signal is carried at 900MHz, the corresponding velocity of the desired Rx is 50m/s.

In Fig. 1.2, we show the channel estimation error due to our proposed design for different values of N_{d} (equivalently, different values of pilot density), when there is no interference (IF) and when there is interference (IP). When N_{d} increases, the channel estimation mean squared error also increases as expected. For the interference-free scenario, the corresponding error curves converge to each other and decrease almost linearly as the SNR increases (both curves are plotted in the log scale). This means that the impact of the fast fading is diminished in the high SNR regime. When the interference is present, there is a performance floor for channel estimation error.

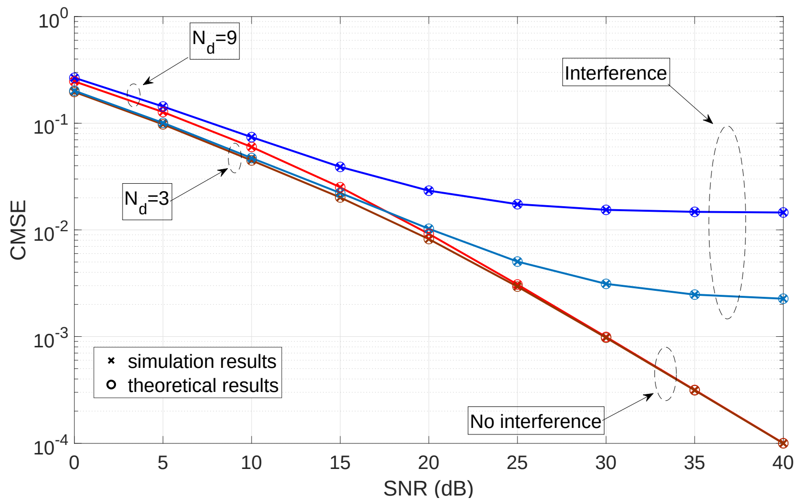

Figure 1.2: Channel estimation mean squared error, $\alpha = 0.99$

b) Performance of the Proposed Symbol Detection Methods

We now compare the SER performance of series symbol MAP detection (S-MAP), individual symbol MAP detection (I-MAP) and optimum diversity detection (ODD) [27, 28] methods. The ODD method is the optimum individual symbol detection with imperfect CSI[11].

Fig. 1.3a illustrates the SER achieved by these detection methods for the interference-free and interference scenarios, which are denoted as IF and IP in this section, respectively. It can be seen that the SER of the proposed I-MAP is almost identical to that achieved by the ODD method. Moreover, the S-MAP detector outperforms both I-MAP and ODD and the performance gap is larger in the interference-free scenario. Note that, in the IP scenario, the residual interference still presents, which causes the error floors in these SER curves. We further show in Fig. 1.3b the SNR

[11]Basically, in the ODD method, the channel gains at data positions are interpolated from the MMSE-estimated channel gains at pilot positions. Then, the zero-forcing based symbol detection is employed (please refer to Sections III and IV in [28] for more details).

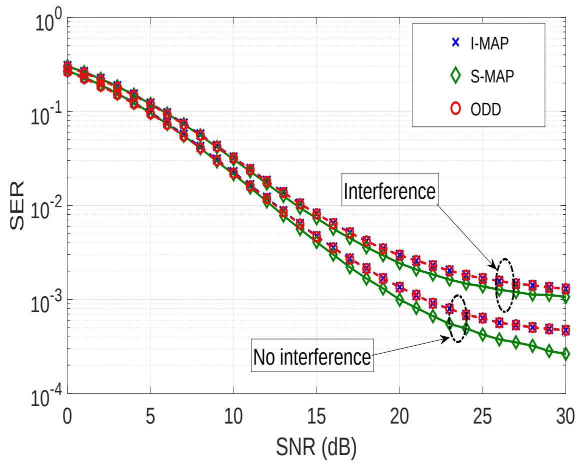

(a)

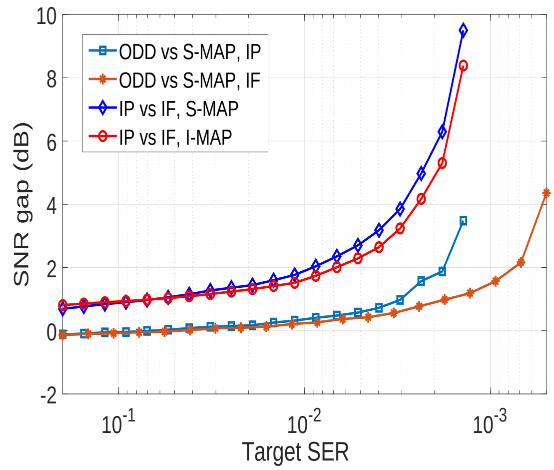

(b)

Figure 1.3: a) SER achieved by different detection methods, $N_\text{d} = 3$; b) SNR gap for specific target SER, $N_\text{d} = 3$

gap to achieve the same SER between different symbol detection methods (S-MAP, I-MAP) and scenarios (IF, IP). Particularly, a value of 3dB SNR gap at 5×10^{-3} target SER of the curve A *vs* B means that method A needs 3dB higher in SNR to achieve the same target SER achieved by method B. For the same scenario (IF or IP), the SNR gap between the proposed S-MAP and ODD becomes larger as the required SER decreases. Note again that there is a performance floor in the IP scenario; nevertheless, our proposed detection method achieves more than 3dB SNR gain compared to the existing ODD method for the same detection performance in the low target SER regime (see the curve with square markers). Moreover, to achieve the same SER performance under the high reliability condition (i.e., low SER), the SNR required in the interference scenario is much higher than that required in the interference free scenario (illustrated by IP vs IF curves).

c) Performance of the Iterative Algorithm

We now study the performance of the iterative algorithm for channel estimation, interference cancellation, and symbol detection. First, we show the performance of channel estimation over iterations in Fig. 1.4a where the CMSE of estimated channel gains is shown for both IF and IP scenarios. In the figure, the iterative algorithm converges after only a few iterations. And the converged channel estimation performance in the presence of interference (IP) is almost identical to that of the interference free scenario (IF) in the low SNR regime (less then 30dB), which implies that the proposed iterative method cancels very well the interference in this SNR region. When the SNR is higher than 30dB, the performance in the IP case is still limited by the fast fading noise. However,

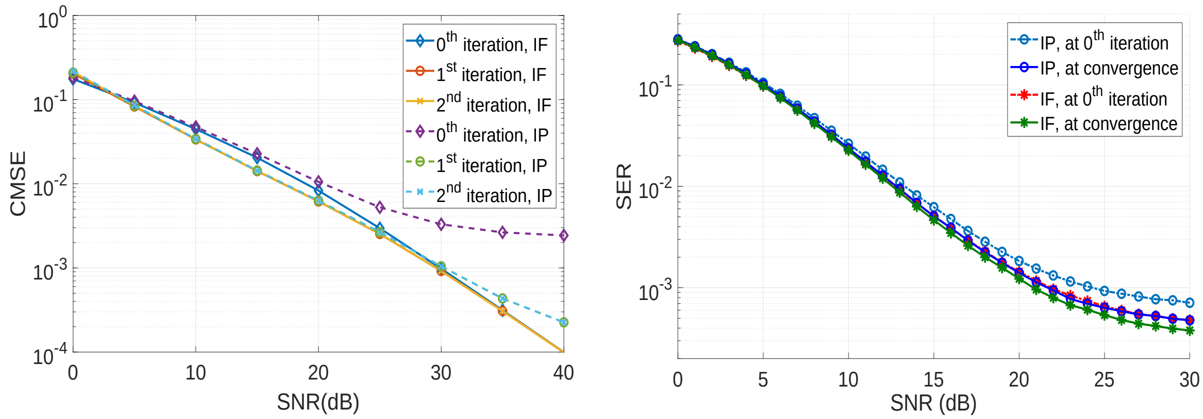

(a) (b)

Figure 1.4: a) Performance of channel estimation for iterative algorithm; b) SER achieved by iterative and non-iterative algorithms

the performance floor of the iterative channel estimation approach is much lower than that of the non-iterative counterpart (the 0^{th}-iteration versus the 2^{nd}-iteration curves in the IP scenario). We then show the SERs achieved by the non-iterative and iterative algorithms[12] in Fig. 1.4b. We can see that the iterative algorithm improves the SER in both IF and IP scenarios. Furthermore, the improvement is higher for larger values of SNR. This is because that the high SNR regime allows more reliable data detection, which boosts the performance of interference cancellation and channel estimation.

d) Throughput Achieved by Proposed Framework

In Fig. 1.5, we show the variations of the throughput with the pilot density for different values of SNR ρ and channel correlation coefficient α. For given α and ρ, there exists an optimal pilot density that achieves the maximum throughput. The maximum throughput increases as the SNR ρ increases, and larger α leads to higher maximum throughput and lower optimal pilot density. This is because when the channel varies more slowly, the performance of interference cancellation and channel estimation is improved, which results in more reliable transmission and higher throughput. The results in this figure demonstrate the tradeoff between the throughput and communication reliability in the fast fading environment.

[12] The SER of the non-iterative algorithm is the SER computed at the 0^{th} iteration and the SER of the iterative algorithm is the SER achieved at convergence.

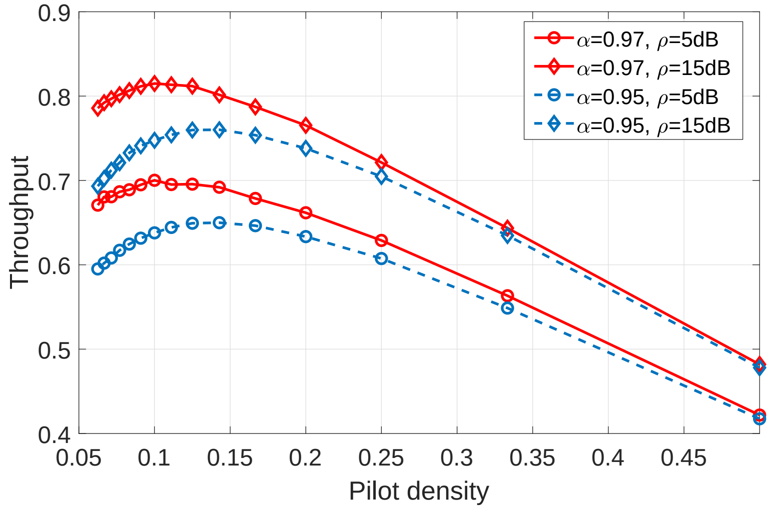

Figure 1.5: Throughput variations with the pilot density

1.2.2 Resource Allocation, Trajectory Optimization, and Admission Control in UAV-based Wireless Networks

In this contribution, we consider the resource allocation and trajectory optimization for multi-UAV based wireless networks, where the main contributions of our work can be summarized as follows:

- Our design maximizes the number of admitted users while satisfying their data transmission demands.
- The formulated problem is MINLP. We propose an iterative algorithm to solve the problem efficiently where the number of admitted users increases over iterations until convergence.

1.2.2.1 System Models

We consider downlink communications in a UAV-based wireless network. There are N UAVs and a set $\mathcal{K} = \{1, ..., K\}$ ground users. User k, whose 2-D coordinate is $\mathbf{u}_k$, demands to receive an amount of data D_k from the UAVs. The service period consists of T time slots, each time slot has length of δ. UAV n flies at altitude h and its 2-D coordinate at t is $\mathbf{c}_n[t]$. The total system bandwidth of B (Hz) is shared by users in an orthogonal manner. The bandwidth and transmit power of the communication between UAV n and user k at t are $b_{n,k}[t]$ and $p_{n,k}[t]$, respectively. The communication channels between UAVs and users are assumed to be dominated by Line of

Sight (LoS) components. Therefore, the channel power gain between UAV n and user k at t is $\rho_0/(h^2 + \|\mathbf{c}_n[t] - \mathbf{u}_k\|^2)$, where ρ_0 is the channel power gain at the reference distance of 1m from the UAV. The amount of data received by user k at t is expressed as

$$d_k[t] = \delta \sum_{n=1}^{N} b_{n,k}[t] \log_2 \left(1 + \frac{\gamma}{b_{n,k}[t]} \frac{p_{n,k}[t]}{h^2 + \|\mathbf{c}_n[t] - \mathbf{u}_k\|^2} \right), \tag{1.28}$$

where $\gamma = \rho_0/\sigma^2$ is the normalized Signal to Noise Ratio (SNR) and σ^2 is the white noise power density (W/Hz).

We consider user admission design where each user k is admitted if the UAVs can transmit at least D_k bits to it during the service period. We denote s_k as the admission decision variable which is equal to 1 if $\sum_{t=1}^{T} d_k[t] \geq D_k$ and equal to 0, otherwise. Our design aims to maximize the number of admitted users. The admission maximization problem can be formulated as follows:

$$\mathcal{P}^{\mathsf{AM}}(\mathcal{K}) : \max_{\{b_{n,k}[t]\},\{p_{n,k}[t]\},\{\mathbf{c}_n[t]\},\{s_k\}} \sum_{k \in \mathcal{K}} s_k,$$

$$\text{s.t.} \quad \sum_{t=1}^{T} d_k[t] \geq s_k D_k, \forall k, \tag{1.29a}$$

$$\sum_{n=1}^{N} \sum_{k=1}^{K} b_{n,k}[t] \leq B, \forall t, \tag{1.29b}$$

$$\sum_{k=1}^{K} p_{n,k}[t] \leq P_{\mathsf{max}}, \forall n, t, \tag{1.29c}$$

$$\|\mathbf{c}_n[t] - \mathbf{c}_n[t-1]\| \leq \min\left(V_{\mathsf{max}}\delta, D_{\mathsf{max}}\right), \forall n, t, \tag{1.29d}$$

$$\|\mathbf{c}_n[t] - \mathbf{c}_m[t]\| \geq D_{\mathsf{O}}, \forall n \neq m, t, \tag{1.29e}$$

$$\mathbf{c}_n[1] = \mathbf{c}_n[T] = \mathbf{c}_{\mathsf{o}}, \forall n, \tag{1.29f}$$

$$s_k \in \{0, 1\}, \forall k, \tag{1.29g}$$

where V_{max} is the maximum speed of a UAV, D_{max} is the maximum displacement to ensure the LoS channel conditions stay approximately the same, D_{O} is the safely distance, and $\mathbf{c}_{\mathsf{o}}$ is the coordinate of the launching station. Constraints (1.29b) and (1.29c) limits the communication resources used, where constraints (1.29d), (1.29e) and (1.29f) are for trajectory control.

1.2.2.2 Proposed Algorithm

First, we define the demand-aware transmission data, and soft admission (SA) decision, for user k, denoted as $\bar{D}_k$ and $\bar{s}_k$, respectively, as follows:

$$\bar{D}_k = \min\left(D_k, \sum_{t=1}^{T} d_k[t]\right), \tag{1.30a}$$

$$\bar{s}_k = \frac{\bar{D}_k}{D_k}, \forall k, \tag{1.30b}$$

We then consider the following SA maximization problem:

$$\begin{aligned}
\mathcal{P}^{\mathsf{SAM}}(\mathcal{K}): \quad & \max_{\{b_{n,k}[t]\},\{p_{n,k}[t]\},\{\mathbf{c}_n[t]\},\{\bar{D}_k,\bar{s}_k\}} \sum_{k\in\mathcal{K}} \bar{s}_k, \\
\text{s.t.} \quad & \bar{D}_k \leq D_k, \forall\, k \in \mathcal{K}, && (1.31\text{a}) \\
& \sum_{t=1}^{T} d_k[t] \geq \bar{D}_k, \forall\, k \in \mathcal{K}, && (1.31\text{b}) \\
& (1.29\text{b}), (1.29\text{c}), (1.29\text{d}), (1.29\text{e}), (1.29\text{f}), (1.30\text{b}).
\end{aligned}$$

The set of admitted users is denoted as $\mathcal{K}_{\mathsf{a}} = \{k : \bar{D}_k = D_k\}$. Note that the feasible set of $\mathcal{P}^{\mathsf{AM}}(\mathcal{K})$ contains the resource allocation and UAV trajectories that realize $\mathcal{K}_{\mathsf{a}}$. This relation provides connections between problem $\mathcal{P}^{\mathsf{AM}}(\mathcal{K})$ and problem $\mathcal{P}^{\mathsf{SAM}}(\mathcal{K})$.

★ *Step 1-Soft Admission Maximization*:

We develop an algorithm to solve problem $\mathcal{P}^{\mathsf{SAM}}(\mathcal{K})$ by using the combination of the BCA and successive convex approximation (SCA) methods.[13] Specifically, the BCA method is applied to optimize the objective function of $\mathcal{P}^{\mathsf{SAM}}(\mathcal{K})$ with respect to one set of variables given other sets of variables while the SCA is applied to approximate and convexify the trajectory control optimization sub-problem.

[13] Note that the user set at outer iteration m is denoted as $\mathcal{K}^m$. However, in this section, we are only interested in solving problem $\mathcal{P}^{\mathsf{SAM}}(\mathcal{K})$ for a certain set of users $\mathcal{K}$. So the index m is omitted for brevity.

The bandwidth and power allocation optimization sub-problem can be written as follows:

$$\begin{aligned}\mathcal{P}_{\mathsf{BP}}(\mathcal{K}):\ &\max_{\left\{b_{n,k}[t],p_{n,k}[t],\bar{D}_k,\bar{s}_k\right\}}\sum_{k\in\mathcal{K}}\bar{s}_k,\\ &\text{s.t.}\ \ (1.29\text{b}),(1.29\text{c}),(1.30\text{b}),(1.31\text{a}),(1.31\text{b}).\end{aligned}$$

Problem $\mathcal{P}_{\mathsf{BP}}(\mathcal{K})$ is convex, so it can be solved optimally using standard solvers such as CVX.

Given the bandwidth and power allocation, the UAV trajectory optimization sub-problem can be stated as follows:

$$\begin{aligned}\mathcal{P}_{\mathsf{C}}(\mathcal{K}):\ &\max_{\left\{\mathbf{c}_n[t],\bar{D}_k,\bar{s}_k\right\}}\sum_{k\in\mathcal{K}}\bar{s}_k,\\ &\text{s.t.}\ \ (1.29\text{d}),(1.29\text{e}),(1.29\text{f}),(1.30\text{b}),(1.31\text{a}),(1.31\text{b}).\end{aligned}$$

We convexify the nonconvex constraints (1.31b) and (1.29e) and apply the SCA method to solve the problem efficiently. Let the set of UAV coordinates from the previous iteration be $\mathbf{c}_n^i[t]$ and $\mathbf{c}_m^i[t]$, constraint (1.29e) can be squared and then approximated by the following inequality.

$$2\left(\mathbf{c}_m^i[t]-\mathbf{c}_n^i[t]\right)^T\left(\mathbf{c}_m[t]-\mathbf{c}_n[t]\right)-\left\|\mathbf{c}_m^i[t]-\mathbf{c}_n^i[t]\right\|^2\geq D_{\mathsf{O}}^2. \tag{1.34}$$

The logarithm terms in (1.28) can be approximated as follows:

$$\log_2\left(1+\frac{\bar{\gamma}_{n,k}[t]}{h^2+\|\mathbf{c}_n[t]-\mathbf{u}_k\|^2}\right)\geq\log_2\left(1+\frac{\bar{\gamma}_{n,k}[t]}{h^2+\|\mathbf{c}_n^i[t]-\mathbf{u}_k\|^2}\right)-\left(\|\mathbf{c}_n[t]-\mathbf{u}_k\|^2-\left\|\mathbf{c}_n^i[t]-\mathbf{u}_k\right\|^2\right)X_{n,k}^i[t], \tag{1.35}$$

where $\bar{\gamma}_{n,k}[t]=\gamma p_{n,k}[t]/b_{n,k}[t]$, and

$$X_{n,k}^i[t]=\frac{\log_2(e)\bar{\gamma}_{n,k}[t]}{\left(h^2+\|\mathbf{c}_n^i[t]-\mathbf{u}_k\|^2\right)\left(\bar{\gamma}_{n,k}[t]+h^2+\|\mathbf{c}_n^i[t]-\mathbf{u}_k\|^2\right)}.$$

Using these approximations, the problem $\mathcal{P}_{\mathsf{C}}(\mathcal{K})$ can be solved by solving the following convex optimization problem:

$$\bar{\mathcal{P}}_{\mathsf{C}}(\mathcal{K}): \quad \max_{\{\mathbf{c}_n[t], \bar{D}_k, \bar{s}_k\}} \quad \sum_{k\in\mathcal{K}} \bar{s}_k,$$

$$\text{s.t.} - \sum_{n=1}^{N}\sum_{t=1}^{T} \delta b_{n,k}[t] \left[\log_2\left(1+\frac{\bar{\gamma}_{n,k}[t]}{h^2+\|\mathbf{c}_n^i[t]-\mathbf{u}_k\|^2}\right) - \left(\|\mathbf{c}_n[t]-\mathbf{u}_k\|^2 - \left\|\mathbf{c}_n^i[t]-\mathbf{u}_k\right\|^2\right) X_{n,k}^i[t]\right] \geq \bar{D}_k, \tag{1.36a}$$

$$(1.29\text{d}), (1.29\text{e}), (1.29\text{f}), (1.30\text{b}), (1.31\text{a}).$$

Finally, problem $\mathcal{P}^{\mathsf{SAM}}(\mathcal{K})$ is solved by using an iterative algorithm where we solve problems $\mathcal{P}_{\mathsf{BP}}(\mathcal{K})$ and $\bar{\mathcal{P}}_{\mathsf{C}}(\mathcal{K})$ sequentially in each iteration.

★ *Step 2-User Removal*:

Let the set of users at iteration m after solving problem $\mathcal{P}^{\mathsf{SAM}}(\mathcal{K}^m)$ be $\mathcal{K}^m$. We want to remove the user who is unlikely to get admitted so that we can efficiently utilize the network resources for other users, so we propose a user removal strategy where the user with the largest gap between its required transmission data and demand-aware transmission data will be removed, as follows:

$$k_{\mathsf{min}}^m = \underset{k\in\mathcal{K}^m}{\operatorname{argmax}} \; D_k - \bar{D}_k^*, \tag{1.37}$$

where $\bar{D}_k^*$ is the demand-aware transmission data of user k expressed in (1.30a) after solving problem $\mathcal{P}^{\mathsf{SAM}}(\mathcal{K}^m)$. The set of users in the next iteration is $\mathcal{K}^{m+1} = \mathcal{K}^m \setminus \{k_{\mathsf{min}}\}$. Let $\mathcal{K}_{\mathsf{a}}^m$ be the set of admitted users after solving $\mathcal{P}^{\mathsf{SAM}}(\mathcal{K}^m)$. We introduce the admitted condition constraint for users $k \in \mathcal{K}_{\mathsf{a}}^m$ to the soft admission maximization problem so that admitted users at iteration m will still be admitted at iteration $m+1$ and express the problem as follows:

$$\mathcal{P}^{\mathsf{SAM}}(\mathcal{K}^{m+1}): \quad \max_{\mathbf{\Theta}, \{\bar{D}_k, \bar{s}_k\}} \; \bar{S}(\mathcal{K}^{m+1}),$$

$$\text{s.t.} \quad \bar{s}_k = 1, \forall k \in \mathcal{K}_{\mathsf{a}}^m, \tag{1.38a}$$

$$(1.29\text{b}), (1.29\text{c}), (1.29\text{d}), (1.29\text{e}), (1.29\text{f}), (1.30\text{b}),$$

Let $\mathcal{K}_{\mathsf{a}}^{m+1}$ be the set of admitted users after solving $\mathcal{P}^{\mathsf{SAM}}(\mathcal{K}^{m+1})$, it can be shown that $|\mathcal{K}_{\mathsf{a}}^{m+1}| \geq |\mathcal{K}_{\mathsf{a}}^{m}|$. Finally, the following table describes our algorithm.

Algorithm 1.4. Admission Maximization

Initiate $\mathbf{\Theta}, m = 1, \mathcal{K}^1 = \mathcal{K}$
while 1 **do**
  (*Soft admission maximization*) Solve problem $\mathcal{P}^{\mathsf{SAM}}(\mathcal{K}^m)$.
  if $|\mathcal{K}_{\mathsf{a}}^{m}| = |\mathcal{K}^m|$ **then**
    Break the loop.
  else
    (*User removal*) Let $\mathcal{K}^{m+1} = \mathcal{K}^m \setminus \{k_{\mathsf{min}}^m\}$, where k_{min}^m is defined in (1.37). Increase m by 1.
  end if
end while
End of algorithm.

1.2.2.3 Numerical Results

We consider the simulation setting where users are randomly located in a circular network area with the radius of 2km. The UAVs is assumed to fly at 100m, the maximum power P_{max} is set at 20dBm, σ^2 is -174dBm/Hz, and $\rho_0 = 4 \times 10^{-5}$. The flight duration is 120s, which is divided into 120 time slots. User transmission demand is 45Mbits, the total bandwidth is $B = 1$MHz, and the total number of users is 20, unless stated otherwise. We will numerically compare our proposed algorithm with a baseline. For this baseline, the problem $\mathcal{P}^{\mathsf{AM}}(\mathcal{K})$ is solved by applying the BCA method, where the sub-problems are MILPs. Specifically, in each iteration of this baseline, the bandwidth-power allocation, and trajectory optimization sub-problems with integer variables $\{s_k\}$ are solved by using the MOSEK solver. This baseline algorithm terminates when no more users can be admitted. This baseline is denoted as BCA-MILP in the following.

In Fig. 1.6a, we show the number of admitted users versus varying user data demand. Two observations can be drawn from the figure. First, deploying more UAVs allows us to admit more users. Second, our proposed methods can admit significantly more users than that achieved by the BCA-MILP baseline. This can be explained as follows. First, the SA maximization step in our algorithm optimizes a continuous objective function, so the algorithm can find better UAVs trajectories over iterations before convergence. This is not the case for the BCA-MILP in which convergence is reached after only a few iterations due to integer-valued objective function. Moreover, our developed user removal step efficiently removes poor users and thus their resources can be

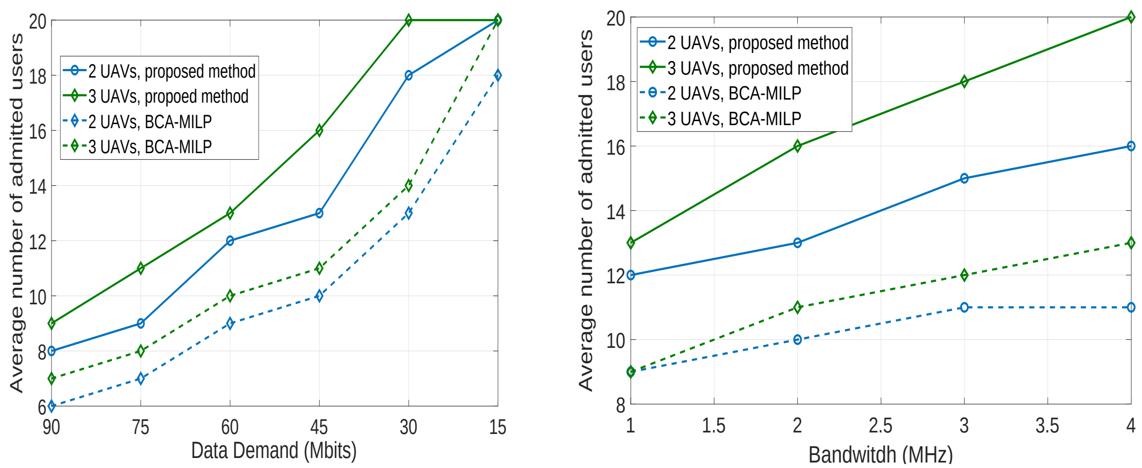

(a) (b)

Figure 1.6: a) Number of served users versus data demand per user; b) Number of served users versus total bandwidth

reserved and used more efficiently to serve better users. Fig. 1.6b presents the number of admitted users versus varying bandwidth. When there is more bandwidth available, the network can admit more users. However, the performance gain of the proposed algorithm versus the baseline increases as the bandwidth grows, which implies that our approach utilizes radio resources more efficiently.

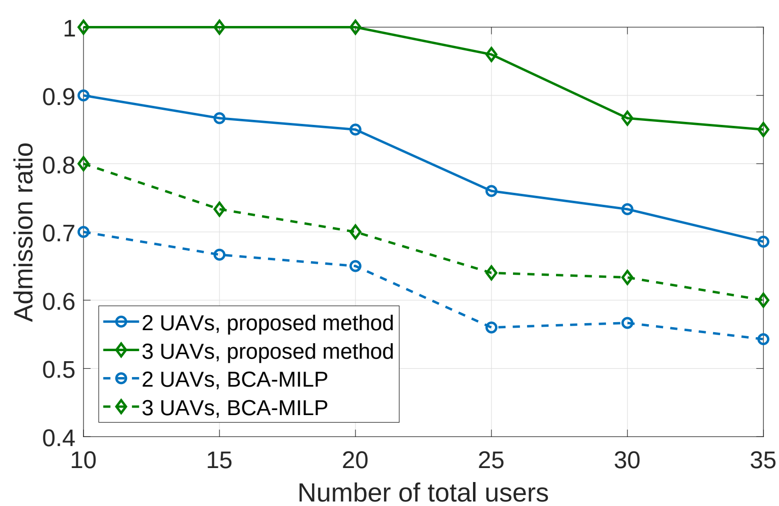

Figure 1.7: Coverage probability versus total number of users

Finally, we show the admission ratio with varying number of users in Fig. 1.7. It can be seen that the admission ratio decreases when there are more users. However, our proposed approach still achieves better performance than the BCA-MILP baseline.

1.2.3 Multi-UAV Trajectory Control, Resource Allocation, and NOMA User Pairing for Uplink Energy Minimization

In this contribution, we study the joint optimization of multiple UAVs' trajectories, transmit power allocation, user-UAV association, and user pairing for UAV-assisted wireless networks employing the non-orthogonal multiple access (NOMA) for uplink communications. The design aims to minimize the total energy consumption of ground users while guaranteeing to successfully transmit their required amount of data to the UAV-mounted base stations. The key contributions of our work are as follows:

- We formulate the total energy minimization problem where NOMA user pairing, transmit power allocation, user-UAV association, and multi-UAV trajectory control are jointly optimized. We derive the optimal power allocation solution, which is expressed explicitly as a function of other optimization variables.
- We develop an efficient algorithm to solve the considered problem by using the BCD approach.
- We compare the proposed algorithm with two other baselines: one is the Data Collection Optimization Algorithm (DCOA) from [29], and the other baseline which employs the same design principles as for our proposed algorithm; however, the conventional OMA instead of NOMA is used. We show the superior performance of our algorithm compared to the two considered baselines via numerical studies and demonstrate the tradeoff between the flight time and the total energy as well as the impacts of different parameters such as the numbers of users and UAVs on the total energy consumption.

1.2.3.1 System Model and Problem Formulation

a) System Model

We consider uplink communications in an UAV-assisted wireless network with N flying UAVs and K ground users. The UAV flying duration T is divided into a number of small time slots, each of which has an identical length of δ. We assume that UAV n flies at the fixed altitude h and its 2-D coordinate at time slot t is denoted as $\mathbf{c}_n[t]$. The 2-D coordinate of ground user k is denoted as $\mathbf{u}_k$. We assume that NOMA is employed to support the uplink communications where users are grouped into two-user pairs which transmit on orthogonal channels. It is assumed that each user k requires to transmit an amount of data D_k to the UAVs by the end of the service period.

The communication channels between UAVs and users are assumed to be dominated by the Line of Sight (LoS) component. The channel power gain between UAV n and user k at t, denoted as $\tau_{k;n}[t]$, is $\tau_{k;n}[t] = \frac{\mu}{\|\mathbf{c}_n[t]-\mathbf{u}_k\|^2+h^2}$, where μ is the channel power gain at the reference distance of 1m from the transmitter. We denote $x_{k,l}[t]$ as the user pairing decision variable which is equal to 1 if user k is paired with user l in time slot t and equal to 0, otherwise. We then have $x_{k,l} = 0$ if $k = l$, and $x_{k,l}[t] = x_{l,k}[t]$ for all k and l. Furthermore, we denote $a_{k;n}[t]$ as the association between UAV n and user k in time slot t where $a_{k;n}[t]$ is equal to 1 if user k is associated[14] with UAV n and equal to 0, otherwise. Each user can only connect to one UAV but each UAV can connect multiple users in any time slot. The channel condition of user k at t can be expressed as follows:

$$\tau_k[t] = \sum_{n=1}^{N} a_{k;n}[t]\tau_{k;n}[t], \quad \forall k, t. \tag{1.39}$$

We assume that users are paired and each user pair transmits data to the associated UAV in the uplink NOMA direction. If user k is the strong user in a particular pair, its achieved data rate in time slot t can be expressed as follows:

$$\mathsf{R}_k[t] = B\log\left(1+\frac{\tau_k[t]p_k[t]}{\sigma^2 + \tau_k^{\mathsf{p}}[t]p_k^{\mathsf{p}}[t]}\right), \tag{1.40}$$

where B is the channel bandwidth assigned for the underlying user pair, $\tau_k^{\mathsf{p}}[t]$ and $p_k^{\mathsf{p}}[t]$ are the channel power gain and the transmit power of its paired user, which can be expressed as follows:

$$\tau_k^{\mathsf{p}}[t] = \sum_{l=1}^{K} x_{k,l}[t]\tau_l[t], \tag{1.41a}$$

$$p_k^{\mathsf{p}}[t] = \sum_{l=1}^{K} x_{k,l}[t]p_l[t]. \tag{1.41b}$$

If user k is the weak user in the considered pair in time slot t, its achieved data rate can be expressed as follows:

$$\mathsf{r}_k[t] = B\log\left(1+\frac{\tau_k[t]p_k[t]}{\sigma^2}\right). \tag{1.42}$$

[14]In this chapter, ‘connected’ and ‘associated’ are used interchangeably to describe the user-UAV association.

We use $\lambda_k[t]$ to describe the strong-weak role[15] of user k where it is equal to 1 if user k is the strong user and equal to 0 if it is the weak user in its associated pair and time slot t. There is a coupling between the strong-weak variables and the user-pairing optimization variables which can be expressed in the following constraints:

$$x_{k,l}[t]\left(\lambda_k[t]+\lambda_l[t]-1\right)=0, \quad \forall(k,l),t. \tag{1.43}$$

Finally, the relationship between channel conditions and strong-weak variables can be stated as follows:

$$\left(2\lambda_k[t]-1\right)\left(\tau_k[t]-\tau_k^{\mathsf{p}}[t]\right)\geq 0, \quad \forall k,t, \tag{1.44}$$

We note here that the values of strong-weak variables can be readily determined (as values of the indicator function $\mathbb{1}_{\tau_k[t]>\tau_k^{\mathsf{p}}[t]}$) when the UAV trajectories, user association, and user pairing variables are given. In the following, the strong-weak variables are occasionally omitted if they can be readily determined from the given values of other variables without causing any ambiguity.

b) Problem Formulation

Our design aims to minimize the energy consumption of all users by optimizing the user association ($\mathbf{A}[t]$), user pairing ($\mathbf{X}[t]$), the strong-weak variables ($\mathbf{\Lambda}[t]$), the power allocation ($\mathbf{P}[t]$), and the UAV trajectories $\{\mathbf{c}_n[t]\}$ while users are ensured to transmit their required amount of data to the UAVs within the service duration. The considered optimization problem can be stated as

[15]Note that a user is strong or weak depending on its channel condition and the channel condition of its partner. In our design, the channel condition of a particular user depends on the coordinates of the associated UAV and the UAVs' coordinates are optimization variables. So it is necessary to define variables capturing the strong-weak roles of individual users.

follows:

$$
\begin{aligned}
\mathcal{P}_0 : & \min_{\{\mathbf{A}[t],\mathbf{X}[t],\mathbf{\Lambda}[t],\mathbf{P}[t],\mathbf{c}_n[t]\}} E_{\mathsf{all}}, \\
\text{s.t.} \quad & \sum_{t=1}^{T} \delta \left(\lambda_k[t]\mathsf{R}_k[t] + (1-\lambda_k[t])\, \mathsf{r}_k[t]\right) \geq D_k, \forall k, && (1.45a) \\
& \sum_{n=1}^{N} a_{k;n}[t] = 1, \quad \forall k, t && (1.45b) \\
& \mathbf{X}[t] = \mathbf{X}^T[t], \quad \forall t, && (1.45c) \\
& \sum_{l=1}^{K} x_{k,l}[t] = 1, \forall k, t, && (1.45d) \\
& x_{k,l}[t](a_{k;n}[t] - a_{l;n}[t]) = 0, \quad \forall (k,l), n, t, && (1.45e) \\
& p_k[t] \leq P_{\mathsf{max}}, \forall k, t, && (1.45f) \\
& \|\mathbf{c}_n[t] - \mathbf{c}_n[t-1]\| \leq \delta V_{\mathsf{max}}, \forall n, t, && (1.45g) \\
& \|\mathbf{c}_n[t] - \mathbf{c}_m[t]\| \geq D_{\mathsf{safe}}, \forall t, \forall n \neq m, && (1.45h) \\
& \mathbf{c}_n[1] = \mathbf{c}_n[T] = \mathbf{c}_{\mathsf{o}}, \forall n, && (1.45i) \\
& \lambda_k \in \{0,1\}, a_{k;n} \in \{0,1\}, x_{k,l} \in \{0,1\}, \forall k, l, n, && (1.45j) \\
& \text{constraints} \quad (1.43), (1.44),
\end{aligned}
$$

where P_{max} denotes the maximum transmit power of each user, and the total energy can be expressed as

$$E_{\mathsf{all}} = \delta \sum_{t=1}^{T} \sum_{k=1}^{K} p_k[t]. \tag{1.46}$$

Constraints (1.45a) ensure that every user can transmit their required amount of data to the UAVs. Constraints (1.45b), (1.45e), (1.45c) and (1.45d) are imposed to make sure that the user pairing and association solution are valid. Constraints (1.45f) describe the maximum transmit powers of users. Constraints (1.45g), (1.45h) and (1.45i) are for UAV trajectory control, where V_{max} is the maximum speed of a UAV, D_{safe} is the safety distance between any two UAVs, $\mathbf{c}_{\mathsf{o}}$ is the coordinate of the launching station. The formulated problem is a mixed-integer nonlinear program, which is nontrivial to solve. In the next section, we propose an algorithm to solve problem $\mathcal{P}_0$ efficiently.

1.2.3.2 Proposed Solution

a) Equivalent Problem

First, we introduce a set of auxiliary variables $\{\mathbf{r}[t]\}$, where $r_k[t]$ is target the data rate that user k transmits to their associated UAV in time slot t. The problem $\mathcal{P}_0$ is equivalent to the following problem with additional variables $\{\mathbf{r}[t]\}$.

$$
\begin{aligned}
\mathcal{P}_1 : & \min_{\{\mathbf{A}[t],\mathbf{X}[t],\mathbf{\Lambda}[t],\mathbf{P}[t],\mathbf{c}_n[t],\mathbf{r}[t]\}} E_{\mathsf{all}}, \\
\text{s.t.} \;\; & \lambda_k[t]\mathsf{R}_k[t] + (1-\lambda_k[t])\mathsf{r}_k[t] \geq r_k[t], \forall k, t, && (1.47a)\\
& \sum_{k=1}^{K} \delta r_k[t] \geq D_k, \forall k, && (1.47b)\\
& (1.45b), (1.45e), (1.43), (1.44), (1.45c), (1.45d), (1.45f), (1.45g), (1.45h), (1.45i), (1.45j).
\end{aligned}
$$

It is easy to see that the equality of (1.47a) holds at the optimum. Since one can always increase $r_k[t]$ to realize the equality of (1.47a) without violating other constraints. We will describe how to solve problem $\mathcal{P}_1$ in the following.

b) Proposed Solution

In the considered optimization problem, we will show in Lemma 1.1 that the optimal power $\{\mathbf{P}^*[t]\}$ can be expressed explicitly in terms of other variables ($\{\mathbf{c}_n[t], \mathbf{X}[t], \mathbf{A}[t], \mathbf{r}[t]\}$). This optimal power $\{\mathbf{P}^*[t]\}$ expression enables us to apply the BCD technique to solve problem $\mathcal{P}_1$ effectively. We then propose to solve problem $\mathcal{P}_1$ by iteratively solving three following sub-problems. In the first sub-problem, we assume that values of $\{\mathbf{c}_n[t], \mathbf{r}[t]\}$ are given and solve for the optimal power consumption where all other variables are the optimization variables. In the second sub-problem, we optimize the data rate variables $\{\mathbf{r}[t]\}$ given $\{\mathbf{c}_n[t]\}$ and the optimal values of other variables obtained from solving the first sub-problem,. Finally, in the third problem, the UAVs' trajectories are optimized given values of other variables. It can be shown that the total energy consumption is reduced over iterations, hence, the iterative process is guaranteed to converge.

★ *Optimizations Of Power and Integer Variables Given UAVs' Trajectories and Rates:*

Assuming that $\{\mathbf{c}_n[t], \mathbf{r}[t]\}$ are given, we find the optimal power $\{\mathbf{P}^*[t]\}$ with respect to $\{\mathbf{c}_n[t], \mathbf{r}[t]\}$, and other integer variables. Specifically, we solve for the optimal power and user association when the pairing scenario is known. Then, the user pairing optimization is solved by tackling the underlying maximum weighted graph matching problem. Then, the optimal user association is derived.

If the values of $\{\mathbf{c}_n[t], \mathbf{r}[t]\}$, and $\mathbf{X}[t]$ are given, the problem $\mathcal{P}_1$ is reduced to the following problem.

$$\begin{aligned}\mathcal{P}_{\mathsf{A,P}} : &\min_{\mathbf{A}[t]\mathbf{\Lambda}[t],\mathbf{P}[t]} E_{\mathsf{all}}, \\ \text{s.t.}\ \ &(1.45\text{b}), (1.45\text{e}), (1.43), (1.44), (1.45\text{f}), (1.45\text{j}), (1.47\text{a}).\end{aligned}$$

Problem $\mathcal{P}_{\mathsf{A,P}}$ can be decoupled into several subproblems denoted as $\tilde{\mathcal{P}}_{\mathsf{A,P}}(k,l;t)$. The subproblem $\tilde{\mathcal{P}}_{\mathsf{A,P}}(k,l;t)$ minimizes the total energy consumed by users k and l in time slot t, where the transmit power $p_k[t], p_l[t]$, the user association $\mathbf{a}_k[t], \mathbf{a}_l[t]$, and the strong-weak variables $\lambda_k[t], \lambda_l[t]$ need to be optimized[16]. This sub-problem can be expressed as follows:

$$\begin{aligned}\tilde{\mathcal{P}}_{\mathsf{A,P}}(k,l;t) : &\min_{\{\mathbf{a}_i[t],\lambda_i[t],p_i[t]\}_{i=k,l}} \delta(p_k[t] + p_l[t]), \\ \text{s.t.}\ \ &a_{k;n}[t] = a_{l;n}[t], &(1.49\text{a}) \\ &\lambda_k[t] + \lambda_l[t] = 1, &(1.49\text{b}) \\ &(2\lambda_k[t] - 1)(\tau_k[t] - \tau_l[t]) \geq 0, &(1.49\text{c}) \\ &(1.45\text{b}), (1.45\text{f}), (1.45\text{j}), (1.47\text{a}).\end{aligned}$$

where (1.49a), (1.49b), and (1.49c) are deduced from (1.45e), (1.43), and (1.44), respectively, given that $x_{k,l}[t] = 1$.

Let the sum power of two users k and l in the objective function of $\tilde{\mathcal{P}}_{\mathsf{A,P}}(k,l;t)$ be $p_{k,l}[t]$, then the total energy consumption can be expressed as follows:

$$E_{\mathsf{all}} = \frac{\delta}{2}\sum_{t=1}^{T}\sum_{k=1}^{K}\sum_{l=1}^{K} x_{k,l}[t] p_{k,l}[t]. \tag{1.50}$$

[16]Note that $\mathbf{a}_k[t] = [a_{k;1}[t], ..., a_{k;N}[t]]$ denotes the user association vector corresponding to user k at t.

In the following, we find the optimal value of $p_{k,l}[t]$ for all t and all combinations of k and l. *First*, we find the optimal power allocation with respect to the user association variables (i.e., if $\mathbf{a}_k[t]$ and $\mathbf{a}_l[t]$ are known). Note that when the user association solution is given, the channel conditions for k and l are determined by (1.39). Then the strong-weak variables can also be readily determined by (1.49b) and (1.49c).[17]. *Second*, we substitute the optimal power allocation solution as a function of the user association variables into the objective function of $\tilde{\mathcal{P}}_{\mathsf{A,P}}(k,l;t)$ from which the optimal association with respect to every pair (k,l) will be determined.

Let us consider a particular pair of users k and l associated with UAV n. Assume that the channel of user k is stronger than that of user l (i.e., $\lambda_k[t]=1$ and $\lambda_l[t]=0$). Then, the problem $\tilde{\mathcal{P}}_{\mathsf{A,P}}(k,l;t)$ can be deduced further into the following problem:

$$\begin{aligned}\tilde{\mathcal{P}}_{\mathsf{P}}(k,l;t;n): &\min_{\{p_i[t]\}_{i=k,l}} \delta(p_k[t]+p_l[t]),\\ &\text{s.t.} \;\; (1.45\text{f}),(1.47\text{a}).\end{aligned}$$

Lemma 1.1. *If the problem $\tilde{\mathcal{P}}_{\mathsf{P}}(k,l;t;n)$ is feasible, the optimal solution of it can be written as follows:*

$$\begin{aligned} p_k^*[t] &= \sigma^2 \tau_{k;n}^{-1}[t](\beta^{r_k[t]}-1)\beta^{r_l[t]},\\ p_l^*[t] &= \sigma^2 \tau_{l;n}^{-1}[t](\beta^{r_l[t]}-1), \end{aligned} \tag{1.52}$$

where $\beta = 2^{1/B}$. The problem is feasible if both $p_k^*[t]$ and $p_l^*[t]$ in (1.52) *are no greater than P_{max}.*

Lemma 1.1 allow us to explicitly express the optimal transmit powers of users k and l in terms of their channel conditions which depend on the user association and distances from the users to their associated UAV. Hereafter we will use the right hand side of (1.52) instead of $p_k[t], p_l[t]$.

[17]Specifically, if users k and l are associated with UAV n in time slot t, we can compute their channel conditions. Then $\lambda_k[t]=1$ if $\tau_{k;n}[t] \geq \tau_{l;n}[t]$ and $\lambda_l[t]=0$, otherwise.

Let $p_{k,l;n}[t]$ be the optimal allocated power of users k and l in case they are paired and connected to UAV n in time slot t. Then, $p_{k,l;n}[t]$ can be expressed as follows:[18]

$$p_{k,l;n}[t] = \begin{cases} \sigma^2 \left(\tau_{k;n}^{-1}[t](\beta^{r_k[t]} - 1)\beta^{r_l[t]} + \tau_{l;n}^{-1}[t](\beta^{r_l[t]} - 1) \right), & \text{if} \max(p_k^*[t], p_l^*[t]) \leq P_{\mathsf{max}}, \\ \infty, & \text{otherwise}. \end{cases} \tag{1.53}$$

The optimal value of the objective function of $\tilde{\mathcal{P}}_{\mathsf{A,P}}(k, l; t)$ with respect to the user association variables can be expressed as follows:

$$p_{k,l}[t] = \sum_{n=1}^{N} a_{k;n}[t] p_{k,l;n}[t]. \tag{1.54}$$

Note that (1.54) is realized with the assumption that $x_{k,l}[t] = 1$, and hence $a_{k;n}[t] = a_{l;n}[t]$. The result in (1.54) allows us to find the optimal association for users k, l by the following Lemma.

Lemma 1.2. *If $x_{k,l}[t] = 1$, the optimal association for users k and l at t can be found as follows:*

$$a_{k;n}^*[t] = a_{l;n}^*[t] = \begin{cases} 1, & \textit{if } n = \operatorname*{argmin}_n p_{k,l;n}[t] \\ 0, & \textit{otherwise}. \end{cases} \tag{1.55}$$

Substituting the user association solution obtained from Lemma 1.2, we can find the optimal value of $p_{k,l}[t]$ from $p_{k,l}[t]$ from (1.54).

Upon obtaining the optimal user association and corresponding power allocation solution, the user pairing optimization problem can be expressed as follows:

$$\begin{aligned} \mathcal{P}_{\mathsf{X}} : & \min_{\mathbf{X}[t]} \frac{\delta}{2} \sum_{t=1}^{T} \sum_{k=1}^{K} \sum_{l=1}^{K} x_{k,l}[t] p_{k,l}[t], \\ & \text{s.t.} \quad (1.45\text{c}), (1.45\text{d}), (1.45\text{j}). \end{aligned}$$

Similarly, problem $\mathcal{P}_{\mathsf{X}}$ can be decomposed into several subproblems each of which optimizes the user pairing for one corresponding t. The subproblem at t is indeed the Maximum Weight Perfect

[18] We use the convention in [30] where the optimal value of a minimization problem is infinity if the problem is infeasible.

Matching (MWPM) problem for a graph whose vertices are users, and the weight of the edge between users k and l is $p_{k,l}[t]$. These MWPM problems can be solved efficiently and optimally [31].

In the following sections, the optimizations of other variables, given user association and pairing solutions, are developed. We denote $(k, l)[t]$ as the users k and l to be paired in time slot t. Without loss of generality, it is the convention in the following sections that k is the strong user and l is the weak user.

★ *Data Rate Optimization Problem:*

From (1.46) and (1.53), the total energy consumption E_{all} can be expressed with respect to the data rates $\{\mathbf{r}[t]\}$ as follows:

$$E_{\mathsf{all}} = \delta\sigma^2 \sum_{t=1}^{T} \sum_{(k,l)[t]} \beta^{r_k[t]+r_l[t]} \tau_k^{-1}[t] + \beta^{r_l[t]} \left(\tau_l^{-1}[t] - \tau_k^{-1}[t]\right) - \delta\sigma^2 \sum_{t=1}^{T} \sum_{(k,l)[t]} \tau_l^{-1}[t], \tag{1.57}$$

When UAV trajectory, user association, and user pairing solutions are given, the optimization of data rates can be stated as follows:

$$\mathcal{P}_{\mathsf{R}} : \min_{\{\mathbf{r}[t]\}} E_{\mathsf{all}},$$

$$\text{s.t.} \sum_{k=1}^{K} \delta r_k[t] \geq D_k, \forall k, \tag{1.58a}$$

$$\beta^{r_l[t]} - 1 \leq \frac{P_{\mathsf{max}}}{\sigma^2} \tau_k[t], \forall (k, l)[t], \tag{1.58b}$$

$$\beta^{r_k[t]+r_l[t]} - \beta^{r_l[t]} \leq \frac{P_{\mathsf{max}}}{\sigma^2} \tau_l[t], \forall (k, l)[t], \tag{1.58c}$$

$$(1.45c), (1.45d), (1.45f), (1.45g), (1.45h), (1.45j).$$

Since $\tau_l^{-1}[t] - \tau_k^{-1}[t] \geq 0$ for all user pairs $(k, l)[t]$, the objective function of problem $\mathcal{P}_{\mathsf{R}}$ is convex; but problem $\mathcal{P}_{\mathsf{R}}$ is still non-convex due to the non-convexity of constraint (1.58c). However, (1.58c) is the difference of two convex functions, so we can approximate (1.58c) by the following constraint [30]:

$$\beta^{r_k[t]+r_l[t]} - \beta^{\bar{r}_l[t]}(1 + \ln(\beta)(r_l[t] - \bar{r}_l[t]))\tau_{l;n}^{-1}[t] \leq \frac{P_{\mathsf{max}}}{\sigma^2}, \tag{1.59}$$

where we have replaced $\beta^{r_l[t]}$ by its first order Taylor approximation at local point $\bar{r}_l[t]$. The constraint (1.59) is convex with respect to the optimization variables $(r_k[t], r_l[t])$, Then we apply the Successive Convex Approximation (SCA) technique to solve the problem $\mathcal{P}_{\mathsf{R}}$ iteratively where constraint (1.58c) is replaced by constraint (1.59) in each iteration of the iterative process.

★ *UAV Trajectory Optimization:*

The overall objective function E_{all} can also be expressed with respect to the UAV trajectories $\{\mathbf{c}_n[t]\}$ as follows:

$$E_{\mathsf{all}} = \delta\sigma^2 \sum_{t=1}^{T} \sum_{(k,l)[t]} \zeta_k[t] \|\mathbf{c}_{n_{(k,l)}}[t] - \mathbf{u}_k\|^2 + \zeta_l[t] \|\mathbf{c}_{n_{(k,l)}}[t] - \mathbf{u}_l\|^2 + \delta\sigma^2 \sum_{t=1}^{T} \sum_{(k,l)[t]} (\zeta_k[t] + \zeta_l[t]) h^2, \quad (1.60)$$

where $\zeta_k[t] = \mu^{-1}(\beta^{r_k[t]} - 1)\beta^{r_l[t]}$ and $\zeta_l[t] = \mu^{-1}(\beta^{r_l[t]} - 1)$; $\mathbf{c}_{n_{(k,l)}}[t]$ is the coordinate of the UAV that is associated with user pair $(k,l)[t]$. Note that the second term does not depend on $\{\mathbf{c}_n[t]\}$.

The UAV trajectory optimization problem can be expressed as follows:

$$\begin{aligned}
\mathcal{P}_{\mathsf{C}} : & \min_{\{\mathbf{c}_n[t]\}} E_{\mathsf{all}} \\
\text{s.t. } & \zeta_k[t] \left(\|\mathbf{c}_{n_{(k,l)}}[t] - \mathbf{u}_k\|^2 + h^2 \right) \leq \frac{P_{\mathsf{max}}}{\sigma^2}, \forall (k,l)[t], && (1.61a) \\
& \zeta_l[t] \left(\|\mathbf{c}_{n_{(k,l)}}[t] - \mathbf{u}_l\|^2 + h^2 \right) \leq \frac{P_{\mathsf{max}}}{\sigma^2}, \forall (k,l)[t], && (1.61b) \\
& (1.44), (1.45g), (1.45i), (1.45h).
\end{aligned}$$

Even though problem $\mathcal{P}_{\mathsf{C}}$ is non-convex due to the non-convex constraint (1.45h), we can solve it by applying the SCA method. Specifically, we first square both sides of (1.45h) and then approximate the left hand side with its lower bound at the local point $\{\bar{\mathbf{c}}_n[t], \bar{\mathbf{c}}_m[t]\}$ by using the first-order Taylor expansion. We then can obtain the following approximated constraint:

$$2\left(\bar{\mathbf{c}}_m[t] - \bar{\mathbf{c}}_n[t]\right)^T (\mathbf{c}_m[t] - \mathbf{c}_n[t]) - \|\bar{\mathbf{c}}_m[t] - \bar{\mathbf{c}}_n[t]\|^2 \geq D_{\mathsf{safe}}^2. \quad (1.62)$$

As constraints (1.45h) are approximated by (1.62), the resulting approximated problem of problem $\mathcal{P}_{\mathsf{C}}$ is convex with respect to the UAV trajectory variables. Therefore, the obtained convex problem can be solved optimally using standard solvers.

Our proposed iterative algorithm, named Multi-UAV NOMA Energy minimization (MUNE), is described in Algorithm 1.5, where ϵ is a small number that is set to balance between the desired accuracy and convergence time of this algorithm.

Algorithm 1.5. Multi-UAV NOMA Energy minimization (MUNE)

Initiate values for UAV trajectories $\left\{\mathbf{c}_n^0[t], \mathbf{R}^0[t]\right\}$, set $i = 1$, $E_{\mathsf{all}}^0 = TKP_{\mathsf{max}}$.
while 1 **do**
  Given $\left\{\mathbf{c}_n^{i-1}[t], \mathbf{R}^{i-1}[t]\right\}$, solve problem $\tilde{\mathcal{P}}_{\mathsf{A,P}}(k, l; t)$ for all t and all possible combinations of (k, l), obtain optimal $\{p_{k,l}[t]\}$ from (1.54).
  From the obtained $\{p_{k,l}[t]\}$, solve problem $\mathcal{P}_{\mathsf{X}}$ for optimal pairing variables $\left\{\mathbf{X}^i[t]\right\}$, and the corresponding association $\left\{\mathbf{A}^i[t]\right\}$.
  Solve problem $\mathcal{P}_{\mathsf{R}}$ with given other variables iteratively until convergence, obtain the values of $\left\{\mathbf{R}^i[t]\right\}$.
  Solve problem $\mathcal{P}_{\mathsf{C}}$ with given other variables iteratively until convergence. Denote the obtained solution as $\{\mathbf{c}_n^i[t]\}$, and the total energy consumption as E_{all}^i.
  if $E_{\mathsf{all}}^i \geq E_{\mathsf{all}}^{i-1} - \epsilon$ **then**
    Break the loop.
  else
    Let $i = i + 1$.
  end if
end while
End of algorithm.

1.2.3.3 Numerical Results

We consider a circular network with radius of 1000m in which users are placed randomly and uniformly. We assume that UAVs fly at the constant altitude $h = 100$m and all users require the same amount of data to be collected $D_k = 6$Mbits $\forall k$, unless stated otherwise. The bandwidth allocated for each user pair is 100kHz, the noise power is set to -105dBm, and μ is set equal to 6.5×10^{-4}. The number of time slots is $T = 60$, unless stated otherwise and each time slot has the length of $\delta = 1$s. The maximum transmit power is $P_{\mathsf{max}} = 0.1$W and the value of ϵ in Algorithm 1.5 is 10^{-2}. The UAV station is located at the center of the network area, $\mathbf{c}_{\mathsf{o}} = (0, 0)$. Initially, we let $r_k[t] = D_k/T$ for all user k, i.e., the initial data rates in each time slot are identical for all users. For the UAVs' initial trajectories, we let UAV n start at $\mathbf{c}_{\mathsf{o}} = (0, 0)$ and fly in counter clockwise direction along a circular trajectory with radius of $r_{\mathsf{o}} = 300$m and center at $(r_{\mathsf{o}} \cos \frac{n2\pi}{N}, r_{\mathsf{o}} \sin \frac{n2\pi}{N})$.

We introduce two baseline algorithms whose performances are to be compared with that achieved by our proposed algorithm. *First,* the Data Collection Optimization Algorithm (DCOA) which was developed in [29] for single-UAV setting only. The DCOA uses the Generalized Benders Decomposition [32] to solve the joint NOMA user pairing and power allocation optimization problem, and then optimizes the UAV trajectory to maximize the total transmitted data from all users. *Second,* we also present another baseline algorithm, called Multi-UAV OMA Energy Minimization (MUOE), whose details are given in Appendix 7.A, where the orthogonal multiple access (OMA) strategy is used instead of NOMA. In this strategy, each user is connected to the closest UAV and they have an assigned bandwidth of $B/2$ in each time slot. There are 18 users in this simulation scenario. We present numerical results for single-UAV and multiple-UAV settings in the following.

a) Single UAV Setting

We show the performances achieved by our proposed MUNE algorithm, the MUOE algorithm, and the DCOA algorithm from [29] for the network setting with one UAV and varying number of users. Specifically, in Fig. 1.8, we show the total energy consumption of all users as these algorithms are applied. This figure shows that the proposed MUNE algorithm achieves the lowest energy consumption. Furthermore, the gaps between the total energy consumption due to the proposed algorithm and the two baselines increases when the number of users increases.

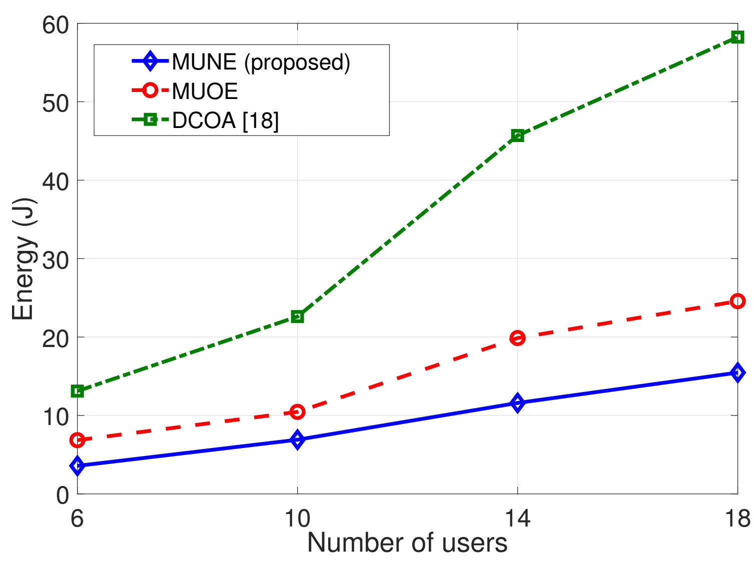

Figure 1.8: Total energy consumption versus number of users, single-UAV setting.

b) Multi-UAV Settings

We now present numerical results for multi-UAV settings. Note that the DCOA algorithm cannot be applied in multi-UAV settings; therefore, we only show the performance achieved by the proposed MUNE and MUOE algorithms.

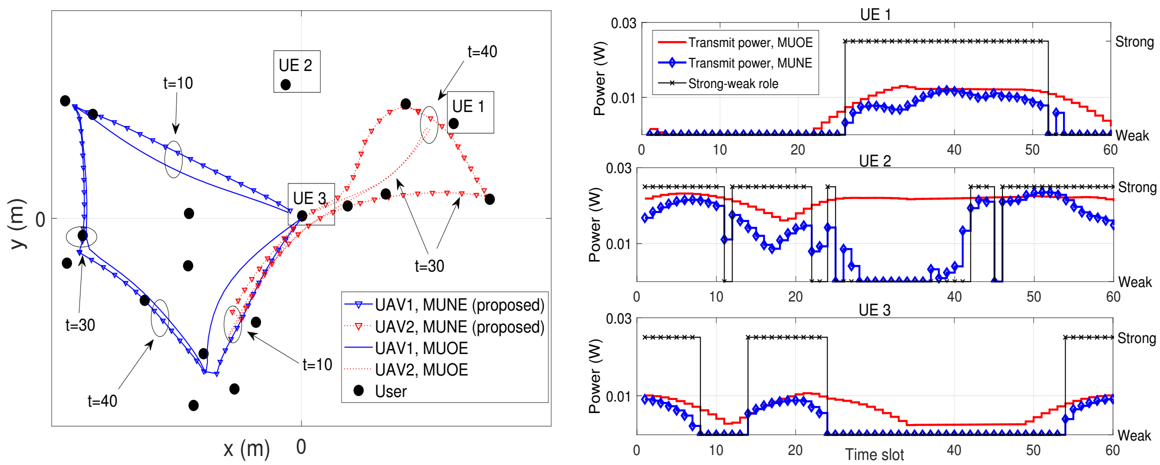

(a) (b)

Figure 1.9: a) Converged UAV trajectories, obtained by different algorithms; b) User transmit powers over time

We first study a particular network scenario. In Fig. 1.9a, we show the UAVs' trajectories obtained by the MUNE and MUOE algorithms at convergence. Several interesting observations can be drawn from this figure. First, the trajectories of UAV 1 achieved by both algorithms seem to follow a convex boundary established by edge users who are closer to the initial trajectory of UAV 1 than that of UAV 2. While the trajectories of UAV 1 due to both algorithms are quite close to each other, there is a clear difference in the trajectories of UAV 2 obtained from the two algorithms. The trajectory obtained from the MUNE algorithm also follows the convex boundary of the edge users that are closer to the initial trajectory of UAV 2. However, the trajectory obtained from the MUOE algorithm squeezes tightly to almost a curve. This can be explained by carefully inspecting the users' locations. In particular, at the beginning of the flight ($t = 0$ to $t = 10$), UAV 2 has to fly down to serve users on the bottom left side. At the second half on the flight ($t \geq 30$), it has to serve users on the top right, and user 2 indicated in the figure. In order to serve a set of spatially diverged users, the UAV has to stay around certain locations that balance its served users' channel conditions due to the nature of the OMA scheme. Specifically, OMA assigns each user a non-zero amount of bandwidth; hence, the assigned bandwidth could be wasted if the corresponding user does not transmit data. On the other hand, the NOMA scheme is more flexible and efficient in bandwidth utilization where the total assigned bandwidth to a user pair can be used efficiently by both users or either one of the two paired users.

We investigate the resource allocation solutions due to MUNE and MUOE in figure 1.9b by studying the transmit powers over time of three typical users indicated in Fig. 1.9b: *i)* (edge) user 1 that lies close to the initial trajectory of one UAV and far from the initial trajectory of the other UAV, *ii)* (edge) user 2 who is far from the initial trajectories of both UAVs, and *iii)* (center) user 3. We also indicate their roles (strong or weak, or $\lambda_k[t] = 1$ or $\lambda_k[t] = 0$, respectively) in this figure. Note that when $p_k[t] = 0$, it does not matter if user k is assigned as a strong or weak user[19]. Therefore, if $p_k[t] = 0$, we assume that user k is a weak user for convenience. Several interesting observations can be drawn from the figure. First, the user transmit power of users in the NOMA case is usually smaller than that in the OMA case. Second, NOMA allows users to be inactive more frequently compared to OMA (e.g., see the transmit powers of users 2, 3). For instance, when both UAVs are far away from user 2 (from $t = 20$ to $t = 40$), NOMA enables the user to be inactive while OMA most lets the user transmit with pretty high power so that user 2 can successfully transmit the required amount of data to the UAVs).

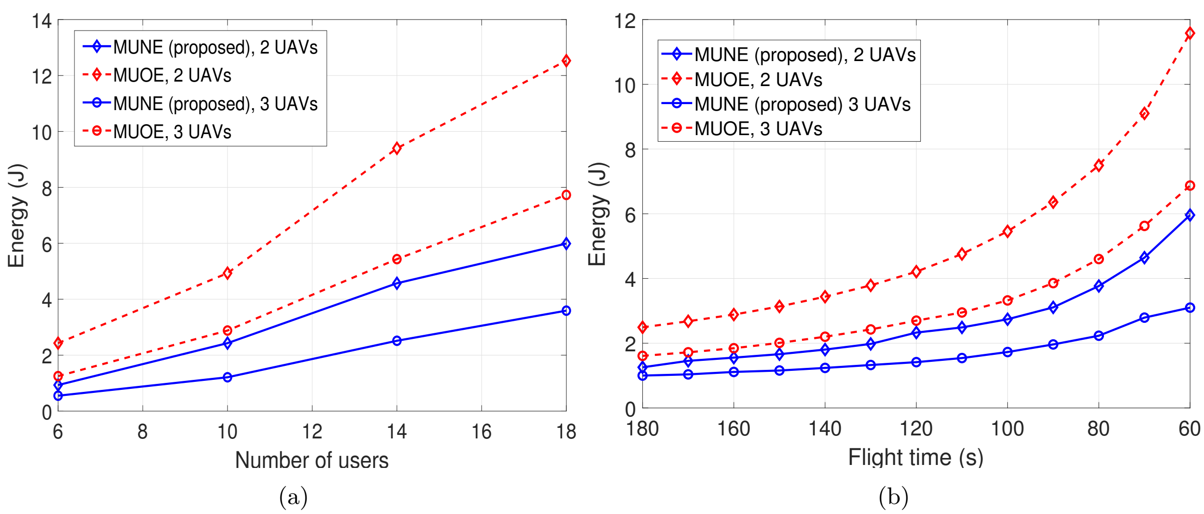

Figure 1.10: a) Total energy used versus number of users, different number of UAVs; b) Total energy used versus flight time

We now study the total energy required by MUNE and MUOE as different key system parameters vary. Specifically, Fig. 1.10a and 1.10b show the total energy as the number of users and the flight time (δT) vary, respectively for network settings with 2, 3 UAVs. It can be seen from Fig. 1.10a that less energy is required with more UAVs in the networks for both algorithms. This can be

[19]It can be verified easily by looking at the optimal power formula (1.52).

explained as follows. Each UAV tends to serve a smaller number of users in each time slot when there are more UAVs in the network. Hence, each UAV can establish a trajectory to serve a subset of users more efficiently with a larger number of UAVs. Fig. 1.10a again confirms that the MUNE algorithm outperforms the MUOE algorithm.

In Fig. 1.10b, we plot the total energy versus the flight time by varying T from $T = 60$ to $T = 180$). At first, it seems surprising that the longer the flight time is, the less total energy is. However, the result in Fig. 1.10b can be explained by referring to the results in Fig. 1.9b. In fact, both MUNE and MUOE algorithms allow a user to stay inactive when there is no UAV sufficiently close to it. In this regard, the proposed MUNE algorithm tends to provide more 'active-inactive' cycles for individual users compared to the MUOE algorithm, as can be observed in Fig. 1.9b and Fig. 1.10b. The results in Fig. 1.10b shows that the MUNE algorithm outperforms the MUOE algorithm. Lastly, Fig. 1.10b shows us that there is a tradeoff between the total energy consumption and flight time to fulfill data collection tasks for all users. Specifically, one can decreases the flight time at the cost of higher users' energy consumption or one can reduce the energy consumption if the time required for the data collection can be stretched.

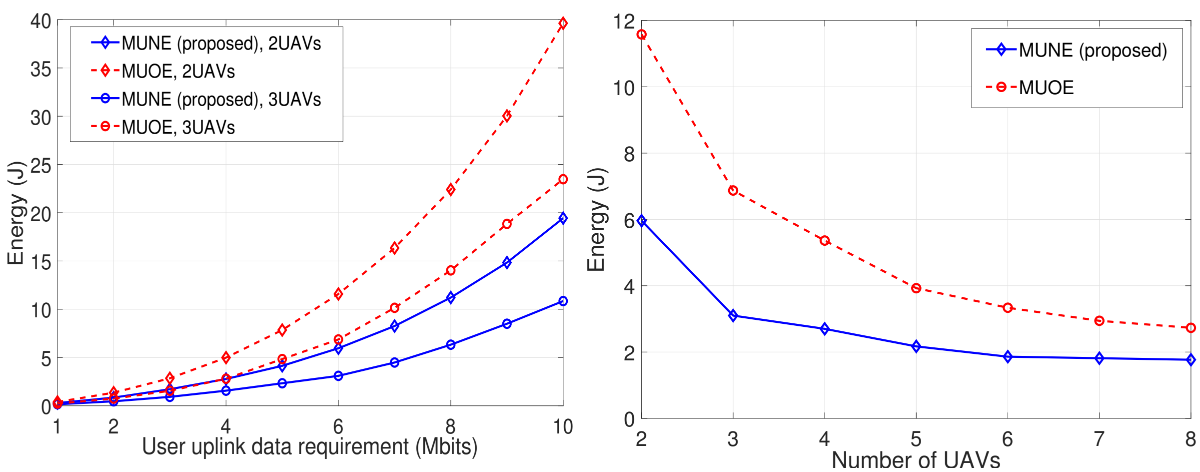

(a) (b)

Figure 1.11: a) Total energy used versus user demand; b) Total energy used versus number of UAVs

Fig. 1.11a presents the variations of total energy with required amount of transmission data D_k (i.e., data demand) of each user for network settings with 2 or 3 UAVs, and $T = 60$. The figure shows that the energy consumption increases rapidly when the amount of required data increases. This can be explained by noticing the logarithmic form of the achievable data rate with respect to the transmit power. However, as the required amount of transmission data increases, the increasing rate of the energy consumption due to by the MUNE algorithm is much lower than that due to the MUOE algorithm. This again confirms the superiority of our proposed algorithm leveraging NOMA compared to the MUOE counterpart. Finally, we plot the energy consumption versus the number of UAVs, which varies from 2 to 8 UAVs in Fig. 1.11b. It is expected that the energy consumption decreases when the number of UAVs increases. However, it is interesting to observe that the difference in energy consumption between the MUNE and MUOE algorithms decreases as the number of UAVs becomes larger, which suggests that the gain due to NOMA over OMA is more significant in denser networks (i.e., each UAV must serve a large number of users on average). The results also suggest that for network settings in which the number of users per UAV is sufficiently high (e.g., more than 10 users per UAV), employment of NOMA instead of OMA for data collection tasks in multi-UAV based wireless networks is very rewarding.

1.3 Concluding Remarks

In this doctoral dissertation, we have developed various novel interference and resource management techniques for future wireless networks where many aerial components are involved to support different applications that demand diverse qualities of services. Specifically, we made three important research contributions. *First*, we develop a new interference cancellation, fast fading channel estimation and symbol detection in a general setting where the interfering and interfered communication operate on overlapping channels and their signals have different bandwidths. The proposed algorithm can cancel the interference and estimate fast fading channel accurately, while the proposed symbol detection methods provide a good tradeoff between accuracy and complexity. *Second*, we consider resource allocation and multi-UAV trajectory optimization where we maximize the number of admitted users. The proposed algorithm greatly outperforms the conventional solution which applies Block Coordinate Ascent method and integer linear programming. *Third*, we study the joint optimization of multi-UAV's trajectories, transmit power, user-UAV association, and NOMA user pairing for multi-UAV based wireless networks to minimize the total user's energy consumption. Our proposed algorithm provides efficient active-inactive schedules, and significantly lower energy consumption compared to an existing baseline, and a joint UAV-trajectory and OMA-based resource allocation optimization strategy.

Chapter 2

Résumé Long

Ce chapitre est le résumée en français de la thèse intitulée:

"Techniques De Gestion D'interférences Et De Ressources Pour Les Réseaux Sans Fil"

2.1 Contexte et Motivations

Les demandes de communications sans fil mondiales ont considérablement augmenté au cours de la dernière décennie, parallèlement à l'augmentation rapide du nombre de connexions humaines et de machines. En fait, Ericsson prévoit que le volume total du trafic mobile pourra atteindre 131 exaoctets par mois d'ici la fin de 2024. [1]. De plus, des prévisions récentes montrent que des milliards d'appareils sans fil, des appareils Internet des objets (IoT) à faible coût, des appareils portables, des appareils de réalité virtuelle/augmentée/mixte et des véhicules intelligents, seront connectés aux réseaux sans fil au cours des prochaines années [2, 3]. De plus, les réseaux sans fil de nouvelle génération et des techniques doivent être développés pour répondre à diverses exigences en matière de débit de données, de latence, de fiabilité pour différentes applications verticales telles que la santé en ligne, les usines intelligentes et les villes intelligentes. Pour répondre à ces exigences compte tenu des ressources spectrales limitées; il devient essentiel de tirer parti des bandes de fréquences utilisables sous-utilisées et d'améliorer l'efficacité du spectre. En général, il faut relever de grands défis dans l'ingénierie des composants matériels tels que antennes et circuits de radiofréquence pour exploiter efficacement les bandes de fréquences plus élevées tout en l'amélioration de l'efficacité du spectre nécessite des techniques de communication plus sophistiquées et l'allocation des ressources telles que les nouvelles stratégies d'interférence et de gestion des ressources.

Exploiter différentes bandes de fréquences et améliorer l'efficacité du spectre sont deux directions essentielles pour améliorer fondamentalement la capacité et les performances du réseau sans fil. En particulier, plusieurs bandes de fréquences sous explorées telles que celles au-dessus de 6 Ghz sont à l'étude depuis réseaux sans fil 5G récemment. Notez que les bandes de garde minimales définies dans [4] sont plus grands que ceux définis dans LTE [5] pour les mêmes valeurs de bande passante du canal. Cela permet d'atténuer les effets négatifs des émissions hors bande indésirables ou des interférences des canaux adjacents. Cependant, du point de vue de l'efficacité du spectre, il est souhaitable de réduire les bandes de garde, ou même permettre la transmission/réception simultanée de données sur des bandes qui se chevauchent, et appliquer des techniques avancées d'annulation des interférences pour gérer les interférences comme dans le cas des radios Full Duplex (FD) [6]. En outre, les futurs réseaux sans fil devront prendre en charge différentes applications ayant des exigences différentes en matière de débit de données; par conséquent, les signaux de communication générés par différents les applications peuvent nécessiter différentes largeurs de bande de communication. En général, le développement de techniques avancées de gestion des interférences pour les les communications sur des bandes de fréquences adjacentes et qui se chevauchent sont difficiles et nécessitent des recherches beaucoup plus approfondies [7].

Une autre approche prometteuse pour améliorer l'efficacité du spectre consiste à utiliser des stratégies avancées d'accès multiple non orthogonale (Non-Orthogonal Multiple Access-NOMA) [8]. Plus précisément, NOMA permet aux réseaux sans fil de desservir plusieurs utilisateurs à l'aide du même ressource dans le temps, la fréquence ou l'espace. En fait, NOMA a montré divers avantages du point de vue de la théorie de l'information [9]. De plus, NOMA est également plus économe en énergie que l'accès multiple orthogonal conventionnel (OMA) [10] sous divers paramètres. Pour réaliser NOMA, annulation d'interférences successives (SIC) est généralement utilisé pour décoder les messages prévus tout en atténuant efficacement les interférences [11]. Cependant, le procédé SIC augmente la complexité des récepteurs. De plus, il faut effectuer un regroupement d'utilisateurs pour déterminer les utilisateurs utilisant la même ressource et optimiser l'allocation des ressources pour optimiser davantage les performances du réseau. Par conséquent, de nombreuses recherches supplémentaires sur NOMA sont nécessaires avant que la technologie ne soit prête pour un déploiement pratique.

Il y a eu un intérêt croissant pour l'exploitation de différentes plates-formes aériennes, y compris véhicules aériens sans pilote (UAV) à basse altitude, UAV à haute altitude, ballons, constellations denses de satellites en orbite basse ces dernières années pour fournir des services sans fil fiables, omniprésents et économiques [12, 13]. Parmi elles, les plates-formes de communication basées sur les drones peuvent fournir des solutions à faible coût pour divers scénarios de communication (par exemple, les zones sans fil avec une infrastructure limitée ou à haute demande de trafic) et les réseaux sans fil basés sur les drones (appelés ci-après UWN) offrent des degrés supplémentaires de liberté d'optimiser le réseau sans fil sous-jacent pour améliorer la couverture, le débit et l'efficacité énergétique grâce aux attributs uniques du drone tel que la mobilité, la flexibilité et l'altitude contrôlable. Avec un déploiement approprié, les communications basées sur les UAV peuvent fournir une visibilité directe favorables (LoS) canaux de communication [14] pour les utilisateurs à la sole. Les communications UAV peuvent également être exploitées pour améliorer la qualité des communications des réseaux cellulaires sans fil et pour prendre en charge diverses applications de l'Internet des objets (IoT) telles que la diffusion ou la collecte de données [15]. Par conséquent, les UWN devraient jouer un rôle important dans les systèmes sans fil 5G et au-delà de ces 5G [16].

Dans cette thèse, notre objectif principal est de développer des stratégies de gestion des interférences et des ressources pour les réseaux sans fil de nouvelle génération où de nombreux composants aériens sont impliqués pour prendre en charge différentes applications qui exigent une qualité de services diversifiés. Plus précisément, les contributions à la recherche de cette thèse sont résumées dans les sections suivantes.

2.2 Contributions à la Recherche

Dans cette thèse, notre objectif principal est de développer des stratégies de gestion des interférences et des ressources pour les réseaux sans fil de nouvelle génération où de nombreux composants aériens sont impliqués pour prendre en charge différentes applications qui exigent diverses qualités de services. En particulier, nos travaux portent sur deux aspects. Le premier aspect est l'annulation des interférences dans un cadre généra où les signaux de communication brouilleurs et brouillés ont des bandes passantes différentes. Dans le deuxième aspect, nous étudions les problèmes d'allocations de ressources dans les UWN où nos conceptions se concentrent sur deux objectifs importants: la maximisation de l'admission dans le sens descendant et la minimisation de la consommation d'énergie de l'utilisateur dans le sens montant. Les sections suivantes décrivent les principales contributions de cette thèse.

2.2.1 Annulation des Interférences, Estimation de Canal et Détection de Symboles pour les Communications sur des Canaux qui se Shevauchent

Dans cette contribution, nous proposons l'annulation d'interférence conjointe, l'estimation de canal à évanouissement rapide, et détection de symboles de données pour un réglage général des interférences où le signal d'émission de la communication brouilleuse et le signal reçu de la communication brouillée (désirée) occupent des canaux se chevauchant de différentes largeurs de bande. Les travaux existant en littérature n'ont pas pris en conte estimation conjointe des canaux, suppression des interférences, et détection de symboles pour le scénario dans lequel deux signaux interférents mutuels non synchronisés ont des bandes passantes différentes dans l'environnement à évanouissement rapide. Notre travail vise à combler cette lacune dans la littérature où nous apportons les contributions suivantes.

- Tout d'abord, nous proposons un cadre en deux phases pour l'annulation conjointe des interférences, l'estimation de canal et la détection de symboles. Dans la première phase, nous estimons les coefficients d'interférence et puis soustraire l'interférence estimée. Après cela, les coefficients de canal à évanouissement rapide au niveau pilote les postes sont estimés. Dans la deuxième phase, nous dérivons les probabilités a posteriori pour les deux séries et symboles individuels, étant donné les coefficients de canal aux positions pilotes, à partir desquels nous proposons des méthodes de détection correspondante qui offrent un compromis entre précision et complexité. Dans la deuxième phase, nous dérivons les probabilités a posteriori pour les deux séries et symboles individuels, étant donné les coefficients de canal aux positions pilotes, à partir desquels nous proposons des méthodes de détection correspondante qui offrent un compromis entre précision et complexité.

- Deuxièmement, nous proposons plusieurs analyses sur les performances de la technique non itérative proposée en matière d'interférence résiduelle et de taux d'erreur global sur les symboles L'analyse montre que l'interférence résiduelle a une puissance bornée car la puissance d'interférence tend vers l'infini. Cependant, l'effet du canal à évanouissement rapide sur les interférences résiduelles est irréductible peu importe la taille du SNR. Par conséquent, il existe

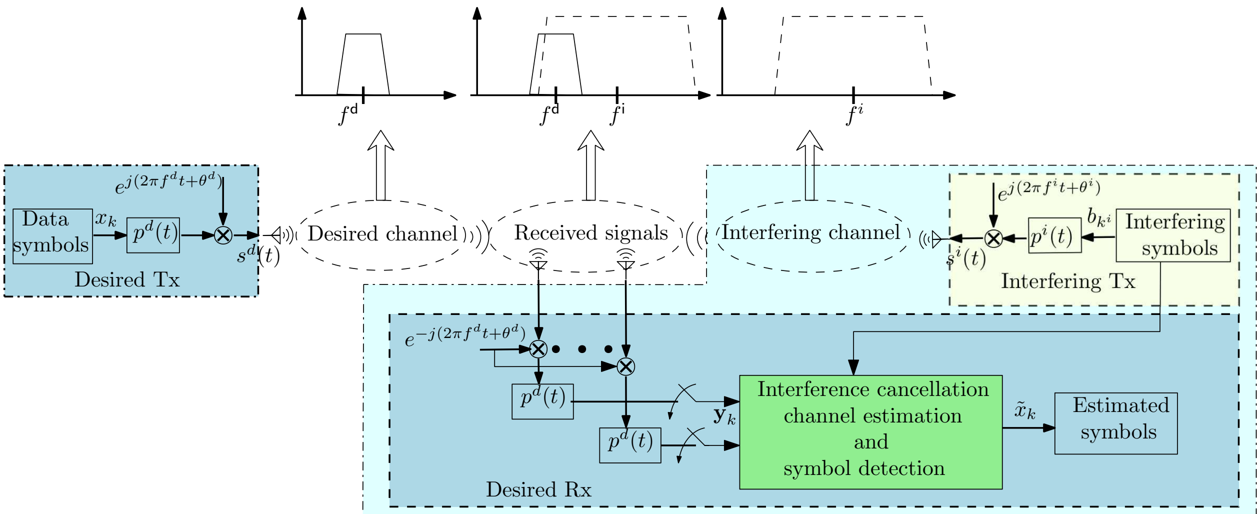

Figure 2.1: Considered interference scenario

des planchers fondamentaux pour les performances d'estimation de canal et de détection de symboles en raison de l'évanouissement rapide.

- Enfin, nous discutons et montrons numériquement qu'il existe une structure de trame optimale (c'est-à-dire une densité de pilotes optimale) pour atteindre le débit maximal du système.

Dans cette section, $\mathbf{I}_N$ représente la matrice d'identité $N \times N$, $\mathbf{1}_{M,N}$ est la matrice $M \times N$ tout un, $\mathbf{A}^H$ est la *transposition hermitienne* de la matrice $\mathbf{A}$, x^* est le *conjugué* de valeur complexe x, $(\star)$ désigne l'opération de convolution et $(\propto)$ désigne '*proportionnel à*'. Puisqu'il s'agit d'une version résumée, les théorèmes et les propositions sont énoncés sans preuves suivantes. Veuillez vous référer au chapitre 5 pour la version complète où les preuves de chaque théorème et proposition sont présentées.

2.2.1.1 Modèle de Système et Énoncé du Problème

Le réglage considéré est illustré sur la Fig. 2.1. Dans le scénario, deux liens de communication notés $\mathbb{S}^{\mathsf{d}}$ (lien souhaité) et $\mathbb{S}^{\mathsf{i}}$ (liaison interférente) fonctionnent sur des bandes de fréquences se chevauchant arbitrairement. Le signal transmis de $\mathbb{S}^{\mathsf{i}}$ interfère avec le signal reçu de $\mathbb{S}^{\mathsf{d}}$ dans un scénario général où leur rapport de bande passante est un entier[1]. Le canal brouilleur de la source brouilleuse aux antennes du récepteur souhaité est supposé être en ligne de mire. Le canal de communication

[1] Le réglage considéré correspond aux scénarios d'interférence pratiques dans communications par satellite [17, 18] et les communications terrestres [19, 20].

souhaité subit un évanouissement rapide où le coefficient du canal change de symbole en symbole selon le processus de Markov du premier ordre [21, 22]. Le scénario de brouillage étudié se produit en pratique lorsque le Tx brouilleur et le Rx souhaité sont situés à proximité l'un de l'autre et le Rx souhaité a accès aux symboles perturbateurs (par exemple, via une connexion dédiée) comme dans le full duplex relais [19, 20]. Le signal transmis de la communication souhaitée avec la fréquence porteuse f^{d} peut être écrit comme

$$s^{\mathsf{d}}(t) = \sum_{k=-\infty}^{\infty} x_k p^{\mathsf{d}}\left(t - kT^{\mathsf{d}} + \epsilon^{\mathsf{d}}\right) e^{j\left(2\pi f^{\mathsf{d}} t + \theta^{\mathsf{d}}\right)}, \tag{2.1}$$

où x_k est le $k$ème symbole transmis. La fonction de mise en forme d'impulsion $p^{\mathsf{d}}(t)$ a un gain unitaire; T^{d}, ϵ^{d} et θ^{d} représentent respectivement la durée, le temps et les décalages de phase du symbole. Le signal de la source interférente peut être exprimé de la même manière.

$$s^{\mathsf{i}}(t) = \sum_{k^{\mathsf{i}}=-\infty}^{\infty} b_{k^{\mathsf{i}}} p^{\mathsf{i}}\left(t - k^{\mathsf{i}}T^{\mathsf{i}} - t^{\mathsf{i}}\right) e^{j\left(2\pi f^{\mathsf{i}} t + \theta^{\mathsf{i}}\right)}, \tag{2.2}$$

où $p^{\mathsf{i}}(t)$ désigne le filtre de mise en forme d'impulsion avec un gain unitaire, le signal brouilleur a la fréquence centrale $f^{\mathsf{i}} = f^{\mathsf{d}} - \Delta f$, le k^{i}ème symbole est $b_{k^{\mathsf{i}}}$; t^{i} et θ^{i} tiennent compte de la différence de temps/phase des deux systèmes et du délai de transmission de l'émetteur brouilleur au récepteur brouillé, respectivement. Supposons qu'il y ait N_{r} antennes réceptrices pour $\mathbb{S}^{\mathsf{d}}$, alors le signal reçu est

$$\mathbf{y}(t) = \mathbf{h}^{\mathsf{d}}(t) \star s^{\mathsf{d}}(t) + \mathbf{h}^{\mathsf{i}}(t) \star s^{\mathsf{i}}(t) + \mathbf{w}(t), \tag{2.3}$$

où $\mathbf{w}(t)$ est le bruit thermique, $\mathbf{h}^{\mathsf{d}}(t)$, $\mathbf{h}^{\mathsf{i}}(t)$ désigne $N_{\mathsf{r}} \times 1$ vecteurs de réponses impulsionnelles de canal souhaitées et brouilleuses. Au récepteur de $\mathbb{S}^{\mathsf{d}}$, les signaux sont down-converti en bande de base. Ensuite, les signaux de sortie passent à travers un filtre adapté avec la réponse impulsionnelle $p^{\mathsf{d}}(t)$. Les signaux continus filtrés sont échantillonnés à $\left(kT^{\mathsf{d}} + \epsilon^{\mathsf{d}}\right)$ pour donner le signal temporel discret $\mathbf{y}_k = \mathbf{h}_k^{\mathsf{d}} x_k + \mathcal{I}_k + \mathbf{w}_k$, où $\mathbf{w}_k$ représente le vecteur de bruit ayant une distribution gaussienne complexe avec une matrice de covariance $\sigma^2 \mathbf{I}_{N_{\mathsf{r}}}$ ($\mathbf{w}_k$ est appelé ci-après AWGN); $\mathcal{I}_k$ désigne la bande de base équivalente, signal interférant à temps discret qui sera dérivé sous peu. Premièrement, nous exprimons les termes d'interférence dans le domaine temporel continu comme suit:

$$\mathcal{I}(t) = \left\{ \left(\mathbf{h}^{\mathsf{i}}(t) \star s^{\mathsf{i}}(t) \right) e^{-j(2\pi f^{\mathsf{d}} t + \theta^{\mathsf{d}})} \right\} \star p^{\mathsf{d}}(t). \tag{2.4}$$

En substituant $s^{\mathsf{i}}(t)$ de (2.2) dans (2.4), on obtient le signal d'interférence en bande de base équivalente dont le signal échantillonné au temps $(kT^{\mathsf{d}}+\epsilon^{\mathsf{d}})$ est $\mathcal{I}_k = \mathcal{I}(t)|_{t=kT^{\mathsf{d}}+\epsilon^{\mathsf{d}}} = \mathbf{h}_k^{\mathsf{i}} \sum_{k^{\mathsf{i}}} b_{k^{\mathsf{i}}} c_{k,k^{\mathsf{i}}}$, où $c_{k,k^{\mathsf{i}}}$ représente l'EIC qui est défini par l'équation suivante.

$$c_{k,k^{\mathsf{i}}} = \int_{-\infty}^{\infty} p^{\mathsf{d}}(kT^{\mathsf{d}} + \epsilon^{\mathsf{d}} - \tau) p^{\mathsf{i}}(\tau - k^{\mathsf{i}}T^{\mathsf{i}} - t^{\mathsf{i}}) e^{j\left(2\pi(f^{\mathsf{i}}-f^{\mathsf{d}})\tau + \theta^{\mathsf{i}} + \theta^{\mathsf{d}}\right)} d\tau. \tag{2.5}$$

Dans ce scénario étudié, la bande passante du signal brouilleur est M fois plus grande que celle du signal désiré. Et il y a des symboles L de $b_{k^{\mathsf{i}}}$ qui interfèrent avec chaque symbole désiré x_k où L doit être un multiple du rapport de bande passante M pour tenir compte l'interférence dans la plage de filtrage du signal souhaité. Puisque le rapport de bande passante est un entier, $c_{k,k^{\mathsf{i}}}$ dans (2.5) ne dépend que de la différence relative de k, k^{i}. Nous les notons donc $\mathbf{c} = [c_1, c_2, ..., c_L]^T$ dans la suite par souci de concision.

Le canal à évanouissement rapide de la liaison de communication souhaitée est supposé suivre le modèle de Markov du premier ordre où la relation des coefficients du canal aux instants $(k+1)$ème et $k$ème peut être décrit comme [21]:

$$\mathbf{h}_{k+1}^{\mathsf{d}} = \alpha \mathbf{h}_k^{\mathsf{d}} + \sqrt{1-\alpha^2}\boldsymbol{\Delta}_k, \tag{2.6}$$

où $\boldsymbol{\Delta}_k$ indique un vecteur de bruit Circular Symetric Complex Gaussian (CSCG) avec des moyennes nulles et une matrice de covariance $\sigma_{\mathsf{h}}^2 \mathbf{I}_{N_{\mathsf{r}}}$. Le terme de bruit additif dans (2.6) est appelé bruit évolutif du canal et α est le coefficient de corrélation du canal. Le rapport signal sur bruit (SNR) moyen est de $\rho = \sigma_{\mathsf{h}}^2/\sigma^2$. Sans perte de généralité, on laisse $\sigma_{\mathsf{h}}^2 = 1$. Cependant, σ_{h}^2 peut apparaître occasionnellement dans plusieurs expressions chaque fois que nécessaire. De l'équation ci-dessus, nous pouvons réécrire le signal reçu $\mathbf{y}_k$ sous la forme matricielle comme suit:

$$\mathbf{y}_k = \mathbf{h}_k^{\mathsf{d}} x_k + \mathbf{B}_k \mathbf{c} + \mathbf{w}_k, \tag{2.7}$$

où $\mathbf{b}_{k,l} = \mathbf{h}_k^{\mathsf{i}} b_{Mk+l}$, $\mathbf{B}_k$ est la matrice $N_{\mathsf{r}} \times L$ dont la $l$ème colonne est $\mathbf{b}_{k,l}$. Nous appellerons par la suite $\mathbf{B}_k$ la matrice d'interférence. Rappelons que $\mathbf{b}_{Mk+l}$ et $\mathbf{h}_k^{\mathsf{i}}$ sont connus[2]. donc $\mathbf{B}_k$ est connu du récepteur souhaité. Dans ce travail, $\mathbf{y}_k$ est appelé *signal reçu* ou *observation* indifféremment.

[2]On suppose que le récepteur a parfait les informations sur le canal brouilleur gagnent $\mathbf{h}_k^{\mathsf{i}}$ qui correspondent au lien de ligne de mire dans ce travail. Par conséquent, les gains des canaux brouilleurs varient lentement dans le temps et peuvent être estimés avec précision.

Étant donné que les canaux brouilleurs sont connus et capturés dans la matrice d'interférence $\mathbf{B}_k$, nous omettons l'exposant d dans la notation de canal souhaitée, c'est-à-dire que $\mathbf{h}_k^{\mathsf{d}}$ devient $\mathbf{h}_k$. Et ci-après *canal* signifie les canaux souhaités discutés dans les sections précédentes. L'estimation de canal et la détection de symbole sont effectuées dans chaque trame. Nous considérons la structure de trame pilote dispersée dans le domaine temporel avec N_{d} symboles de données entre deux symboles pilotes consécutifs, et il y a N_{p} symboles pilotes dans un cadre [23, 24]. La disposition typique des symboles dans un cadre est exprimée par $[x_1^{\mathsf{p}}, x_{1,1}^{\mathsf{d}}, ..., x_{1,N_{\mathsf{d}}}^{\mathsf{d}}, x_2^{\mathsf{p}}, x_{1,2}^{\mathsf{d}}, ..., x_{2,N_{\mathsf{d}}}^{\mathsf{d}}, ..., x_{N_{\mathsf{p}}-1,N_{\mathsf{d}}}^{\mathsf{d}}, x_{N_{\mathsf{p}}}^{\mathsf{p}}]$, où x_i^{p} désigne le $i$ième symbole pilote, et $[x_{1,i}^{\mathsf{d}}, ..., x_{i,N_{\mathsf{d}}}^{\mathsf{d}}]$ désigne des symboles de données entre le $i$ième et le $(i+1)$ième symboles pilotes.

Ce travail répond aux questions suivantes:

1) Étant donné la matrice d'interférence $\mathbf{B}_k$, les observations $\mathbf{y}_k$ et les symboles pilotes, comment annuler les interférences et détecter les symboles de données de manière fiable?

2) Quels sont les effets du bruit évolutif du canal à évanouissement rapide sur les performances globales du système (estimation EIC, suppression des interférences, estimation de canal et détection de symboles)?

3) Existe-t-il une conception de trame optimale (c'est-à-dire une densité de pilotes optimale) qui maximise le débit en présence d'évanouissements et d'interférences rapides?

2.2.1.2 Algorithme Proposé

a) Estimation des Interférences et des Coefficients de Canal

Dans la première phase, nous estimons $\mathbf{c}$ et $\mathbf{h}_n^{\mathsf{p}}, n = 1, ..., N_{\mathsf{p}}$ étant donné les observations $\mathbf{y}_{1:N_{\mathsf{p}}}^{\mathsf{p}}$. Par souci de concision, l'exposant p est omis dans cette section, c'est-à-dire que x_i^{p} devient x_i. On note $\mathbf{Y} = [\mathbf{y}_{1:n-1}, \mathbf{y}_n, \mathbf{y}_{n+1:N_{\mathsf{p}}}]$. L'estimation des critères pour $\mathbf{c}$ et $\mathbf{h}_n$ sont exprimés comme suit:[3]

$$\left\{\tilde{\mathbf{c}}_n, \tilde{\mathbf{h}}_n\right\} = \text{argmax} \quad p(\mathbf{h}_n, \mathbf{Y}|\mathbf{c}). \tag{2.8}$$

[3]Nous utilisons les critères MAP pour estimer $\mathbf{h}_n$. Notez que $p(\mathbf{h}_n|\mathbf{Y})$ ou $p(\mathbf{h}_n, \mathbf{Y})$ peuvent être utilisés, puisque $p(\mathbf{h}_n, \mathbf{Y}) = p(\mathbf{h}_n|\mathbf{Y})p(\mathbf{Y})$ et $p(\mathbf{Y})$ est indépendant du paramètre d'intérêt $\mathbf{h}_n$. Et les EIC $\mathbf{c}$ sont des paramètres déterministes inconnus dans une trame.

Pour estimer $\mathbf{h}_n$ et $\mathbf{c}$ selon (2.8), nous devons trouver $p(\mathbf{h}_n, \mathbf{Y})$[4] dont le logarithme est exprimé dans le théorème suivant.

Theorem 2.1. *Le log de vraisemblance des signaux reçus et des coefficients de canal à la position pilote n est*

$$\mathcal{L}_{\mathbf{h}_n,\mathbf{Y}} = \log(p(\mathbf{h}_n, \mathbf{Y})) = -\sum_{i=1}^{N_\mathsf{p}} \left(\mathbf{y}_i - \boldsymbol{\mu}_{i,n}\right)^H \boldsymbol{\Sigma}_{i,n}^{-1} \left(\mathbf{y}_i - \boldsymbol{\mu}_{i,n}\right) - \mathbf{h}_n^H \mathbf{h}_n + const.. \tag{2.9}$$

Les paramètres associés ($\boldsymbol{\mu}_{i,n}, \boldsymbol{\Sigma}_{i,n}$) peut être trouvée dans l'annexe 5.A. Par ailleurs, les premiers termes du membre de droite de (2.9) peuvent être décomposé en deux termes quadratiques où un terme contient $\mathbf{h}_n$ et l'autre ne contient que $\mathbf{c}$. Puisqu'il y a deux variables à optimiser (c'est-à-dire $\mathbf{h}_n$ et $\mathbf{c}$), nous dérivons d'abord le $\mathbf{h}_n$ optimal par rapport à $\mathbf{c}$ alors nous dérivons le $\mathbf{c}$ optimal en maximisant la fonction objectif correspondante obtenue avec le $\mathbf{h}_n$ optimal.

★ *Étape 1-Dérivation du $\mathbf{h}_n$ optimal pour un $\mathbf{c}$ connu*: La somme des termes quadratiques dans (2.9) peut être réécrite comme

$$\tilde{\mathcal{L}}_{\mathbf{h}_n,\mathbf{Y}} = -(\mathbf{h}_n - \tilde{\mathbf{h}}_n)^H \mathbf{A}_n (\mathbf{h}_n - \tilde{\mathbf{h}}_n) - \mathcal{C}_n, \tag{2.10}$$

où $\mathbf{A}_n, \tilde{\mathbf{h}}_n$ et $\mathcal{C}_n$ sont définis comme

$$\begin{aligned} &\mathbf{A}_n = \mathbf{I}_{N_\mathsf{r}} + \sum_{i=1}^{N_\mathsf{p}} \omega_{i,n}^2 \boldsymbol{\Sigma}_{i,n}^{-1}, \qquad \tilde{\mathbf{h}}_n = \mathbf{A}_n^{-1} \left(\sum_{i=1}^{N_\mathsf{p}} x_{i,n}^* \boldsymbol{\Sigma}_{i,n}^{-1} \left(\mathbf{y}_{i,n} - \mathbf{B}_{i,n}\mathbf{c}\right) \right), \\ &\mathcal{C}_n = -\tilde{\mathbf{h}}_n^H \mathbf{A}_n \tilde{\mathbf{h}}_n + \sum_{i=1}^{N_\mathsf{p}} \left(\mathbf{y}_{i,n} - \mathbf{B}_{i,n}\mathbf{c}\right)^H \boldsymbol{\Sigma}_{i,n}^{-1} \left(\mathbf{y}_{i,n} - \mathbf{B}_{i,n}\mathbf{c}\right), \end{aligned} \tag{2.11}$$

où $\omega_{i,n}, x_{i,n}, \mathbf{y}_{i,n}, \mathbf{B}_{i,n}$ et les paramètres associés sont définis dans ce qui suit équations[5]

$$x_{i,n} = \omega_{i,n} x_i, \quad \mathbf{y}_{i,n} = \mathbf{y}_i - \beta_{i,n} \mathbf{y}_{i+j_{i,n}}, \quad \mathbf{B}_{i,n} = \mathbf{B}_i - \beta_{i,n} \mathbf{B}_{i+j_{i,n}}, \tag{2.12a}$$

$$\omega_{i,n} = \begin{cases} \frac{\alpha_\mathsf{p}^{|n-i|}}{1+\rho(1-\alpha_\mathsf{p}^{2(|n-i|-1)})}, & i \neq n \\ 1, & i = n \end{cases}, \qquad \beta_{i,n} = \begin{cases} \frac{x_i x_{i+j_{i,n}}^* \rho \alpha_\mathsf{p} \left(1-\alpha_\mathsf{p}^{2(|n-i|-1)}\right)}{1+\rho\left(1-\alpha_\mathsf{p}^{2(|n-i|-1)}\right)}, & i \neq n \\ 0, & i = n \end{cases}. \tag{2.12b}$$

[4]Pour simplifier, nous omettons $\mathbf{c}$ dans les distributions suivantes, c'est-à-dire que $p(\mathbf{h}_n, \mathbf{Y}|\mathbf{c})$ s'écrit simplement $p(\mathbf{h}_n, \mathbf{Y})$.

[5]On note l' 'indicateur de signe' $j_{i,n} = -1$ pour $i > n$, $j_{i,n} = 1$ pour $i < n$ et $j_{i,n} = 0$ pour $i = n$.

Puisque $\mathbf{A}_n$ est défini positif, le $\mathbf{h}_n$ optimal qui maximise $\tilde{\mathcal{L}}_{\mathbf{h}_n,\mathbf{Y}}$ dans (2.10) est $\tilde{\mathbf{h}}_n$.

★ *Étape 2- Dérivation du* $\mathbf{c}$ *optimal*: Lorsque $\mathbf{h}_n = \tilde{\mathbf{h}}_n$, la fonction dans (2.10) est égale à $-\mathcal{C}_n$ qui ne dépend que de $\mathbf{c}$ où

$$\mathcal{C}_n = (\mathbf{c} - \tilde{\mathbf{c}}_n)^H \mathbf{D}_n \left(\mathbf{c} - \tilde{\mathbf{h}}_n\right) + const., \tag{2.13}$$

où $\mathbf{D}_n$ et $\tilde{\mathbf{c}}_n$ sont définis dans les équations suivantes.

$$\mathbf{D}_n = \sum_{i=1}^{N_\mathsf{p}} \mathbf{B}_{i,n}^H \mathbf{\Sigma}_{i,n}^{-1} \mathbf{B}_{i,n} - \left(\sum_{i=1}^{N_\mathsf{p}} x_{i,n}^* \mathbf{\Sigma}_{i,n}^{-1} \mathbf{B}_{i,n}\right)^H \mathbf{A}_n^{-1} \left(\sum_{i=1}^{N_\mathsf{p}} x_{i,n}^* \mathbf{\Sigma}_{i,n}^{-1} \mathbf{B}_{i,n}\right), \tag{2.14a}$$

$$\tilde{\mathbf{c}}_n = \mathbf{D}_n^{-1} \left\{ \sum_{i=1}^{N_\mathsf{p}} \mathbf{B}_{i,n}^H \mathbf{\Sigma}_{i,n}^{-1} \mathbf{y}_{i,n} - \left(\sum_{i=1}^{N_\mathsf{p}} x_{i,n}^* \mathbf{\Sigma}_{i,n}^{-1} \mathbf{B}_{i,n}\right)^H \mathbf{A}_n^{-1} \left(\sum_{i=1}^{N_\mathsf{p}} x_{i,n}^* \mathbf{\Sigma}_{i,n}^{-1} \mathbf{y}_{i,n}\right) \right\}. \tag{2.14b}$$

On peut vérifier que $\mathbf{D}_n$ est défini positif en utilisant l'inégalité *Cauchy-Schwarz*. Alors le $\mathbf{c}$ optimal qui maximise $\tilde{\mathcal{L}}_{\mathbf{h}_n,\mathbf{Y}}$ dans (2.10) est $\tilde{\mathbf{c}}_n$. On fait la moyenne sur tout $\tilde{\mathbf{c}}_n, n = 1, ..., N_\mathsf{p}$ pour produire une estimation à variance réduite de $\mathbf{c}$ comme suit:

$$\tilde{\mathbf{c}} = \frac{1}{N_\mathsf{p}} \sum_{n=1}^{N_\mathsf{p}} \tilde{\mathbf{c}}_n. \tag{2.15}$$

En résumé, l'algorithme conjoint d'estimation d'interférence, d'annulation et d'estimation de canal est décrit dans Algorithme 2.1.

Algorithm 2.1. Estimation des EIC, des Coefficients de Canal Souhaités et de la Suppression des Interférences

1: **for** $n = 1 : N_\mathsf{p}$ **do**
2:     **for** $i = 1 : N_\mathsf{p}$ **do**
3:         Compute $x_{i,n}, \mathbf{y}_{i,n}, \mathbf{B}_{i,n}, \mathbf{\Sigma}_{i,n}$ in (2.11), (2.12a).
4:     **end for**
5:     Compute $\mathbf{A}_n, \mathbf{D}_n$, and then $\tilde{\mathbf{c}}_n$ in (2.11), (2.14a), (2.14b).
6: **end for**
7: Compute $\tilde{\mathbf{c}}$ in (2.15) and subtract the interference.
8: **for** $n = 1 : N_\mathsf{p}$ **do**
9:     Estimate $\mathbf{h}_n$ as $\tilde{\mathbf{h}}_n$ in (2.11).
10: **end for**
11: End of algorithm.

b) Détection de Symboles

Avec le $\tilde{\mathbf{c}}$ estimé, nous pouvons soustraire l'interférence. Ensuite, les coefficients de canal aux positions pilotes sont estimés comme $\tilde{\mathbf{h}}_n$ donne dans (2.11) avec $\mathbf{c}$ remplacé par $\tilde{\mathbf{c}}$ dans (2.15). Les coefficients de canal estimés aux positions pilotes seront utilisés pour le détection de symboles comme décrit ci-dessous. Nous décrirons la détection de symbole pour l'intervalle $\left[x_i^{\mathsf{p}}, x_{i,1}^{\mathsf{d}}, x_{i,2}^{\mathsf{d}}, ..., x_{i,N_{\mathsf{d}}}^{\mathsf{d}}, x_{i+1}^{\mathsf{p}}\right]$. La méthode peut être appliquée et répétée pour d'autres intervalles. Pour plus de simplicité, nous omettons l'index pilote i et l'exposant (d) dans cette section, c'est-à-dire que les coefficients du canal sont notés $[\mathbf{h}_h, \mathbf{h}_{1:N_{\mathsf{d}}}, \mathbf{h}_t]$, où $\mathbf{h}_h$ et $\mathbf{h}_t$ représentent le coefficient de canal connu au niveau du symbole pilote juste avant et juste après l'intervalle considéré, respectivement. Nous proposons deux méthodes de détection de symboles différentes dans ce qui suit.

★ *Détection de symboles de série (S-MAP):* Les symboles dans un intervalle sont détectés comme

$$\tilde{\mathbf{x}}_{1:N_{\mathsf{d}}} = \operatorname{argmax} \quad p\left(\mathbf{x}_{1:N_{\mathsf{d}}} | \mathbf{h}_h, \mathbf{h}_t, \mathbf{y}_{1:N_{\mathsf{d}}}\right). \tag{2.16}$$

Nous caractérisons maintenant la fonction de log vraisemblance dans le théorème suivant.

Theorem 2.2. *Le log de vraisemblance des symboles de données conditionnés sur les signaux reçus et les coefficients de canal aux positions pilotes juste après et avant l'intervalle peut être exprimé en une somme de fonctions quadratiques de symboles de données* $\mathbf{x}$ *comme*

$$\log\left(p\left(\mathbf{x}_{1:N_{\mathsf{d}}} | \mathbf{h}_h, \mathbf{h}_t, \mathbf{y}_{1:N_{\mathsf{d}}}\right)\right) = const. + \\ \sum_{i=1}^{N_{\mathsf{d}}} \left[\left(\tau_2 \mathbf{\Gamma}_{i,1} \mathbf{h}_h + \mathbb{1}_{i=N_{\mathsf{d}}} \tau_2 \mathbf{h}_t + \sum_{j=1}^{i} \frac{x_j^*}{\sigma^2} \mathbf{\Gamma}_{i,j} \mathbf{y}_j \right)^H \mathbf{S}_i \left(\tau_2 \mathbf{\Gamma}_{i,1} \mathbf{h}_h + \mathbb{1}_{i=N_{\mathsf{d}}} \tau_2 \mathbf{h}_t + \sum_{j=1}^{i} \frac{x_j^*}{\sigma^2} \mathbf{\Gamma}_{i,j} \mathbf{y}_j \right) \right], \tag{2.17}$$

où les paramètres associés sont définis dans (2.18) et Annexe 5.C.

$$\mathbf{S}_i^{-1} = \left(\frac{1}{\sigma^2} + (1+\alpha^2)\tau_1\right) \mathbf{I}_{N_{\mathsf{r}}} - \mathbb{1}_{i>1} \tau_2^2 \mathbf{S}_{i-1}, \tag{2.18a}$$

$$\bar{\mathbf{h}}_i = \begin{cases} \mathbf{S}_i \left(\tau_2 \mathbf{\Gamma}_{i,1} \mathbf{h}_h + \tau_2 \mathbf{h}_{i+1} + \sum_{j=1}^{i} \frac{x_j^*}{\sigma^2} \mathbf{\Gamma}_{i,j} \mathbf{y}_j \right), & i < N_{\mathsf{d}} \\ \mathbf{S}_i \left(\tau_2 \mathbf{\Gamma}_{i,1} \mathbf{h}_h + \tau_2 \mathbf{h}_t + \sum_{j=1}^{i} \frac{x_j^*}{\sigma^2} \mathbf{\Gamma}_{i,j} \mathbf{y}_j \right), & i = N_{\mathsf{d}} \end{cases}. \tag{2.18b}$$

En calculant les valeurs de $\log\left(p\left(\mathbf{x}_{1:N_\mathsf{d}}|\mathbf{h}_h, \mathbf{h}_t, \mathbf{y}_{1:N_\mathsf{d}}\right)\right)$ de tous les vecteurs possibles $\mathbf{x} = [x_1, ..., x_{N_\mathsf{d}}]$ des points de constellation, nous obtenons les symboles détectés de manière optimale par (2.16).

★ *Détection de symboles individuels (I-MAP):* Nous proposons d'estimer x_i individuellement comme

$$\tilde{x}_i = \operatorname{argmax} \quad p\left(x_i|\mathbf{h}_h, \mathbf{h}_t, \mathbf{y}_i\right). \tag{2.19}$$

En utilisant des dérivations similaires à celles utilisées pour obtenir les résultats du théorème 2.2, on a

$$\tilde{x}_i = \frac{\breve{\mathbf{h}}_i^H \mathbf{y}_i}{\|\breve{\mathbf{h}}_i^H \mathbf{y}_i\|}, \qquad \breve{\mathbf{h}}_i = \frac{\alpha^i}{1-\alpha^{2i}}\mathbf{h}_h + \frac{\alpha^{N_\mathsf{d}+1-i}}{1-\alpha^{2(N_\mathsf{d}+1-i)}}\mathbf{h}_t, \quad \text{for} \quad i = 1, ..., N_\mathsf{d}. \tag{2.20}$$

Ensuite, les symboles détectés peuvent être trouvés en mappant $\tilde{x}_i$ au point le plus proche de la constellation. Nous résumons l'estimation de canal conjointe et la détection de symboles proposées dans l'algorithme 2.2.

Algorithm 2.2. Détection de Symboles Individuels sur un Canal à Evanouissement Rapide (I-MAP)

```
for n = 1 : N_p do
    for i = 1 : N_d do
        Estimate x̃^d_{i,n} from (2.20) and assign x̃^d_{i,n} to the closest point in the constellation.
    end for
end for
End of algorithm.
```

c) Algorithme Itératif pour L'annulation des Interférences, L'estimation de Canal et la Détection de Symboles

En pratique, l'estimation conjointe du canal, l'annulation des interférences et la détection des données sont souvent effectuées de manière itérative, où les symboles de données détectés peuvent agir en tant que symboles pilotes pour prendre en charge l'annulation d'interférence et l'estimation de canal. Ce qui améliore potentiellement les performances de détection. Nous proposons une approche itérative pour annulation d'interférence, estimation de canal et détection de symbole sur la base de la méthode à deux phases précédente. Nous désignons maintenant les symboles souhaités dans le cadre comme $x_n, n = 1, ..., (N_\mathsf{p} - 1)(N_\mathsf{d} + 1) + 1$, où $x_n, n = 1, 1 + N_\mathsf{d} + 1, 1 + 2(N_\mathsf{d} + 1), ...$ sont des symboles pilotes dans les notations précédentes.

Dans la première phase, l'estimation d'interférence, l'annulation d'interférence et l'estimation de canal sont effectuées comme présenté précédemment. Excepté le nombre de symboles pilotes nouvellement considérés[6] est maintenant $\hat{N}_\mathsf{p} = (N_\mathsf{d} + 1)(N_\mathsf{p} - 1) + 1$ (symboles dans la trame entière) et le coefficient de corrélation des gains de canal à deux positions pilotes consécutives est $\hat{\alpha}_\mathsf{p} = \alpha$.

Dans la deuxième phase, laissez les gains estimés du canal à la position n être $\breve{\mathbf{h}}_n$. Afin de détecter le symbole x_n, on utilise maintenant la connaissance de $\breve{\mathbf{h}}_{n+1}$ et $\breve{\mathbf{h}}_{n-1}$ comme si $n + 1$ et $n - 1$ sont deux postes de pilotes. Appliquer la technique I-MAP[7] dans (2.20), on a

$$\begin{aligned} \tilde{x}_n &= \frac{\hat{\mathbf{h}}_n^H \mathbf{y}_n}{\|\hat{\mathbf{h}}_n^H \mathbf{y}_n\|}, n = 2, ..., (N_\mathsf{p} - 1)(N_\mathsf{d} + 1), \\ \hat{\mathbf{h}}_i &= \frac{\alpha}{1 - \alpha^2} \left(\breve{\mathbf{h}}_{n-1} + \breve{\mathbf{h}}_{n+1}\right). \end{aligned} \tag{2.21}$$

Une fois que $\tilde{x}_n$ sont détectés, dans les prochaines itérations, l'annulation des interférences, l'estimation du canal et la détection des données sont effectuées jusqu'à ce que la convergence soit atteinte. L'algorithme converge lorsqu'il n'y a pas de changement dans la détection symboles de données. Nous résumons cette approche itérative dans Algorithme 2.3.

2.2.1.3 Analyse de Performance

Dans cette section, nous effectuons une analyse des performances pour le cadre de conception proposé[8] et présenter les informations clés de l'analyse. Spécifiquement, nous montrons *première*, les caractéristiques de l'erreur d'estimation du canal et de l'interférence résiduelle, *deuxième*, le SER réalisable de nos méthodes de détection proposées, et *enfin*, l'analyse du débit.

[6]Puisque tous les symboles x_n sont connus (aux positions pilotes) ou détectés (aux positions de données), ils sont tous traités comme des symboles pilotes.

[7]Maintenant qu'il n'y a qu'un seul symbole de données entre deux symboles pilotes, S-MAP et I-MAP produisent des résultats identiques.

[8]En raison de la nature stochastique du modèle de canal et de la conception, l'analyse de l'algorithme itératif est très impliquée, ce qui dépasse le cadre de ce travail. Néanmoins, l'analyse de la conception non itérative en deux phases proposées fournit de nombreuses informations qui aident à expliquer les comportements de l'algorithme itératif.

Algorithm 2.3. Algorithme Itératif pour L'estimation des Canaux, L'annulation des Interférences et la Détection des Données

Perform Algorithm 2.1 for interference cancellation and channel estimation.
Perform Algorithm 2.2 for I-MAP symbol detection.
while (true) **do**
  Perform Algorithm 2.1 for interference cancellation and channel estimation with $\hat{\alpha}_{\mathsf{p}} = \alpha$ and $\hat{N}_{\mathsf{p}} = (N_{\mathsf{d}} + 1)(N_{\mathsf{p}} - 1) + 1$.
  Perform Algorithm 2.2 for I-MAP symbol detection with $\hat{N}_{\mathsf{d}} = 1$. The detected data symbols are denoted as $\bar{\mathbf{x}}^{\mathsf{i}}$.
  if $\bar{\mathbf{x}}^{\mathsf{i}} == \bar{\mathbf{x}}^{(\mathsf{i}-1)}$ **then**
    Break the loop (Convergence is reached).
  else
    Increase i and go to the next iteration.
  end if
end while
End of algorithm.

Dans l'analyse suivante, nous étudions l'interférence résiduelle (notée $\boldsymbol{\upsilon}_n$) et l'erreur d'estimation de canal (CEE, notée $\boldsymbol{\nu}_n$) qui sont définies comme suit:

$$\begin{aligned} \boldsymbol{\upsilon}_n &= \mathbf{B}_n \left(\mathbf{c} - \tilde{\mathbf{c}}\right), \\ \boldsymbol{\nu}_n &= \mathbf{h}_n - \tilde{\mathbf{h}}_n. \end{aligned} \tag{2.22}$$

a) Caractéristiques de L'erreur D'estimation du Canal et de L'interférence Résiduelle

Tout d'abord, nous fournissons la remarque suivante sur l'erreur d'estimation de canal dans le cas de sans interférence.

Remark 2.1. *En cas d'absence d'interférence, l'erreur d'estimation de canal $\boldsymbol{\nu}_n$ a une distribution gaussienne avec une moyenne nulle. De plus, l'effet du bruit évolutif du canal sur l'erreur d'estimation du canal est négligeable lorsque le SNR tend vers l'infini.*

Le fait que le l'effet du bruit évolutif du canal diminue à mesure quand le SNR tend vers l'infini suggère que le plancher d'erreur dans le canal l'estimation rapportée dans [25] provient de l'interférence résiduelle. Par conséquent, nous effectuons une analyse et caractérisons l'estimation d'interférence $\tilde{\mathbf{c}}$ et l'interférence résiduelle dans les remarques suivantes.

Remark 2.2. *L'estimation EIC $\tilde{\mathbf{c}}$ est sans biais et l'interférence résiduelle suit la distribution gaussienne avec une moyenne nulle. De plus, l'interférence résiduelle est indépendante de $\mathbf{c}$ et a une puissance bornée lorsque la puissance d'interférence tend vers l'infini.*

Remark 2.3. *La puissance d'interférence résiduelle ne peut pas être complètement éliminée, même avec un SNR très élevé. Spécifiquement, quand le SNR tend vers l'infini, il existe un plancher de puissance résiduelle d'interférence*

b) Analyse de SER

Le $\tilde{x}_i$ non normalisé dans (2.20) est $\breve{\mathbf{h}}_i^H(\mathbf{h}_i x_i + \tilde{\mathbf{w}}_i)$, où $\tilde{\mathbf{w}}_i$ est la somme du bruit gaussien additif et de l'interférence résiduelle[9]. Conditionné sur $\mathbf{h}_h$ et $\mathbf{h}_t$, le SNR équivalent pour la détection de symboles de x_i peut être exprimé comme

$$\rho_i^{\mathsf{e}} = \frac{\alpha^{2i}\left|\|\mathbf{h}_h\|^2 \frac{\alpha^i}{1-\alpha^{2i}} + \mathbf{h}_h^H \mathbf{h}_t \frac{\alpha^j}{1-\alpha^{2j}}\right|^2}{(\sigma^2 + \sigma_{\mathsf{i}}^2 + 1 - \alpha^{2i})\left|\mathbf{h}_h^H \mathbf{1}_{N_{\mathsf{r}}} \frac{\alpha^i}{1-\alpha^{2i}} + \mathbf{h}_t^H \mathbf{1}_{N_{\mathsf{r}}} \frac{\alpha^j}{1-\alpha^{2j}}\right|^2}, \tag{2.23}$$

où $j = N_{\mathsf{d}} + 1 - i$. Le SER à la position du symbole i peut être calculé comme suit

$$P_i^{\mathsf{e}} = \int p(\mathbf{h}_h, \mathbf{h}_t) f_{\mathsf{e}}(\rho_i^{\mathsf{e}}) d\mathbf{h}_h d\mathbf{h}_t, \tag{2.24}$$

où $f_{\mathsf{e}}(\rho)$ est le taux d'erreur correspondant à instantané ρ. L'expression fermée pour P_i^{e} dans (2.24) est difficile à dériver. Cependant, P_i^{e} peut être calculé avec précision en utilisant l'intégration numérique ou par simulation Monte Carlo. Enfin, le SER moyen global peut être exprimé sous la forme

$$P^{\mathsf{e}} = \frac{1}{N_{\mathsf{d}}} \sum_{i=1}^{N_{\mathsf{d}}} P_i^{\mathsf{e}}. \tag{2.25}$$

c) Analyse de Débit

Le débit est défini comme le nombre moyen de symboles de données transmis avec succès par période de symbole, qui est moyenné sur l'intervalle de trame. Notez qu'il y a N_{d} symboles de données transmis entre deux symboles pilotes consécutifs et que la trame se compose de N_{p} symboles

[9]En cas d'absence d'interférence, la matrice de covariance est $\sigma^2\mathbf{I}_{N_r}$. Et s'il y a interférence, la matrice de covariance est $(\sigma^2 + \sigma_{\mathsf{i}}^2)\mathbf{I}_{N_r}$, où σ_{i}^2 est la puissance de l'interférence résiduelle qui peut être calculée à partir de (5.49)

pilotes. Considérant le SER moyen P^{e} dans (2.25), le débit peut être calculé comme

$$\mathsf{TP} = (1 - P^{\mathsf{e}}) \frac{N_{\mathsf{d}}(N_{\mathsf{p}} - 1)}{(N_{\mathsf{d}} + 1)(N_{\mathsf{p}} - 1) + 1}, \tag{2.26}$$

La densité pilote est définie comme $1/(N_{\mathsf{d}} + 1)$. On peut vérifier que lorsque nous augmentons la densité du pilote (c'est-à-dire que N_{d} diminue), P_{e} diminue ; ainsi le premier terme de (2.26) augmente. Cependant, l'augmentation de la densité de pilotes entraîne un surcoût de pilote plus élevé, ce qui réduit le deuxième terme dans (2.26) et vice versa. Par conséquent, il existe un compromis entre la fiabilité de la transmission et le débit, ce qui suggère qu'il existe une valeur optimale de la densité pilote qui atteint le débit maximum. Bien qu'il soit difficile d'exprimer la forme fermée de P^{e} dans (2.25), la densité pilote optimale pour α et ρ donnés peuvent être trouvés efficacement en utilisant des méthodes de recherche numérique.

2.2.1.4 Résultats Numériques

On considère le cadre de simulation dans lequel le récepteur souhaité a $N_{\mathsf{r}} = 2$ antennes, le coefficient α est choisi dans l'ensemble $\{0.95, 0.97, 0.99, 0.995, 0.999\}$[10]. La bande passante du signal interférant est le double de la bande passante du signal souhaité, elles sont respectivement 30 kHz et 15 kHz. L'espacement de fréquence Δ_f entre les signaux interférents et souhaités est normalisé par $\Delta_f T^{\mathsf{d}}$ où T^{d} désigne le temps de symbole du signal souhaité. Nous supposons que la modulation QPSK est utilisée; le signal brouilleur et le signal souhaité utilisent la fonction de mise en forme d'impulsion root-raise-cosine. De plus, les fonctions de mise en forme des impulsions $p^{\mathsf{d}}(t)$ et $p^{\mathsf{i}}(t)$ sont supposés avoir le facteur d'amortissement égale à 0,25. La puissance d'interférence est réglée aussi forte que la puissance du signal souhaité et la fréquence espacement $\Delta_f = 1/T^{\mathsf{d}}$ sauf indication contraire. Le nombre de symboles pilotes est fixé égal à 51. De plus, la densité pilote est choisie dans l'ensemble $\{25\%, 10\%\}$ correspondant à $\{3, 9\}$ symboles de données entre deux symboles pilotes, respectivement. De plus, pour les résultats de simulation de débit, nous montrons les débits obtenus pour différentes densités de pilotes allant de 50 % à 6,25 %. Les résultats présentés dans cette section sont obtenus en faisant la moyenne de 10^4 réalisations aléatoires.

[10]En mode Clarke, $\alpha = J_0(2\pi f_D T^{\mathsf{d}})$, où f_D est l'écart Doppler maximal [26] (rappelez-vous que T^{d} est la période de symbole du signal désiré). Plus précisément, $\alpha = 0.999$ correspond à 150 Hz de propagation Doppler avec un débit de symboles de 15 Kbps. Si le signal souhaité est transporté à 900 MHz, la vitesse correspondante du Rx souhaité est de 50 m/s.

a) Performance de la Technique D'estimation du Canal Proposée

Pour le scénario sans interférence, nous étudions l'effet de différents paramètres sur les erreurs d'estimation de canal. Nous notons que les performances de la technique d'estimation de canal présentée dans cette section dépendent principalement de N_{d} et α. Plus précisément, la performance dépend de α_{p} qui est le coefficient de corrélation de gain de canal à deux positions pilotes consécutives. Différentes valeurs de N_{d} (différentes densités de pilotes) ont les valeurs correspondantes de α_{p}. Nous montrerons l'erreur quadratique moyenne d'estimation de canal numérique (CMSE) qui est calculé comme

$$\mathsf{CMSE} = \frac{1}{N_{\mathsf{p}} N_{\mathsf{r}}} \sum_{n=1}^{N_{\mathsf{p}}} \mathbf{tr}\left(\mathbb{E}\left[\left(\mathbf{h}_n - \tilde{\mathbf{h}}_n\right)\left(\mathbf{h}_n - \tilde{\mathbf{h}}_n\right)^H\right]\right). \tag{2.27}$$

Dans la figure 2.2, nous montrons l'erreur d'estimation de canal due à notre proposition conception pour différentes valeurs de N_{d} (équivalent, différentes valeurs de densité pilote), lorsqu'il n'y a pas d'interférences (IF) et lorsqu'il y a des interférences (IP). Lorsque N_{d} augmente, l'erreur quadratique moyenne d'estimation de canal augmente également comme prévu. Pour le scénario sans interférence, les courbes d'erreur correspondantes convergent les unes vers les autres et diminuent presque linéairement à mesure que le SNR augmente (les deux courbes sont tracées dans l'échelle logarithmique). Cette signifie que l'impact de l'évanouissement rapide est diminué dans le régime SNR élevé. Lorsque l'interférence est présente, il existe un plancher de performance pour l'erreur d'estimation de canal.

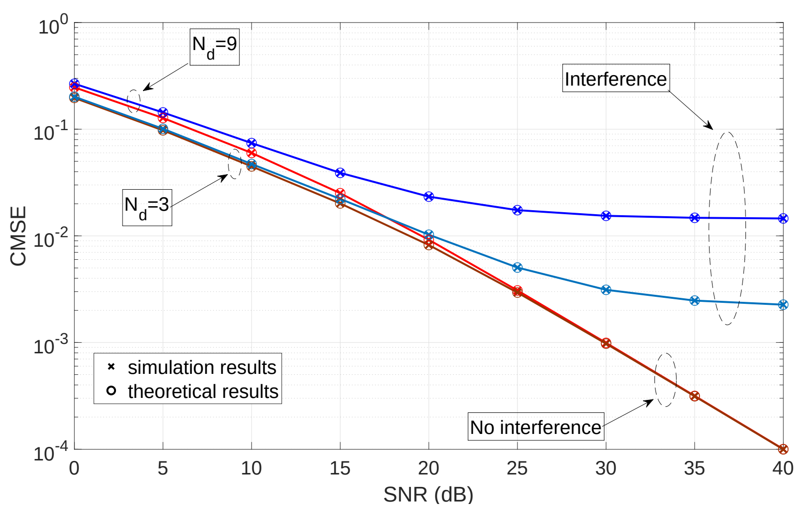

Figure 2.2: Channel estimation mean squared error, $\alpha = 0.99$

b) Performances des Méthodes de Détection de Symboles Proposées

Nous comparons maintenant les performances SER de la détection MAP des symboles en série (S-MAP), de la détection MAP des symboles individuels (I-MAP) et les méthodes de détection de diversité optimale (ODD) [27, 28]. La méthode ODD est la détection optimale de symboles individuels avec un CSI imparfait[11].

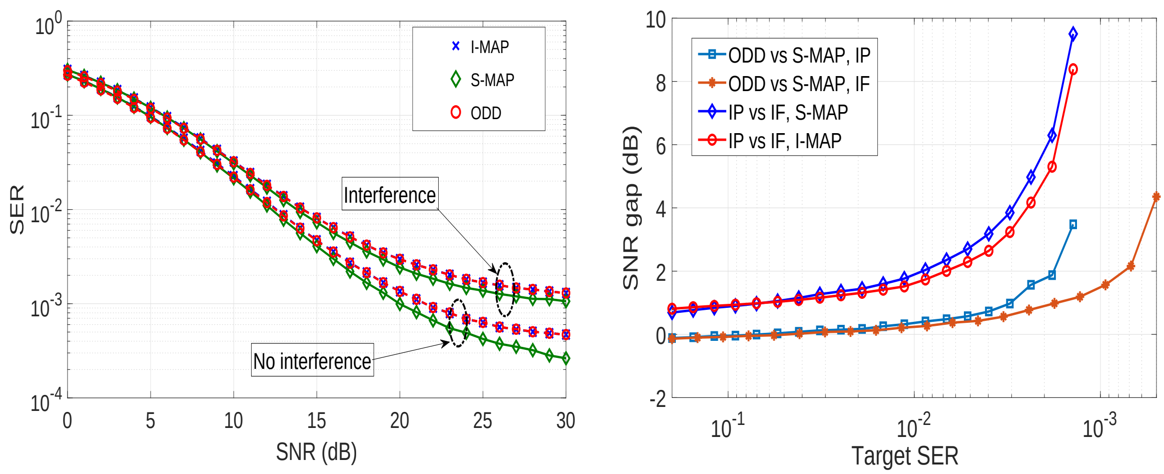

(a) (b)

Figure 2.3: a) SER achieved by different detection methods, $N_\mathsf{d} = 3$; b) SNR gap for specific target SER, $N_\mathsf{d} = 3$

La figure 2.3a illustre le SER obtenu par ces méthodes de détection pour les scénarios sans interférence et interférence, qui sont désignés par IF et IP dans cette section, respectivement. On peut voir que le SER de l'I-MAP proposé est presque identique à celui obtenu par la méthode ODD. De plus, le détecteur S-MAP surpasse à la fois I-MAP et ODD et l'écart de performance est plus important dans le scénario sans interférence. Notez que, dans le scénario IP, l'interférence résiduelle est toujours présente, ce qui provoque les planchers d'erreur dans ces courbes SER. Nous montrons en outre sur la figure 2.3b l'écart SNR pour obtenir le même SER entre différentes méthodes de détection de symboles (S-MAP, I-MAP) et scénarios (IF, IP). Particulièrement, une valeur de 3dB d'écart SNR à 5×10^{-3} cible SER de la courbe A *vs* B signifie que la méthode A a besoin de 3dB plus élevé en SNR pour atteindre le même SER cible atteint par la méthode B. Pour le même scénario (IF ou IP), l'écart SNR entre le S-MAP proposé et l'ODD augmente à mesure que le SER requis diminue. Notez à nouveau qu'il existe un plancher de performance dans le scénario IP; néanmoins,

[11] Fondamentalement, dans la méthode ODD, les gains de canal aux positions de données sont interpolés à partir des gains de canal estimés par le MMSE aux positions pilotes. Ensuite, la détection de symbole basée sur le forçage zéro est utilisée (veuillez vous référer aux sections III et IV dans [28] pour plus de détails).

notre méthode de détection proposée atteint plus de 3 db de gain SNR par rapport à la méthode ODD existant pour les mêmes performances de détection dans le régime cible faible SER (voir la courbe avec des marqueurs carrés). De plus, pour obtenir les mêmes performances SER dans des conditions de fiabilité élevée (c'est-à-dire, faible SER); le SNR requis dans le scénario de brouillage est beaucoup plus élevé que celui-ci requis dans le scénario sans interférence (illustré par les courbes IP vs IF).

c) Performance de L'algorithme Itératif

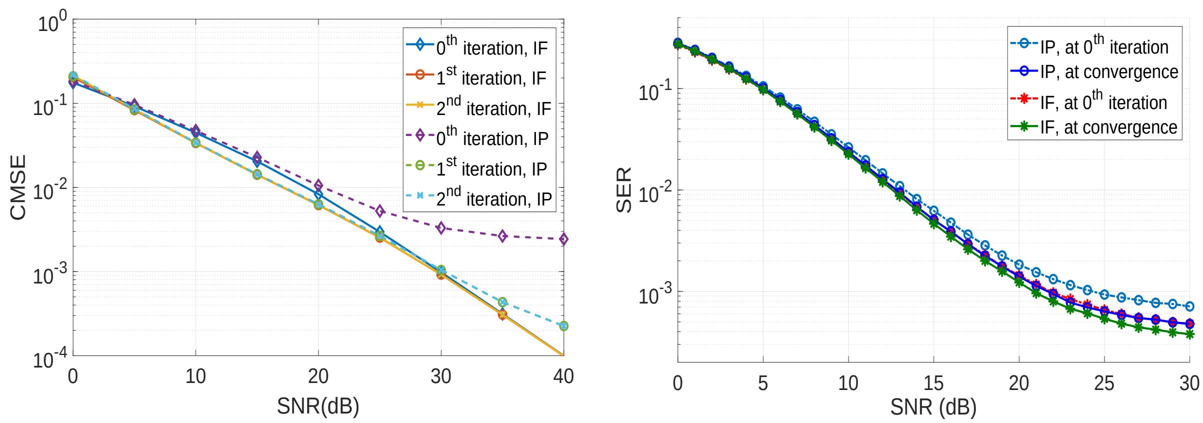

(a) (b)

Figure 2.4: a) Performance of channel estimation for iterative algorithm; b) SER achieved by iterative and non-iterative algorithms

Nous étudions maintenant les performances de l'algorithme itératif pour l'estimation de canal, l'annulation d'interférence et la détection de symboles. Tout d'abord, nous montrons les performances de l'estimation de canal au cours des itérations dans la figure 2.4a où le CMSE du canal estimé gagne est affiché pour les scénarios IF et IP. Dans la figure, l'algorithme itératif converge après seulement quelques itérations. Et la performance d'estimation de canal convergé en présence d'interférence (IP) est presque identique à celle du scénario sans interférence (FI) en régime SNR bas (inférieur à 30dB), ce qui implique que la méthode itérative proposée annule très bien l'interférence dans cette région SNR. Lorsque le SNR est supérieur à 30 dB, les performances dans le cas IP sont toujours limitées par le bruit de décoloration rapide. Cependant, le plancher de performance de l'approche d'estimation de canal itérative est bien inférieur à celui de la contrepartie non itérative (l'itération 0^{th} par rapport aux courbes d'itération de 2^{nd} dans le scénario IP). Nous montrons ensuite les SER obtenus par les méthodes non itératives et itératives algorithmes[12] dans la figure 2.4b. Nous pouvons voir que l'algorithme itératif améliore le SER dans les deux scénarios IF et IP. De plus, l'amélioration est plus importante pour des valeurs plus élevées de SNR. En effet, le régime SNR élevé permet une détection de données plus fiable, ce qui augmente les performances de annulation d'interférence et estimation de canal.

d) Débit Atteint par le Cadre Proposé

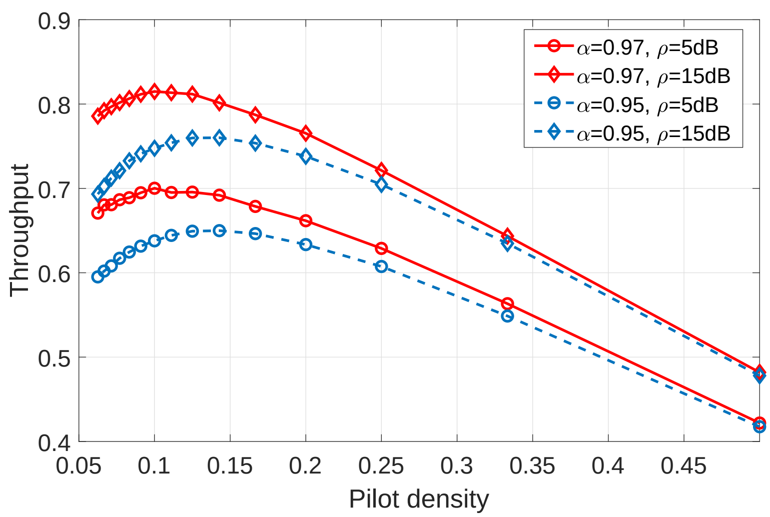

Figure 2.5: Throughput variations with the pilot density

Dans la figure 2.5, nous montrons les variations du débit avec la densité du pilote pour différentes valeurs de SNR ρ et le coefficient de corrélation de canal α. Pour α et ρ donnés, il existe une densité de pilotes optimales qui atteint le débit maximal. Le débit ne maximum augmente au fur et à mesure que le SNR ρ augmente, et un α plus grand conduit à un débit maximum plus élevé et à une densité de pilote optimale plus faible. En effet, lorsque le canal varie plus lentement, les performances d'annulation d'interférence et d'estimation de canal sont amélioré, ce qui se traduit par une transmission plus fiable et un débit plus élevé. Les résultats de cette figure démontrent le compromis entre le débit et la fiabilité de la communication dans l'environnement à évanouissement rapide.

[12]Le SER de l'algorithme non itératif est le SER calculé à l'itération 0^{th} et le SER de l'algorithme itératif est le SER atteint à la convergence.

2.2.2 Allocation de Ressources, Optimisation de Trajectoire et Contrôle D'admission dans les Réseaux Sans Fil basés sur UAV

Dans cette contribution, nous considérons l'allocation des ressources et l'optimisation de la trajectoire pour les réseaux sans fil multi-UAV, où les principaux apports de nos travaux peuvent être résumés comme suit:

- Notre conception maximise le nombre d'utilisateurs admis tout en satisfaisant leurs demandes de transmission de données.
- Le problème formulé est MINLP, nous proposons donc un algorithme itératif pour résoudre le problème efficacement où le nombre d'utilisateurs admis augmente au fil des itérations jusqu'à convergence.

2.2.2.1 Modèles de Système

Nous considérons les communications de liaison descendante dans un réseau sans fil basé sur UAV. Il y a N UAV et un ensemble $\mathcal{K} = \{1, ..., K\}$ utilisateurs au sol. Utilisateur k, dont la coordonnée 2-D est $\mathbf{u}_k$, exige de recevoir une quantité de données D_k des drones. La période de service se compose de tranches horaires T, chaque intervalle de temps a une longueur de δ. UAV n vole à l'altitude h et ses coordonnées 2-D à t est $\mathbf{c}_n[t]$. La bande passante totale du système de B (Hz) est partagé par les utilisateurs de manière orthogonale. La bande passante et la puissance de transmission de la communication entre le drone n et l'utilisateur k à t sont respectivement $b_{n,k}[t]$ et $p_{n,k}[t]$. Les canaux de communication entre les UAV et les utilisateurs sont supposés être dominés par les composants de la ligne de vue (LoS). Par conséquent, le gain de puissance du canal entre UAV n et l'utilisateur k à t est $\rho_0/(h^2 + \|\mathbf{c}_n[t] - \mathbf{u}_k\|^2)$, où ρ_0 est le gain de puissance du canal à la distance de référence de 1m de l'UAV. La quantité de données reçues par l'utilisateur k à t est exprimée comme

$$d_k[t] = \delta \sum_{n=1}^{N} b_{n,k}[t] \log_2 \left(1 + \frac{\gamma}{b_{n,k}[t]} \frac{p_{n,k}[t]}{h^2 + \|\mathbf{c}_n[t] - \mathbf{u}_k\|^2} \right), \tag{2.28}$$

où $\gamma = \rho_0/\sigma^2$ est le rapport signal sur bruit (SNR) normalisé et σ^2 est la densité de puissance du bruit blanc (W/Hz).

Nous considérons la conception d'admission d'utilisateurs où chaque utilisateur k est admis si les drones peuvent lui transmettre au moins D_k bits pendant la période de service. On note s_k comme variable de décision d'admission qui est égale à 1 si $\sum_{t=1}^{T} d_k[t] \geq D_k$ et égal à 0, sinon. Notre conception vise à maximiser le nombre d'utilisateurs admis. Le problème de maximisation d'admission peut être formulé comme suit:

$$
\begin{aligned}
\mathcal{P}^{\mathsf{AM}}(\mathcal{K}) : \quad & \max_{\{b_{n,k}[t]\},\{p_{n,k}[t]\},\{\mathbf{c}_n[t]\},\{s_k\}} \sum_{k\in\mathcal{K}} s_k, \\
\text{s.t.} \quad & \sum_{t=1}^{T} d_k[t] \geq s_k D_k, \forall k, && \text{(2.29a)} \\
& \sum_{n=1}^{N}\sum_{k=1}^{K} b_{n,k}[t] \leq B, \forall t, && \text{(2.29b)} \\
& \sum_{k=1}^{K} p_{n,k}[t] \leq P_{\mathsf{max}}, \forall n, t, , && \text{(2.29c)} \\
& \|\mathbf{c}_n[t] - \mathbf{c}_n[t-1]\| \leq \min\left(V_{\mathsf{max}}\delta, D_{\mathsf{max}}\right), \forall n, t, && \text{(2.29d)} \\
& \|\mathbf{c}_n[t] - \mathbf{c}_m[t]\| \geq D_{\mathsf{O}}, \forall n \neq m, t, && \text{(2.29e)} \\
& \mathbf{c}_n[1] = \mathbf{c}_n[T] = \mathbf{c}_{\mathsf{o}}, \forall n, && \text{(2.29f)} \\
& s_k \in \{0, 1\}, \forall k, , && \text{(2.29g)}
\end{aligned}
$$

où V_{max} est la vitesse maximale d'un drone, D_{max} est le déplacement maximum pour garantir que les conditions du canal LoS restent approximativement les mêmes, D_{O} est la distance de sécurité, et $\mathbf{c}_{\mathsf{o}}$ est la coordonnée de la station de lancement. Les contraintes (2.29b) et (2.29c) limitent les ressources de communication utilisées, où les contraintes (2.29d), (2.29e) et (2.29f) sont pour le contrôle de trajectoire.

2.2.2.2 Algorithme Proposé

Tout d'abord, nous définissons les données de transmission sensibles à la demande et la décision d'admission douce (SA), pour l'utilisateur k, noté respectivement $\bar{D}_k$ et $\bar{s}_k$, comme suit:

$$\bar{D}_k = \min\left(D_k, \sum_{t=1}^{T} d_k[t]\right). \quad \text{(2.30a)}$$

$$\bar{s}_k = \frac{\bar{D}_k}{D_k}, \forall k, \quad \text{(2.30b)}$$

On considère alors le problème de maximisation SA suivant:

$$\begin{aligned}
\mathcal{P}^{\mathsf{SAM}}(\mathcal{K}): \quad & \max_{\{b_{n,k}[t]\},\{p_{n,k}[t]\},\{\mathbf{c}_n[t]\},\{\bar{D}_k,\bar{s}_k\}} \sum_{k\in\mathcal{K}} \bar{s}_k, \\
\text{s.t.} \quad & \bar{D}_k \leq D_k, \forall\, k \in \mathcal{K}, && (2.31a)\\
& \sum_{t=1}^{T} d_k[t] \geq \bar{D}_k, \forall\, k \in \mathcal{K}, && (2.31b)\\
& (2.29b), (2.29c), (2.29d), (2.29e), (2.29f), (2.30b).
\end{aligned}$$

L'ensemble des utilisateurs admis est noté $\mathcal{K}_{\mathsf{a}} = \{k : \bar{D}_k = D_k\}$. Notez que l'ensemble des possibles de $\mathcal{P}^{\mathsf{AM}}(\mathcal{K})$ contient l'allocation des ressources et les trajectoires UAV qui réalisent $\mathcal{K}_{\mathsf{a}}$. Cette relation fournit des connexions entre le problème $\mathcal{P}^{\mathsf{AM}}(\mathcal{K})$ et problème $\mathcal{P}^{\mathsf{SAM}}(\mathcal{K})$.

★ *Étape 1-Maximisation de l'admission en douceur*:

Nous développons un algorithme pour résoudre le problème $\mathcal{P}^{\mathsf{SAM}}(\mathcal{K})$ en utilisant la combinaison du BCA et des méthodes d'approximation convexe (SCA)[13]. Plus précisément, la méthode BCA est appliquée pour optimiser la fonction objectif de $\mathcal{P}^{\mathsf{SAM}}(\mathcal{K})$ par rapport à un ensemble de variables étant donné d'autres ensembles de variables tandis que le SCA est appliqué approximer et convexifier le sous-problème d'optimisation du contrôle de trajectoire.

Le sous-problème d'optimisation de la bande passante et de l'allocation de puissance peut s'écrire comme suit :

$$\begin{aligned}
\mathcal{P}_{\mathsf{BP}}(\mathcal{K}): \quad & \max_{\{b_{n,k}[t],p_{n,k}[t],\bar{D}_k,\bar{s}_k\}} \sum_{k\in\mathcal{K}} \bar{s}_k, \\
\text{s.t.} \quad & (2.29b), (2.29c), (2.30b), (2.31a), (2.31b).
\end{aligned}$$

Le problème $\mathcal{P}_{\mathsf{BP}}(\mathcal{K})$ est convexe, il peut donc être résolu de manière optimale à l'aide de solveurs standard tels que CVX.

[13]Notez que l'utilisateur défini à l'itération externe m est noté $\mathcal{K}^m$. Cependant, dans cette section, nous ne sommes que intéressé à résoudre le problème $\mathcal{P}^{\mathsf{SAM}}(\mathcal{K})$ pour un certain ensemble d'utilisateurs $\mathcal{K}$. L'index m est donc omis par souci de concision.

Compte tenu de la bande passante et de l'allocation de puissance, le sous-problème d'optimisation de trajectoire d'UAV peut être énoncé comme suit :

$$\begin{aligned} \mathcal{P}_{\mathsf{C}}(\mathcal{K}): \quad & \max_{\{\mathbf{c}_n[t], \bar{D}_k, \bar{s}_k\}} \sum_{k \in \mathcal{K}} \bar{s}_k, \\ \text{s.t.} \quad & (2.29\text{d}), (2.29\text{e}), (2.29\text{f}), (2.30\text{b}), (2.31\text{a}), (2.31\text{b}). \end{aligned}$$

On convexe les contraintes non convexes (2.31b) et (2.29e) et appliquons la méthode SCA pour résoudre le problème efficacement. Soit l'ensemble des coordonnées du drone de l'itération précédente être $\mathbf{c}_n^i[t]$ et $\mathbf{c}_m^i[t]$, contrainte (2.29e) peut être mis au carré puis approximé par l'inégalité suivante.

$$2\left(\mathbf{c}_m^i[t] - \mathbf{c}_n^i[t]\right)^T (\mathbf{c}_m[t] - \mathbf{c}_n[t]) - \left\|\mathbf{c}_m^i[t] - \mathbf{c}_n^i[t]\right\|^2 \geq D_{\mathsf{O}}^2. \tag{2.34}$$

Les termes du logarithme dans (2.28) peuvent être approximés comme suit:

$$\log_2\left(1 + \frac{\bar{\gamma}_{n,k}[t]}{h^2 + \|\mathbf{c}_n[t] - \mathbf{u}_k\|^2}\right) \geq \log_2\left(1 + \frac{\bar{\gamma}_{n,k}[t]}{h^2 + \|\mathbf{c}_n^i[t] - \mathbf{u}_k\|^2}\right) - \left(\|\mathbf{c}_n[t] - \mathbf{u}_k\|^2 - \left\|\mathbf{c}_n^i[t] - \mathbf{u}_k\right\|^2\right) X_{n,k}^i[t], \tag{2.35}$$

où $\bar{\gamma}_{n,k}[t] = \gamma p_{n,k}[t]/b_{n,k}[t]$, et

$$X_{n,k}^i[t] = \frac{\log_2(e)\bar{\gamma}_{n,k}[t]}{\left(h^2 + \|\mathbf{c}_n^i[t] - \mathbf{u}_k\|^2\right)\left(\bar{\gamma}_{n,k}[t] + h^2 + \|\mathbf{c}_n^i[t] - \mathbf{u}_k\|^2\right)}.$$

En utilisant ces approximations, le problème $\mathcal{P}_{\mathsf{C}}(\mathcal{K})$ peut être résolu par résoudre le problème d'optimisation convexe suivant:

$$\begin{aligned} \bar{\mathcal{P}}_{\mathsf{C}}(\mathcal{K}): \quad & \max_{\{\mathbf{c}_n[t], \bar{D}_k, \bar{s}_k\}} \sum_{k \in \mathcal{K}} \bar{s}_k, \\ \text{s.t.} \ - & \sum_{n=1}^{N} \sum_{t=1}^{T} \delta b_{n,k}[t] \left[\log_2\left(1 + \frac{\bar{\gamma}_{n,k}[t]}{h^2 + \|\mathbf{c}_n^i[t] - \mathbf{u}_k\|^2}\right) - \left(\|\mathbf{c}_n[t] - \mathbf{u}_k\|^2 - \left\|\mathbf{c}_n^i[t] - \mathbf{u}_k\right\|^2\right) X_{n,k}^i[t]\right] \geq \bar{D}_k, \qquad (2.36\text{a}) \\ & (2.29\text{d}), (2.29\text{e}), (2.29\text{f}), (2.30\text{b}), (2.31\text{a}). \end{aligned}$$

Enfin, problème $\mathcal{P}^{\mathsf{SAM}}(\mathcal{K})$ est résolu en utilisant un algorithme itératif où nous résolvons les problèmes $\mathcal{P}_{\mathsf{BP}}(\mathcal{K})$ et $\bar{\mathcal{P}}_{\mathsf{C}}(\mathcal{K})$ séquentiellement à chaque itération.

★ *Étape 2-Suppression de l'utilisateur*:

Soit $\mathcal{K}^m$ l'ensemble des utilisateurs à l'itération m après avoir résolu le problème $\mathcal{P}^{\mathsf{SAM}}(\mathcal{K}^m)$. Nous voulons supprimer l'utilisateur qui est peu susceptible d'être admis, donc que nous pouvons utiliser efficacement les ressources du réseau pour d'autres utilisateurs, nous proposons donc une stratégie de suppression des utilisateurs où l'utilisateur ayant le plus grand écart entre ses données de transmission requises et les données de transmission sensibles à la demande sera supprimé, comme suit:

$$k_{\mathsf{min}}^m = \underset{k \in \mathcal{K}^m}{\operatorname{argmax}} \ D_k - \bar{D}_k^*, \tag{2.37}$$

où $\bar{D}_k^*$ sont les données de transmission sensibles à la demande de l'utilisateur k exprimées dans (2.30a) après avoir résolu le problème $\mathcal{P}^{\mathsf{SAM}}(\mathcal{K}^m)$. L'ensemble d'utilisateurs dans l'itération suivante est $\mathcal{K}^{m+1} = \mathcal{K}^m \setminus \{k_{\mathsf{min}}\}$. Soit $\mathcal{K}_{\mathsf{a}}^m$ l'ensemble des utilisateurs admis après avoir résolu $\mathcal{P}^{\mathsf{SAM}}(\mathcal{K}^m)$. Nous introduisons la contrainte de condition admise pour les utilisateurs $k \in \mathcal{K}_{\mathsf{a}}^m$ au problème de maximisation de l'admission douce afin que les utilisateurs admis à l'itération m soient toujours admis à l'itération $m+1$ et exprimer le problème comme suit:

$$\begin{aligned} \mathcal{P}^{\mathsf{SAM}}(\mathcal{K}^{m+1}) : \quad & \max_{\boldsymbol{\Theta}, \{\bar{D}_k, \bar{s}_k\}} \ \bar{S}(\mathcal{K}^{m+1}), \\ \text{s.t.} \quad & \bar{s}_k = 1, \forall k \in \mathcal{K}_{\mathsf{a}}^m, \qquad (2.38a) \\ & (2.29b), (2.29c), (2.29d), (2.29e), (2.29f), (2.30b), \end{aligned}$$

Soit $\mathcal{K}_{\mathsf{a}}^{m+1}$ l'ensemble des utilisateurs admis après avoir résolu $\mathcal{P}^{\mathsf{SAM}}(\mathcal{K}^{m+1})$, on peut montrer que $|\mathcal{K}_{\mathsf{a}}^{m+1}| \geq |\mathcal{K}_{\mathsf{a}}^m|$. Enfin, le tableau suivant décrit notre algorithme.

2.2.2.3 Résultats Numériques

Nous considérons le cadre de simulation où les utilisateurs sont localisés au hasard dans une zone de réseau circulaire d'un rayon de 2 km. Les drones sont supposés voler à 100m, la puissance maximale P_{max} est fixée à 20dBm, σ^2 est de -174dBm/Hz, et $\rho_0 = 4 \times 10^{-5}$. La durée du vol est de 120s, qui est divisée en 120 tranches horaires. La demande de transmission des utilisateurs est

Algorithm 2.4. Maximisation des Admissions

Initiate $\mathbf{\Theta}, m = 1, \mathcal{K}^1 = \mathcal{K}$
while 1 **do**
  (*Soft admission maximization*) Solve problem $\mathcal{P}^{\mathsf{SAM}}(\mathcal{K}^m)$.
  if $|\mathcal{K}_{\mathsf{a}}^m| = |\mathcal{K}^m|$ **then**
    Break the loop.
  else
    (*User removal*) Let $\mathcal{K}^{m+1} = \mathcal{K}^m \setminus \{k_{\mathsf{min}}^m\}$, where k_{min}^m is defined in (2.37). Increase m by 1.
  end if
end while
End of algorithm.

de 45Mbits, la bande passante totale est de $B = 1$MHz, et le nombre total d'utilisateurs est de 20, sauf indication contraire. Nous comparerons numériquement notre algorithme proposé avec une ligne de base. Pour cette ligne de base, le problème $\mathcal{P}^{\mathsf{AM}}(\mathcal{K})$ est résolu en appliquant la méthode BCA, où les sous-problèmes sont des MILP. Plus précisément, à chaque itération de cette ligne de base, l'allocation de bande passante-puissance et les sous-problèmes d'optimisation de trajectoire avec des variables entières $\{s_k\}$ sont résolus en utilisant le solveur MOSEK. Cet algorithme de base se termine lorsque plus aucun utilisateur ne peut être admis. Cette ligne de base est désignée par BCA-MILP dans ce qui suit.

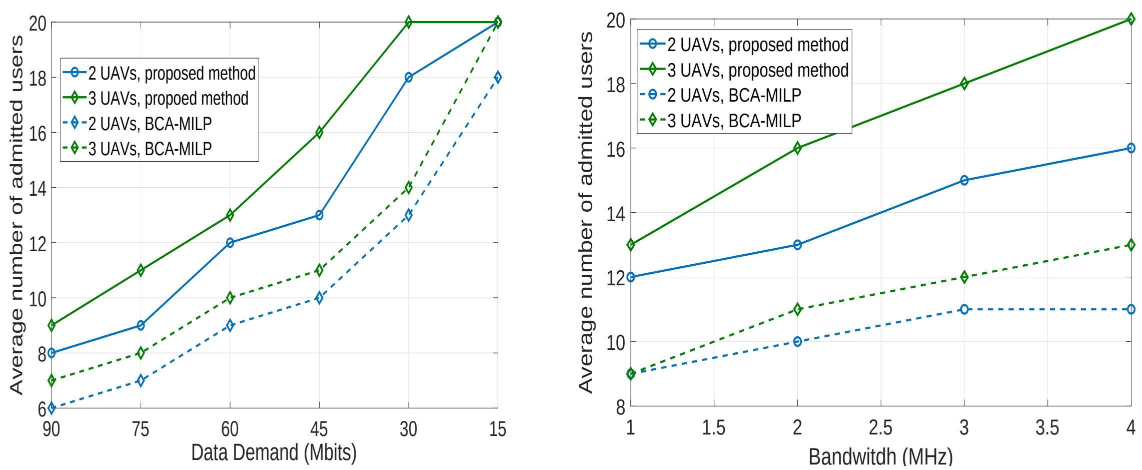

(a) (b)

Figure 2.6: a) Number of served users versus data demand per user; b) Number of served users versus total bandwidth

Dans la figure 2.6a, nous montrons le nombre d'utilisateurs admis en fonction de la demande de données utilisateur variable. Deux observations peuvent être tirées de la figure. Premièrement, le déploiement de plus de drones nous permet d'admettre plus d'utilisateurs. Deuxièmement, nos méthodes proposées peuvent admettre beaucoup plus d'utilisateurs que celle obtenue par la ligne de base BCA-MILP. Cela peut s'expliquer comme suit. Premièrement, l'étape de maximisation SA dans notre algorithme optimise une fonction objective continue, ainsi, l'algorithme peut trouver de meilleures trajectoires de drones au cours des itérations avant la convergence. Ce n'est pas le cas pour le BCA-MILP dans lequel la convergence est atteinte après seulement quelques itérations en raison de fonction objective à valeurs entières. De plus, notre étape de suppression d'utilisateurs développée supprime efficacement les utilisateurs pauvres et donc leurs ressources peuvent être réservés et utilisés plus efficacement pour servir de meilleurs utilisateurs. La figure 2.6b présente le nombre d'utilisateurs admis en fonction de la bande passante variable. Lorsqu'il y a plus de bande passante disponible, le réseau peut admettre plus d'utilisateurs. Cependant, le gain de performances de l'algorithme proposé par rapport à la ligne de base augmente à mesure que la bande passante augmente, ce qui implique que notre approche utilise les ressources radio plus efficacement.

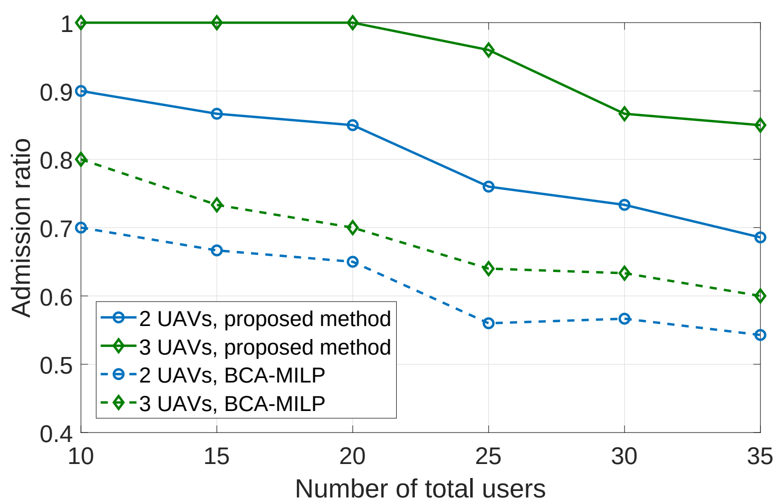

Figure 2.7: Coverage probability versus total number of users

Enfin, nous montrons le taux d'admission avec un nombre variable d'utilisateurs sur la figure 2.7. On constate que le taux d'admission diminue lorsqu'il y a plus d'utilisateurs. Cependant, notre approche proposée atteint toujours de meilleures performances que la ligne de base BCA-MILP.

2.2.3 Contrôle de Trajectoire Multi-UAV, Allocation de Ressources et Appariement D'utilisateurs NOMA pour la Minimisation de L'énergie de Liaison Montante

Dans ce travail, nous étudions l'optimisation conjointe des trajectoires de plusieurs drones, l'allocation de puissance d'émission, l'association utilisateur-UAV, et l'appariement des utilisateurs pour les réseaux sans fil assisté par UAV utilisant l'accès multiple non orthogonal (NOMA) pour les communications montantes. La conception vise à minimiser la consommation totale d'énergie des utilisateurs au sol tout en garantissant de transmettre avec succès la quantité de données requises aux stations de base montées sur UAV. Les principales contributions de notre travail sont les suivantes:

- Nous formulons le problème de minimisation de l'énergie totale où l'appariement d'utilisateurs NOMA, l'allocation de puissance de transmission, l'association utilisateur-UAV et le contrôle de trajectoire multi-UAV sont optimisés conjointement. Nous dérivons la solution d'allocation de puissance optimale, qui est exprimée explicitement en fonction d'autres variables d'optimisation.
- Nous développons un algorithme efficace pour résoudre le problème considéré en utilisant l'approche BCD.
- Nous comparons l'algorithme proposé avec deux autres lignes de base : l'un est l'algorithme d'optimisation de la collecte de données (DCOA) de [29], et l'autre ligne de base qui utilise les mêmes principes de conception comme pour notre algorithme proposé; cependant, l'OMA conventionnel au lieu du NOMA est utilisé. Nous montrons les performances supérieures de notre algorithme par rapport aux deux lignes de base considérées via des études numériques et démontrer le compromis entre le temps de vol et l'énergie totale ainsi que les impacts de différents paramètres tels que le nombre d'utilisateurs et de drones sur la consommation totale d'énergie.

2.2.4 Modèle de Système et Formulation de Problèmes

a) Modèle de Système

Nous considérons les communications de liaison montante dans un réseau sans fil assisté par UAV avec N de drones volants et K d'utilisateurs au sol. La durée de vol du drone T est divisée en un certain nombre de petites plages horaires, dont chacun a une longueur identique de δ. Nous supposons que le drone n vole à l'altitude fixe h et sa coordonnée 2-D à l'intervalle de temps t est notée $\mathbf{c}_n[t]$. La coordonnée 2-D de l'utilisateur au sol k est notée $\mathbf{u}_k$. Nous supposons que NOMA est utilisé pour prendre en charge la liaison montante communications où les utilisateurs sont regroupés en paires de deux utilisateurs qui transmettent sur des canaux orthogonaux. On suppose que chaque utilisateur k a besoin de transmettre une quantité de données D_k aux drones avant la fin de la période de service.

Les canaux de communication entre les UAV et les utilisateurs sont supposés être dominés par la composante Ligne de Vue (LoS). Le gain de puissance du canal entre UAV n et l'utilisateur k à t, noté $\tau_{k;n}[t]$, est $\tau_{k;n}[t] = \frac{\mu}{\|\mathbf{c}_n[t]-\mathbf{u}_k\|^2+h^2}$, où μ est le gain de puissance du canal à la distance de référence de $1m$ de l'émetteur. Nous notons $x_{k,l}[t]$ comme variable de décision d'appariement de l'utilisateur qui est égale à 1 si l'utilisateur k est apparié avec l'utilisateur l dans la tranche de temps t et égale à 0, sinon. On a alors $x_{k,l} = 0$ si $k = l$, et $x_{k,l}[t] = x_{l,k}[t]$ pour tout k et l. Par ailleurs, on note $a_{k;n}[t]$ comme l'association entre le drone n et l'utilisateur k dans la tranche de temps t où $a_{k;n}[t]$ est égal à 1 si l'utilisateur k est associé[14] avec UAV n et égal à 0, sinon. Chaque utilisateur ne peut se connecter qu'à un seul drone, mais chaque drone peut connecter plusieurs utilisateurs dans n'importe quel créneau horaire. La condition de canal de l'utilisateur k à t peut être exprimée comme suit :

$$\tau_k[t] = \sum_{n=1}^{N} a_{k;n}[t]\tau_{k;n}[t], \quad \forall k, t. \tag{2.39}$$

Nous supposons que les utilisateurs sont appariés et que chaque paire d'utilisateurs transmet des données à l'UAV associé dans le sens NOMA de la liaison montante. Si l'utilisateur k est l'utilisateur fort d'une paire particulière, son débit de données atteint dans l'intervalle de temps t peut être exprimé comme suit :

$$\mathsf{R}_k[t] = B\log\left(1+\frac{\tau_k[t]p_k[t]}{\sigma^2 + \tau_k^{\mathsf{p}}[t]p_k^{\mathsf{p}}[t]}\right), \tag{2.40}$$

où B est la bande passante du canal attribuée à la paire d'utilisateurs sous-jacente, $\tau_k^{\mathsf{p}}[t]$ et $p_k^{\mathsf{p}}[t]$ sont le gain de puissance du canal et la puissance d'émission de son utilisateur apparié, qui peut

[14]Dans ce chapitre, « connecté » et « associé » sont utilisés de manière interchangeable pour décrire l'association utilisateur-UAV.

être exprimé comme suit :

$$\tau_k^{\mathsf{p}}[t] = \sum_{l=1}^{K} x_{k,l}[t]\tau_l[t], \tag{2.41a}$$

$$p_k^{\mathsf{p}}[t] = \sum_{l=1}^{K} x_{k,l}[t]p_l[t]. \tag{2.41b}$$

Si l'utilisateur k est l'utilisateur faible dans la paire considérée dans l'intervalle de temps t, son débit de données atteint peut être exprimé comme suit :

$$\mathsf{r}_k[t] = B\log\left(1 + \frac{\tau_k[t]p_k[t]}{\sigma^2}\right). \tag{2.42}$$

Nous utilisons $\lambda_k[t]$ pour décrire le rôle fort-faible[15] de l'utilisateur k où il est égal à 1 si l'utilisateur k est l'utilisateur fort et égal à 0 s'il s'agit de l'utilisateur faible dans sa paire associée et sa tranche horaire t. Il existe un couplage entre les variables fortes-faibles et les variables d'optimisation d'appariement utilisateur qui peut s'exprimer dans les contraintes suivantes:

$$x_{k,l}[t]\left(\lambda_k[t] + \lambda_l[t] - 1\right) = 0, \quad \forall(k,l), t. \tag{2.43}$$

Enfin, la relation entre les conditions du canal et les variables fortes-faibles peuvent être énoncées comme suit:

$$\left(2\lambda_k[t] - 1\right)\left(\tau_k[t] - \tau_k^{\mathsf{p}}[t]\right) \geq 0, \quad \forall k, t, \tag{2.44}$$

Nous notons ici que les valeurs des variables fortes-faibles peuvent être facilement déterminées (comme les valeurs de la fonction indicatrice $\mathbb{1}_{\tau_k[t] > \tau_k^{\mathsf{p}}[t]}$) lorsque les trajectoires d'UAV, l'association d'utilisateurs et les variables d'appariement d'utilisateurs sont fournies. Dans ce qui suit, les variables fortes-faibles sont parfois omises si elles peuvent être facilement déterminées à partir des valeurs données d'autres variables sans provoquer d'ambiguïté.

b) Formulation du Problème

[15] Notez qu'un utilisateur est fort ou faible selon sa condition de canal et la condition de canal de son partenaire. Dans notre conception, l'état du canal d'un utilisateur particulier dépend des coordonnées du drone associé et les coordonnées des drones sont des variables d'optimisation. Il faut donc définir des variables capturant les rôles forts-faibles des utilisateurs individuels.

Notre conception vise à minimiser la consommation d'énergie de tous les utilisateurs en l'optimisation de l'association des utilisateurs ($\mathbf{A}[t]$), le couplage des utilisateurs ($\mathbf{X}[t]$), le variables fort-faibles ($\mathbf{\Lambda}[t]$), l'allocation de puissance ($\mathbf{P}[t]$), et les trajectoires du drone $\{\mathbf{c}_n[t]\}$ tandis que les utilisateurs sont assurés de transmettre la quantité de données requise aux drones pendant la durée du service. Le problème d'optimisation considéré peut être énoncé comme suit:

$$
\begin{aligned}
\mathcal{P}_0 : & \min_{\{\mathbf{A}[t],\mathbf{X}[t],\mathbf{\Lambda}[t],\mathbf{P}[t],\mathbf{c}_n[t]\}} E_{\mathsf{all}}, \\
\text{s.t.} \quad & \sum_{t=1}^{T} \delta \left(\lambda_k[t]\mathsf{R}_k[t] + (1-\lambda_k[t])\, \mathsf{r}_k[t]\right) \geq D_k, \forall k, && \text{(2.45a)} \\
& \sum_{n=1}^{N} a_{k;n}[t] = 1, \quad \forall k, t && \text{(2.45b)} \\
& \mathbf{X}[t] = \mathbf{X}^T[t], \quad \forall t, && \text{(2.45c)} \\
& \sum_{l=1}^{K} x_{k,l}[t] = 1, \forall k, t, && \text{(2.45d)} \\
& x_{k,l}[t](a_{k;n}[t] - a_{l;n}[t]) = 0, \quad \forall (k,l), n, t, && \text{(2.45e)} \\
& p_k[t] \leq P_{\mathsf{max}}, \forall k, t, && \text{(2.45f)} \\
& \|\mathbf{c}_n[t] - \mathbf{c}_n[t-1]\| \leq \delta V_{\mathsf{max}}, \forall n, t, && \text{(2.45g)} \\
& \|\mathbf{c}_n[t] - \mathbf{c}_m[t]\| \geq D_{\mathsf{safe}}, \forall t, \forall n \neq m, && \text{(2.45h)} \\
& \mathbf{c}_n[1] = \mathbf{c}_n[T] = \mathbf{c}_{\mathsf{o}}, \forall n, && \text{(2.45i)} \\
& \lambda_k \in \{0,1\}, a_{k;n} \in \{0,1\}, x_{k,l} \in \{0,1\}, \forall k, l, n, && \text{(2.45j)} \\
& \text{constraints} \quad (2.43), (2.44),
\end{aligned}
$$

où P_{max} désigne la puissance d'émission maximale de chaque utilisateur, et le l'énergie totale peut être exprimée comme

$$E_{\mathsf{all}} = \delta \sum_{t=1}^{T} \sum_{k=1}^{K} p_k[t]. \tag{2.46}$$

Les contraintes (2.45a) garantissent que chaque utilisateur peut transmettre la quantité de données requise aux drones. Contraintes (2.45b), (2.45e), (2.45c) et (2.45d) sont imposées pour s'assurer que la solution d'appariement et d'association d'utilisateurs est valide. Les contraintes (2.45f) décrivent les puissances de transmission maximales des utilisateurs. Contraintes (2.45g), (2.45h) et (2.45i) sont pour le contrôle de trajectoire d'UAV, où V_{max} est la vitesse maximale d'un drone, D_{safe} est la distance de sécurité entre deux drones, $\mathbf{c}_{\mathsf{o}}$ est la coordonnée de la station de lancement. Le problème formulé est un programme non linéaire à nombres entiers mixtes, qui n'est pas trivial à résoudre. Dans la section suivante, nous proposons un algorithme pour résoudre efficacement le problème $\mathcal{P}_0$.

2.2.4.1 Solution Proposée

a) Problème Équivalent

Tout d'abord, nous introduisons un ensemble de variables auxiliaires $\{\mathbf{r}[t]\}$, où $r_k[t]$ est la cible du débit de données que l'utilisateur k transmet à son drone associé dans la tranche de temps t. Le problème $\mathcal{P}_0$ est équivalent au problème suivant avec des variables supplémentaires $\{\mathbf{r}[t]\}$.

$$\mathcal{P}_1 : \min_{\{\mathbf{A}[t],\mathbf{X}[t],\mathbf{\Lambda}[t],\mathbf{P}[t],\mathbf{c}_n[t],\mathbf{r}[t]\}} E_{\mathsf{all}},$$

$$\text{s.t.} \quad \lambda_k[t]\mathsf{R}_k[t] + (1-\lambda_k[t])\mathsf{r}_k[t] \geq r_k[t], \forall k, t, \tag{2.47a}$$

$$\sum_{k=1}^{K} \delta r_k[t] \geq D_k, \forall k, \tag{2.47b}$$

$$(2.45b), (2.45e), (2.43), (2.44), (2.45c), (2.45d), (2.45f), (2.45g), (2.45h), (2.45i), (2.45j).$$

Il est facile de voir que l'égalité de (2.47a) est optimale. Comme on peut toujours augmenter $r_k[t]$ pour réaliser l'égalité de (2.47a) sans violer les autres contraintes. Nous décrirons ci-dessous comment résoudre le problème $\mathcal{P}_1$.

b) Solution Proposée

Dans le problème d'optimisation considéré, nous allons montrer dans le lemme 2.1 que la puissance optimale $\{\mathbf{P}^*[t]\}$ peut être exprimé explicitement en termes d'autres variables ($\{\mathbf{c}_n[t], \mathbf{X}[t], \mathbf{A}[t], \mathbf{r}[t]\}$). Cette puissance optimale $\{\mathbf{P}^*[t]\}$ expression nous permet d'appliquer la technique BCD pour résoudre efficacement le problème $\mathcal{P}_1$. Nous proposons alors de résoudre le problème $\mathcal{P}_1$ en résolvant itérativement les trois sous-problèmes suivants. Dans le premier sous-problème, nous supposons que les valeurs de $\{\mathbf{c}_n[t], \mathbf{r}[t]\}$ sont donnés et résolvent pour la consommation d'énergie optimale où toutes les autres variables sont les variables d'optimisation. Dans le deuxième sous-problème, nous optimisons les variables de débit de données $\{\mathbf{r}[t]\}$ étant donné $\{\mathbf{c}_n[t]\}$ et les valeurs optimales des autres variables obtenues en résolvant le premier sous-problème. Enfin, dans le troisième problème, les trajectoires des drones sont optimisées compte tenu des valeurs d'autres variables. On peut montrer que la consommation totale d'énergie est réduite au fil des itérations, par conséquent, le processus itératif est garanti de converger.

★ *Optimisations de la puissance et des variables entières compte tenu des trajectoires et des taux des drones:*

En supposant que $\{\mathbf{c}_n[t], \mathbf{r}[t]\}$ sont donnés, nous trouvons le puissance optimale $\{\mathbf{P}^*[t]\}$ par rapport à $\{\mathbf{c}_n[t], \mathbf{r}[t]\}$, et d'autres variables entières. Plus précisément, nous résolvons la puissance optimale et l'association d'utilisateurs lorsque le scénario d'appariement est connu. Ensuite, l'optimisation de l'appairage des utilisateurs est résolue en s'attaquant au problème sous-jacent d'appariement de graphe à pondération maximale. Puis, l'association optimale d'utilisateurs est dérivée.

Si les valeurs de $\{\mathbf{c}_n[t], \mathbf{r}[t]\}$, et $\mathbf{X}[t]$ sont donnés, le problème $\mathcal{P}_1$ se réduit au problème suivant.

$$\begin{aligned} \mathcal{P}_{\mathsf{A,P}} : & \min_{\mathbf{A}[t]\mathbf{\Lambda}[t],\mathbf{P}[t]} E_{\mathsf{all}}, \\ \text{s.t.} \;\; & (2.45\text{b}), (2.45\text{e}), (2.43), (2.44), (2.45\text{f}), (2.45\text{j}), (2.47\text{a}). \end{aligned}$$

Le problème $\mathcal{P}_{\mathsf{A,P}}$ peut être découplé en plusieurs sous-problèmes noté $\tilde{\mathcal{P}}_{\mathsf{A,P}}(k,l;t)$. Le sous-problème $\tilde{\mathcal{P}}_{\mathsf{A,P}}(k,l;t)$ minimise l'énergie totale consommée par les utilisateurs k et l dans la tranche de temps t, où la puissance d'émission $p_k[t], p_l[t]$, l'association d'utilisateurs $\mathbf{a}_k[t], \mathbf{a}_l[t]$, et les variables fortes-faibles $\lambda_k[t], \lambda_l[t]$ doivent être optimisées[16]. Ce sous-problème peut être exprimé comme suit:

$$\begin{aligned} \tilde{\mathcal{P}}_{\mathsf{A,P}}(k,l;t) : & \min_{\{\mathbf{a}_i[t],\lambda_i[t],p_i[t]\}_{i=k,l}} \delta(p_k[t]+p_l[t]), \\ \text{s.t.} \;\; & a_{k;n}[t] = a_{l;n}[t], && (2.49\text{a}) \\ & \lambda_k[t] + \lambda_l[t] = 1, && (2.49\text{b}) \\ & (2\lambda_k[t]-1)(\tau_k[t]-\tau_l[t]) \geq 0, && (2.49\text{c}) \\ & (2.45\text{b}), (2.45\text{f}), (2.45\text{j}), (2.47\text{a}). \end{aligned}$$

[16]Notez que $\mathbf{a}_k[t] = [a_{k;1}[t], ..., a_{k;N}[t]]$ désigne le vecteur d'association d'utilisateurs correspondant à l'utilisateur k à t.

où (2.49a), (2.49b), et (2.49c) se déduisent respectivement de (2.45e), (2.43), et (2.44), étant donné que $x_{k,l}[t] = 1$.

Soit $p_{k,l}[t]$ la somme des puissances de deux utilisateurs k et l dans la fonction objectif de $\tilde{\mathcal{P}}_{\mathsf{A,P}}(k,l;t)$, alors la consommation totale d'énergie peut être exprimée comme suit:

$$E_{\mathsf{all}} = \frac{\delta}{2}\sum_{t=1}^{T}\sum_{k=1}^{K}\sum_{l=1}^{K} x_{k,l}[t] p_{k,l}[t]. \tag{2.50}$$

Dans ce qui suit, nous trouvons la valeur optimale de $p_{k,l}[t]$ pour tout t et toutes les combinaisons de k et l. *Première*, nous trouvons l'allocation de puissance optimale par rapport aux variables d'association d'utilisateurs (c'est-à-dire si $\mathbf{a}_k[t]$ et $\mathbf{a}_l[t]$ sont connus). Notez que lorsque la solution d'association d'utilisateurs est donnée, les conditions de canal pour k et l sont déterminées par (2.39). Ensuite, les variables fortes-faibles peuvent également être facilement déterminé par (2.49b) and (2.49c).[17]. *Deuxième*, nous substituons la solution d'allocation de puissance optimale en fonction des variables d'association d'utilisateurs dans la fonction objectif de $\tilde{\mathcal{P}}_{\mathsf{A,P}}(k,l;t)$ d'où l'association optimale par rapport à chaque paire (k,l) sera déterminée.

Considérons un couple particulier d'utilisateurs k et l associé au drone n. Supposons que le canal de l'utilisateur k soit plus fort que celui de l'utilisateur l (i.e., $\lambda_k[t] = 1$ et $\lambda_l[t] = 0$). Ensuite, le problème $\tilde{\mathcal{P}}_{\mathsf{A,P}}(k,l;t)$ peut être déduit plus loin dans le problème suivant:

$$\begin{aligned} \tilde{\mathcal{P}}_{\mathsf{P}}(k,l;t;n) : &\min_{\{p_i[t]\}_{i=k,l}} \ \delta(p_k[t] + p_l[t]), \\ &\text{s.t.} \ \ (2.45\text{f}), (2.47\text{a}). \end{aligned}$$

Lemma 2.1. *Si le problème $\tilde{\mathcal{P}}_{\mathsf{P}}(k,l;t;n)$ est réalisable, la solution optimale de celui-ci peut être écrite comme suit :*

$$\begin{aligned} p_k^*[t] &= \sigma^2 \tau_{k;n}^{-1}[t](\beta^{r_k[t]} - 1)\beta^{r_l[t]}, \\ p_l^*[t] &= \sigma^2 \tau_{l;n}^{-1}[t](\beta^{r_l[t]} - 1), \end{aligned} \tag{2.52}$$

où $\beta = 2^{1/B}$. Le problème est réalisable si $p_k^*[t]$ et $p_l^*[t]$ dans (2.52) ne sont pas supérieurs à P_{max}.

[17] Plus précisément, si les utilisateurs k et l sont associés au drone n dans la tranche horaire t, nous pouvons calculer leurs conditions de canal. Alors $\lambda_k[t] = 1$ si $\tau_{k;n}[t] \geq \tau_{l;n}[t]$ et $\lambda_l[t] = 0$, sinon.

Le lemme 2.52 permet d'exprimer explicitement les puissances de transmission optimales des utilisateurs k et l en termes de conditions de canal qui dépendent de l'association d'utilisateurs et des distances entre les utilisateurs et leur drone associé. Ci-après, nous utiliserons le membre de droite de (2.52) au lieu de $p_k[t], p_l[t]$.

Soit $p_{k,l;n}[t]$ la puissance allouée optimale des utilisateurs k et l au cas où ils seraient appariés et connectés au drone n dans la tranche horaire t. Alors, $p_{k,l;n}[t]$ peut être exprimé comme suit :[18]

$$p_{k,l;n}[t] = \begin{cases} \sigma^2 \left(\tau_{k;n}^{-1}[t](\beta^{r_k[t]} - 1)\beta^{r_l[t]} + \tau_{l;n}^{-1}[t](\beta^{r_l[t]} - 1)\right), & \text{if} \max(p_k^*[t], p_l^*[t]) \leq P_{\mathsf{max}}, \\ \infty, & \text{autrement.} \end{cases} \tag{2.53}$$

La valeur optimale de la fonction objectif de $\tilde{\mathcal{P}}_{\mathsf{A,P}}(k, l; t)$ par rapport à l'association utilisateur Les variables peuvent être exprimées comme suit:

$$p_{k,l}[t] = \sum_{n=1}^{N} a_{k;n}[t] p_{k,l;n}[t]. \tag{2.54}$$

Notez que (2.54) est réalisé avec l'hypothèse que $x_{k,l}[t] = 1$, et donc $a_{k;n}[t] = a_{l;n}[t]$. Le résultat dans (2.54) nous permet de trouver l'association optimale pour les utilisateurs k, l par le lemme suivant.

Lemma 2.2. *Si $x_{k,l}[t] = 1$, l'association optimale pour les utilisateurs k et l à t peut être trouvée comme suit :*

$$a_{k;n}^*[t] = a_{l;n}^*[t] = \begin{cases} 1, & si \;\; n = \operatorname*{argmin}_n p_{k,l;n}[t] \\ 0, & autrement. \end{cases} \tag{2.55}$$

En substituant la solution d'association d'utilisateurs obtenue à partir du Lemme 2.2, nous pouvons trouver la valeur optimale de $p_{k,l}[t]$ à partir de $p_{k,l}[t]$ à partir de (2.54).

Après avoir obtenu l'association d'utilisateurs optimale et la solution d'allocation de puissance correspondante, le problème d'optimisation de l'appariement des utilisateurs peut être exprimé

[18]Nous utilisons la convention dans [30] où la valeur optimale d'un problème de minimisation est l'infini si le problème est infaisable.

comme suit :

$$
\begin{aligned}
\mathcal{P}_{\mathsf{X}} :& \min_{\mathbf{X}[t]} \frac{\delta}{2} \sum_{t=1}^{T} \sum_{k=1}^{K} \sum_{l=1}^{K} x_{k,l}[t] p_{k,l}[t], \\
\text{s.t.} \ & (2.45\text{c}), (2.45\text{d}), (2.45\text{j}).
\end{aligned}
$$

De même, le problème $\mathcal{P}_{\mathsf{X}}$ peut être décomposé en plusieurs sous-problèmes dont chacun optimise l'appariement d'utilisateurs pour un t correspondant. Le sous-problème à t est en effet le Maximum Weight Perfect Matching (MWPM) problème pour un graphe dont les sommets sont des utilisateurs, et le poids de l'arête entre les utilisateurs k et l est $p_{k,l}[t]$. Ces problèmes MWPM peuvent être résolus de manière efficace et optimale [31].

Dans les sections suivantes, les optimisations d'autres variables, compte tenu des solutions d'association d'utilisateurs et d'appariement, sont développées. On note $(k,l)[t]$ comme les utilisateurs k et l à apparier dans la tranche de temps t. Sans perte de généralité, c'est la convention dans les sections suivantes que k est l'utilisateur fort et l est l'utilisateur faible.

★ *Problème d'optimisation du débit de données:*

A partir de (2.46) et (2.53), la consommation totale d'énergie E_{all} peut être exprimée par rapport aux débits de données $\{\mathbf{r}[t]\}$ comme suit :

$$
E_{\mathsf{all}} = \delta\sigma^2 \sum_{t=1}^{T} \sum_{(k,l)[t]} \beta^{r_k[t]+r_l[t]} \tau_k^{-1}[t] + \beta^{r_l[t]} \left(\tau_l^{-1}[t] - \tau_k^{-1}[t] \right) - \delta\sigma^2 \sum_{t=1}^{T} \sum_{(k,l)[t]} \tau_l^{-1}[t], \tag{2.57}
$$

Lorsque des solutions de trajectoire d'UAV, d'association d'utilisateurs et d'appariement d'utilisateurs sont données, l'optimisation des débits de données peut être énoncée comme suit :

$$
\begin{aligned}
\mathcal{P}_{\mathsf{R}} :& \min_{\{\mathbf{r}[t]\}} E_{\mathsf{all}}, \\
\text{s.t.} \ & \sum_{k=1}^{K} \delta r_k[t] \geq D_k, \forall k, && (2.58\text{a}) \\
& \beta^{r_l[t]} - 1 \leq \frac{P_{\mathsf{max}}}{\sigma^2} \tau_k[t], \forall (k,l)[t], && (2.58\text{b}) \\
& \beta^{r_k[t]+r_l[t]} - \beta^{r_l[t]} \leq \frac{P_{\mathsf{max}}}{\sigma^2} \tau_l[t], \forall (k,l)[t], && (2.58\text{c}) \\
& (2.45\text{c}), (2.45\text{d}), (2.45\text{f}), (2.45\text{g}), (2.45\text{h}), (2.45\text{j}).
\end{aligned}
$$

Puisque $\tau_l^{-1}[t] - \tau_k^{-1}[t] \geq 0$ pour toutes les paires d'utilisateurs $(k,l)[t]$, la fonction objectif du problème $\mathcal{P}_{\mathsf{R}}$ est convexe ; mais le problème $\mathcal{P}_{\mathsf{R}}$ est toujours non convexe en raison de la non-convexité de la contrainte (2.58c). Cependant, (2.58c) est la différence de deux fonctions convexes, on peut donc approximer (2.58c) par la contrainte suivante [30]:

$$\beta^{r_k[t]+r_l[t]} - \beta^{\bar{r}_l[t]}(1 + \ln(\beta)(r_l[t] - \bar{r}_l[t]))\tau_{l;n}^{-1}[t] \leq \frac{P_{\mathsf{max}}}{\sigma^2}, \tag{2.59}$$

où nous avons remplacé $\beta^{r_l[t]}$ par son approximation de Taylor du premier ordre au point local $\bar{r}_l[t]$. La contrainte (2.59) est convexe par rapport aux variables d'optimisation $(r_k[t], r_l[t])$, Ensuite, nous appliquons la technique d'approximation convexe successive (SCA) pour résoudre le problème $\mathcal{P}_{\mathsf{R}}$ itérativement où la contrainte (2.58c) est remplacée par la contrainte (2.59) à chaque itération du processus itératif.

★ *Optimisation de la trajectoire des drones:*

La fonction objectif globale E_{all} peut également être exprimée par rapport aux trajectoires du drone $\{\mathbf{c}_n[t]\}$ comme suit :

$$E_{\mathsf{all}} = \delta\sigma^2 \sum_{t=1}^{T} \sum_{(k,l)[t]} \zeta_k[t] \|\mathbf{c}_{n_{(k,l)}}[t] - \mathbf{u}_k\|^2 + \zeta_l[t] \|\mathbf{c}_{n_{(k,l)}}[t] - \mathbf{u}_l\|^2 + \delta\sigma^2 \sum_{t=1}^{T} \sum_{(k,l)[t]} (\zeta_k[t] + \zeta_l[t]) h^2, \tag{2.60}$$

où $\zeta_k[t] = \mu^{-1}(\beta^{r_k[t]} - 1)\beta^{r_l[t]}$ et $\zeta_l[t] = \mu^{-1}(\beta^{r_l[t]} - 1)$; $\mathbf{c}_{n_{(k,l)}}[t]$ est la coordonnée du drone associé à la paire d'utilisateurs $(k,l)[t]$. Notez que le deuxième terme ne dépend pas de $\{\mathbf{c}_n[t]\}$.

Le problème d'optimisation de trajectoire d'UAV peut être exprimé comme suit:

$$\begin{aligned} \mathcal{P}_{\mathsf{C}} : \min_{\{\mathbf{c}_n[t]\}} \; & E_{\mathsf{all}} \\ \text{s.t.} \; & \zeta_k[t] \left(\|\mathbf{c}_{n_{(k,l)}}[t] - \mathbf{u}_k\|^2 + h^2 \right) \leq \frac{P_{\mathsf{max}}}{\sigma^2}, \forall (k,l)[t], && \text{(2.61a)} \\ & \zeta_l[t] \left(\|\mathbf{c}_{n_{(k,l)}}[t] - \mathbf{u}_l\|^2 + h^2 \right) \leq \frac{P_{\mathsf{max}}}{\sigma^2}, \forall (k,l)[t], && \text{(2.61b)} \\ & (2.44), (2.45\text{g}), (2.45\text{i}), (2.45\text{h}). \end{aligned}$$

Même si le problème $\mathcal{P}_{\mathsf{C}}$ est non convexe en raison de la contrainte non convexe (2.45h), nous pouvons le résoudre en appliquant la méthode SCA. Plus précisément, nous commençons par élever au carré les deux côtés de (2.45h), puis approchons le côté gauche avec sa borne inférieure au point local $\{\bar{\mathbf{c}}_n[t], \bar{\mathbf{c}}_m[t]\}$ en utilisant le développement de Taylor au premier ordre. On obtient alors la contrainte approchée suivante:

$$2\,(\bar{\mathbf{c}}_m[t]-\bar{\mathbf{c}}_n[t])^T(\mathbf{c}_m[t]-\mathbf{c}_n[t])-\|\bar{\mathbf{c}}_m[t]-\bar{\mathbf{c}}_n[t]\|^2 \geq D^2_{\mathsf{safe}}. \tag{2.62}$$

Comme les contraintes (2.45h) sont approximées par (2.62), le problème approximatif résultant du problème $\mathcal{P}_{\mathsf{C}}$ est convexe par rapport aux variables de trajectoire du drone. Par conséquent, le problème convexe obtenu peut être résolu de manière optimale à l'aide de solveurs standard.

Notre algorithme itératif proposé, nommé Multi-UAV NOMA Energy minimization (MUNE), est décrit dans l'algorithme 2.5, où ϵ est un petit nombre qui est réglé pour équilibrer la précision souhaitée et le temps de convergence de cet algorithme.

Algorithm 2.5. Multi-UAV NOMA Energy minimization (MUNE)

1: Initiate values for UAV trajectories $\left\{\mathbf{c}_n^0[t], \mathbf{R}^0[t]\right\}$, set $i=1$, $E^0_{\mathsf{all}} = TKP_{\mathsf{max}}$.
2: **while** 1 **do**
3: Given $\left\{\mathbf{c}_n^{i-1}[t], \mathbf{R}^{i-1}[t]\right\}$, solve problem $\tilde{\mathcal{P}}_{\mathsf{A,P}}(k,l;t)$ for all t and all possible combinations of (k,l), obtain optimal $\{p_{k,l}[t]\}$ from (2.54).
4: From the obtained $\{p_{k,l}[t]\}$, solve problem $\mathcal{P}_{\mathsf{X}}$ for optimal pairing variables $\left\{\mathbf{X}^i[t]\right\}$, and the corresponding association $\left\{\mathbf{A}^i[t]\right\}$.
5: Solve problem $\mathcal{P}_{\mathsf{R}}$ with given other variables iteratively until convergence, obtain the values of $\left\{\mathbf{R}^i[t]\right\}$.
6: Solve problem $\mathcal{P}_{\mathsf{C}}$ with given other variables iteratively until convergence. Denote the obtained solution as $\{\mathbf{c}_n^i[t]\}$, and the total energy consumption as E^i_{all}.
7: **if** $E^i_{\mathsf{all}} \geq E^{i-1}_{\mathsf{all}} - \epsilon$ **then**
8: Break the loop.
9: **else**
10: Let $i = i+1$.
11: **end if**
12: **end while**
13: End of algorithm.

2.2.4.2 Résultats Numériques

Nous considérons un réseau circulaire d'un rayon de 1000m dans lequel les utilisateurs sont placés de manière aléatoire et uniforme. Nous supposons que les drones volent à l'altitude constante $h = 100$m et tous les utilisateurs ont besoin de collecter la même quantité de données $D_k = 6$Mbits

$\forall k$, sauf indication contraire. La bande passante allouée pour chaque paire d'utilisateurs est de 100 kHz, la puissance de bruit est définie sur -105dBm, et μ est égal à 6.5×10^{-4}. Le nombre de tranches horaires est de $T = 60$, sauf indication contraire et chaque tranche horaire a une longueur de $\delta = 1$s. La puissance d'émission maximale est $P_{\mathsf{max}} = 0.1$W et la valeur de ϵ dans l'algorithme 2.5 est 10^{-2}. La station UAV est située au centre de la zone du réseau, $\mathbf{c}_{\mathsf{o}} = (0, 0)$. Initialement, nous laissons $r_k[t] = D_k/T$ pour tout utilisateur k, c'est-à-dire que les débits de données initiaux dans chaque tranche de temps sont identiques pour tous les utilisateurs. Pour les trajectoires initiales des drones, nous laissons le drone n commencer à $\mathbf{c}_{\mathsf{o}} = (0, 0)$ et voler dans le sens antihoraire le long d'une trajectoire circulaire avec un rayon de $r_{\mathsf{o}} = 300$m et un centre à $(r_{\mathsf{o}} \cos \frac{n2\pi}{N}, r_{\mathsf{o}} \sin \frac{n2\pi}{N})$.

Nous introduisons deux algorithmes de base dont les performances sont à comparer avec celles atteintes par notre algorithme proposé. *Première,* le Data Collection Optimization Algorithm (DCOA) qui a été développé dans [29] pour le réglage d'un seul drone uniquement. Le DCOA utilise la décomposition en courbes généralisées [32] pour résoudre le problème commun d'appariement d'utilisateurs NOMA et d'optimisation d'allocation de puissance, puis optimise la trajectoire de l'UAV pour maximiser le total des données transmises par tous les utilisateurs. *Deuxièmement,* nous présentons également un autre algorithme de base, appelé Multi-UAV OMA Energy Minimization (MUOE), dont les détails sont donnés dans l'annexe 7.A, où la stratégie d'accès multiple orthogonal (OMA) est utilisée au lieu de NOMA. Dans cette stratégie, chaque utilisateur est connecté au drone le plus proche et une bande passante de $B/2$ lui est attribuée dans chaque tranche de temps. Il y a 18 utilisateurs dans ce scénario de simulation. Nous présentons ci-après les résultats numériques pour les paramètres d'UAV unique et multi-UAV.

a) Paramètres Seul-UAV

Nous montrons les performances atteintes par notre algorithme MUNE proposé, l'algorithme MUOE, et l'algorithme DCOA de [29] pour la configuration du réseau avec un UAV et un nombre variable d'utilisateurs. Plus précisément, dans la figure 2.8, nous montrons la consommation totale d'énergie de tous les utilisateurs lorsque ces algorithmes sont appliqués. Cette figure montre que l'algorithme MUNE proposé atteint la plus faible consommation d'énergie. De plus, les écarts entre la consommation totale d'énergie due à l'algorithme proposé et les deux lignes de base augmente lorsque le nombre d'utilisateurs augmente.

b) Paramètres Multi-UAV

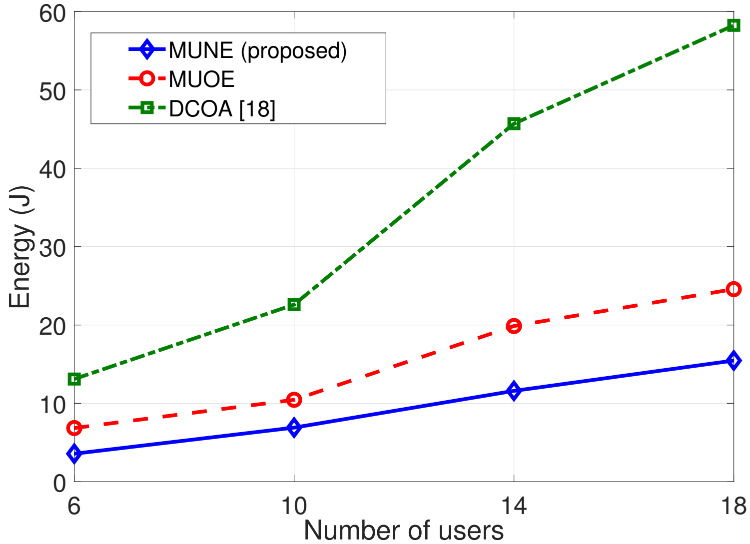

Figure 2.8: Total energy consumption versus number of users, single-UAV setting.

Nous présentons maintenant les résultats numériques pour les paramètres multi-UAV. Notez que l'algorithme DCOA ne peut pas être appliqué dans les paramètres multi-UAV ; donc, nous ne montrons que les performances obtenues par les algorithmes MUNE et MUOE proposés.

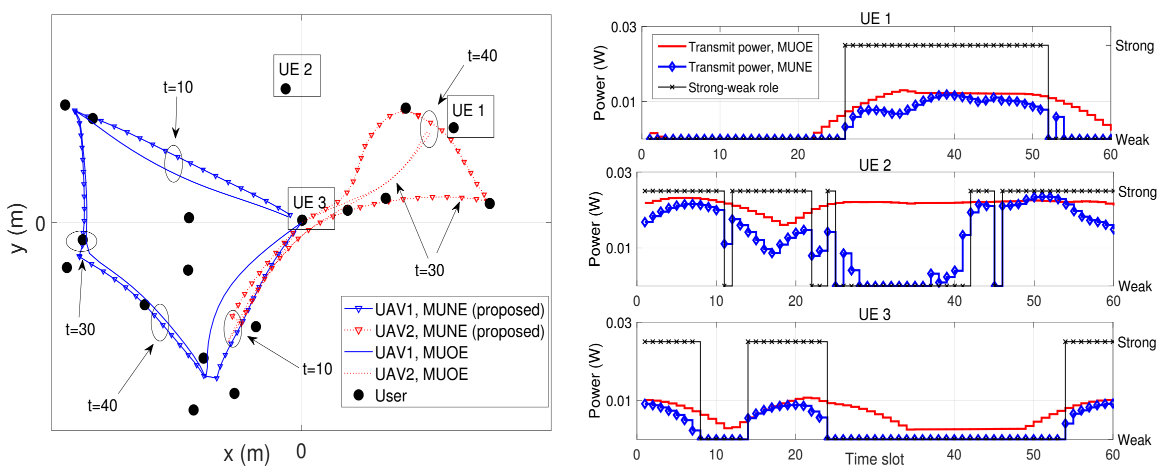

(a) (b)

Figure 2.9: a) Converged UAV trajectories, obtained by different algorithms; b) User transmit powers over time

Nous étudions d'abord un scénario de réseau particulier. Dans la Fig. 2.9a, nous montrons les trajectoires des drones obtenues par les algorithmes MUNE et MUOE à la convergence. Plusieurs observations intéressantes peuvent être tirées de cette figure. Premièrement, les trajectoires du drone 1 obtenues par les deux algorithmes semblent suivre une frontière convexe établie par les utilisateurs de bord qui sont plus proches de la trajectoire initiale du drone 1 que de celle du drone

2. Alors que les trajectoires du drone 1 dues aux deux algorithmes sont assez proches l'une de l'autre, il y a une nette différence dans les trajectoires du drone 2 obtenues à partir des deux algorithmes. La trajectoire obtenue à partir de l'algorithme MUNE suit également la frontière convexe des utilisateurs de bord qui sont plus proches de la trajectoire initiale du drone 2. Cependant, la trajectoire obtenue à partir de l'algorithme MUOE se contracte étroitement jusqu'à presque une courbe. Cela peut s'expliquer en inspectant soigneusement les emplacements des utilisateurs. En particulier, au début du vol ($t = 0$ à $t = 10$), L'UAV 2 doit descendre pour servir les utilisateurs en bas à gauche. A la seconde moitié du vol ($t \geq 30$), il doit servir les utilisateurs en haut à droite, et l'utilisateur 2 a indiqué dans la figure. Afin de desservir un ensemble d'utilisateurs spatialement divergents, le drone doit rester autour de certains endroits qui équilibrent les conditions de canal de ses utilisateurs desservis en raison de la nature du système OMA. Plus précisément, OMA attribue à chaque utilisateur une quantité de bande passante non nulle ; par conséquent, la bande passante attribuée pourrait être gaspillée si l'utilisateur correspondant ne transmet pas de données. D'autre part, le schéma NOMA est plus flexible et efficace dans l'utilisation de la bande passante où la bande passante totale attribuée à une paire d'utilisateurs peut être utilisée efficacement par les deux utilisateurs ou par l'un des deux utilisateurs appariés.

Nous étudions les solutions d'allocation de ressources dues à MUNE et MUOE dans la figure 2.9b en étudiant les puissances de transmission dans le temps de trois utilisateurs types indiqués sur la figure 2.9b: *i)* (périphérique) utilisateur 1 qui se trouve à proximité de la trajectoire initiale d'un drone et loin de la trajectoire initiale de l'autre drone, *ii)* (périphérique) user 2 qui est loin des trajectoires initiales des deux drones, et *iii)* (centre) utilisateur 3. Nous indiquons également leurs rôles (fort ou faible, ou $\lambda_k[t] = 1$ ou $\lambda_k[t] = 0$, respectivement) dans cette figure. Notez que lorsque $p_k[t] = 0$, peu importe que l'utilisateur k soit affecté en tant qu'utilisateur fort ou faible[19]. Donc,si $p_k[t] = 0$, nous supposons que l'utilisateur k est un utilisateur faible pour plus de commodité. Plusieurs observations intéressantes peuvent être tirées de la figure. Premièrement, la puissance de transmission des utilisateurs dans le cas NOMA est généralement inférieure à celle dans le cas OMA. Deuxièmement, NOMA permet aux utilisateurs d'être inactifs plus fréquemment par rapport à OMA (par exemple, voir les puissances de transmission des utilisateurs 2, 3). Par exemple, lorsque les deux drones sont éloignés de l'utilisateur 2 (de $t = 20$ à $t = 40$), NOMA permet à l'utilisateur d'être inactif tandis que OMA permet à l'utilisateur de transmettre avec une puissance assez élevée de sorte que l'utilisateur 2 peut transmettre avec succès la quantité de données requise aux drones).

[19]Cela peut être vérifié facilement en examinant la formule de puissance optimale (2.52).

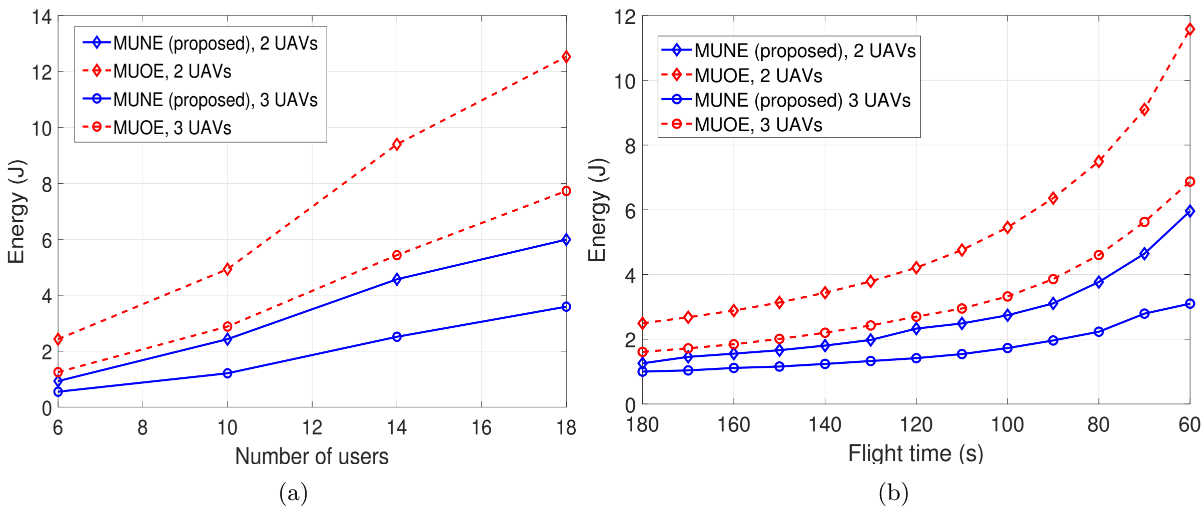

Figure 2.10: a) Total energy used versus number of users, different number of UAVs; b) Total energy used versus flight time

Nous étudions maintenant l'énergie totale requise par MUNE et MUOE car différents paramètres clés du système varient. Plus précisément, Fig. 2.10a et 2.10b montrer l'énergie totale comme le nombre d'utilisateurs et le temps de vol (δT) varient respectivement pour les paramètres réseau avec 2, 3 drones. On peut le voir sur la figure 2.10a que moins d'énergie est nécessaire avec plus de drones dans les réseaux pour les deux algorithmes. Ceci peut être expliqué comme suit. Chaque UAV a tendance à servir un plus petit nombre d'utilisateurs dans chaque créneau horaire lorsqu'il y a plus d'UAV dans le réseau. Par conséquent, chaque UAV peut établir une trajectoire pour desservir plus efficacement un sous-ensemble d'utilisateurs avec un plus grand nombre d'UAV. La figure 2.10a confirme à nouveau que l'algorithme MUNE surpasse l'algorithme MUOE.

Dans la figure 2.10b, nous traçons l'énergie totale en fonction du temps de vol en faisant varier T de $T = 60$ à $T = 180$). Au début, il semble surprenant que plus le temps de vol est long, moins l'énergie totale est. Cependant, le résultat de la figure 2.10b peut être expliqué en se référant aux résultats de la figure 2.9b. En fait, les algorithmes MUNE et MUOE permettent à un utilisateur de rester inactif lorsqu'il n'y a pas de drone suffisamment proche de lui. À cet égard, l'algorithme MUNE proposé tend à fournir plus de cycles 'actif-inactif' pour les utilisateurs individuels par rapport à l'algorithme MUOE, comme on peut l'observer sur la figure 2.9b et la figure 2.10b. Les résultats de la figure 2.10b montrent que l'algorithme MUNE surpasse l'algorithme MUOE. Enfin, la figure 2.10b nous montre qu'il y a un compromis entre la consommation totale d'énergie et temps de vol pour accomplir les tâches de collecte de données pour tous les utilisateurs. Spécifiquement, on peut diminuer le temps de vol au prix d'une consommation d'énergie plus élevée des utilisateurs ou on peut réduire la consommation d'énergie si le temps requis pour la collecte de données peut être allongé.

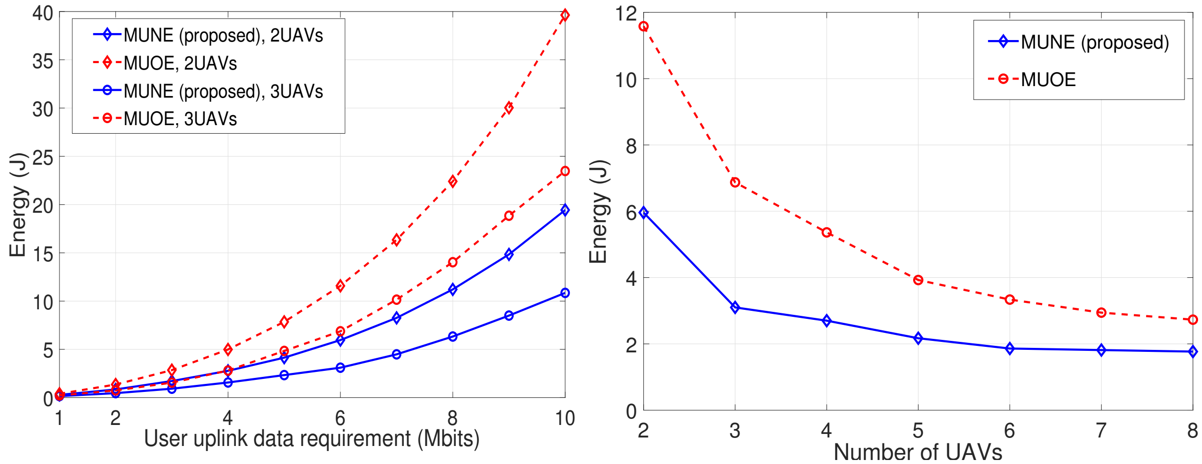

(a) (b)

Figure 2.11: a) Total energy used versus user demand; b) Total energy used versus number of UAVs

La figure 2.11a présente les variations de l'énergie totale avec la quantité requise de données de transmission D_k (c'est-à-dire la demande de données) de chaque utilisateur pour les paramètres réseau avec 2 ou 3 drones, et $T = 60$. La figure montre que la consommation d'énergie augmente rapidement lorsque la quantité de données requises augmente. Cela peut s'expliquer en remarquant la forme logarithmique du débit de données atteignable par rapport à la puissance d'émission. Cependant, à mesure que la quantité requise de données de transmission augmente, le taux croissant de la consommation d'énergie dû à l'algorithme MUNE est beaucoup plus faible que cela en raison de l'algorithme MUOE. Cela confirme à nouveau la supériorité de notre algorithme proposé tirant parti de NOMA par rapport à son homologue MUOE. Enfin, nous traçons la consommation d'énergie en fonction du nombre de drones, qui varient de 2 à 8 drones dans la figure 2.11b. On s'attend à ce que la consommation d'énergie diminue lorsque le nombre de drones augmente. Cependant, il est intéressant d'observer que la différence de consommation d'énergie entre les algorithmes MUNE et MUOE diminue à mesure que le nombre de drones augmente, ce qui suggère que le gain dû au NOMA par rapport à l'OMA est plus important dans les réseaux plus denses (c'est-à-dire que chaque drone doit servir un grand nombre d'utilisateurs en moyenne). Les résultats suggèrent également que pour les paramètres de réseau dans lesquels le nombre d'utilisateurs par drone est suffisamment élevé (par exemple, plus de 10 utilisateurs par drone), emploi de NOMA au lieu d'OMA pour les tâches de collecte de données dans les réseaux sans fil multi-UAV est très enrichissant.

2.3 Remarques Finales

Dans cette thèse de doctorat, nous avons développé diverses nouvelles techniques de gestion des interférences et des ressources pour les futurs réseaux sans fil où de nombreux composants aériens sont impliqués pour prendre en charge différentes applications qui exigent diverses qualités de services. Spécifiquement, nous avons apporté trois contributions importantes à la recherche. *Première*, nous développons une nouvelle annulation d'interférence, une estimation de canal à évanouissement rapide et une détection de symboles dans un cadre général où les communications brouilleuses et brouillées fonctionnent sur des canaux qui se chevauchent et leurs signaux ont des bandes passantes différentes. L'algorithme proposé peut annuler les interférences et estimer avec précision le canal à évanouissement rapide, tandis que les méthodes de détection de symboles proposées fournissent un compromis entre précision et complexité. *Deuxième*, nous considérons l'allocation des ressources et l'optimisation de la trajectoire multi-UAV où l'on maximise le nombre d'utilisateurs admis. L'algorithme proposé surpasse considérablement la solution conventionnelle qui applique la méthode Block Coordinate Ascent et la programmation linéaire en nombres entiers. *Troisième*, nous étudions l'optimisation conjointe des trajectoires multi-UAV, la puissance d'émission, l'association utilisateur-UAV, et l'appariement d'utilisateurs NOMA pour les réseaux sans fil multi-UAV afin de minimiser la consommation d'énergie totale de l'utilisateurs. Notre algorithme proposé fournit des horaires actifs-inactifs efficaces, et une consommation d'énergie nettement inférieure par rapport à une référence existante, et une stratégie conjointe d'optimisation de la trajectoire des drones et de l'allocation des ressources basée sur l'OMA.

Chapter 3

Introduction

3.1 Background and Motivations

Global wireless communication demands have seen dramatic growth over the past decade along the rapid increase in the numbers of human and machine based connections. In fact, it is predicted by Ericsson that total mobile traffic volume can reach 131 exabytes per month by the end of 2024 [1]. Moreover, recent forecast shows that billions of wireless devices, from low-cost internet of things (IoT) devices, wearables, to virtual/augmented/mixed reality devices, and smart vehicles will be connected with wireless networks over the next few years [2, 3]. Furthermore, next-generation wireless networks and technologies must be developed to support diverse requirements in terms of data rate, latency, reliability for different vertical applications such as e-health, smart factories, and smart cities. To meet these requirements given limited spectrum resource, it becomes critical to leverage under-utilized usable frequency bands and to enhance the spectrum efficiency. In general, one must address great challenges in engineering hardware components such as antennas and radio frequency circuits to effectively exploit higher frequency bands while improvement of spectrum efficiency requires more sophisticated communications techniques and resource allocation such as novel interference and resource management strategies.

There has been growing interests in leveraging different aerial platforms including low-altitude unmanned aerial vehicles (UAVs), high-altitude UAVs, balloons, dense low-orbit satellite constellations in recent years for providing reliable, ubiquitous, and economical wireless services [12, 13].

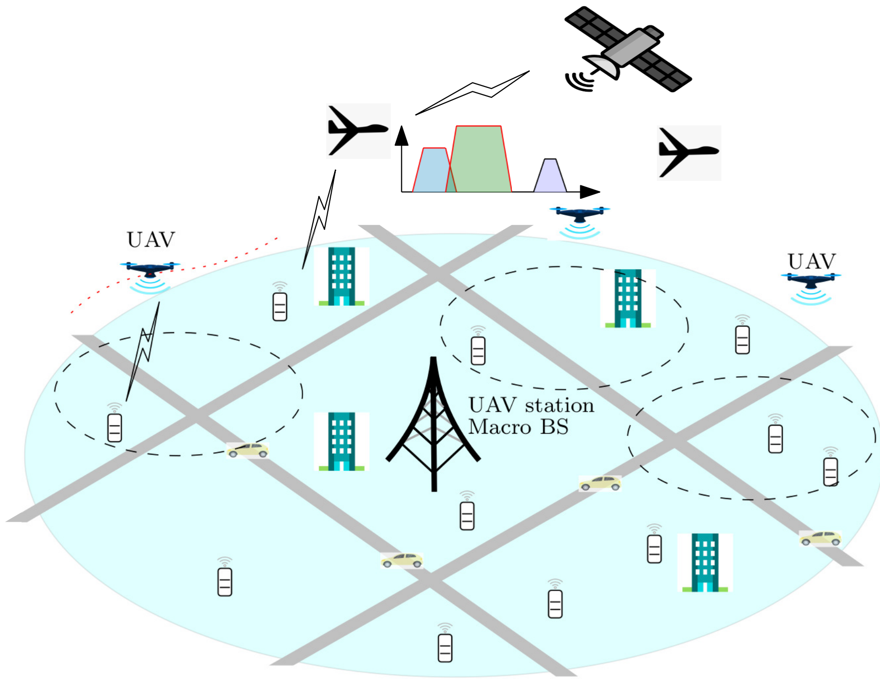

Figure 3.1: Next-generation wireless networks

Among them, UAVs-based communications platforms can provide low-cost solutions for various communications scenarios (e.g., wireless areas with limited infrastructure or high traffic demand) and the UAV-based wireless networks (called UWNs hereafter) offer extra degrees of freedom to optimize the underlying wireless network to enhance the coverage, throughput, and energy efficiency thanks to unique UAV's attributes such as mobility, flexibility, and controllable altitude. With appropriate deployment, UAV-based communications can provide favorable Line-of-Sight (LoS) communications channels [14] for ground users. UAV communications can also be leveraged to enhance the communications quality of wireless cellular networks and to support various Internet of Thing (IoT) applications such as data dissemination or data collection [15]. Therefore, UWNs are expected to play an important role in 5G and beyond-5G wireless systems [16].

In this dissertation, our main objective is to develop interference and resource management techniques for next-generation wireless networks where various aerial components are leveraged to effectively support different applications with diverse QoS requirements. We illustrate the wireless networks considered in our research in Fig. 3.1. In the following, we discuss motivations for our research, the involved research challenges, then we perform literature survey for the considered research issues and summarize key contributions of this dissertation.

3.1.1 Spectrum and Interference Management, and Non-Orthogonal Multiple Access

Exploiting different frequency bands and improving the spectrum efficiency are two critical directions to fundamentally enhance the wireless network capacity and performance. In particular, several under-explored frequency bands such as those above 6Ghz have been under study for 5G wireless networks recently. For example, from [4], 5G New Radio and NB-IoT are designed to operate in several frequency bands from n1 to n96 in frequency range 1 (FR1) and some other operating bands in frequency range 2 (FR2) (please refer to [4], section 5 for more details). Note that the minimum guard-bands defined in [4] are larger than those defined in LTE [5] for the same values of channel bandwidth. This is to mitigate the negative effects of unwanted out-of-band emissions, or adjacent channel interference. However, from the spectrum efficiency perspective, it is desirable to squeeze the guard-bands, or even allow simultaneous data transmission/reception on overlapping bands, and apply advanced interference cancellation techniques to manage the interference such as in the case of Full Duplex (FD) radios [6]. Furthermore, future wireless networks must support different applications with diverse requirements in terms of data rates; therefore, communication signals generated by different applications can require different communication bandwidths. In general, developing advanced interference management techniques for concurrent communications over adjacent and overlapping frequency bands is challenging and it requires much further research [7].

Another promising approach to enhance the spectrum efficiency is to employ advanced Non-Orthogonal Multiple Access (NOMA) strategies [8]. Specifically, NOMA enables wireless networks to serve multiple users using the same resource in time, frequency, or space. In fact, NOMA has shown to have various advantages from the information theory perspective [9]. Moreover, NOMA is also more energy efficient than the conventional Orthogonal Multiple Access (OMA) [10] under various settings. To realize NOMA, successive interference cancellation (SIC) is typically employed to decode the intended messages while effectively mitigating the interference [11]. However, the SIC process increases the complexity of receivers. Moreover, one must perform user grouping to determine users using the same resource and optimize the resource allocation to further optimize the network performance. Therefore, much further research for NOMA is needed before the technology is ready for practical deployment.

3.1.2 UAV Communications

There has been strong interest in providing wireless coverage in the 3D space and leveraging different flying platforms to enhance wireless connectivity and/or the performance of the terrestrial wireless networks. In 2018, 3GPP considered UAVs as a new type of user equipment (UE) in cellular networks in their study item [33]. Recent research has taken a step further when considering UAVs as flying base stations [12,34]. Various studies [16,35,36] have showed that UAV communications can be employed to improve system performances such as coverage, throughput, and energy efficiency. Specifically, UAVs's flying trajectories can be efficiently controlled and optimized to provide reliable and line of sight (LoS) wireless connectivity for ground users. Moreover, a sufficiently large number of UAVs should be deployed and adjusted to cope with dynamic traffic [37]. Joint optimization of the UAVs' trajectories and resource allocation allows to potentially support more users with limited radio resources, which is highly desirable in various application scenarios such as massive connectivity and data dissemination for internet of things (IoTs).

The number of IoT devices has been increasing rapidly in recent years [3] together with many new applications. Energy-efficient design for IoT networks is very important because it helps elongate working durations of IoT devices and networks [38]. Energy-efficient deployment of fixed base stations can be challenging in certain scenarios such as remote areas with limited infrastructure or disaster response and recovery. Some recent works [39–41] show that UAV communications can provide promising solutions to improve the energy efficiency of IoT wireless networks. Succinctly, efficient design of UAVs' trajectories or placement can enable to achieve LoS communications between the IoT devices and UAVs, which significantly improve the energy efficiency of the IoT devices and networks. However, joint design of resource allocation and multi-UAV trajectories to optimize the energy efficiency still requires further research.

3.2 Research Challenges

3.2.1 Advanced Interference Cancellation in Different Scenarios

Interference occurs in many practical network deployment scenarios when the spectrum is reused over time, space, and code domains. To mitigate the negative impacts of interference to the communication quality and network performance, effective interference management and cancellation are critical tasks in network design. Different interference scenarios require different management and cancellation techniques. In particular, interference management becomes difficult to address when interference occurs between concurrent communications on adjacent/overlapping channels in the fast fading environment where channel estimation and interference cancellation must be jointly performed.

Several advanced interference cancellation techniques have been developed for In-Band Full-Duplex (IBFD) communications to effectively mitigate the strong self-interference. Specifically, a combination of various interference management and cancellation strategies spanning over the propagation, analog, and digital domains can be employed to achieve desirable interference cancellation performance [42–44]. Digital interference cancellation for the more general scenario where the interfering and desired signals have different bandwidths have been considered in the past [45–47]. This interference scenario is difficult to tackle since certain weights of interfering symbols (called equivalent interference coefficients (EIC) [48]) must be derived to perform the interference cancellation and symbol detection tasks. However, the EICs change from symbol to symbol; therefore, the derivations of these coefficients are quite involved. Because of these challenges, most existing interference cancellation strategies for concurrent communications on overlapping bands with different bandwidths [45] assume perfect channel state information (CSI) and/or synchronization between the underlying communications, which is hard to realize in the fast fading environment. Moreover, channel estimation techniques developed for the fast fading environment may not be reliable in the presence of strong interference. Therefore, joint design of interference cancellation and channel estimation that can effectively cope with a strong interfering signal having different bandwidth with that of the desired signal in the fast fading environment is a challenging problem that needs further study.

3.2.2 Joint UAV Deployment, Control, and Resource Allocation

The joint optimization of UAV deployment or control (e.g., UAV placement or trajectory control) and resource allocation often results in optimization problems in the form of Mixed-Integer Nonlinear Program (MINLP). In general, it is non-trivial to develop an efficient algorithm to solve these MINLP problems. Several existing works in the literature (e.g., [29, 49–52], to name a few), propose to solve these MINLP problems by using a *heuristic/non-iterative multi-step* strategy [29, 52] or an *iterative Block Coordinate Descent (BCD)* method [49, 51], where the variable set is decomposed into smaller sets (e.g., variables related to bandwidth, power allocation, UAVs' locations), then, individual sets of variables are solved iteratively in the corresponding subproblems given the values of other variables until convergence. Among these approaches, the BCD-based approaches are numerically efficient and they typically result in high-quality solutions since the objective function's value can be improved over iterations.

In some cases, non-trivial problem transformations must be performed before the BCD-based method can be applied to tackle underlying optimization problems. This is the case for the joint resource allocation and UAV deployment/control optimization problems where the objective functions do not directly depend on all optimization variables. For example, when the design objectives are to minimize the total energy consumption, or to maximize the number of admitted users, the objective function contains only a sub-set of all optimization variables. In fact, subproblems that solve for variables that are not present in the objective function are just feasibility verification problems. However, solving feasibility checking problems does not improve the objective function over iterations. This explains why further analysis and transformations are required before the BCD-based method can be applied.

The joint design sometime requires to solve optimization problems where the objective function contains only integer variables. Since the objective functions in these problems may be non-differentiable, employment of BCD-based methods can lead to to inefficient solutions [53]. Furthermore, most existing designs employ the branch-and-bound method to solve MILP sub-problems which has non-polynomial complexity [54].

3.2.3 NOMA Employment in UAV-based Wireless Networks

Employment of NOMA in UAV-based wireless networks can potentially enhance the achievable performance; however, such the employment introduces additional challenges besides those discussed in the previous section. One important problem relates to the joint optimization of NOMA user grouping/paring and UAV placement/control where NOMA grouping design must decide groups of users sharing the same resource and NOMA pairing is the special case where two users share the same resource. The NOMA user paring/grouping design involves optimization of binary variables (i.e. combinatorial characteristics), which is, therefore, challenging to tackle.

Though the NOMA user pairing problem has been studied under various circumstances in the conventional network with fixed deployment of base stations [55–57]. The NOMA user pairing problem in the UAV-based wireless network is more complicated to address because the mobility of UAVs renders the channel conditions being dependent on UAV locations, which need to be optimized. Succinctly, the joint optimization of NOMA user paring and UAV placement/control results in MINLP problems which are difficult to solve in general.

Most previous works either consider joint optimization of NOMA user pairing and *i)* multi-UAV placement [50–52, 58–61] or *ii)* single-UAV trajectory [29, 41, 62, 63]. To leverage the full benefits of UAV's mobility, joint optimization of NOMA user pairing and multi-UAV trajectories should be considered. In the multi-UAV setting, user-UAV associations are also optimization variables where the wireless channels between users and their associated UAVs strongly depend on the association decisions. Furthermore, there is strong coupling between integer optimization variables relating to user pairing variables and user-UAV association variables since users in a same pair should be associated with the same UAV.

3.3 Literature Review

In the following, we survey existing literature on the research issues considered in this dissertation. First, we describe the existing works on interference cancellation and channel estimation for different scenarios in section 3.3.1. Then, we survey the researches on joint resource allocation and UAV deployment in section 3.3.2 Finally, we discuss the research works on energy-efficient design in NOMA-enabled UAV-based wireless networks in section 3.3.4.

3.3.1 Interference Cancellation and Channel Estimation

In IBFD communications, wireless devices transmit and receive signals simultaneously over the same frequency band. Thus, there is strong interference caused by the transmitter to the receiver of the same device. This interference is called *self interference* (or just *interference* when there is no ambiguity) that must be canceled effectively to achieve the throughput gain of IBFD communications with respect to half-duplex communications. Various self-interference cancellation techniques for IBFD have been developed over the past years which can be categorized into cancellation techniques in propagation, analog, and digital domains [44]. In the propagation domain, one can exploit certain characteristics of electromagnetic signals to passively [64–73] or actively [74–76] mitigate the effects of self interference, while an IBFD interference cancellation strategy in the analog domain typically generates an analog signal that can negate the self interference signal [42, 77–80].

Several IBFD interference cancellation techniques to cancel residual interference in the digital domain are also proposed in the literature [81–84]. When using combination of different interference cancellation strategies from the three domains, a full-duplex (FD) receiver can usually achieve sufficient cancellation performance (from 100 to 120dB in suppression of self interference signal) [43, 44, 77, 85–89].

Note, however, that FD communication possesses a special interference structure where the interfering and interfered signals have the same bandwidth and symbol rate. This interference structure allows more tractable designs of interference cancellation techniques, especially in the digital domain [81, 82]. Interference cancellation in a more general scenario where the interfering and interfered signals have different bandwidths is more challenging to tackle. In fact, this interfering scenario can occur in both terrestrial communications [46] and satellite communications [17, 18]. Only a few research works [45, 90, 91] have studied this interference scenario. However, the interference cancellation techniques developed in these works assume perfect channel state information and/or synchronization between the underlying communications.

Channel estimation for the fast fading environment [92] has been studied quite extensively in the literature [27, 93–117]. In particular, various channel estimation strategies have been developed for single-carrier systems [27, 95–97, 99, 101, 103], and for multi-carrier systems [98, 100, 104–117], to name a few notable works. Specifically, super-imposed or interleaved pilot frame structures are usually used to enable joint channel estimation and data detection. Moreover, channel estimation can be performed jointly and iteratively with data detection and channel decoding to achieve desirable performances [97, 99]. Among the aforementioned works, some of them address the joint channel estimation and interference mitigation in Orthogonal Frequency Division Multiplexing (OFDM) systems [100, 113–117] or single carrier settings [96, 101, 103]. The designs of these joint channel estimation and interference mitigation algorithms are crucially facilitated by certain favorable assumptions about the interference. In particular, the considered inter-channel interference (ICI) in the OFDM system and the interfering signals in [96,101,103] all have the same bandwidth and symbol rate with those of the desired signals. In addition, the interfering signal considered in previous works is mostly assumed to have similar or smaller power than that of the desired signal. In severe interference scenarios (e.g., full-duplex self interference), the interference should be canceled before the channel estimation can be performed.

In summary, joint interference cancellation and channel estimation has been studied quite extensively in the past mostly for the scenario where the interfering and interfered signals have the same bandwidth. However, joint channel estimation, interference cancellation, and symbol detection for the more general setting in which two un-synchronized communications over overlapping channels of different bandwidths in the fast fading environment has been under-explored and this scenario deserves further detailed study.

3.3.2 UAV Deployment/Control and Resource Allocation

In this section, we provide a brief review of existing research on UAV deployment/control and resource allocation for UAV-based wireless networks. The survey will group the works according to their considered network settings, design objectives, and approaches. Moreover, we focus on research studies in which UAVs act as flying base stations providing wireless connectivity to ground users. We would like to refer the reader to recent surveys [118–120] for other use cases and design settings. For the topics considered in this dissertation, there are some existing surveys [12,16,121] discussing relevant performance analysis, modeling, and optimization issues in UAV-based wireless networks.

For the performance analysis and modeling fronts, there have been several studies on UAV-to-ground channel models [122,123] and ergodic/outage performance analysis [124–140] under different settings. These research works provide fundamental understanding of the achievable performance of UWNs, which would be useful for other studies on the network optimization.

In general, the spatial and temporal flexibility of UAVs make the deployment optimization for UWNs different from that for conventional wireless networks with fixed base stations. In particular, optimizations of UAV deployment can be divided into two categories, namely UAV placement and UAV trajectory optimization. While researches on UAV placement aim to determine locations for UAVs to optimize certain objectives [50–52, 58–61, 141], researches on UAV trajectory optimizations exploit the mobility of UAVs to further improve the system performance [29, 41, 62, 63, 142, 143].

Existing research studies on the optimization of UWNs consider different design objectives related to throughput, flight time, coverage, user admission, and energy efficiency. In particular, joint optimization of resource allocation and UAVs' trajectories is considered in [144] and [145–147] for throughput and common throughput[1] maximization, respectively. On the other hand, the authors in [148] consider maximizing the UAV hovering time while flight time is minimized in [40, 149, 150] for different network scenarios. Moreover, wireless coverage optimization is studied in [151, 152] and admission maximization problems for UWNs are investigated in [35, 153]. Finally, energy-efficient designs for UWNs are addressed in [36, 39, 57, 62, 142, 143, 154–160] which consider both communication and propulsion energy consumptions. Mathematically, optimization problems that arise in these joint resource allocation and UAV deployment optimizations are usually nonconvex optimization problems and even MINLP in some cases. To tackle these optimization problems, different solution approaches including non-iterative multi-step algorithms, iterative block coordinate descent (BCD) method are employed.

The above review suggests that even though the joint optimization of resource allocation and UAV deployment/control has been an active research topic, only a few notable works consider the admission control problem. In particular, the works in [35, 153], tackle the placement optimization of a single UAV and it is not trivial to extend the proposed designs to the multi-UAV setting. Moreover, one may not be able to directly apply the BCD method to solve an optimization problem if its objective function contains a single type of optimization variables (e.g., admission control variables, or transmit power allocation variables,...).

[1] 'Throughput' refers to the sum rate of all users while 'common throughput' is the minimum of the data rates of all users.

3.3.3 Non-Orthogonal Multiple Access

Research on Non-Orthogonal Multiple Access (NOMA) [8] has been attracting a great deal of attention over the past ten years.[2] It has been shown that NOMA can greatly outperform conventional Orthogonal Multiple-Access (OMA) schemes in terms of throughput and energy efficiency under various settings [9, 10]. Recent surveys [162, 163] categorize NOMA schemes into two main groups: code-based NOMA (code domain multiplexing) and power-based NOMA (power domain multiplexing). While the code-based NOMA schemes assign different users with different codes, users are allocated different power levels based on their channel conditions in the power-based NOMA schemes. Then, the multiplexed signals are transmitted using the same resource. At the receiver, successive interference cancellation (SIC) is used to decode and then cancel interference from unintended users so that the message of an intended user can be decoded reliably.[3]

Furthermore, multiple-input-multiple-output (MIMO) communications and NOMA can be jointly employed to further enhance the achievable spectral efficiency [168, 169]. In this dissertation, we focus on the single-input-single-output (SISO) NOMA setting, which is more suitable for practical implementation on UAV-mounted base stations. Moreover, we also focus on power-based NOMA schemes whose information-theoretic insights have been studied in [9, 10]. The following literature survey is conducted for this specific class of power-based NOMA schemes.

Many recent research works study different optimization aspects of NOMA. In particular, throughput maximization and performance analysis are studied for the downlink NOMA communications in [170–173] and uplink communications in [170, 174]. Moreover, energy efficiency or power consumption based optimization problems for NOMA are studied in [55–57]. Particularly, the authors in [55] prove the NP-hardness of user grouping problem for downlink power minimization, and employ the heuristic approach to solve the underlying problem. When each NOMA group has 2 users (i.e., user pairing problem), the authors in [56] show that the optimal solution for down-

[2] Although NOMA generally refers to any communication schemes where multiple users transmit/receiver signals over a non-orthogonal resource. While the non-orthogonal transmission concept has been studied before 2013 (e.g., [161]), it has been observed that research NOMA has received significantly higher attention after the work [8] was published.

[3] For code-based NOMA, the separation created by using different codes could be sufficient so the receiver may not need to decode and then subtract the message of unintended users. There are various code-based NOMA schemes, some notable schemes are described in [164–166]. Detailed discussions of different code-based NOMA schemes for different communication directions (uplink, downlink) and network settings can be found in recent surveys [162, 167].

link power minimization can be obtained by an efficient algorithm. Finally, energy-efficient user association and power allocation for uplink hybrid NOMA-OMA is studied in [57].

It has been shown in several existing works that even though the general NOMA user grouping (i.e., more than 2 users in each NOMA group) may provide some performance benefits, much higher computational complexity is required for the SIC-based decoding process. These drawbacks hinder the application of large NOMA groups in practice [162]. Because of this, we focus on the NOMA user pairing design in this dissertation. Additionally, though these research works provide some fundamental understanding and address various design aspects of NOMA such as user pairing/grouping and power allocation, further efforts are needed to employ NOMA in UAV-based wireless networks.

3.3.4 NOMA in UAV-based Wireless Networks

Employment of NOMA in UWMs is quite natural since the NOMA performance can be greatly enhanced when different users have different channel conditions [163, 169], which can be strategically controlled by optimizing the UAVs' positions or trajectories. Therefore, there have been growing interests in engineering NOMA-enabled UWNs. In particular, resource allocation optimization problems to maximize the system throughput of UAV-based wireless networks in uplink and downlink scenarios are considered in [52, 141], respectively. Maximization of the minimum achievable rate of ground users in the downlink NOMA communications is studied in [175] by optimizing the UAV trajectory, transmit power allocation, and user association. Moreover, the work in [41] considers the minimization of UAV's flight time for the data collection task where device NOMA scheduling, transmit power allocation, and UAVs' locations are optimized.

In energy-efficient designs, the work in [29] minimizes the total energy consumption of ground devices by jointly performing user pairing and single UAV's trajectory optimization for data collection tasks. Recently, the authors in [59] study a power minimization problem in a wireless network where a single UAV is deployed to assist a base station in ensuring the required Quality of Service (QoS) of users. Moreover, an energy minimization problem is considered in [142] for the multi-UAV setting; however, each user is assumed to communicate with all the UAVs concurrently using fixed bandwidths, which may not best exploit the benefits created by UAV's mobility. Note that when all users are clustered into a single NOMA group, the decoding complexity can increase and the reliability of the SIC process can decrease significantly [162, 176]. In summary, most previous research works either consider NOMA user pairing and multi-UAV placement [51, 52, 58–61] or single-UAV trajectory optimization [29, 41, 62, 63]. To further elevate the benefits of UAV's mobility, joint optimization of NOMA user pairing and multi-UAV trajectories should be studied. This is indeed performed in this dissertation.

3.4 Research Objectives and Contributions

The general objective of my Ph.D research is to develop novel interference and resource management strategies for future wireless networks. Specifically, its main contributions can be summarized as follows:

1. *Interference cancellation, channel estimation, and symbol detection for communications on overlapping channels*:

   We consider the joint interference cancellation, fast fading channel estimation, and data symbol detection design for a general interference setting where the interfering source and the interfered receiver are un-synchronized and their communications occur over overlapping channels of different bandwidths. First, we construct a two-phase framework where the Effective Interference Coefficients (EICs) and desired channel coefficients are estimated by using the joint maximum likelihood-maximum a posteriori probability (JML-MAP) criteria in the first phase; and the MAP based data symbol detection is performed in the second phase. Based on this two-phase framework, we propose an iterative algorithm for interference cancellation, channel estimation, and data detection. We analyze the channel estimation error, residual interference, symbol error rate (SER) achieved by the proposed design. We then discuss how to optimize the pilot density to achieve the maximum throughput. Via numerical studies, we show that our design can effectively mitigate the interference for a wide range of SNR values, our proposed channel estimation and symbol detection design can achieve better performances compared to an existing method. Moreover, we demonstrate the improved performance of the iterative algorithm with respect to the non-iterative counterpart.

2. *Resource allocation, trajectory optimization, and admission control in UAV-based wireless networks*:

We study the resource allocation, trajectory optimization, and admission control for the multi-UAV based wireless networks. Our design maximizes the number of admitted users while satisfying their data transmission demands. We formulate an admission maximization problem which is an MINLP problem. Then, we introduce soft admission variables and propose an iterative algorithm to solve this problem where each iteration comprises two steps, namely soft admission maximization and user removal. Our method guarantees that the number of admitted users increases over iterations. Numerical results show that our algorithm outperforms the conventional scheme based on block coordinate ascent and mixed-integer linear programming.

3. *Multi-UAV trajectories and NOMA user pairing optimization for energy minimization*:

   We consider the energy minimization problem in multi-UAV based wireless networks, where NOMA is employed for uplink communications. Our design aims to minimize the total energy consumption of ground devices (users) while users are guaranteed to successfully transmit their data to the UAV-mounted base stations. Toward this end, we consider optimizing the transmit power, NOMA user pairing, user-UAV association, and multi-UAV trajectories. The formulation results in a mixed-integer nonlinear programming (MINLP) problem which is difficult to solve optimally. We then propose an iterative three-step algorithm to solve the problem. In the first step, we optimize transmit powers, NOMA pairing, and user association given the UAV trajectories and users' data rates. Even though the problem is an MINLP, we are able to solve it optimally by exploiting its special structure. In the second step, the users' data rates at each time slot are optimized given the other parameters while the UAV trajectory optimization is performed in the third step. Numerical results show that our proposed algorithm can provide better active-inactive schedules and lower energy consumption compared to an existing technique, and a OMA-based resource allocation and UAV-trajectory optimization strategy.

3.5 Dissertation Outline

The remaining of this dissertation is organized as follows. Chapter 4 reviews some fundamental background about mathematical optimization, NOMA, and UAV-based wireless networks. Chapter 5 covers our study about joint interference cancellation, channel estimation, and data symbol detection for concurrent communications over overlapping channels. Then, we study the resource allocation and trajectory optimization for admission maximization in multi-UAV based wireless networks in Chapter 6. Finally, we present our study on NOMA user pairing, resource allocation, and multi-UAV trajectory optimization in Chapter 7. The main contributions of the dissertation and some potential direction for future research are discussed in Chapter 8.

Chapter 4

Background

In this chapter, we present some fundamentals of mathematical optimization, NOMA, and UAV communications. Particularly, basic concepts of mathematical optimization and some popular techniques to solve optimization problems are introduced in section 4.1 while we present working principles of NOMA and UAV communications in section 4.2 and section, respectively.

4.1 Mathematical Optimization

4.1.1 Fundamental Concepts

A mathematical optimization problem can be written in the following form [30]

$$\begin{aligned} \underset{\mathbf{x}}{\text{minimize}} \quad & f_0(\mathbf{x}), \\ \text{subject to} \quad & f_i(\mathbf{x}) \leq 0, \quad i = 1, 2, ..., m, \end{aligned} \tag{4.1}$$

where the vector $\mathbf{x} \in \mathbb{R}^n$ is the *optimization variable*, and $f_0(\mathbf{x})$ is the *objective function*. The inequalities $f_i(\mathbf{x}) \leq 0,\ i = 1, 2, ..., m$ are the *constraints* of the problem. Let $\mathcal{D}$ be the intersection of the domains of $f_i(\mathbf{x}),\ i = 0, 1, ..., m$, the *feasible set* of the problem is the set of all $\mathbf{x} \in \mathcal{D}$ that satisfies all these m constraints. A vector $\mathbf{x}^*$ is called *optimal*, or *optimal solution*, of the problem if $f_0(\mathbf{x}^*)$ achieves the smallest value among all values of $f_0(\mathbf{x})$ where $\mathbf{x}$ belongs to the feasible set, and the value of $f_0(\mathbf{x}^*)$ is called *optimal value*. If the feasible set is empty, the problem is *infeasible*.

Conventionally, the optimal value of the problem is $+\infty$ if the problem is infeasible [30]. Hereafter, the term 'subject to' is written as 's.t.'.

4.1.2 Convex Optimization

Among many classes of optimization problems, convex optimization problems are of particular interest. First, it is a fundamental property of convex optimization problems that any locally optimal point is also globally optimal. Hence, compared to a generic optimization problem, it is generally easier to solve a convex optimization problem as one only needs to find a local optimal solution. Second, many sub-classes of convex optimization problems are well-studied, and the technologies to solve most of problems in these sub-classes are mature and can be deployed in many applications. In the following sections, some fundamentals of convex optimization are briefly introduced.

Convex set: A set S is convex if for any vectors $\mathbf{x}, \mathbf{y} \in S$, the following holds for any value of θ where $\theta \in [0, 1]$

$$\theta \mathbf{x} + (1 - \theta)\mathbf{y} \in S. \tag{4.2}$$

Convex function: A function $f : \mathbb{R}^n \to \mathbb{R}$ is convex if its domain (denoted as $\mathcal{D}$) is a convex set and the following inequality holds for any $\mathbf{x}, \mathbf{y} \in \mathcal{D}$ and any $\theta \in [0, 1]$

$$f\left(\theta \mathbf{x} + (1 - \theta)\mathbf{y}\right) \leq \theta f(\mathbf{x}) + (1 - \theta) f(\mathbf{y}). \tag{4.3}$$

Convex optimization problem: An optimization problem is convex if it can be written in the following form

$$\begin{aligned} \underset{\mathbf{x}}{\text{minimize}} \quad & f_0(\mathbf{x}) \\ \text{s. t.} \quad & f_i(\mathbf{x}) \leq 0, \quad i = 1, ..., m, \\ & h_j(\mathbf{x}) = 0, \quad j = 1, ..., p, \end{aligned} \tag{4.4}$$

where the functions $f_i, \; i = 0, 1, ..., m$, are convex and the functions $h_j, \; j = 1, ..., p$ are linear. Convex optimization problems can be called 'convex problems' for short.

4.1.3 Methods to Solve Optimization Problems

It is known that there is no efficient methods that can find a global solution of a generic nonconvex optimization problem in polynomial time [30]. However, various methods that can solve some classes of convex optimization problems with desired accuracy and in polynomial time with respect to the problem dimensions have been developed and used for decades [177, 178]. Particularly, the interior-point (or barrier) methods are currently considered the most powerful algorithms for large-scale problems. The interior-point methods are already used in many optimization solvers. For brevity, we do not intend to go into details about these methods. Interested readers are encouraged to read [30, 179] where many rigorous definitions of mathematical optimization and solving techniques are presented in details. Furthermore, since available solvers already do a decent job in solving popularly encountered convex problems, we use them to solve convex problems that arise in our research, rather than developing specific numerical methods. In particular, we use the CVX [180] on Matlab to solve convex problems in our research where the underlying solver is Mosek academic version [181]. That being said, several formulated problems arising in our studies are nonconvex, so techniques other than interior-point methods have to be devised to tackle them. In this dissertation, two main techniques that we use to find sub-optimal solutions of the formulated nonconvex problems are Block Coordinate Descent (BCD) and Successive Convex Approximation (SCA) where a nonconvex problem is solved sub-optimally by iteratively solving a series of convex optimization problems. Details of these techniques are presented in the following.

4.1.3.1 Block Coordinate Descent

First, let us consider an optimization problem as follows:

$$\begin{aligned} \mathcal{P}: \quad \underset{\mathbf{x}}{\text{minimize}} \quad & f_0(\mathbf{x}), \\ \text{s.t.} \quad & f_i(\mathbf{x}) \leq 0, \quad i = 1, 2, ..., m, \end{aligned} \tag{4.5}$$

A widely used approach for solving the optimization problem in (4.5) is the block coordinate descent (BCD). In this approach, the optimization variable set $\mathbf{x}$ is split into smaller blocks (subsets) of variables, i.e., $\mathbf{x} = [\mathbf{x}_1, \mathbf{x}_2, ..., \mathbf{x}_b]$, where $\mathbf{x}_i, i = 1, ..., b$ are vectors who together form $\mathbf{x}$. Note that $\mathbf{x}_i$ can have more than one dimension. The BCD method is an iterative method where at each iteration[1], the variable blocks are optimized sequentially[2] and when a particular variable block is optimized, other blocks are fixed. Let $\mathcal{P}_i$ be the optimization problem at iteration r where $f_0(\mathbf{x}_1^r, ..., \mathbf{x}_{i-1}^r, \mathbf{x}_i, \mathbf{x}_{i+1}^{r-1} ..., \mathbf{x}_b^{r-1})$ is optimized with respect to $\mathbf{x}_i$, while other variables are fixed, we illustrate a typical BCD algorithm in Algorithm 4.1.

Algorithm 4.1. Typical BCD algorithm

```
Initiate [x_1^0, x_2^0, ..., x_b^0] and r = 1
while 1 do
    for i=1,2,...,b do
        Solve problem P_i, update x_i^r by the obtained solution.
    end for
    if f_0(x_1^{r-1}, ..., x_b^{r-1}) - f_0(x_1^r, ..., x_b^r) ≤ ϵ then
        Break the loop.
    else
        Let r = r + 1.
    end if
end while
End of algorithm.
```

Where ϵ is the desired accuracy. Because the BCD algorithms are simple and have good scalability, they have been widely applied in many fields, e.g., resource allocation in wireless communication systems [144], or image classification in computer vision [183]. In this dissertation, we apply the BCD method to solve resource allocation problems in UWNs in chapters 6 and 7.

4.1.3.2 Successive Convex Approximation

The BCD method is widely used to solve optimization problem by dividing the original problem into subproblems and solve them iteratively. However, in many cases, as one attempts to apply the BCD method to tackle a complex nonconvex problem, some corresponding subproblems are also nonconvex. Fortunately, there are approaches to tackle the nonconvexity of optimization problems. We will describe one popular approach in this regard which is the Successive Convex Approximation (SCA) method. In the SCA method, nonconvex functions are approximated by convex functions and the resulting approximated convex problem is solved iteratively until convergence. In this iterative

[1] Definitions of an iteration may vary depending on the referred literature. In this work, an iteration in a BCD algorithm ends where all of the variable blocks are updated. This aligns with popular conventions in the literature.

[2] We note that there are many ways to choose the updating order of the blocks. Some popular choice of orders are cyclic (Gauss-Seidel), greedy (Gauss-Southwell), or randomized [182]. The choice of orders depends on particular applications and no choice has been proved to have notably advantages over other choices. In this work, we use Gauss-Seidel (cyclic) updating order.

process, the solution obtained in each iteration is used in the new approximations of the objective and constraint functions in the next iteration.

Consider the following nonconvex optimization problem

$$\begin{aligned} \mathcal{P}: \quad & \underset{\mathbf{x}}{\text{minimize}} \quad f_0(\mathbf{x}), \\ & \text{s.t.} \quad f_i(\mathbf{x}) \leq 0, \quad i = 1, 2, ..., m. \end{aligned} \tag{4.6}$$

Assume that the local point $\mathbf{x}^r$ is given, in iteration $r+1$, the SCA method approximates functions $f_i(\mathbf{x})$ by $\tilde{f}_i(\mathbf{x}|\mathbf{x}^r)$ and solves the following approximated optimization problem

$$\begin{aligned} \mathcal{P}^{r+1}: \quad & \underset{\mathbf{x}}{\text{minimize}} \quad \tilde{f}_0(\mathbf{x}|\mathbf{x}^r), \\ & \text{s.t.} \quad \tilde{f}_i(\mathbf{x}|\mathbf{x}^r) \leq 0, \quad i = 1, 2, ..., m, \end{aligned} \tag{4.7}$$

where the following conditions hold [182]

$$\text{Upper-bound:} \quad \tilde{f}_i(\mathbf{x}|\mathbf{x}^r) \geq f_i(\mathbf{x}), \tag{4.8a}$$

$$\text{Function value consistency:} \quad \tilde{f}_i(\mathbf{x}^r|\mathbf{x}^r) = f_i(\mathbf{x}^r), \tag{4.8b}$$

$$\text{Gradient consistency:} \quad \nabla\tilde{f}_i(\mathbf{x}^r|\mathbf{x}^r) = \nabla f_i(\mathbf{x}^r), \tag{4.8c}$$

$$\text{Convexity:} \quad \tilde{f}_i(\mathbf{x}|\mathbf{x}^r) \text{ is convex with respect to } \mathbf{x}. \tag{4.8d}$$

These conditions guarantee that in each iteration, an original function is approximated by a upper-bound whose first order derivative is equal to that of the original function. The typical SCA based algorithm to solve problem $\mathcal{P}$ is described in Table 4.2.

Algorithm 4.2. Typical SCA algorithm

Initiate $\mathbf{x}$ by a feasible $\mathbf{x}^0$ and set $r = 0$
while 1 **do**
  Solve problem $\mathcal{P}^{r+1}$, update $\mathbf{x}^r$ by the obtained solution.
  if Convergence condition is met **then**
    Break the loop.
  else
    Let $r = r + 1$.
  end if
end while
End of algorithm.

4.2 Non-Orthogonal Multiple Access

While there are several variants of NOMA with their own strength and weaknesses, NOMA performances have been studied from the information theoretic perspective [9]. Following the direction of [9], we discuss the power-domain NOMA hereafter. In particular, we present some fundamentals of power-domain NOMA in terms of achievable data rates and corresponding power consumptions. We refer to [163,184] for detailed descriptions of various NOMA schemes. In the following, downlink NOMA is discussed in section 4.2.1 and uplink NOMA is presented in section 4.2.2.

4.2.1 Downlink NOMA

Consider a scenario in which the base station sends messages to two users[3] in the downlink direction by using the same resource block. Let the allocated power and channel power gain of user $i, i = 1, 2$ be p_i and g_i, respectively. Then, the signals received at the receivers of users 1 and 2 can be expressed as follows:

$$\begin{aligned} y_1 &= g_1(\sqrt{p_1}x_1 + \sqrt{p_2}x_2) + n_1, \\ y_2 &= g_2(\sqrt{p_1}x_1 + \sqrt{p_2}x_2) + n_2, \end{aligned} \tag{4.9}$$

where n_i denotes the thermal noise and x_1, x_2 are the unity-power signals intended for users 1 and 2, respectively. Let $h_i = |g_i|^2, i = 1, 2$ denote the channel power gains of users 1 and 2, respectively. Without loss of generality, we assume that user 1 has better channel condition than that of user 2[4] (i.e., $h_1 > h_2$). In downlink NOMA, the user with better channel condition is allocated less power than the user with worse channel condition, i.e., $p_1 < p_2$. At the receiver of user 2, the received power of user 2's message is $h_2 p_2$ which is larger than the received power of user 1's message ($h_2 p_1$). Moreover, user 2 treats user 1's message as noise and tries to decode its own message. Thus, the achievable rate of user 2 can be expressed as follows:

$$r_2 = B \log\left(1 + \frac{h_2 p_2}{h_2 p_1 + \sigma^2}\right), \tag{4.10}$$

[3]Even though NOMA can be applied for more than two users, the high complexity of the SIC process hinders the practicality of large NOMA groups, as discussed in section 3.3.3. Therefore, the majority of papers in this topic focuses on the 2-user NOMA scenario, which is referred to as 2-NOMA in the following.

[4]Most works in the literature, user 1 is called the strong user and user 2 is referred to as the weak user in the considered user pair.

where B is the bandwidth allocated for the user pair, σ^2 is the power of noise n_2 and we assume that n_1 and n_2 have the same power.

At the receiver of user 1, the power of user 2's message is $h_1 p_2$ which is larger than the power of user 1's message ($h_1 p_1$). Therefore, user 1 will decode the message of user 2 first, then subtract the message and decode its own message. Thus, the achievable rate of user 1 can be written as follows:

$$r_1 = B \log \left(1 + \frac{p_1 h_1}{\sigma^2}\right). \tag{4.11}$$

We also note that the frequently used assumption in downlink 2-NOMA is that the message of the weak user can be decoded effectively at the strong user's receiver. This is because the effective achievable rate of the weak user's message at the strong user' receiver is larger than the rate of weak user's message at its own receiver, i.e.,

$$B \log \left(1 + \frac{h_1 p_2}{h_1 p_1 + \sigma^2}\right) \geq B \log \left(1 + \frac{h_2 p_2}{h_2 p_1 + \sigma^2}\right). \tag{4.12}$$

In downlink NOMA, the total power allocated for paired used is limited by the maximum power that the base station can transmit, denoted as P_{max}. Therefore, we have

$$p_1 + p_2 \leq P_{max}. \tag{4.13}$$

This constraint should be considered in NOMA resource allocation optimization.

4.2.2 Uplink NOMA

In uplink NOMA, let us consider users 1 and 2 and assume g_i and p_1 denote user i's channel gain and transmit power, respectively. Moreover, let $h_i = |g_i|^2, i = 1, 2$ denote the channel power gains of users 1 and 2, respectively. Without loss of generality, we assume that user 1 has better channel condition than that of user 2. The received signal at the base station can be expressed as follows:

$$y = g_1 \sqrt{p_1} x_1 + g_2 \sqrt{p_2} x_2 + n, \tag{4.14}$$

where n is the thermal noise which has power of σ^2, x_1, x_2 denote the unity-power messages transmitted from users 1 and 2, respectively. The SIC process will first decode the message of user 1 and subtract this message afterward. Then, the message of user 2 is decoded. Therefore, the achievable rates of users 1 and 2 can be expressed as follows:

$$\begin{aligned} r_1 &= B \log\left(1 + \frac{h_1 p_1}{h_2 p_2 + \sigma^2}\right), \\ r_2 &= B \log\left(1 + \frac{h_2 p_2}{\sigma^2}\right). \end{aligned} \tag{4.15}$$

Different from downlink NOMA, in uplink NOMA, the transmit power of each user is limited by the maximum power of its own device. Therefore we have

$$\begin{aligned} p_1 &\leq P_{max}, \\ p_2 &\leq P_{max}, \end{aligned} \tag{4.16}$$

where we assume that the maximum transmit powers of user 1 and 2 are P_{max}.

4.3 UAV Communications and Networks

In this section, we introduce some fundamental concepts of UAV communications and UAV-based wireless networks. In particular, we present widely adopted channel models in UWNs in section 4.3.1 and typical optimization formulations for UWNs in section 4.3.2.

4.3.1 Channel Models in UAV-based Wireless Networks

Most studies on channel modeling for air-to-ground and ground-to-air communications in UWNs are fairly recent compared to those on channel modeling for the conventional cellular networks. One popular air-to-ground channel model considers a binomial random event in which the LoS and non-line-of-sight (NLoS) communications between the UAV and the ground users occur with certain probabilities [185]. Specifically, these occurrence probabilities depend on the elevation angle, types of communications environment (e.g., urban, sub-urban, rural,...), and the relative locations of the UAV and users. We denote the 2-D coordinate of the considered ground user as $\mathbf{u}$ and the 2-D coordinate of the UAV as $\mathbf{c}$. For convenience, we assume that the ground user has altitude of

0 meters and the UAV has altitude of h meters. Then, the LoS and NLoS probabilities can be calculated as follows:

$$\begin{aligned} P_{LoS} &= \alpha \left(\frac{180}{\pi}\theta - 15 \right)^{\gamma}, \\ P_{NLoS} &= 1 - P_{LoS}, \end{aligned} \tag{4.17}$$

where α and γ are the constants which depend on the communications environment, and θ is the elevation angle that can be calculated as

$$\theta = \tan^{-1} \left(\frac{h}{\|\mathbf{u} - \mathbf{c}\|} \right). \tag{4.18}$$

Moreover, the shadow fading components for the LoS and NLoS links (denoted as ξ_{LoS} and ξ_{NLoS}, respectively) are assumed to follow log-normal distribution, which means their logarithms are normal distribution with mean 0 and variances defined as follows:

$$\begin{aligned} \sigma_{LoS} &= k_{LoS} \exp \left(-g_{LoS}\theta \right), \\ \sigma_{NLoS} &= k_{NLoS} \exp \left(-g_{NLoS}\theta \right), \end{aligned} \tag{4.19}$$

where $k_{LoS}, g_{LoS}, k_{NLoS}$ and g_{NLoS} are positive constants depending on the communications environment. Then, the channel power gains (τ_{LoS}, τ_{NLoS}) can be computed for the LoS and NLoS communications scenarios as follows [185]:

$$\begin{aligned} \tau_{LoS} &= \frac{\zeta}{\xi_{LoS}} \left(\frac{4\pi f_c (h^2 + \|\mathbf{u} - \mathbf{c}\|^2)^{1/2}}{c} \right)^{-\kappa}, \\ \tau_{NLoS} &= \frac{\zeta}{\xi_{NLoS}} \left(\frac{4\pi f_c (h^2 + \|\mathbf{u} - \mathbf{c}\|^2)^{1/2}}{c} \right)^{-\kappa}, \end{aligned} \tag{4.20}$$

where ζ is the constant that accounts for the antenna gain, κ is the free-space path loss exponent, f_c and c are the carrier frequency and the speed of light, respectively.

Even though the above probabilistic channel model accounts for several factors that affect the channel power gain, it can be difficult to estimate the involved constants for different types of communications environment. Moreover, in the multi-UAV based wireless networks, it is natural to associate users with their closest UAVs [34], which would increase the elevation angle θ. Besides, the high elevation angle significantly reduces the effect of shadowing (from (4.19)) and increases the

LoS probability (from (4.17)). Therefore, in multi-UAV deployments with high elevation angles, the air-to-ground channel can be considered effectively LoS. As a result, many research studies in UAV communications have adopted a simplified channel model in which the air-to-ground channel power gain can be expressed as follows:

$$\tau = \mu(h^2 + \|\mathbf{u} - \mathbf{c}\|^2)^{-\kappa/2}, \tag{4.21}$$

where μ is the channel power gain at a reference distance. In fact, μ accounts for the antenna gain ζ and other constants in (4.20).

Despite its simplicity, the channel model in (4.21) and its results can serve as benchmarks and help gain insights about efficient network designs and achievable performance.

4.3.2 Design Optimization in UAV-based Wireless Networks

In this section, we discuss a generic design optimization formulation in UWNs where there are N UAVs communicating with K users in the downlink direction. The service period is divided into T time slots ($t = 1, 2, ..., T$), each having equal length of δ seconds. The slot length δ should be chosen appropriately such that network conditions stay approximately the same during each time slot. We consider a communication system in which users and UAVs communicate via orthogonal resource blocks.[5] Let the channel power gain, bandwidth, and transmit power allocated for user k associated with UAV n in time slot t be $h_{n,k}[t]$, $b_{n,k}[t]$, and $p_{n,k}[t]$, respectively. The achievable data rate of user k associated with UAV n at t, denoted as $r_{n,k}[t]$, can be expressed as follows:

$$r_{n,k}[t] = b_{n,k}[t] \log\left(1 + \frac{h_{n,k}[t]p_{n,k}[t]}{\delta^2 b_{n,k}[t]}\right), \tag{4.22}$$

where δ^2 denotes the white noise power density (W/Hz).

[5] Note that co-channel interference among user-UAV communications can occur and it has been considered in some existing works where non-orthogonal resource blocks are allocated for nearby communication links/users. However, for the introductory purpose of this section, we choose to present a design optimization for an interference-free scenario.

The total transmit power of each UAV, and bandwidth of the system, denoted as B, are limited. Hence, we have the following constraints:

$$\sum_{k=1}^{K} p_{n,k}[t] \leq P_{max}, \quad \forall n, t, \tag{4.23a}$$

$$\sum_{k=1}^{K}\sum_{n=1}^{N} b_{n,k}[t] \leq B, \quad \forall t, \tag{4.23b}$$

where P_{max} is the maximum total power of each UAV.

Let the 3-D coordinate of UAV n in time slot t be $\mathbf{c}_n[t] = (x_n[t], y_n[t], z_n[t])$, the following constraints are usually considered for the UAV's trajectory control:

$$\|\mathbf{c}_n[t] - \mathbf{c}_n[t-1]\| \leq \delta V_{max}, \quad \forall n, t, \tag{4.24a}$$

$$\|\mathbf{c}_n[t] - \mathbf{c}_m[t]\| \geq D_{safe}, \quad \forall n \neq m, t, \tag{4.24b}$$

$$\mathbf{c}_n[1] = \mathbf{c}_{start}, \quad \forall n, \tag{4.24c}$$

$$\mathbf{c}_n[T] = \mathbf{c}_{end}, \quad \forall n, \tag{4.24d}$$

where V_{max} is the maximum speed of a UAV, D_{safe} is the safety distance between any two UAVs to avoid collision, and $\mathbf{c}_{start}$ and $\mathbf{c}_{end}$ are the starting and final positions on the trajectory of a UAV.

A generic resource allocation optimization problem in UWNs can be stated as follows:

$$\begin{aligned} \mathcal{P}: \min_{\{\mathbf{B}[t], \mathbf{P}[t], \mathbf{C}[t]\}} \; & \mathcal{F}, & (4.25a)\\ \text{s.t.} \; & \text{constraints related to } r_{n,k}[t] \text{ in (4.22)}, \\ & \text{constraints (4.23a), (4.23b), (4.24a), (4.24b), (4.24c), (4.24d)}, \end{aligned}$$

where $\mathcal{F}$ is the objective function that depends on the optimization variables, $\mathbf{B}[t], \mathbf{P}[t], \mathbf{C}[t]$ are the matrices of resource allocation variables and the matrix of UAVs' coordinates in time slot t, respectively, and $\{\mathbf{B}[t], \mathbf{P}[t], \mathbf{C}[t]\}$ denotes the set of all optimization variables for all values of t. In the single-UAV setting, we have $N = 1$ and constraints (4.24b) are omitted. Furthermore, there may be more variables and constraints to be added in optimization problems for more complicated designs and network settings.

Optimization problems formulated in UWNs that similar to (4.25a) are usually complicated and non-convex which involves both resource allocation and spatial variables which need to be optimized in each time slot. Solving these types of optimization problems usually requires sophisticated algorithms which are developed specifically to exploit certain structure of the underlying problem. Beside analysis, modeling, and formulations, developing algorithms to solve different design optimization problems is the core part of many existing studies in the literature.

Chapter 5

Interference Cancellation, Channel Estimation, and Symbol Detection for Communications on Overlapping Channels

The content of this chapter was published in the following paper:

Minh Tri Nguyen and Long Bao Le, "Interference Cancellation, Channel Estimation, and Symbol Detection for Communications on Overlapping Channels," *IEEE Access,* vol. 8, pp. 89 822-89 838, May 2020.

5.1 Abstract

In this paper, we propose the joint interference cancellation, fast fading channel estimation, and data symbol detection for a general interference setting where the interfering source and the interfered receiver are unsynchronized and occupy overlapping channels of different bandwidths. The interference must be canceled before the channel estimation and data symbol detection of the desired communication are performed. To this end, we have to estimate the Effective Interference

Coefficients (EICs) and then the desired fast fading channel coefficients. We construct a two-phase framework where the EICs and desired channel coefficients are estimated using the joint maximum likelihood-maximum a posteriori probability (JML-MAP) criteria in the first phase; and the MAP based data symbol detection is performed in the second phase. Based on this two-phase framework, we also propose an iterative algorithm for interference cancellation, channel estimation and data detection. We analyze the channel estimation error, residual interference, symbol error rate (SER) achieved by the proposed framework. We then discuss how to optimize the pilot density to achieve the maximum throughput. Via numerical studies, we show that our design can effectively mitigate the interference for a wide range of SNR values, our proposed channel estimation and symbol detection design can achieve better performances compared to the existing method. Moreover, we demonstrate the improved performance of the iterative algorithm with respect to the non-iterative counterpart.

5.2 Introduction

Traffic demand from wireless networks has been increasing dramatically over the last decades while the spectrum resource is limited. This has motivated the development of efficient and flexible spectrum utilization and sharing techniques. Moreover, future wireless networks are expected to support a massive number of connections to enable many emerging applications requiring diverse communication rates and qualities of service [186]. Therefore, effective spectrum reuses using robust interference cancellation and management are essential in maintaining and enhancing the communication rates and reliability in next-generation wireless systems [187]. In particular, future wireless systems must be able to support different applications and use cases, e.g., highly mobile scenarios in which users move at high speeds (up to 500 km/hr) [188–190]. Thus, developing wireless communication techniques for high mobility environments is of high importance and has attracted increasing research attention [191–193].

Non-Orthogonal Multiple Access (NOMA) [194] and Full Duplex (FD) communication [6] are among the advanced frequency reuse techniques. In NOMA, signals from different sources are allowed to be transmitted simultaneously over the same channel, and successive interference cancellation is typically employed to decode these messages. Moreover, a FD transceiver allows to transmit and receive at the same time over the same channel, thus, the receiver experiences severe self-interference from the transmitter. As a result, advanced interference cancellation techniques are required to realize a practical FD system where combined analog and digital interference cancellation strategies are usually employed to achieve sufficient cancellation performance [43].

Note, however, that FD communication has a special interference structure where the interfering and interfered communications have the same bandwidth (hence, the same symbol rate). This interference structure plays a crucial role in designing interference cancellation techniques, especially in the digital domain [81, 82]. Interference cancellation in the more general scenario where the interfering source and victim have different bandwidths is more challenging to tackle because of the following reasons. First, the equivalent interference coefficients (EIC) [48] vary from symbol to symbol and they are difficult to capture. Second, when operating over different bandwidths, these concurrent communications are likely not synchronized, which creates a fundamental limitation in cancellation performance [195].

Various interference cancellation techniques, including passive interference cancellations [64], active interference cancellations in the analog domain [42,77] and in the digital domain [81,82], have been proposed for full-duplex systems. However, only a few works study interference cancellation for the concurrent communications with different bandwidths even though this interfering scenario can arise in both terrestrial communications [46] and satellite communications [17]. In fact, this interference scenario occurs between the Iridium satellite system operating in the band 1621.35 - 1626.5 MHz and the Inmarsat satellite system operating in the adjacent band 1626.5 - 1660.5 MHz, as reported in [18]. Thus, development of robust interference cancellation methods that effectively address the general interference scenario between two communications of different bandwidths is highly important.

Interference cancellation for communications with different bandwidths has been investigated in some previous works [45, 48] assuming perfect CSI and/or synchronization between the underlying communications. The problem becomes much more challenging when the desired channel experiences the fast fading where the time-varying channel can be modeled by using the Gauss-Markov process [21, 22, 101, 103, 192, 196]. For the fast fading channel, MMSE-based channel estimators are derived in [27, 102] requiring the knowledge of the channel correlation matrix, which may not be readily usable in the presence of interference. Therefore, it is highly desirable to develop robust interference cancellation techniques that can effectively cope with a strong interfering signal with different bandwidth from the victim in the fast fading environment.

Data symbol detection in the fast fading environment is another challenging task, especially with the presence of strong interference. A well-known approach for symbol detection in fast fading environments is the message-passing detection technique in which the posterior probability of data symbols is estimated. In [101], it is shown that this detection technique can function well if the interfering signal has similar characteristics with the desired signal. However, the method works well only if the interfering and desired signals are synchronized and have the same symbol rate. Furthermore, an approximated distribution of data symbols by the Gaussian mixture with a limited number of terms may yield unacceptable error rate with a large signal constellation size. Another approach is considered in [28] where the channel gains at data symbols are interpolated by the imperfect CSI at pilot symbols. Then, the zero-forcing based symbol detection is employed, the technique is called optimum diversity detection (ODD). However, this detection technique does not fully exploit the correlations of channel gains at consecutive data symbols, and the required inverse matrix operations result in high computational complexity. This motivates us to develop a new detection strategy that has low complexity and can achieve the performance close to that of the ODD technique.

The above survey suggests that joint channel estimation, interference cancellation, and symbol detection for the scenario in which two un-synchronized mutual interfering signals have different bandwidths in the fast fading environment has been under-explored. This paper aims to fill this gap in the literature where we make the following contributions.

- Firstly, a two-phase framework for joint interference cancellation, channel estimation, and symbol detection is proposed. In the first phase, the EICs are estimated and the interference is subtracted. Then, fast-fading channel coefficients at pilot positions are estimated. In the second phase, we derive the *a posteriori probabilities* for both series and individual symbols, given the channel coefficients at pilot positions. Based on these probabilities, we propose corresponding detection methods. Specifically, our series symbol detection (S-MAP) outperforms the existing ODD technique [28] while our individual symbol detection (I-MAP) achieves almost identical result to the ODD technique with much lower complexity as confirmed by numerical studies.

- Secondly, based on the proposed two-phase framework, we propose an iterative algorithm for interference cancellation, channel estimation, and data detection. Numerical studies show that the proposed iterative algorithm converges quite quickly and it performs better than the non-iterative counterpart.

- Thirdly, we analyze the residual interference and symbol error rate achieved by the proposed non-iterative algorithm. Specifically, we provide an exact expression for channel estimation error in the interference-free scenario, and an approximated residual interference and channel estimation error for the case with interference. The analysis shows that the residual interference has bounded power as the interference power tends to infinity. However, the effect of the fast fading channel to the residual interference is irreducible no matter how large the SNR or the number of pilot symbols is. Hence, there are fundamental floors for the channel estimation and symbol detection performances.

- Finally, we conduct simulation studies and draw several insightful observations from the results. Particularly, the performance floor exists for the considered interference scenario while it is not the case for the interference free scenario. It is also shown that the existing symbol detection method may need more than 3dB increment in SNR to achieve the same symbol error rate (SER) obtained from our S-MAP method, while our I-MAP method achieves very close performance to the existing optimum detection method. Finally, we show that there exists an optimal frame structure (i.e., optimal pilot density) to achieve the maximum system throughput.

While preliminary results of this paper were published in [25], the current paper makes several significant contributions compared to this conference version. Specifically, the current journal paper proposes two detection methods with improved performances compared to the method introduced in the conference version. The new iterative algorithm is also proposed in this journal version. The theoretical performance analysis and throughput optimization were not conducted in the conference version. Moreover, the current journal paper presents much more extensive numerical results which provide useful insights into the proposed design.

The chapter is structured as follows. The system model and problem formulation are presented in Section 5.3. Section 5.4 describes the proposed channel estimation, interference cancellation, and the symbol detection techniques. In Section 5.5, we analyze the residual interference, SER, and

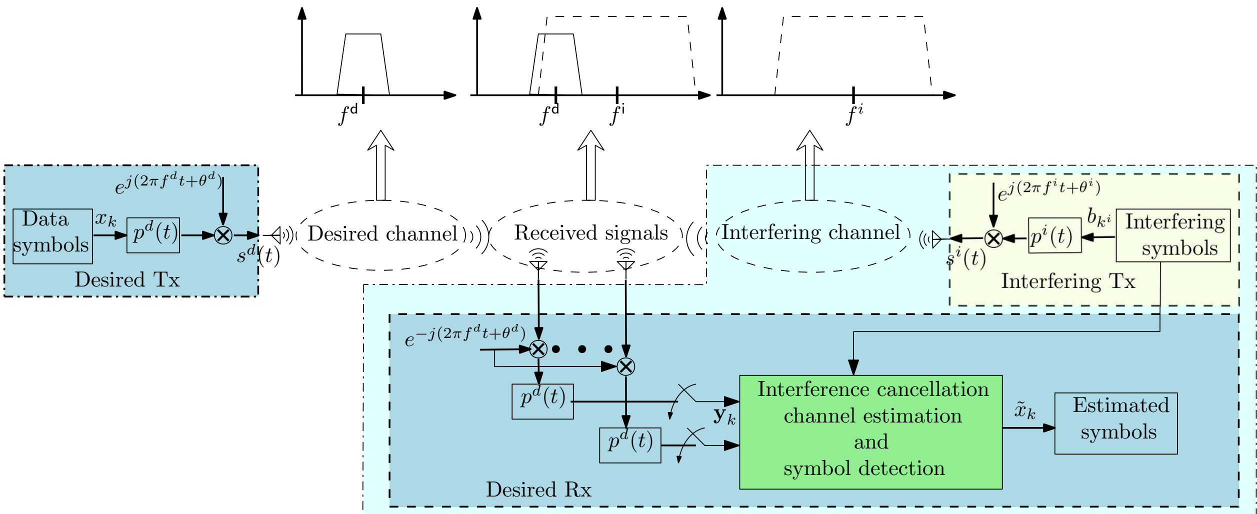

Figure 5.1: Considered interference scenario

optimal frame design for the fast fading and interference scenario. Numerical results are presented in Section 5.6 and Section 5.7 concludes the chapter.

Some important notations used in the paper are summarized as follows: $\mathbf{I}_N$ represents the $N \times N$ identity matrix, $\mathbf{1}_{M,N}$ is the $M \times N$ all-one matrix, $\mathbf{A}^H$ is the *Hermitian transpose* of matrix $\mathbf{A}$, x^* is the *conjugate* of complex value x, $\mathbb{1}_{i=j}$ is the indicator function equal to one when $i = j$ and equal to zero otherwise, *const.* represents a constant independent of the variables of interest, $(\star)$ denotes the convolution operation and $(\propto)$ denotes '*proportional to*'.

5.3 System Model and Problem Statement

We consider the scenario where two communication links denoted by $\mathbb{S}^{\mathsf{d}}$ (desired link) and $\mathbb{S}^{\mathsf{i}}$ (interfering link) operate on overlapping frequency bands. The transmitted signal from $\mathbb{S}^{\mathsf{i}}$ interferes with the received signal of $\mathbb{S}^{\mathsf{d}}$. One popular assumption usually made in the literature is that interfering and desired signals have identical bandwidths where the full-duplex system is a special setting attracting great interests recently. Our current paper considers the more general scenario in which the frequency bands of the two communication links can be arbitrarily aligned and their bandwidth ratio is an integer. The considered setting corresponds to the practical interference scenarios in satellite communications [17, 18] and terrestrial communications, e.g., full-duplex relay [19, 20].

We further assume that the desired communication channel experiences the fast fading where the channel coefficient changes from symbol to symbol according to the first order Markov process [21, 22]. In addition, the interfering channel from the interfering source to the antennas of the desired receiver is assumed to be line of sight. In this interference scenario, the involved signals have different bandwidths and are not synchronized with each other. This induces a dynamic interference pattern to the desired received signal, which can be captured by the EICs [45, 48]. We propose to jointly estimate the desired channel coefficients and the EICs with the knowledge of transmitted symbols from the interfering source and the pilot symbols of the desired signal.

The considered setting with desired and interfering communications is illustrated in Fig. 5.1. The studied interference scenario occurs in practice when the interfering Tx and the desired Rx are located close to each other and the desired Rx has access to the interfering symbols (e.g., via a dedicated connection) as in the full-duplex relay [19, 20]. More details about the system are introduced in the followings.

5.3.1 Signal Models

The transmitted signal of the desired communication with the carrier frequency f^{d} can be written as follows:

$$s^{\mathsf{d}}(t) = \sum_{k=-\infty}^{\infty} x_k p^{\mathsf{d}} \left(t - kT^{\mathsf{d}} + \epsilon^{\mathsf{d}}\right) e^{j\left(2\pi f^{\mathsf{d}} t + \theta^{\mathsf{d}}\right)}, \tag{5.1}$$

where x_k is the kth transmitted symbol. The pulse shaping function $p^{\mathsf{d}}(t)$ has unity gain; T^{d}, ϵ^{d} and θ^{d} represent the symbol duration, time and phase offsets, respectively. Similarly, the signal from the interfering source can be written as follows:

$$s^{\mathsf{i}}(t) = \sum_{k^{\mathsf{i}}=-\infty}^{\infty} b_{k^{\mathsf{i}}} p^{\mathsf{i}} \left(t - k^{\mathsf{i}} T^{\mathsf{i}} - t^{\mathsf{i}}\right) e^{j\left(2\pi f^{\mathsf{i}} t + \theta^{\mathsf{i}}\right)}, \tag{5.2}$$

where $p^{\mathsf{i}}(t)$ denotes the pulse shaping filter with unity gain, the interfering signal has the center frequency $f^{\mathsf{i}} = f^{\mathsf{d}} - \Delta f$, the k^{i}th symbol is $b_{k^{\mathsf{i}}}$; t^{i} and θ^{i} account for the time/phase difference of the two systems and transmission time delay from the interfering transmitter to the interfered receiver, respectively. Assume that there are N_{r} receiver antennas for $\mathbb{S}^{\mathsf{d}}$, then the received signal is

$$\mathbf{y}(t) = \mathbf{h}^{\mathsf{d}}(t) \star s^{\mathsf{d}}(t) + \mathbf{h}^{\mathsf{i}}(t) \star s^{\mathsf{i}}(t) + \mathbf{w}(t), \tag{5.3}$$

where $\mathbf{h}^{\mathsf{d}}(t)$ and $\mathbf{h}^{\mathsf{i}}(t)$ denote $N_{\mathsf{r}}\times 1$ vectors of desired and interfering channel impulse responses.

At the receiver of $\mathbb{S}^{\mathsf{d}}$, the signals are down-converted to baseband by using $e^{-j(2\pi f^{\mathsf{d}}t+\theta^{\mathsf{d}})}$. The output signals then pass through a matched filter having the impulse response $p^{\mathsf{d}}(t)$; and the filtered continuous signals are sampled at $(kT^{\mathsf{d}}+\epsilon^{\mathsf{d}})$ to yield the following discrete time signal

$$\mathbf{y}_k = \mathbf{h}_k^{\mathsf{d}} x_k + \mathcal{I}_k + \mathbf{w}_k, \tag{5.4}$$

where $\mathbf{w}_k$ represents the vector of noise having complex Gaussian distribution with covariance matrix $\sigma^2\mathbf{I}_{N_{\mathsf{r}}}$ ($\mathbf{w}_k$ is called AWGN hereafter); $\mathcal{I}_k$ denotes the equivalent baseband, discrete time interfering signal which will be derived shortly. Firstly, we express the interference terms in the continuous time domain as follows:

$$\mathcal{I}(t) = \left\{\left(\mathbf{h}^{\mathsf{i}}(t)\star s^{\mathsf{i}}(t)\right) e^{-j(2\pi f^{\mathsf{d}}t+\theta^{\mathsf{d}})}\right\}\star p^{\mathsf{d}}(t). \tag{5.5}$$

Substituting $s^{\mathsf{i}}(t)$ from (5.2) into (5.5), we obtain the equivalent baseband interference signal whose sampled signal at time $(kT^{\mathsf{d}}+\epsilon^{\mathsf{d}})$ is

$$\mathcal{I}_k = \mathcal{I}(t)|_{t=kT^{\mathsf{d}}+\epsilon^{\mathsf{d}}} = \mathbf{h}_k^{\mathsf{i}} \sum_{k^{\mathsf{i}}} b_{k^{\mathsf{i}}} c_{k,k^{\mathsf{i}}}, \tag{5.6}$$

where $c_{k,k^{\mathsf{i}}}$ represents the EIC which is defined in the following equation.

$$c_{k,k^{\mathsf{i}}} = \int_{-\infty}^{\infty} p^{\mathsf{d}}(kT^{\mathsf{d}}+\epsilon^{\mathsf{d}}-\tau)p^{\mathsf{i}}(\tau-k^{\mathsf{i}}T^{\mathsf{i}}-t^{\mathsf{i}})e^{j\left(2\pi(f^{\mathsf{i}}-f^{\mathsf{d}})\tau+\theta^{\mathsf{i}}+\theta^{\mathsf{d}}\right)}d\tau. \tag{5.7}$$

Suppose that the interfering signal's bandwidth is M times larger than that of the interfered signal's bandwidth and there are L symbols of $b_{k^{\mathsf{i}}}$'s interfering to each desired symbol x_k where L should be a multiple of the bandwidth ratio M to account for the interference in the filter span of the desired signal[1]. For the considered interference scenario, the bandwidth of the interfering signal is multiple times larger than that of the desired signal. Since the bandwidth ratio is an integer, $c_{k,k^{\mathsf{i}}}$ in (5.7) depends only on the relative difference of k, k^{i}. Hence, for brevity, we denote them as $\mathbf{c} = [c_1, c_2, ..., c_L]^T$ in the sequel.

[1]For tractability, the bandwidth ratio M is an integer. As a result, the achieved results provide performance bounds and approximation for the case where M is a real number.

5.3.2 Channel Model

The fast fading channel of the desired communication link $\mathbf{h}_k^{\mathsf{d}}$ in (5.4) is assumed to follow the first-order Markov model where the relation of channel coefficients at instants $(k+1)$th and kth can be described as [21]:

$$\mathbf{h}_{k+1}^{\mathsf{d}} = \alpha \mathbf{h}_k^{\mathsf{d}} + \sqrt{1-\alpha^2}\boldsymbol{\Delta}_k, \tag{5.8}$$

where $\boldsymbol{\Delta}_k$ denotes a vector of Circular Symmetric Complex Gaussian (CSCG) noise with zero means and covariance matrix $\sigma_{\mathsf{h}}^2 \mathbf{I}_{N_{\mathsf{r}}}$. The additive noise term in (5.8) is called channel evolutionary noise and α is the channel correlation coefficient. The average Signal to Noise Ratio (SNR) is $\rho = \sigma_{\mathsf{h}}^2/\sigma^2$ (called SNR without fading in some previous works [27]). Without loss of generality, we let $\sigma_{\mathsf{h}}^2 = 1$. However, σ_{h}^2 may appear occasionally in several expressions whenever needed.

The Markovian channel model can accurately capture the practical Clarke channel model, which has been validated in [21, 22]. Moreover, the Markovian channel model has been widely adopted in the literature [22, 27, 92, 101, 103, 197, 198]. In fact, the authors of [101] have conducted the model mismatching study, where the actual channel follows the Clarke model and the assumed channel is the Gaussian-Markov model, and they have found that the mismatch is negligible.

We assume that the receiver has perfect information about the interfering channel gains $\mathbf{h}_k^{\mathsf{i}}$ which correspond to the line of sight link as assumed. Therefore, the interfering channel gains vary slowly over time and they can be estimated accurately.

5.3.3 Problem Statement

Using the result of $\mathcal{I}_k$ in (5.6), we can rewrite the received signal in (5.4) as

$$\begin{aligned} \mathbf{y}_k &= \mathbf{h}_k^{\mathsf{d}} x_k + \sum_{l=1}^{L} \left(\mathbf{h}_k^{\mathsf{i}} b_{Mk+l} \right) c_l + \mathbf{w}_k \\ &= \mathbf{h}_k^{\mathsf{d}} x_k + \sum_{l=1}^{L} \mathbf{b}_{k,l} c_l + \mathbf{w}_k, \end{aligned} \tag{5.9}$$

where $\mathbf{b}_{k,l} = \mathbf{h}_k^{\mathsf{i}} b_{Mk+l}$. Then, we can rewrite (5.9) in a matrix form as follows:

$$\mathbf{y}_k = \mathbf{h}_k^{\mathsf{d}} x_k + \mathbf{B}_k \mathbf{c} + \mathbf{w}_k, \tag{5.10}$$

where $\mathbf{B}_k$ is the $N_\mathsf{r} \times L$ matrix whose lth column is $\mathbf{b}_{k,l}$. We will call $\mathbf{B}_k$ the interference matrix hereafter. Recall that the interfering symbols $\mathbf{b}_{Mk+l}$ and the interfering channel gains $\mathbf{h}_k^\mathsf{i}$ are assumed to be known. Therefore, $\mathbf{B}_k$ is known by the desired receiver.

In this paper, $\mathbf{y}_k$ is referred to as the *received signal* or *observation* interchangeably. Since the interfering channels are known and captured in the interference matrix $\mathbf{B}_k$, we will omit the superscript d in the desired channel notation, i.e., $\mathbf{h}_k^\mathsf{d}$ becomes $\mathbf{h}_k$. From now on, *channels* means desired channels discussed in the previous sections.

This paper aims to address the following questions:

1) Given the interference matrix $\mathbf{B}_k$, the observations $\mathbf{y}_k$ and the pilot symbols, how can one cancel the interference and detect data symbols reliably?
2) What are the effects of fast fading channel evolutionary noise to the overall system performances (EIC estimation, interference cancellation, channel estimation, and symbol detection)?
3) Is there an optimal frame design (i.e., optimal pilot density) that maximizes the throughput in the presence of fast fading and interference?

In the next sections, we will provide the answers for these questions.

5.4 Proposed Algorithms

Even though the MMSE method has been widely used in channel estimation, this method relies heavily on the knowledge of the time-domain channel correlation [102, 199–201]. In the presence of interference, MMSE can only be applied after the interference is canceled out. Moreover, its achieved performance depends on the interference cancellation techniques and the resulted residual interference. In addition, MMSE estimators typically require matrix inversion with complexity scaling with the number of pilot symbols, which may become unaffordable for long frames. These drawbacks of the MMSE method motivate us to use the MAP estimator instead where the MAP estimator can be used to estimate the channel coefficients. Furthermore, the MAP estimator is usually preferable to other estimation techniques regarding both bias and variance for the setting with a small number of observations, which corresponds to the small number of pilot symbols in our considered frame [202].

In this section, we propose a two-phase design framework for estimation of the EICs and symbol detection. In the first phase, the EICs are estimated at each pilot position using the maximum likelihood (ML) approach. Then, we take the average of the estimates of $\mathbf{c}$ over all pilot positions to obtain a reduced-variance estimate of $\mathbf{c}$ compared to its estimates at different pilot positions. After that the interference is subtracted from the received signal and the channel coefficients are estimated at pilot positions. In the second phase, the *a posteriori probability* of data symbols is derived, given the estimated channel coefficients at the pilot positions before and after the data intervals, then the data symbols are detected based on that probability. Fig. 5.2 illustrates our proposed design for one particular frame.

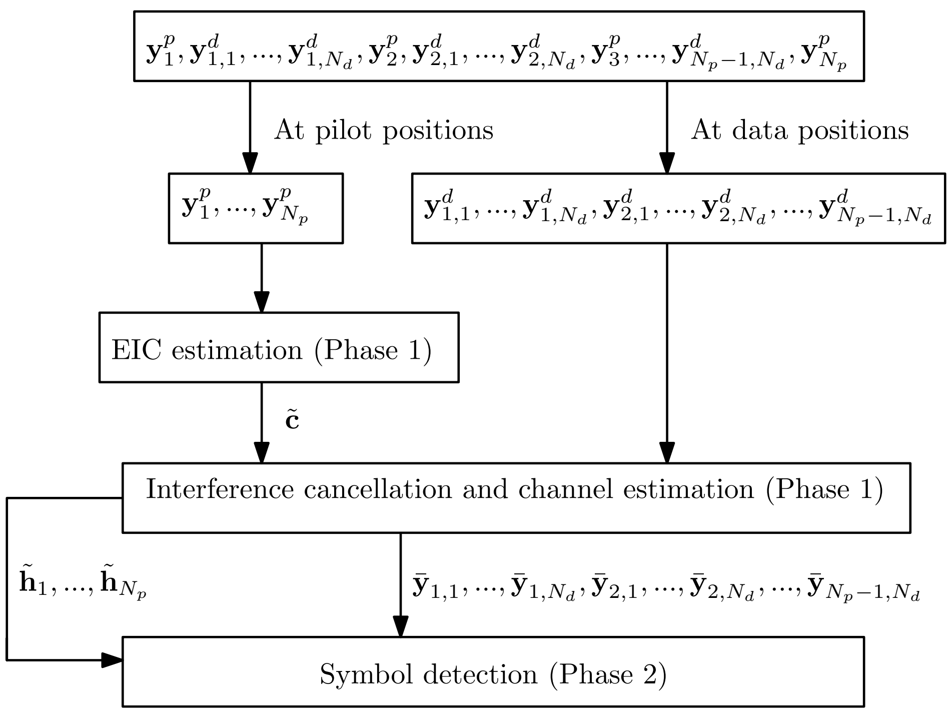

Figure 5.2: Illustration of the proposed design

Channel estimation and symbol detection are performed in each frame. We consider the scattered pilot frame structure in the time domain with N_d data symbols between two consecutive pilot symbols, and there are N_p pilot symbols in a frame [23,24]. Typical symbol arrangement in a frame is expressed as $[x_1^\mathsf{p}, x_{1,1}^\mathsf{d}, ..., x_{1,N_\mathsf{d}}^\mathsf{d}, x_2^\mathsf{p}, x_{1,2}^\mathsf{d}, ..., x_{2,N_\mathsf{d}}^\mathsf{d}, ..., x_{N_\mathsf{p}-1,N_\mathsf{d}}^\mathsf{d}, x_{N_\mathsf{p}}^\mathsf{p}]$, where x_i^p denotes the ith pilot symbol, and $[x^{\mathsf{d}}_{1,i}, ..., x^{\mathsf{d}}_{i,N_{\mathsf{d}}}]$ denotes data symbols between the ith and $(i+1)$th pilot symbols. Fig. 5.3 illustrates this pilot arrangement.

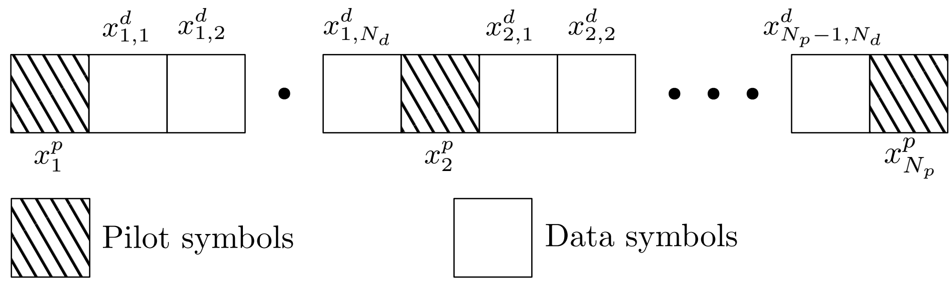

Figure 5.3: Pilot and data symbol arrangement in a frame

5.4.1 Estimation of Interference and Channel Coefficients

In the first phase, we are interested in estimating $\mathbf{c}$ and $\mathbf{h}^{\mathsf{p}}_n, n = 1, ..., N_{\mathsf{p}}$ given the observations $\mathbf{y}^{\mathsf{p}}_{1:N_{\mathsf{p}}}$. For brevity, the superscript p is omitted in this section, i.e., x^{p}_i becomes x_i. We denote $\mathbf{Y} = [\mathbf{y}_{1:n-1}, \mathbf{y}_n, \mathbf{y}_{n+1:N_{\mathsf{p}}}]$. We have the knowledge of the distribution of $\mathbf{h}_n$, so we use the MAP criteria to estimate $\mathbf{h}_n$. Note that either $p(\mathbf{h}_n|\mathbf{Y})$ or $p(\mathbf{h}_n, \mathbf{Y})$ can be used, since $p(\mathbf{h}_n, \mathbf{Y}) = p(\mathbf{h}_n|\mathbf{Y})p(\mathbf{Y})$ and $p(\mathbf{Y})$ is independent of the parameter of interest $\mathbf{h}_n$. Recall also that the EICs $\mathbf{c}$ are unknown, deterministic parameters within a frame. Therefore, the joint estimation criteria for $\mathbf{c}$ and $\mathbf{h}_n$ can be expressed as follows:

$$\left\{\tilde{\mathbf{c}}_n, \tilde{\mathbf{h}}_n\right\} = \text{argmax} \quad p(\mathbf{h}_n, \mathbf{Y}|\mathbf{c}). \tag{5.11}$$

For notational convenience, we omit $\mathbf{c}$ in the following distributions, when there is no confusion, i.e., $p(\mathbf{h}_n, \mathbf{Y}|\mathbf{c})$ is simply written as $p(\mathbf{h}_n, \mathbf{Y})$. In order to estimate $\mathbf{h}_n$ and $\mathbf{c}$ according to (5.11), we need to find $p(\mathbf{h}_n, \mathbf{Y})$. Therefore, we provide the following theorem which states the log likelihood of the received signals and the channel coefficients at pilot positions.

Theorem 5.1. *The log likelihood of the received signals and channel coefficients at pilot position n is*

$$\begin{aligned}\mathcal{L}_{\mathbf{h}_n,\mathbf{Y}} &= \log(p(\mathbf{h}_n, \mathbf{Y})) \\ &= -\sum_{i=1}^{N_{\mathsf{p}}} \left(\mathbf{y}_i - \boldsymbol{\mu}_{i,n}\right)^H \boldsymbol{\Sigma}^{-1}_{i,n} \left(\mathbf{y}_i - \boldsymbol{\mu}_{i,n}\right) - \mathbf{h}^H_n \mathbf{h}_n + const..\end{aligned} \tag{5.12}$$

Proof. The derivation and related parameters $(\boldsymbol{\mu}_{i,n}, \boldsymbol{\Sigma}_{i,n})$ can be found in Appendix 5.A. $\square$

We estimate the desired channel and EIC by maximizing $\mathcal{L}_{\mathbf{h}_n,\mathbf{Y}}$. As can be shown in the derivation later, the exponent of $p(\mathbf{h}_n, \mathbf{Y}|\mathbf{c})$ can be decomposed into two quadratic terms where one term contains $\mathbf{h}_n$ and the other contains only $\mathbf{c}$ and not $\mathbf{h}_n$. Since there are two variables to be optimized (i.e., $\mathbf{h}_n$ and $\mathbf{c}$), we first derive the optimal $\mathbf{h}_n$ with respect to $\mathbf{c}$ then we derive the optimal $\mathbf{c}$ by maximizing the corresponding objective function achieved with the optimal $\mathbf{h}_n$.

★ *Step 1*: Derivation of the optimal $\mathbf{h}_n$ for a given $\mathbf{c}$

The sum of quadratic terms in (5.12) can be re-written as

$$\begin{aligned}\tilde{\mathcal{L}}_{\mathbf{h}_n,\mathbf{Y}} &= -\mathbf{h}_n^H\mathbf{h}_n - \sum_{i=1}^{N_\mathsf{p}} \left(\mathbf{y}_{i,n} - x_{i,n}\mathbf{h}_n - \mathbf{B}_{i,n}\mathbf{c}\right)^H \boldsymbol{\Sigma}_{i,n}^{-1} \left(\mathbf{y}_{i,n} - x_{i,n}\mathbf{h}_n - \mathbf{B}_{i,n}\mathbf{c}\right) \\ &= -(\mathbf{h}_n - \tilde{\mathbf{h}}_n)^H\mathbf{A}_n(\mathbf{h}_n - \tilde{\mathbf{h}}_n) - \mathcal{C}_n,\end{aligned} \tag{5.13}$$

where we omit the constant in (5.12). $\mathbf{A}_n, \tilde{\mathbf{h}}_n$ and $\mathcal{C}_n$ are defined as

$$\begin{aligned}\mathbf{A}_n &= \mathbf{I}_{N_\mathsf{r}} + \sum_{i=1}^{N_\mathsf{p}} \omega_{i,n}^2 \boldsymbol{\Sigma}_{i,n}^{-1}, \\ \tilde{\mathbf{h}}_n &= \mathbf{A}_n^{-1}\left(\sum_{i=1}^{N_\mathsf{p}} x_{i,n}^*\boldsymbol{\Sigma}_{i,n}^{-1}\left(\mathbf{y}_{i,n} - \mathbf{B}_{i,n}\mathbf{c}\right)\right), \\ \mathcal{C}_n &= -\tilde{\mathbf{h}}_n^H\mathbf{A}_n\tilde{\mathbf{h}}_n + \sum_{i=1}^{N_\mathsf{p}} \left(\mathbf{y}_{i,n} - \mathbf{B}_{i,n}\mathbf{c}\right)^H \boldsymbol{\Sigma}_{i,n}^{-1}\left(\mathbf{y}_{i,n} - \mathbf{B}_{i,n}\mathbf{c}\right),\end{aligned} \tag{5.14}$$

where $\omega_{i,n}, x_{i,n}, \mathbf{y}_{i,n}, \mathbf{B}_{i,n}$ and the related parameters are defined in the following equations.

$$x_{i,n} = \omega_{i,n}x_i, \quad \mathbf{y}_{i,n} = \mathbf{y}_i - \beta_{i,n}\mathbf{y}_{i+j_{i,n}}, \quad \mathbf{B}_{i,n} = \mathbf{B}_i - \beta_{i,n}\mathbf{B}_{i+j_{i,n}}, \tag{5.15a}$$

$$\omega_{i,n} = \begin{cases} \frac{\alpha_\mathsf{p}^{|n-i|}}{1+\rho(1-\alpha_\mathsf{p}^{2(|n-i|-1)})}, & i \neq n \\ 1, & i = n \end{cases}, \qquad \beta_{i,n} = \begin{cases} \frac{x_i x_{i+j_{i,n}}^* \rho\alpha_\mathsf{p}\left(1-\alpha_\mathsf{p}^{2(|n-i|-1)}\right)}{1+\rho\left(1-\alpha_\mathsf{p}^{2(|n-i|-1)}\right)}, & i \neq n \\ 0, & i = n \end{cases}. \tag{5.15b}$$

For notational simplicity, we denote the 'sign indicator' $j_{i,n} = -1$ for $i > n$, $j_{i,n} = 1$ for $i < n$ and $j_{i,n} = 0$ for $i = n$. Since $\mathbf{A}_n$ is positive definite, the optimal $\mathbf{h}_n$ that maximizes $\tilde{\mathcal{L}}_{\mathbf{h}_n,\mathbf{Y}}$ in (5.13) is $\tilde{\mathbf{h}}_n$. Note that, when the desired channels are independent, we have $\mathbf{A}_n = a_n \mathbf{I}_{N_\mathsf{r}}$, where

$$a_n = 1 + \sum_{i=1}^{N_\mathsf{p}} \frac{\omega_{i,n}^2}{\sigma_{i,n}^2}. \tag{5.16}$$

★ *Step 2*: Derivation of the optimal $\mathbf{c}$

When $\mathbf{h}_n = \tilde{\mathbf{h}}_n$, the function in (5.13) is equal to $-\mathcal{C}_n$ which only depends on $\mathbf{c}$ where

$$\begin{aligned}\mathcal{C}_n =& \sum_{i=1}^{N_\mathsf{p}} \left(\mathbf{y}_{i,n} - \mathbf{B}_{i,n}\mathbf{c}\right)^H \boldsymbol{\Sigma}_{i,n}^{-1} \left(\mathbf{y}_{i,n} - \mathbf{B}_{i,n}\mathbf{c}\right) \\ &- \left(\sum_{i=1}^{N_\mathsf{p}} x_{i,n}^* \boldsymbol{\Sigma}_{i,n}^{-1} \left(\mathbf{y}_{i,n} - \mathbf{B}_{i,n}\mathbf{c}\right)\right)^H \mathbf{A}_n^{-1} \left(\sum_{i=1}^{N_\mathsf{p}} x_{i,n}^* \boldsymbol{\Sigma}_{i,n}^{-1} \left(\mathbf{y}_{i,n} - \mathbf{B}_{i,n}\mathbf{c}\right)\right) \\ =& \left(\mathbf{c} - \tilde{\mathbf{c}}_n\right)^H \mathbf{D}_n \left(\mathbf{c} - \tilde{\mathbf{h}}_n\right) + const.,\end{aligned} \tag{5.17}$$

where $\mathbf{D}_n$ and $\tilde{\mathbf{c}}_n$ are defined in the following equations.

$$\mathbf{D}_n = \sum_{i=1}^{N_\mathsf{p}} \mathbf{B}_{i,n}^H \boldsymbol{\Sigma}_{i,n}^{-1} \mathbf{B}_{i,n} - \left(\sum_{i=1}^{N_\mathsf{p}} x_{i,n}^* \boldsymbol{\Sigma}_{i,n}^{-1} \mathbf{B}_{i,n}\right)^H \mathbf{A}_n^{-1} \left(\sum_{i=1}^{N_\mathsf{p}} x_{i,n}^* \boldsymbol{\Sigma}_{i,n}^{-1} \mathbf{B}_{i,n}\right), \tag{5.18a}$$

$$\tilde{\mathbf{c}}_n = \mathbf{D}_n^{-1} \left\{\sum_{i=1}^{N_\mathsf{p}} \mathbf{B}_{i,n}^H \boldsymbol{\Sigma}_{i,n}^{-1} \mathbf{y}_{i,n} - \left(\sum_{i=1}^{N_\mathsf{p}} x_{i,n}^* \boldsymbol{\Sigma}_{i,n}^{-1} \mathbf{B}_{i,n}\right)^H \mathbf{A}_n^{-1} \left(\sum_{i=1}^{N_\mathsf{p}} x_{i,n}^* \boldsymbol{\Sigma}_{i,n}^{-1} \mathbf{y}_{i,n}\right)\right\}. \tag{5.18b}$$

It can be verified that $\mathbf{D}_n$ is positive definite by using the *Cauchy-Schwarz* inequality. The proof of this property can be found in Appendix 5.B. Therefore, the optimal $\mathbf{c}$ that maximizes $\tilde{\mathcal{L}}_{\mathbf{h}_n,\mathbf{Y}}$ in (5.13) is $\tilde{\mathbf{c}}_n$. We take the average over all $\tilde{\mathbf{c}}_n, n = 1, ..., N_\mathsf{p}$ to yield a reduced-variance estimate of $\mathbf{c}$. Consequently, the resulting estimated EIC vector can be written as

$$\tilde{\mathbf{c}} = \frac{1}{N_\mathsf{p}} \sum_{n=1}^{N_\mathsf{p}} \tilde{\mathbf{c}}_n. \tag{5.19}$$

The joint interference estimation, cancellation and channel estimation algorithm is described in Algorithm 5.1.

Algorithm 5.1. Estimation of EICs, Desired Channel Coefficients, and Interference Cancellation

for $n = 1 : N_\mathsf{p}$ **do**
  for $i = 1 : N_\mathsf{p}$ **do**
    Compute $x_{i,n}, \mathbf{y}_{i,n}, \mathbf{B}_{i,n}, \mathbf{\Sigma}_{i,n}$ in (5.14), (5.15a).
  end for
  Compute $\mathbf{A}_n, \mathbf{D}_n$, and then $\tilde{\mathbf{c}}_n$ in (5.14), (5.18a), (5.18b).
end for
Compute $\tilde{\mathbf{c}}$ in (5.19) and subtract the interference.
for $n = 1 : N_\mathsf{p}$ **do**
  Estimate $\mathbf{h}_n$ as $\tilde{\mathbf{h}}_n$ in (5.14).
end for
End of algorithm.

5.4.2 Symbol Detection

With the estimated $\tilde{\mathbf{c}}$, we can subtract the interference, and the channel coefficients at pilot positions are estimated as $\tilde{\mathbf{h}}_n$ given in (5.14) with $\mathbf{c}$ substituted by $\tilde{\mathbf{c}}$ in (5.19). The estimated channel coefficients at pilot positions will be used for the symbol detection as described in the following.

We will describe the symbol detection for the interval $\left[x_i^\mathsf{p}, x_{i,1}^\mathsf{d}, x_{i,2}^\mathsf{d}, ..., x_{i,N_\mathsf{d}}^\mathsf{d}, x_{i+1}^\mathsf{p}\right]$. The method can be applied and repeated for other intervals. For simplicity, we omit the pilot index i and superscript (d) in this section, i.e., the channel coefficients are denoted as $[\mathbf{h}_h, \mathbf{h}_{1:N_\mathsf{d}}, \mathbf{h}_t]$, where $\mathbf{h}_h$ represents the known channel coefficient at the pilot symbol right before the considered interval and $\mathbf{h}_t$ represents known channel coefficient at the pilot symbol right after the considered interval.

In [28], the optimum diversity detection (ODD) is derived to detect symbols individually based on the interpolated channel coefficients at the corresponding positions in the interference-free scenario. This method, however, requires expensive matrix inversion because the matrix size corresponds to the number of pilot symbols. Alternatively, we provide two different symbol detection methods where the first method is based on series symbol detection which will be shown to outperform the optimum individual detector ODD at the cost of high complexity, while the second method achieves very close (almost identical) SER to that due to the ODD but with significantly lower complexity. These detection methods are described in the following.

5.4.2.1 Series Symbol MAP Detection (S-MAP)

The symbols in an interval are detected as

$$\tilde{\mathbf{x}}_{1:N_{\mathsf{d}}} = \operatorname{argmax} \quad p\left(\mathbf{x}_{1:N_{\mathsf{d}}} | \mathbf{h}_h, \mathbf{h}_t, \mathbf{y}_{1:N_{\mathsf{d}}}\right). \tag{5.20}$$

We now characterize the log likelihood function in the following theorem.

Theorem 5.2. *The log likelihood of data symbols conditioned on the received signals and the channel coefficients at pilot positions right after and before the interval can be expressed in a sum of quadratic functions of data symbols* $\mathbf{x}$ *as*

$$\log\left(p\left(\mathbf{x}_{1:N_{\mathsf{d}}} | \mathbf{h}_h, \mathbf{h}_t, \mathbf{y}_{1:N_{\mathsf{d}}}\right)\right) = \mathcal{F} + const., \tag{5.21}$$

where

$$\mathcal{F} = \sum_{i=1}^{N_{\mathsf{d}}} \left[\left(\tau_2 \boldsymbol{\Gamma}_{i,1} \mathbf{h}_h + \mathbb{1}_{i=N_{\mathsf{d}}} \tau_2 \mathbf{h}_t + \sum_{j=1}^{i} \frac{x_j^*}{\sigma^2} \boldsymbol{\Gamma}_{i,j} \mathbf{y}_j \right)^H \mathbf{S}_i \left(\tau_2 \boldsymbol{\Gamma}_{i,1} \mathbf{h}_h + \mathbb{1}_{i=N_{\mathsf{d}}} \tau_2 \mathbf{h}_t + \sum_{j=1}^{i} \frac{x_j^*}{\sigma^2} \boldsymbol{\Gamma}_{i,j} \mathbf{y}_j \right) \right], \tag{5.22}$$

and the related parameters are defined in (5.23) and Appendix 5.C.

$$\mathbf{S}_i^{-1} = \left(\frac{1}{\sigma^2} + (1+\alpha^2)\tau_1 \right) \mathbf{I}_{N_{\mathsf{r}}} - \mathbb{1}_{i>1} \tau_2^2 \mathbf{S}_{i-1}, \tag{5.23a}$$

$$\bar{\mathbf{h}}_i = \begin{cases} \mathbf{S}_i \left(\tau_2 \boldsymbol{\Gamma}_{i,1} \mathbf{h}_h + \tau_2 \mathbf{h}_{i+1} + \sum_{j=1}^{i} \frac{x_j^*}{\sigma^2} \boldsymbol{\Gamma}_{i,j} \mathbf{y}_j \right), & i < N_{\mathsf{d}} \\ \mathbf{S}_i \left(\tau_2 \boldsymbol{\Gamma}_{i,1} \mathbf{h}_h + \tau_2 \mathbf{h}_t + \sum_{j=1}^{i} \frac{x_j^*}{\sigma^2} \boldsymbol{\Gamma}_{i,j} \mathbf{y}_j \right), & i = N_{\mathsf{d}} \end{cases}. \tag{5.23b}$$

Proof. The proof and related parameters can be found in Appendix 5.C. □

By enumerating all possible vectors $\mathbf{x} = [x_1, ..., x_{N_{\mathsf{d}}}]$ from the constellation points and calculating the corresponding $p\left(\mathbf{x}_{1:N_{\mathsf{d}}} | \mathbf{h}_h, \mathbf{h}_t, \mathbf{y}_{1:N_{\mathsf{d}}}\right)$, we are able to obtain the optimally detected symbols by (5.20).

5.4.2.2 Individual Symbol MAP Detection (I-MAP)

The individual symbol detection method presented in [25] determines the detected symbol x_i based on (5.20). However, because $\tilde{x}_i$ is computed from $\tilde{x}_j, j < i$, this method suffers from error propagation, which increases the error rates of symbols in the middle of the interval. To address this limitation, we propose to estimate x_i individually as

$$\tilde{x}_i = \text{argmax} \quad p\left(x_i | \mathbf{h}_h, \mathbf{h}_t, \mathbf{y}_i\right). \tag{5.24}$$

Using similar derivations as those used to obtain the results in Theorem 5.2, we have[2]

$$\begin{aligned}\tilde{x}_i &= \frac{\breve{\mathbf{h}}_i^H \mathbf{y}_i}{\|\breve{\mathbf{h}}_i^H \mathbf{y}_i\|}, \quad i = 1, ..., N_{\mathsf{d}}, \\ \breve{\mathbf{h}}_i &= \frac{\alpha^i}{1-\alpha^{2i}} \mathbf{h}_h + \frac{\alpha^{N_{\mathsf{d}}+1-i}}{1-\alpha^{2(N_{\mathsf{d}}+1-i)}} \mathbf{h}_t.\end{aligned} \tag{5.25}$$

Then, the detected symbols can be found by mapping $\tilde{x}_i$ to the closest point on the constellation. This method does not suffer from error propagation and its achievable performance is less sensitive to the positions i of the data symbol in each detection interval. We summarize the proposed joint channel estimation and symbol detection in Algorithm 5.2.

Algorithm 5.2. Individual Symbol MAP Detection Over Fast Fading Channel (I-MAP)

```
1: for n = 1 : N_p do
2:    for i = 1 : N_d do
3:       Estimate x̃^d_{i,n} from (5.25) and assign x̃^d_{i,n} to the closest point in the constellation.
4:    end for
5: end for
6: End of algorithm.
```

5.4.3 Iterative Algorithm for Interference Cancellation, Channel Estimation, and Symbol Detection

In practice, the joint channel estimation, interference cancellation, and data detection are often performed iteratively [203]. Moreover, if the data detection is sufficiently reliable, detected data

[2]Upon deriving $\breve{\mathbf{h}}_i$, the normalized technique employed is similar to that employed in the well-known Maximal Ratio Combining technique.

symbols can act as pilot symbols to support the interference cancellation and channel estimation, which can potentially improve the detection performance. In this section, we propose an iterative approach for interference cancellation, channel estimation, and symbol detection based on the previous two-phase method. For convenience purposes, we now denote the desired symbols in the frame as $x_n, n = 1, ..., (N_\mathsf{p} - 1)(N_\mathsf{d} + 1) + 1$, where $x_n, n = 1, 1 + N_\mathsf{d} + 1, 1 + 2(N_\mathsf{d} + 1), ...$ are pilot symbols in the previous notations.

5.4.3.1 Interference Cancellation and Channel Estimation

Since all symbols x_n are known (at pilot positions) or detected (at data positions), they are all treated as pilot symbols. Therefore, the number of newly considered pilot symbols is now $\hat{N}_\mathsf{p} = (N_\mathsf{d} + 1)(N_\mathsf{p} - 1) + 1$ (symbols in the whole frame) and the correlation coefficient of channel gains at two consecutive pilot positions is $\hat{\alpha}_\mathsf{p} = \alpha$ (instead of $\alpha^{N_\mathsf{d}+1}$). The interference estimation, interference cancellation, and channel estimation are performed as presented in sections 5.4.1 and 5.4.2.

5.4.3.2 Symbol Detection

Let the estimated channel gains at position n be $\breve{\mathbf{h}}_n$. In order to detect the symbol x_n, we now use the knowledge of $\breve{\mathbf{h}}_{n+1}$ and $\breve{\mathbf{h}}_{n-1}$ as if $n+1$ and $n-1$ are two pilot positions. Apply the I-MAP technique[3] in (5.25), we have

$$\begin{aligned} \tilde{x}_n &= \frac{\hat{\mathbf{h}}_n^H \mathbf{y}_n}{\|\hat{\mathbf{h}}_n^H \mathbf{y}_n\|}, n = 2, ..., (N_\mathsf{p} - 1)(N_\mathsf{d} + 1), \\ \hat{\mathbf{h}}_i &= \frac{\alpha}{1 - \alpha^2} \left(\breve{\mathbf{h}}_{n-1} + \breve{\mathbf{h}}_{n+1} \right). \end{aligned} \tag{5.26}$$

After $\tilde{x}_n$ are detected, in the next iterations, interference cancellation, channel estimation and data detection are performed until convergence is reached. The algorithm converges when there is no change in the detected data symbols. Though the convergence guarantee is difficult to prove, simulation results show that the convergence is achieved after only a few iterations. We summarize this iterative approach in Algorithm 5.3.

[3] Now as there is only one data symbol between two 'pilot' symbols, S-MAP and I-MAP produce identical results.

Algorithm 5.3. Iterative Algorithm for Channel Estimation, Interference Cancellation and Data Detection

Perform Algorithm 5.1 for interference cancellation and channel estimation.
Perform Algorithm 5.2 for I-MAP symbol detection.
while (true) **do**
    Perform Algorithm 5.1 for interference cancellation and channel estimation with $\hat{\alpha}_{\mathsf{p}} = \alpha$ and $\hat{N}_{\mathsf{p}} = (N_{\mathsf{d}} + 1)(N_{\mathsf{p}} - 1) + 1$.
    Perform Algorithm 5.2 for I-MAP symbol detection with $\hat{N}_{\mathsf{d}} = 1$. The detected data symbols are denoted as $\bar{\mathbf{x}}^{\mathsf{i}}$.
    if $\bar{\mathbf{x}}^{\mathsf{i}} {==} \bar{\mathbf{x}}^{(\mathsf{i}-1)}$ **then**
        Break the loop (Convergence is reached).
    else
        Increase i and go to the next iteration.
    end if
end while
End of algorithm.

5.5 Performance Analysis

In this section, we conduct performance analysis for the proposed design framework in sections 5.4.1 and 5.4.2[4]. For benchmarking, we first consider the interference-free scenario and inspect the effects of AWGN and channel evolutionary noise to the residual interference $\boldsymbol{\nu}_n$. As shown from the analysis later, the mean square of the channel estimation error (CEE) in the interference-free scenario approaches zero as the SNR tends to infinity. In the considered interference scenario, we prove that the residual interference and the channel estimation error are independent of the interfering power. Finally, based on the analysis of the estimation error, we demonstrate how the actual residual interference affects the symbol detection and derive the achievable SER.

In the following analysis, we investigate the channel estimation error (CEE, denoted as $\boldsymbol{\nu}_n$) and residual interference (denoted as $\boldsymbol{\upsilon}_n$) which are defined as follows.

$$\begin{aligned} \boldsymbol{\nu}_n &= \mathbf{h}_n - \tilde{\mathbf{h}}_n, \\ \boldsymbol{\upsilon}_n &= \mathbf{B}_n \left(\mathbf{c} - \tilde{\mathbf{c}} \right). \end{aligned} \tag{5.27}$$

[4] Due to the stochastic nature of the channel model and the design, analysis of the iterative algorithm is very involved, which is beyond the scope of this work. Nevertheless, the analysis of the proposed non-iterative two-phase design provides many insights that help explain the behaviors of the iterative algorithm. In-depth analysis of the iterative algorithm is left for future extensions.

5.5.1 Channel Estimation in Interference-free Scenario

In the interference-free case, the estimate of $\mathbf{h}_n$ is

$$\tilde{\mathbf{h}}_n = \mathbf{A}_n^{-1} \left(\sum_{i=1}^{N} x_{i,n}^* \mathbf{\Sigma}_{i,n}^{-1} \mathbf{y}_{i,n} \right). \tag{5.28}$$

We characterize the performance of this channel estimator in the following proposition[5].

Proposition 5.1. *The channel estimation error* $\boldsymbol{\nu}_n$ *has Gaussian distribution with zero mean. Moreover, the effect of channel evolutionary noise to the channel estimation error is negligible as the SNR tends to infinity.*

Proof. Please see Appendix 5.D. □

5.5.2 Residual Interference Analysis

For the derived estimators for $\mathbf{c}$ and $\mathbf{h}_n$ under the considered interference scenario, the resulting residual interference is characterized in the following propositions.

Proposition 5.2. *The EIC estimation is unbiased and the residual interference follows the Gaussian distribution with zero mean. Moreover, the residual interference is independent of* $\mathbf{c}$ *and has bounded power as the interference power goes to infinity.*

Proof. Please see Appendix 5.E. □

Proposition 5.3. *There is a floor for the residual interference power, i.e., as* ρ *goes to infinity, the residual interference power approaches* $\tilde{\sigma}_{\mathsf{i}}^2 = \frac{\alpha_{\mathsf{p}}^2(1-\alpha_{\mathsf{p}}^2)}{N_{\mathsf{p}}}$.

Proof. Please see Appendix 5.F. □

The channel estimation is performed based on the observations after interference cancellation. Therefore, the floor of residual interference corresponds to the floor in channel estimation perfor-

[5]The fact that the effect of channel evolutionary noise diminishes as SNR goes to infinity suggests that the error floor in channel estimation reported in [25] comes from the residual interference. The later analysis will confirm this prediction.

mance. This also means that the achieved SINR after cancellation is bounded. This result is stated in the following proposition.

Proposition 5.4. *As the SNR goes to infinity, the SINR after interference cancellation*[6] *approaches* $\tilde{\rho} = \frac{N_{\mathsf{p}}}{\alpha_{\mathsf{p}}^2(1-\alpha_{\mathsf{p}}^2)}$.

Proof. After interference cancellation, the achievable SINR is affected by the channel estimation error and the residual interference. According to Proposition 5.1, the channel estimation error vanishes as $\rho \to \infty$. Hence, the SINR after interference cancellation is $1/\tilde{\sigma}_{\mathsf{i}}^2$, where $\tilde{\sigma}_{\mathsf{i}}^2$ is given in Proposition 5.3. □

5.5.3 SER Analysis

The unnormalized $\tilde{x}_i$ in (5.25) is $\breve{\mathbf{h}}_i^H(\mathbf{h}_i x_i + \tilde{\mathbf{w}}_i)$, where $\tilde{\mathbf{w}}_i$ is the sum of the additive Gaussian noise and residual interference with the corresponding covariance matrix of $(\sigma^2 + \sigma_{\mathsf{i}}^2)\mathbf{I}_{N_{\mathsf{r}}}$. Conditioned on $\mathbf{h}_h$ and $\mathbf{h}_t$, the equivalent SNR for symbol detection of x_i can be expressed as

$$\rho_i^{\mathsf{e}} = \frac{\alpha^{2i}\left|\|\mathbf{h}_h\|^2 \frac{\alpha^i}{1-\alpha^{2i}} + \mathbf{h}_h^H\mathbf{h}_t\frac{\alpha^j}{1-\alpha^{2j}}\right|^2}{(\sigma^2+\sigma_{\mathsf{i}}^2+1-\alpha^{2i})\left|\mathbf{h}_h^H\mathbf{1}_{N_{\mathsf{r}}}\frac{\alpha^i}{1-\alpha^{2i}} + \mathbf{h}_t^H\mathbf{1}_{N_{\mathsf{r}}}\frac{\alpha^j}{1-\alpha^{2j}}\right|^2}, \tag{5.29}$$

where $j = N_{\mathsf{d}} + 1 - i$ and σ_{i}^2 can be computed from (5.49) or approximated by $\tilde{\sigma}_{\mathsf{i}}^2$ in Proposition 5.3 for large ρ. Thus, the SER at symbol position i can be calculated as

$$P_i^{\mathsf{e}} = \int p(\mathbf{h}_h, \mathbf{h}_t) f_{\mathsf{e}}(\rho_i^{\mathsf{e}}) d\mathbf{h}_h d\mathbf{h}_t, \tag{5.30}$$

where $f_{\mathsf{e}}(\rho)$ is the error rate corresponding to instantaneous ρ. For the QPSK modulation,

$$f_{\mathsf{e}}(\rho) = \operatorname{erfc}\left(\sqrt{\rho/2}\right) - \frac{1}{4}\operatorname{erfc}^2\left(\sqrt{\rho/2}\right),$$

and $\operatorname{erfc}(x) = \frac{2}{\sqrt{\pi}}\int_x^\infty e^{-x^2}dx$ is the complementary error function. The closed-form expression for P_i^{e} in (5.30) is difficult to derive. However, P_i^{e} can be computed accurately by using numerical integration or by Monte Carlo simulation. Finally, the overall average SER can be expressed as

[6] Since the interference is efficiently canceled, the probably most important parameter before interference cancellation is the SNR; therefore, we use the term "SNR before cancellation" but not "SINR before cancellation" to reflect this. After interference cancellation, the residual interference is irreducible and affects directly the performance of the detection process; hence, the term "SINR after cancellation" is used.

$$P^{\mathsf{e}} = \frac{1}{N_{\mathsf{d}}} \sum_{i=1}^{N_{\mathsf{d}}} P_i^{\mathsf{e}}. \tag{5.31}$$

5.5.4 Throughput Analysis

The throughput is defined as the average number of successfully transmitted data symbol per symbol period, which is averaged over the frame interval. Note that there are N_{d} transmitted data symbols between two consecutive pilot symbols and the frame consists of N_{p} pilot symbols as shown in Fig. 5.3. Considering the average SER P^{e} in (5.31), the throughput can be calculated as

$$\mathsf{TP} = (1 - P^{\mathsf{e}}) \frac{N_{\mathsf{d}}(N_{\mathsf{p}} - 1)}{(N_{\mathsf{d}} + 1)(N_{\mathsf{p}} - 1) + 1}, \tag{5.32}$$

where, the numerator of the second term of (5.32) is the number of data symbols transmitted, and the denominator is the frame length.

The pilot density is defined as $1/(N_{\mathsf{d}} + 1)$. It can be verified that when we increase the pilot density (i.e., N_{d} is decreased), P_{e} decreases; thus the first term in (5.32) increases. However, the increasing pilot density leads to higher pilot overhead which reduces the second term in (5.32) and vice versa. Therefore, there is a trade-off between transmission reliability and throughput, which suggests that there exists an optimal value of the pilot density that achieves the maximum throughput.

Because the SER in (5.30) and the average SER in (5.31) cannot be expressed in closed form, the optimal pilot density for given α and ρ can be found effectively by using the bisection search method.

5.5.5 Complexity Analysis

For uncorrelated desired channels, the complexity of our proposed interference cancellation, channel estimation and symbol detection is linear in the number of antennas, since all involved matrix inversions simply become divisions. In the first phase, the complexity of EIC estimation is $\mathcal{O}(N_{\mathsf{r}} N_{\mathsf{p}}^2)$ and the complexity of channel estimations at pilot positions is $\mathcal{O}(N_{\mathsf{r}} N_{\mathsf{p}})$. In the second phase, while the exhaustive-search based symbol detection approach has the complexity growing exponentially with the number of data symbols and the constellation size, our proposed I-MAP detection does not depend on the constellation size and has linear complexity in the number of data symbols. Particularly, the complexity of the I-MAP detection is $\mathcal{O}(N_\mathsf{r}N_\mathsf{d}N_\mathsf{p})$ which is also linear in the frame length. Therefore, the overall complexity of the proposed two-phase design with I-MAP is $\mathcal{O}\left(N_\mathsf{r}N_\mathsf{p}(N_\mathsf{p}+N_\mathsf{d})\right)$. The complexity of the iterative method presented in section 5.3 is $\mathcal{O}\left(IN_\mathsf{r}N_\mathsf{p}^2N_\mathsf{d}^2\right)$[7], where I is the average number of iterations to achieve convergence.

5.6 Numerical Results

5.6.1 Simulation Settings

We consider the simulation setting in which the desired receiver has $N_\mathsf{r}=2$ antennas, the coefficient α is chosen in the set $\{0.95, 0.97, 0.99, 0.995, 0.999\}$[8]. The bandwidth of the interfering signal is two times of the bandwidth of the desired signal, which are $30kHz$ and $15kHz$, respectively. The frequency spacing Δ_f between interfering and desired signals will be normalized as $\Delta_f T^\mathsf{d}$ where T^d denotes the symbol time of the desired signal. We assume that the QPSK modulation is employed; both interfering and interfered signals use the root-raised-cosine pulse shaping function. Moreover, the pulse shaping functions $p^\mathsf{d}(t)$ and $p^\mathsf{i}(t)$ are assumed to have the roll-off factor equal to 0.25.

The interference power is set as strong as the power of the desired signal and the frequency spacing $\Delta_f = 1/T^\mathsf{d}$ unless stated otherwise. The number of pilot symbols is set equal to 51. Moreover, the pilot density is chosen in the set $\{25\%, 10\%\}$ corresponding to $\{3, 9\}$ data symbols between two pilot symbols, respectively. Furthermore, for throughput simulation results, we show the throughputs obtained for various pilot densities ranging from 50% to 6.25%. The results presented in this section are obtained by averaging over 10^4 random realizations.

[7] In order to obtain this result, we note that the number of considered pilot symbols in the iterative method is equal to the frame length.

[8] In Clarke's mode, $\alpha = J_0(2\pi f_D T^\mathsf{d})$, where f_D is the maximum Doppler spread [26] (recall that T^d is the symbol period of the desired signal). Specifically, $\alpha = 0.999$ corresponds to 150 Hz of Doppler spread with symbol rate of 15 Kbps. If the desired signal is carried at 900MHz, the corresponding velocity of the desired Rx is 50m/s.

5.6.2 Performance of the Proposed Channel Estimation Technique

For the interference-free scenario, we investigate the effect of different parameters to the channel estimation errors. We note that the performance of the channel estimation technique presented in this section depends mainly on N_{d} and α. Specifically, the performance depends on α_{p} which is the correlation coefficient of channel gains at two consecutive pilot positions (see Appendix 5.A and Theorem 5.1). Different values of N_{d} (different pilot densities) have the corresponding values of α_{p}. We will show the numerical channel estimation mean squared error (CMSE) which is calculated as

$$\mathsf{CMSE} = \frac{1}{N_{\mathsf{p}} N_{\mathsf{r}}} \sum_{n=1}^{N_{\mathsf{p}}} \mathbf{tr}\left(\mathbb{E}\left[\left(\mathbf{h}_n - \tilde{\mathbf{h}}_n\right)\left(\mathbf{h}_n - \tilde{\mathbf{h}}_n\right)^H\right]\right). \tag{5.33}$$

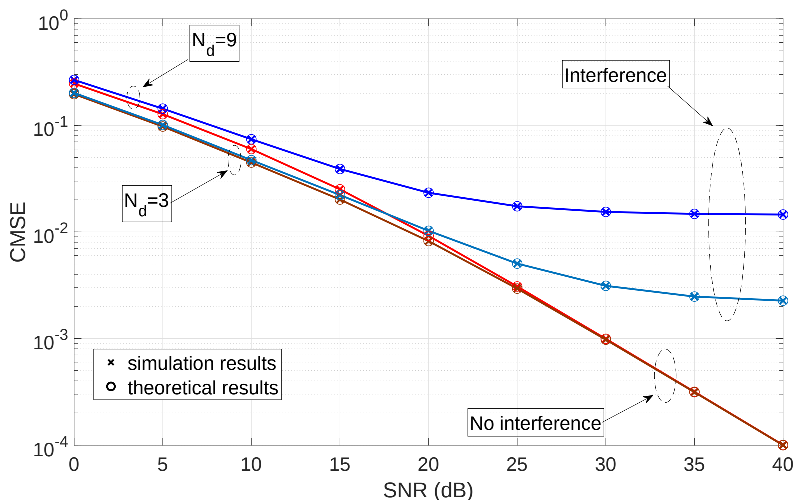

Figure 5.4: Channel estimation mean squared error, $\alpha = 0.99$

In Fig. 5.4, we show the channel estimation error due to our proposed design for different values of N_{d} (equivalently, different values of pilot density), when there is no interference (IF) and when there is interference (IP). When N_{d} increases, the channel estimation mean squared error also increases as expected. For the interference-free scenario, the corresponding error curves converge to each other and decrease almost linearly as the SNR increases (both curves are plotted in the log scale). This means that the impact of the fast fading is diminished in the high SNR regime. When the interference is present, there is a performance floor for channel estimation error. The results in Fig. 5.4 also validate the theoretical results stated in Propositions 5.1, 5.3, and 5.4 about the channel estimation errors in the scenarios without and with interference.

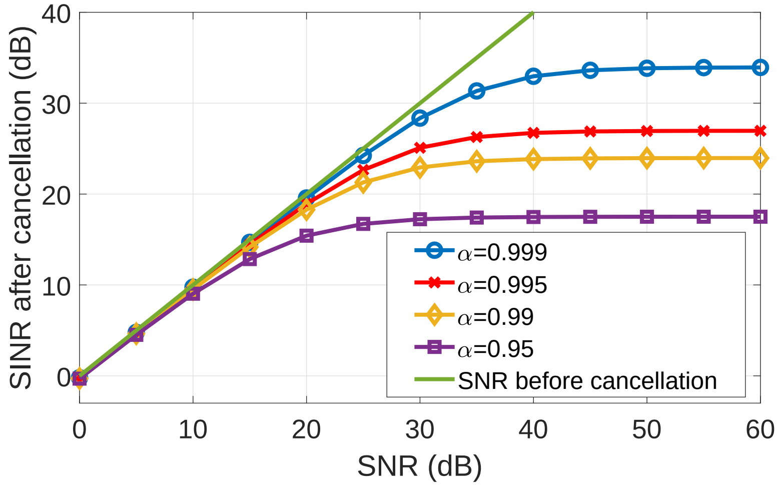

Figure 5.5: SINR after cancellation for different values of channel correlation coefficient, $N_{\mathrm{d}} = 3$

In Fig. 5.5, we show the achieved SINR after interference cancellation versus the SNR for different values of channel correlation coefficient α. Two noticeable observations can be drawn from this figure. First, it can be seen that the achieved SINR increases with increasing SNR before becoming saturated. In the low SNR regime, however, the residual interference has almost no impact on the achieved SINR after interference cancellation, i.e., the SINR curves after interference cancellation are very close to the line showing the SNR before interference cancellation. Second, the achieved SINR after cancellation increases with the increasing values of channel correlation coefficient α. This is because the higher the value of α is, the lower the variance of the channel evolutionary noise and the less severe the impact of the fast fading are. Since the fast fading noise is less disruptive, interference cancellation performance is alleviated (as it is known that the fast fading noise causes the performance floor for the interference cancellation), which in turn reduces the residual interference power and makes the achieved SINR higher.

5.6.3 Performance of the Proposed Symbol Detection Techniques

We now compare the SER performance of series symbol MAP detection (S-MAP), individual symbol MAP detection (I-MAP) and optimum diversity detection (ODD) [27, 28] methods. The ODD method is the optimum individual symbol detection with imperfect CSI. Basically, in the ODD method, the channel gains at data positions are interpolated from the MMSE-estimated channel

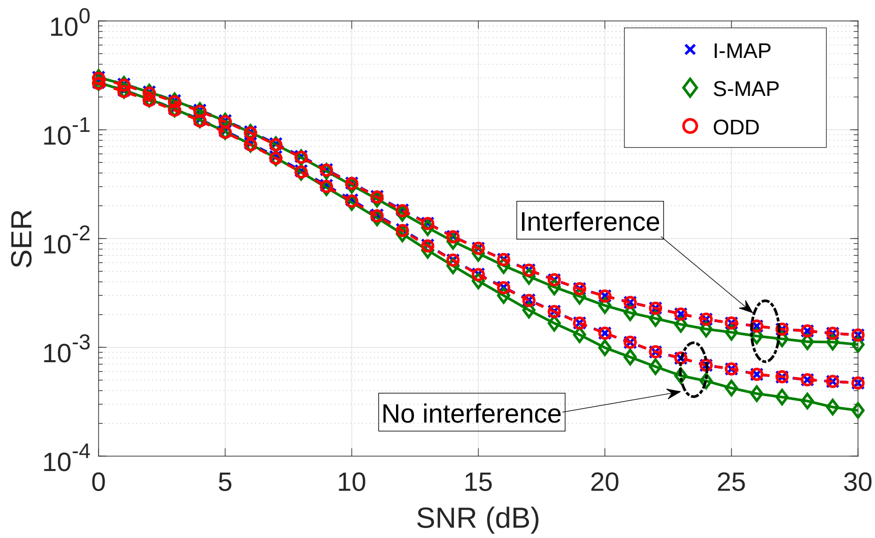

Figure 5.6: SER achieved by different detection methods, $N_{\text{d}} = 3$

gains at pilot positions. Then, the zero-forcing based symbol detection is employed (please refer to Sections III and IV in [28] for more details).

Fig. 5.6 illustrates the SER achieved by these detection methods for the interference-free and interference scenarios, which are denoted as IF and IP in this section, respectively. It can be seen that the SER of the proposed I-MAP is almost identical to that achieved by the ODD method. Moreover, the S-MAP detector outperforms both I-MAP and ODD and the performance gap is larger in the interference-free scenario. Note that, in the IP scenario, the residual interference still presents, which causes the error floors in these SER curves.

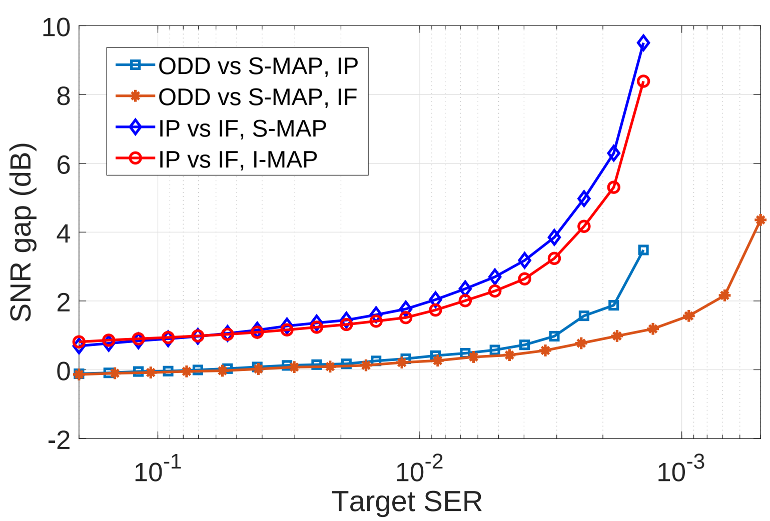

Figure 5.7: SNR gap for specific target SER, $N_{\text{d}} = 3$

For performance comparison between our methods and the existing method, we show in Fig. 5.7 the SNR gap to achieve the same SER between different symbol detection methods (S-MAP, I-MAP) and scenarios (IF, IP). Particularly, a value of 3dB SNR gap at 5×10^{-3} target SER of the curve *A vs B* means that method A needs 3dB higher in SNR to achieve the same target SER achieved by method B. For the same scenario (IF or IP), the SNR gap between the proposed S-MAP and ODD becomes larger as the required SER decreases. Note again that there is a performance floor in the IP scenario; nevertheless, our proposed detection method achieves more than 3dB SNR gain compared to the existing ODD method for the same detection performance in the low target SER regime (see the curve with square markers). Moreover, to achieve the same SER performance under the high reliability condition (i.e., low SER), the SNR required in the interference scenario is much higher than that required in the interference free scenario (illustrated by IP vs IF curves).

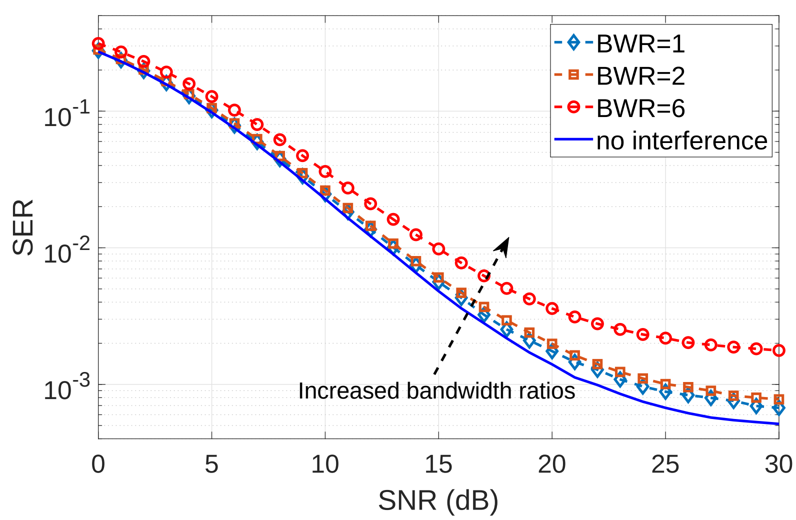

Figure 5.8: SER versus SNR for different values of BWR, $N_{\mathrm{d}} = 3$

Fig. 5.8 illustrates the SER in the interference-free and interference scenarios for different bandwidth ratios, which is denoted as BWR. As can be seen from this figure, higher bandwidth ratios between interfering and desired signals lead to higher SER. This is because higher BWR creates more severe interference for the desired signal and it is not possible to completely remove the interference due to the fast fading.

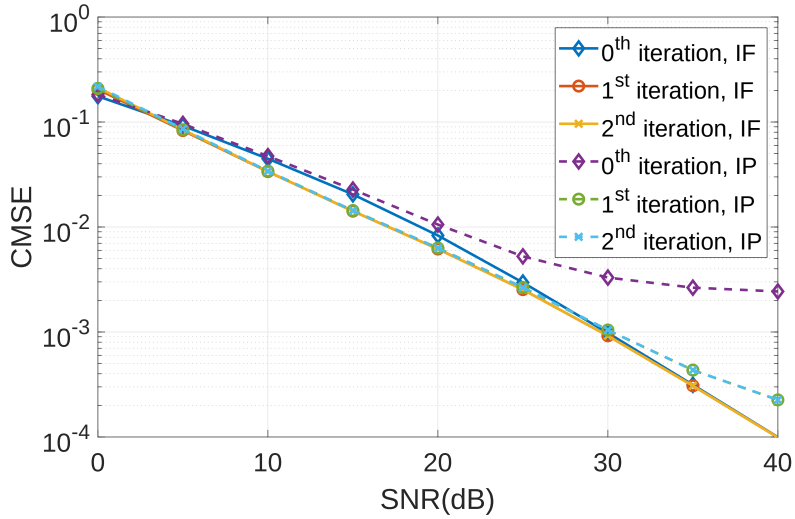

Figure 5.9: Performance of channel estimation for iterative algorithm

5.6.4 Performance of the Iterative Algorithm

We now study the performance of the iterative algorithm for channel estimation, interference cancellation, and symbol detection. First, we present the performance of channel estimation over iterations in Fig. 5.9 where the CMSE of estimated channel gains is shown for both IF and IP scenarios. As can be seen from this figure, the iterative algorithm converges[9] after only a few iterations. The most noticeable observation is that the converged channel estimation performance in the presence of interference (IP) is almost identical to that of the interference free scenario (IF) in the low SNR regime (less then 30dB), which implies that the proposed iterative method cancels very well the interference in this SNR region. When the SNR is higher than 30dB, the performance in the IP case is still limited by the fast fading noise. However, the performance floor of the iterative channel estimation approach is much lower than that of the non-iterative counterpart (the 0^{th}-iteration[10] versus the 2^{nd}-iteration curves in the IP scenario).

We now study how the SER improves over iterations. In Fig. 5.10, the left and right figures show the SERs for the IF and IP cases, respectively. It can be seen from the figure that the SER

[9] In the simulation, the convergence is actually achieved when there is no change in the detected data symbols. For a better illustration, we show the 'convergence' of the CMSE instead. This is because there is no change in the estimated channel if there is no change in the detected data symbols over iterations.

[10] Note that iterations are only counted when the algorithm enters the while loop. In other words, results obtained from the first and second steps in Algorithm 3 are considered at the 0^{th} iteration. In Algorithm 3, we choose I-MAP due to its low complexity, but S-MAP can also be used.

improvement is higher when the interference is present, which suggests that the iterative algorithm estimates and cancels the interference effectively.

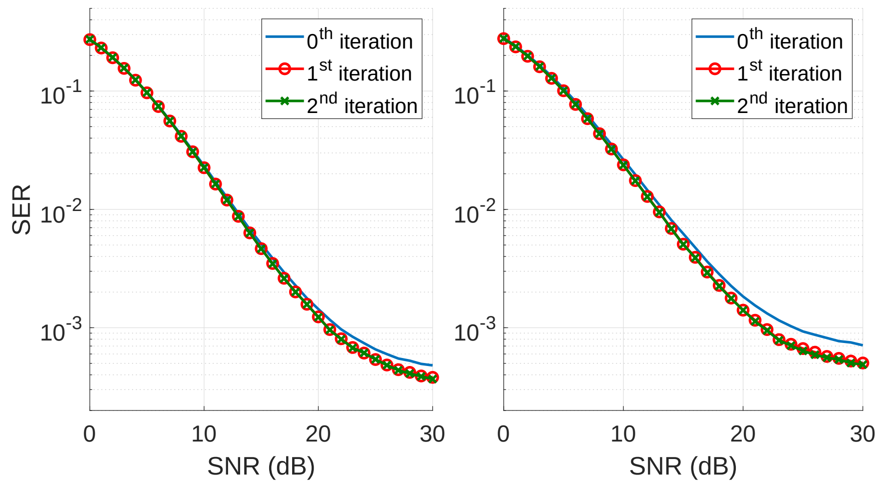

Figure 5.10: SER over iterations

We show the SERs achieved by the non-iterative and iterative algorithms[11]. From Fig. 5.11, we can see that the iterative algorithm improves the SER in both IF and IP scenarios. Furthermore, the improvement is higher for larger values of SNR. This is because that the high SNR regime allows more reliable data detection, which boosts the performance of interference cancellation and channel estimation.

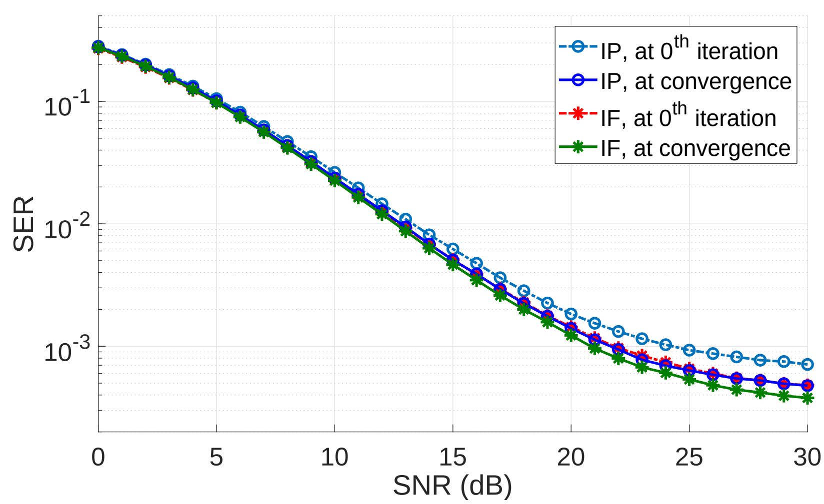

Figure 5.11: SER achieved by iterative and non-iterative algorithms

[11]The SER of the non-iterative algorithm is the SER computed at the 0^{th} iteration and the SER of the iterative algorithm is the SER achieved at convergence.

5.6.5 Throughput Achieved by the Proposed Framework

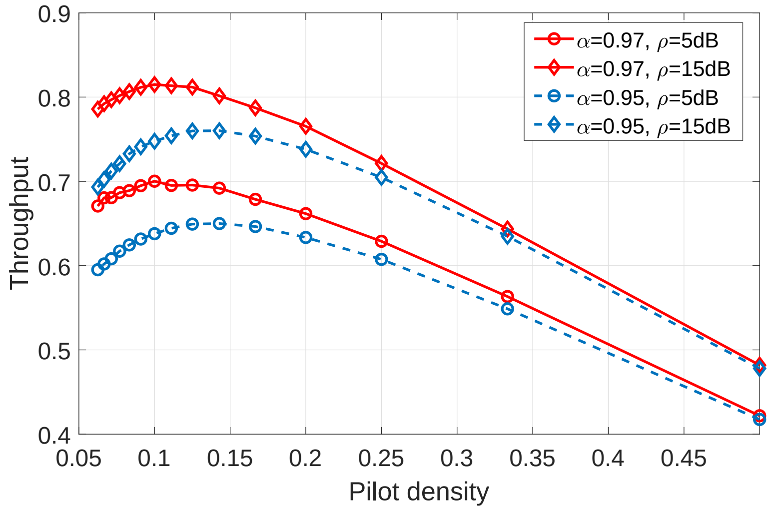

Figure 5.12: Throughput variations with the pilot density

In Fig. 5.12, we show the variations of the throughput with the pilot density for different values of SNR ρ and channel correlation coefficient α. As can be seen from this figure, for given α and ρ, there exists an optimal pilot density that achieves the maximum throughput. Moreover, the maximum throughput increases as the SNR ρ increases. It can also be observed that larger α leads to higher maximum throughput and lower optimal pilot density. This is because when the channel varies more slowly, the performance of interference cancellation and channel estimation is improved, which results in more reliable transmission and higher throughput. The results in this figure demonstrate the tradeoff between the throughput and communication reliability in the fast fading environment.

5.7 Conclusion

We have proposed two frameworks for channel estimation, interference cancellation, and symbol detection for communication signals with different bandwidth in the fast fading environment. Specifically, in the two-phase non-iterative framework, we have derived the channel estimators and studied both series and individual symbol detection methods. The iterative framework performs interference cancellation, channel estimation and data detection based on the detected data symbol from the previous iteration, which can improve the system performance compared to the non-iterative counterpart. Numerical studies have confirmed the existence of the performance floor for SER in the considered interference scenario and illustrated the optimal pilot density to achieve the maximum throughput. Moreover, we have shown that the series symbol detection method outperforms the existing ODD method in terms of SER while the individual symbol detection method achieves the very close performance to the ODD method but with lower complexity.

Appendices

5.A Proof of Theorem 5.1

To compute $p(\mathbf{h}_n, \mathbf{Y})$, we need to find $p(\mathbf{Y}|\mathbf{h}_n)$, since

$$p(\mathbf{h}_n, \mathbf{Y}) = p(\mathbf{Y}|\mathbf{h}_n)p(\mathbf{h}_n), \tag{5.34}$$

and $p(\mathbf{h}_n)$ is known to be $\mathcal{CN}(\mathbf{h}_n, \mathbf{0}, \mathbf{I}_{N_\mathsf{r}})$, where $\mathcal{CN}(\mathbf{x}, \boldsymbol{\mu}, \boldsymbol{\Sigma})$ is the complex Gaussian density of random vector $\mathbf{x}$ having mean $\boldsymbol{\mu}$ and covariance matrix $\boldsymbol{\Sigma}$ [101]. The likelihood of $\mathbf{Y}$, given $\mathbf{h}_n$ can be factorized, thanks to the channel Markovian property, as

$$p(\mathbf{Y}|\mathbf{h}_n) = p(\mathbf{y}_n|\mathbf{h}_n) \prod_{i=1}^{n-1} p(\mathbf{y}_i|\mathbf{y}_{i+1}, \mathbf{h}_n) \prod_{i=n+1}^{N_\mathsf{p}} p(\mathbf{y}_i|\mathbf{y}_{i-1}, \mathbf{h}_n). \tag{5.35}$$

Given $\mathbf{h}_n$, any two consecutive observations are correlated due to the cumulative channel evolutionary noises. Since we consider only received signals at pilot positions, the equivalent correlation coefficient of channel gains at two consecutive pilot positions is $\alpha_\mathsf{p} = \alpha^{N_\mathsf{d}+1}$. To further derive $p(\mathbf{Y}|\mathbf{h}_n)$, we need to find the probabilities $p(\mathbf{y}_i|\mathbf{y}_{i-1}, \mathbf{h}_n)$ for $i > n$ and $p(\mathbf{y}_i|\mathbf{y}_{i+1}, \mathbf{h}_n)$ for $i < n$.

We now show the derivation of $p(\mathbf{y}_i|\mathbf{y}_{i-1}, \mathbf{h}_n)$ for $i > n$. From (5.8), the channel coefficient $\mathbf{h}_i, i > n$ can be expressed with respect to $\mathbf{h}_n$ as

$$\mathbf{h}_i = \alpha_\mathsf{p}^{i-n} \left(\mathbf{h}_n + \eta_\mathsf{p} \sum_{j=1}^{i-n} \alpha_\mathsf{p}^{-j} \boldsymbol{\Delta}_{n+j} \right), \tag{5.36}$$

where $\eta_{\mathsf{p}} = \left(1-\alpha_{\mathsf{p}}^2\right)^{1/2}$. Substituting $\mathbf{h}_n$ in (5.36) into (5.9), it can be seen that $\mathbf{y}_i$ and $\mathbf{y}_{i-1}$ share the common evolutionary noise terms $\mathbf{\Delta}_{n+j}, j = 1, ..., i-n-1$. Then, we can obtain the parameters of the distribution $p(\mathbf{y}_i, \mathbf{y}_{i-1}|\mathbf{h}_n) = \mathcal{CN}\left(\begin{bmatrix} \mathbf{y}_i \\ \mathbf{y}_{i-1} \end{bmatrix}, \begin{bmatrix} \boldsymbol{\mu}_{\mathbf{y}_i|\mathbf{h}_n} \\ \boldsymbol{\mu}_{\mathbf{y}_{i-1}|\mathbf{h}_n} \end{bmatrix}, \begin{bmatrix} \mathbf{\Sigma}_{\mathbf{y}_i|\mathbf{h}_n} & \mathbf{\Sigma}_{\mathbf{y}_i,\mathbf{y}_{i-1}|\mathbf{h}_n} \\ \mathbf{\Sigma}^H_{\mathbf{y}_i,\mathbf{y}_{i-1}|\mathbf{h}_n} & \mathbf{\Sigma}_{\mathbf{y}_{i-1}|\mathbf{h}_n} \end{bmatrix}\right)$ as follows:

$$\begin{aligned}
\boldsymbol{\mu}_{\mathbf{y}_k|\mathbf{h}_n} &= \mathbf{B}_k\mathbf{c} + \alpha_{\mathsf{p}}^{k-n}\mathbf{h}_n x_k,\ k = i, i-1, \\
\mathbf{\Sigma}_{\mathbf{y}_k|\mathbf{h}_n} &= \left(\sigma^2 + \alpha_{\mathsf{p}}^{2(k-n)}\eta_{\mathsf{p}}^2 \sum_{j=1}^{k-n} \alpha_{\mathsf{p}}^{-2j}\right)\mathbf{I}_{N_{\mathsf{r}}} \\
&= \left[1 + \rho\left(1 - \alpha_{\mathsf{p}}^{2(k-n)}\right)\right]\sigma^2\mathbf{I}_{N_{\mathsf{r}}},\ k = i, i-1, \\
\mathbf{\Sigma}_{\mathbf{y}_i,\mathbf{y}_{i-1}|\mathbf{h}_n} &= \mathbb{E}\left[\left(\mathbf{y}_i - \boldsymbol{\mu}_{\mathbf{y}_i|\mathbf{h}_n}\right)\left(\mathbf{y}_{i-1} - \boldsymbol{\mu}_{\mathbf{y}_{i-1}|\mathbf{h}_n}\right)^H|\mathbf{h}_n\right] \\
&= x_i x_{i-1}^* \alpha_{\mathsf{p}}(1 - \alpha_{\mathsf{p}}^{2(i-n-1)})\mathbf{I}_{N_{\mathsf{r}}}.
\end{aligned} \tag{5.37}$$

Next, we apply the conditional probability formula for the multivariate Complex Circular Symmetric Gaussian vector [204] (section 3.7.7, page 153) and obtain $p(\mathbf{y}_i|\mathbf{y}_{i-1}, \mathbf{h}_n) = \mathcal{CN}(\mathbf{y}_i, \boldsymbol{\mu}_{i,n}, \mathbf{\Sigma}_{i,n})$ for $i > n$, where

$$\begin{aligned}
\boldsymbol{\mu}_{i,n} &= \boldsymbol{\mu}_{\mathbf{y}_i|\mathbf{h}_n} + \beta_{i,n}\left(\mathbf{y}_{i-1} - \boldsymbol{\mu}_{\mathbf{y}_{i-1}|\mathbf{h}_n}\right), \quad \mathbf{\Sigma}_{i,n} = \sigma_{i,n}^2\mathbf{I}_{N_{\mathsf{r}}}, \\
\beta_{i,n} &= \frac{x_i x_{i-1}^* \rho\alpha_{\mathsf{p}}\left(1 - \alpha_{\mathsf{p}}^{2(i-n-1)}\right)}{1 + \rho\left(1 - \alpha_{\mathsf{p}}^{2(i-n-1)}\right)}, \\
\sigma_{i,n}^2 &= \sigma^2\left[1 + \rho\left(1 - \alpha_{\mathsf{p}}^{2(i-n)}\right) - \frac{\rho^2\alpha_{\mathsf{p}}^2\left(1 - \alpha_{\mathsf{p}}^{2(i-n-1)}\right)^2}{1 + \rho\left(1 - \alpha_{\mathsf{p}}^{2(i-n-1)}\right)}\right].
\end{aligned} \tag{5.38}$$

For $i < n$, $p(\mathbf{y}_i|\mathbf{y}_{i+1}, \mathbf{h}_n) = \mathcal{CN}(\mathbf{y}_i, \boldsymbol{\mu}_{i,n}, \mathbf{\Sigma}_{i,n})$, where the parameters can be expressed similarly as follows:

$$\begin{aligned}
\boldsymbol{\mu}_{i,n} &= \alpha_{\mathsf{p}}^{n-i}\mathbf{h}_n x_i + \mathbf{B}_i\mathbf{c} + \beta_{i,n}(\mathbf{y}_{i+1} - \alpha_{\mathsf{p}}^{n-i-1}\mathbf{h}_n x_{i+1} - \mathbf{B}_{i+1}\mathbf{c}), \\
\mathbf{\Sigma}_{i,n} &= \sigma_{i,n}^2\mathbf{I}_{N_{\mathsf{r}}}, \quad \beta_{i,n} = \frac{x_i x_{i+1}^* \rho\alpha_{\mathsf{p}}\left(1 - \alpha^{2(n-i-1)}\right)}{1 + \rho\left(1 - \alpha_{\mathsf{p}}^{2(n-i-1)}\right)}, \\
\sigma_{i,n}^2 &= \sigma^2\left[1 + \rho\left(1 - \alpha_{\mathsf{p}}^{2(n-i)}\right) - \frac{\rho^2\alpha_{\mathsf{p}}^2\left(1 - \alpha_{\mathsf{p}}^{2(n-i-1)}\right)^2}{1 + \rho\left(1 - \alpha_{\mathsf{p}}^{2(n-i-1)}\right)}\right].
\end{aligned} \tag{5.39}$$

For $j = n, \boldsymbol{\mu}_{n,n} = \mathbf{h}_n x_n + \mathbf{B}_n \mathbf{c},\ \mathbf{\Sigma}_{n,n} = \sigma^2 \mathbf{I}_{N_\mathsf{r}}$. Substituting the parameters in (5.38) and (5.39) into (5.34) using (5.35), taking the logarithm, we obtain the log-likelihood function in Theorem 5.1. This completes the proof.

5.B Proof for the Positive-definiteness of $\mathbf{D}_n$

For an arbitrary non-zero vector $\mathbf{z} = [z_1, ..., z_L]^T$, we have

$$\begin{aligned}
\mathbf{z}^H \mathbf{D}_n \mathbf{z} &= \operatorname{tr}\left[\left(\sum_{i=1}^{N_\mathsf{p}} \frac{(\mathbf{B}_{i,n}\mathbf{z})^H (\mathbf{B}_{i,n}\mathbf{z})}{\sigma_{i,n}^2}\right)\right] - \operatorname{tr}\left[\left(\sum_{i=1}^{N_\mathsf{p}} \frac{x_{i,n}^* \mathbf{B}_{i,n}}{\sigma_{i,n}^2}\mathbf{z}\right)^H \mathbf{A}_n^{-1} \left(\sum_{i=1}^{N_\mathsf{p}} \frac{x_{i,n}^* \mathbf{B}_{i,n}}{\sigma_{i,n}^2}\mathbf{z}\right)\right] \\
&= \operatorname{tr}\left[\left(\sum_{i=1}^{N_\mathsf{p}} \frac{(\mathbf{B}_{i,n}\mathbf{z}) (\mathbf{B}_{i,n}\mathbf{z})^H}{\sigma_{i,n}^2}\right)\right] - \operatorname{tr}\left[\left(\sum_{i=1}^{N_\mathsf{p}} \frac{x_{i,n}^* \mathbf{B}_{i,n}}{\sigma_{i,n}^2}\mathbf{z}\right) \mathbf{A}_n^{-1} \left(\sum_{i=1}^{N_\mathsf{p}} \frac{x_{i,n}^* \mathbf{B}_{i,n}}{\sigma_{i,n}^2}\mathbf{z}\right)^H\right] \\
&> \operatorname{tr}\left[\left(\sum_{i=1}^{N_\mathsf{p}} \frac{(\mathbf{B}_{i,n}\mathbf{z}) (\mathbf{B}_{i,n}\mathbf{z})^H}{\sigma_{i,n}^2}\right) - \left(\sum_{i=1}^{N_\mathsf{p}} \frac{x_{i,n}^* \mathbf{B}_{i,n}}{\sigma_{i,n}^2}\mathbf{z}\right) (\mathbf{A}_n - \mathbf{I}_{N_\mathsf{r}})^{-1} \left(\sum_{i=1}^{N_\mathsf{p}} \frac{x_{i,n}^* \mathbf{B}_{i,n}}{\sigma_{i,n}^2}\mathbf{z}\right)^H\right],
\end{aligned} \tag{5.40}$$

where tr($\mathbf{X}$) is the sum of diagonal elements of $\mathbf{X}$. In the last two lines of (5.40), the jth diagonal element of the first term is $\sum_{i=1}^{N_\mathsf{p}} \left(\mathbf{b}_{i,n}^{(j)}\mathbf{z}\right)\left(\mathbf{b}_{i,n}^{(j)}\mathbf{z}\right)^H / \sigma_{i,n}^2$, where $\mathbf{b}_{i,n}^{(j)}$ is the jth row of $\mathbf{B}_{i,n}$, and the jth diagonal element of the second term is $\left(\sum_{i=1}^{N_\mathsf{p}} \frac{|x_{i,n}|^2}{\sigma_{i,n}^2}\right)^{-1} \left(\sum_{i=1}^{N_\mathsf{p}} \frac{x_{i,n}^* \mathbf{b}_{i,n}^{(j)}\mathbf{z}}{\sigma_{i,n}^2}\right)\left(\sum_{i=1}^{N_\mathsf{p}} \frac{x_{i,n}^* \mathbf{b}_{i,n}^{(j)}\mathbf{z}}{\sigma_{i,n}^2}\right)^H$, where $\mathbf{A}_n$ from (5.14) is substituted into this term.

We now define the two vectors $\mathbf{u}$ and $\mathbf{v}$ whose ith elements are $\mathrm{u}_i = x_{i,n}^*/\sigma_{i,n}$ and $\mathrm{v}_i = \mathbf{b}_{i,n}^{(j)}\mathbf{z}/\sigma_{i,n}$, respectively. By applying the *Cauchy-Schwarz* inequality:

$$|\mathbf{u}|^2 |\mathbf{v}|^2 \geq |\mathbf{u}.\mathbf{v}|^2, \tag{5.41}$$

it can be verified that each diagonal element of the matrix in the last two lines of (5.40) is positive, which means its trace is also positive. Thus, we have completed the proof.

5.C Proof of Theorem 5.2

We can reformulate $p\left(x_{1:N_\mathsf{d}}|\mathbf{h}_h,\mathbf{h}_t,\mathbf{y}_{1:N_\mathsf{d}}\right)$ as follows.

$$
\begin{aligned}
p\left(x_{1:N_\mathsf{d}}|\mathbf{h}_h,\mathbf{h}_t,\mathbf{y}_{1:N_\mathsf{d}}\right) &\propto \int p(x_{1:N_\mathsf{d}},\mathbf{y}_{1:N_\mathsf{d}},\mathbf{h}_h,\mathbf{h}_{1:N_\mathsf{d}},\mathbf{h}_t)d\mathbf{h}_{1:N_\mathsf{d}} \\
&\overset{(a)}{\propto} \int p(\mathbf{y}_{1:N_\mathsf{d}}|\mathbf{h}_{1:N_\mathsf{d}},x_{1:N_\mathsf{d}})p(\mathbf{h}_h,\mathbf{h}_{1:N_\mathsf{d}},\mathbf{h}_t)d\mathbf{h}_{1:N_\mathsf{d}} \\
&\overset{(b)}{\propto} \int p(\mathbf{h}_h,\mathbf{h}_{1:N_\mathsf{d}},\mathbf{h}_t)\prod_{i=1}^{N_\mathsf{d}} p(\mathbf{y}_i|x_i,\mathbf{h}_i)d\mathbf{h}_{1:N_\mathsf{d}} \\
&\overset{(c)}{\propto} \int p(\mathbf{h}_1|\mathbf{h}_h)p(\mathbf{h}_t|\mathbf{h}_{N_\mathsf{d}})\prod_{i=2}^{N_\mathsf{d}} p(\mathbf{h}_i|\mathbf{h}_{i-1})\prod_{i=1}^{N_\mathsf{d}} p(\mathbf{y}_i|x_i,\mathbf{h}_i)d\mathbf{h}_{1:N_\mathsf{d}} \\
&\overset{(d)}{\propto} e^{\mathcal{F}}\int exp\left\{-\sum_{i=1}^{N_\mathsf{d}}(\mathbf{h}_i-\mathbf{a}_i)^H\mathbf{S}_i^{-1}(\mathbf{h}_i-\mathbf{a}_i)\right\}d\mathbf{h}_{1:N_\mathsf{d}} \\
&\overset{(e)}{\propto} e^{\mathcal{F}}\prod_{i=1}^{N_\mathsf{d}}|\mathbf{S}_i|,
\end{aligned}
\tag{5.42}
$$

where $\mathbf{\Gamma}_{i,j} = \tau_2^{i-j}\prod_{k=j}^{i-1}\mathbf{S}_k, \tau_1 = \frac{1}{(1-\alpha^2)\sigma_\mathsf{h}^2}, \tau_2 = \alpha\tau_1$, and $\mathcal{F}$ is defined in (5.22). Assuming all points in the constellation are transmitted with equal probability, the conditional probabilities in (5.42) are transformed by Baye's rule (a) and the Markovian property of channel (b,c), where these expressions can be obtained by iteratively synthesizing quadratic terms of $\mathbf{h}_i, i = 1,...,N_\mathsf{d}$ in the exponents (d,e).

5.D Proof of Proposition 5.1

The channel estimation error can be written as (see (5.14), (5.15a))

$$
\begin{aligned}
\boldsymbol{\nu}_n &= \mathbf{h}_n - \mathbf{A}_n^{-1}\left(\sum_{i=1}^{N_\mathsf{p}}\frac{x_{i,n}^*}{\sigma_{i,n}^2}\left(\mathbf{y}_i-\beta_{i,n}\mathbf{y}_{i+j_{i,n}}\right)\right) \\
&= \boldsymbol{\nu}_n^\mathsf{g}+\boldsymbol{\nu}_n^\mathsf{c},
\end{aligned}
\tag{5.43}
$$

where $\boldsymbol{\nu}_n^{\mathsf{g}}$ is the error due to the AWGN, and $\boldsymbol{\nu}_n^{\mathsf{c}}$ is the error due to the channel evolutionary noise. Specifically,

$$\begin{aligned} \boldsymbol{\nu}_n^{\mathsf{g}} &= \sum_{i=1}^{N_{\mathsf{p}}} \boldsymbol{\Xi}_{i,n}^{\mathsf{g}} \mathbf{w}_i, \\ \boldsymbol{\nu}_n^{\mathsf{c}} &= \boldsymbol{\Xi}_{0,n}^{\mathsf{c}} \mathbf{h}_0 + \sum_{i=1}^{N_{\mathsf{p}}} \boldsymbol{\Xi}_{i,n}^{\mathsf{c}} \boldsymbol{\Delta}_i, \end{aligned} \tag{5.44}$$

where we decompose $\mathbf{h}_n$ into $\alpha_{\mathsf{p}}^n \left(\mathbf{h}_0 + \sum_{i=1}^{n} \alpha_{\mathsf{p}}^{-i} \boldsymbol{\Delta}_i \right)$. By using this decomposition, it is more convenient to compute the channel estimation error components due to the channel evolutionary noise. Otherwise, one has to determine the dependence structure of $\mathbf{h}_n$ on the preceding channel noise components $\boldsymbol{\Delta}_i, i < n$, which is not trivial.

When the desired channels are independent, $\boldsymbol{\Xi}_{i,n}^{\mathsf{g}} = \xi_{i,n}^{\mathsf{g}} \mathbf{I}_{N_{\mathsf{r}}}$ and $\boldsymbol{\Xi}_{i,n}^{\mathsf{c}} = \xi_{i,n}^{\mathsf{c}} \mathbf{I}_{N_{\mathsf{r}}}$. Substituting $\mathbf{y}_i = \mathbf{h}_i x_i + \mathbf{w}_i$ into (5.43), we have

$$\xi_{i,n}^{\mathsf{g}} = \begin{cases} -\frac{x_{i,n}^*}{a_n \sigma_{i,n}^2}, & i = 1, n, n\pm 1, N_{\mathsf{p}}, \\ -\frac{x_i^*}{a_n} \left(\frac{\omega_{i,n}}{\sigma_{i,n}^2} + \frac{|\beta_{n,i-j_{i,n}}| \omega_{n,i-j_{i,n}}}{\sigma_{n,i-j_{i,n}}^2} \right), & \text{otherwise.} \end{cases}$$

Hence, the AWGN contributes to the CEE with the total power of $\sigma^2 \sum_{i=1}^{N_{\mathsf{p}}} |\xi_{i,n}^{\mathsf{g}}|^2$. As the SNR goes to infinity, $\lim_{\rho\to\infty} \sum_{i=1}^{N_{\mathsf{p}}} |\xi_{i,n}^{\mathsf{g}}|^2 = 1$, and the AWGN contributes σ^2 to the overall CEE. Besides, $\boldsymbol{\nu}_n^{\mathsf{c}}$ is expressed in (5.46), and we can write the multipliers $\xi_{i,n}^{\mathsf{c}}$ as follows.

$$\begin{aligned} \xi_{0,n}^{\mathsf{c}} &= \alpha_{\mathsf{p}}^n - \sum_{i=1}^{N_{\mathsf{p}}} \frac{\omega_{i,n} \alpha_{\mathsf{p}}^i}{a_n \sigma_{i,n}^2} (1 - |\beta_{i,n}| \alpha_{\mathsf{p}}^{j_{i,n}}), \\ \xi_{i,n}^{\mathsf{c}} &= \frac{\alpha_{\mathsf{p}}^{-i}}{a_n} \left(\sum_{k=i-1}^{n-1} \frac{\omega_{k,n}}{\sigma_{k,n}^2} |\beta_{k,n}| \alpha_{\mathsf{p}}^{k+1} - \sum_{k=i}^{N_{\mathsf{p}}} \frac{\omega_{k,n}}{\sigma_{k,n}^2} \alpha_{\mathsf{p}}^k + \alpha_{\mathsf{p}}^n + \sum_{k=n+1}^{N_{\mathsf{p}}} \frac{\omega_{k,n}}{\sigma_{k,n}^2} |\beta_{k,n}| \alpha_{\mathsf{p}}^{k-1} \right), \quad i \le n, \\ \xi_{i,n}^{\mathsf{c}} &= \frac{\alpha_{\mathsf{p}}^{-i}}{a_n} \left(\sum_{k=i+1}^{N_{\mathsf{p}}} \frac{\omega_{k,n}}{\sigma_{k,n}^2} |\beta_{k,n}| \alpha_{\mathsf{p}}^{k-1} - \sum_{k=i}^{N_{\mathsf{p}}} \frac{\omega_{k,n}}{\sigma_{k,n}^2} \alpha_{\mathsf{p}}^k - \frac{1}{\sigma^2} \mathbb{1}_{n<N} \mathbb{1}_{i=N} \right), \quad i > n. \end{aligned} \tag{5.45}$$

$$\begin{aligned}
\boldsymbol{\nu}_n^{\mathsf{c}} &= \mathbf{h}_n - \mathbf{A}_n^{-1}\left\{\sum_{i=1}^{N_{\mathsf{p}}}\frac{\omega_{i,n}\alpha_{\mathsf{p}}^i}{\sigma_{i,n}^2}\left[\mathbf{h}_0 + \sum_{k=1}^{i}\alpha_{\mathsf{p}}^{-k}\boldsymbol{\Delta}_k - |\beta_{i,n}|\alpha_{\mathsf{p}}^{j_{i,n}}\left(\mathbf{h}_0 + \sum_{k=1}^{i+j_{i,n}}\alpha_{\mathsf{p}}^{-k}\boldsymbol{\Delta}_k\right)\right]\right\} \\
&= \mathbf{h}_0\left(\alpha_{\mathsf{p}}^n - \sum_{i=1}^{N_{\mathsf{p}}}\frac{\omega_{i,n}\alpha_{\mathsf{p}}^i}{a_n\sigma_{i,n}^2}(1-|\beta_{i,n}|\alpha_{\mathsf{p}}^{j_{i,n}})\right) - \sum_{k=1}^{N_{\mathsf{p}}}\left(\boldsymbol{\Delta}_k\alpha_{\mathsf{p}}^{-k}\sum_{i=k}^{N_{\mathsf{p}}}\frac{\omega_{i,n}}{a_n\sigma_{i,n}^2}\alpha_{\mathsf{p}}^i\right) + \sum_{i=1}^{n}\alpha_{\mathsf{p}}^{n-i}\boldsymbol{\Delta}_i \\
&\quad + \sum_{k=1}^{n}\left(\boldsymbol{\Delta}_k\alpha_{\mathsf{p}}^{-k}\sum_{i=k-1}^{n-1}\frac{\omega_{i,n}}{a_n\sigma_{i,n}^2}|\beta_{i,n}|\alpha_{\mathsf{p}}^{i+1}\right) + \sum_{k=1}^{N_{\mathsf{p}}-1}\left(\boldsymbol{\Delta}_k\alpha_{\mathsf{p}}^{-k}\sum_{i=k+1,i>n}^{N_{\mathsf{p}}}\frac{\omega_{i,n}}{a_n\sigma_{i,n}^2}|\beta_{i,n}|\alpha_{\mathsf{p}}^{i-1}\right) \\
&= \mathbf{h}_0\left(\alpha_{\mathsf{p}}^n - \sum_{i=1}^{N_{\mathsf{p}}}\frac{\omega_{i,n}\alpha_{\mathsf{p}}^i}{a_n\sigma_{i,n}^2}\left(1-|\beta_{i,n}|\alpha_{\mathsf{p}}^{j_{i,n}}\right)\right) + \sum_{k=n+1}^{N-1}\left[\boldsymbol{\Delta}_k\frac{\alpha_{\mathsf{p}}^{-k}}{a_n}\left(\sum_{i=k+1}^{N_{\mathsf{p}}}\frac{\omega_{i,n}}{\sigma_{i,n}^2}|\beta_{i,n}|\alpha_{\mathsf{p}}^{i-1} - \sum_{i=k}^{N_{\mathsf{p}}}\frac{\omega_{i,n}}{\sigma_{i,n}^2}\alpha_{\mathsf{p}}^i\right)\right] \\
&\quad + \sum_{k=1}^{n}\left[\boldsymbol{\Delta}_k\frac{\alpha_{\mathsf{p}}^{-k}}{a_n}\left(\sum_{i=k-1}^{n-1}\frac{\omega_{i,n}}{\sigma_{i,n}^2}|\beta_{i,n}|\alpha_{\mathsf{p}}^{i+1} - \sum_{i=k}^{N_{\mathsf{p}}}\frac{\omega_{i,n}}{\sigma_{i,n}^2}\alpha_{\mathsf{p}}^i + \sum_{i=n+1}^{N_{\mathsf{p}}}\frac{\omega_{i,n}}{\sigma_{i,n}^2}|\beta_{i,n}|\alpha_{\mathsf{p}}^{i-1}\right)\right] \\
&\quad + \sum_{k=1}^{n}\boldsymbol{\Delta}_k\alpha_{\mathsf{p}}^{n-k} - \boldsymbol{\Delta}_N\frac{\omega_{N,n}}{a_n\sigma_{N,n}^2}\mathbb{1}_{n<N}.
\end{aligned} \tag{5.46}$$

As SNR goes to infinity, $\lim_{\rho\to\infty}\sum_{i=1}^{N_{\mathsf{p}}}|\xi_{i,n}^{\mathsf{c}}|^2 = 0$, the channel evolutionary noises contribute negligible power to the CEE. This completes the proof.

5.E Proof of Proposition 5.2

Substituting $\mathbf{y}_{i,n}$ from (5.15a) into (5.18b), note that $\mathbf{y}_i = \mathbf{h}_i x_i + \mathbf{B}_i\mathbf{c} + \mathbf{w}_i$, and after some manipulations, we have

$$\tilde{\mathbf{c}}_n = \mathbf{c} + \mathbf{D}_n^{-1}\sum_{i=1}^{N_{\mathsf{p}}}\mathbf{G}_{i,n}\left(\mathbf{h}_i x_i + \mathbf{w}_i\right), \tag{5.47}$$

where $\mathbf{K}_n = \left(\sum_{i=1}^{N_{\mathsf{p}}} x_{i,n}^*\boldsymbol{\Sigma}_{i,n}^{-1}\mathbf{B}_{i,n}\right)^H\mathbf{A}_n^{-1}, \mathbf{J}_{i,n} = \left(\mathbf{B}_{i,n}^H - \mathbf{K}_n x_{i,n}^*\right)\boldsymbol{\Sigma}_{i,n}^{-1}$, and

$$\mathbf{G}_{i,n} = \begin{cases} \mathbf{J}_{i,n}, & i = 1, n, N_{\mathsf{p}} \\ \mathbf{J}_{i,n} - \mathbf{J}_{i-1,n}\beta_{i-1,n}, & n > i > 1 \\ \mathbf{J}_{i,n} - \mathbf{J}_{i+1,n}\beta_{i+1,n}, & n < i < N_{\mathsf{p}}. \end{cases} \tag{5.48}$$

The second term in (5.47) represents the estimation error of $\mathbf{c}$ at position n, and it is independent of $\mathbf{c}$. This completes the proof for the first part of the proposition.

Additionally, it can be seen that the estimation error is a linear combination of zero-mean Gaussian random variables, hence it also has zero mean. Therefore, the estimation is unbiased. The covariance matrix of the residual interference at position nth is

$$\begin{aligned}
&(\sigma_{\mathsf{h}}^2+\sigma^2)\,\mathbb{E}_{(\mathbf{x},\mathbf{B})}\left[\mathbf{B}_n\mathbf{D}_n^{-1}\left(\sum_{i=1}^{N_{\mathsf{p}}}\mathbf{G}_{i,n}\mathbf{G}_{i,n}^H\right)\mathbf{D}_n^{-1}\mathbf{B}_n^H\right]+\\
&\sigma_{\mathsf{h}}^2\sum_{i\neq j}\mathbb{E}_{(\mathbf{x},\mathbf{B},\mathbf{h}_i,\mathbf{h}_j)}\left[\mathbf{B}_n\mathbf{D}_n^{-1}\left(\mathbf{G}_{i,n}\mathbf{h}_i\mathbf{h}_j^H\mathbf{G}_{j,n}^H x_i x_j^*\right)\mathbf{D}_n^{-1}\mathbf{B}_n^H\right]\\
&=(\sigma_{\mathsf{h}}^2+\sigma^2)\,\mathbb{E}_{(\mathbf{x},\mathbf{B})}\left[\mathbf{B}_n\mathbf{D}_n^{-1}\left(\sum_{i=1}^{N_{\mathsf{p}}}\mathbf{G}_{i,n}\mathbf{G}_{i,n}^H\right)\mathbf{D}_n^{-1}\mathbf{B}_n^H\right]+\\
&\sigma_{\mathsf{h}}^2\sum_{i\neq j}\alpha_{\mathsf{p}}^{|i-j|}\,\mathbb{E}_{(\mathbf{x},\mathbf{B})}\left[\mathbf{B}_n\mathbf{D}_n^{-1}\left(\mathbf{G}_{i,n}\mathbf{G}_{j,n}^H x_i x_j^*\right)\mathbf{D}_n^{-1}\mathbf{B}_n^H\right].
\end{aligned}\tag{5.49}$$

Deriving the closed-form expression for the covariance matrix is tedious. Hence, we will prove the proposition by using the following arguments. First, note that, $\mathbf{D}_n$ is Hermitian, positive definite, and in quadratic order of interfering matrices $\mathbf{B}_i, i=1,...,N$. Second, $\mathbf{B}_n\mathbf{G}_{i,n}$ is also in quadratic order of interfering matrices. Therefore, the expected covariance matrix is in a fractional function form with total zero-th order of $\mathbf{B}_i$. As a result, the residual interference power is bounded as we increase the interference power to infinity. Furthermore, if all interfering channel coefficients for different antennas have identical value, the residual interference power is *completely* independent of the interference power. Since estimation errors for EICs at any symbol position n are finite, the overall estimation error for EICs is also finite. This completes the proof.

5.F Proof of Proposition 5.3

Since the expression of the power of residual interference in (5.49) contains σ_{h}^2, it does not vanish as $\rho\to\infty$. As ρ goes to infinity, we have

$$
\begin{aligned}
&\omega_{i,n} \to \begin{cases} \alpha_{\mathsf{p}}, & i = n \pm 1 \\ 1, & i = n \\ 0, & \text{otherwise} \end{cases}, \qquad |\beta_{i,n}| \to \begin{cases} 0, & i = n, n \pm 1 \\ \alpha_{\mathsf{p}}, & \text{otherwise} \end{cases}, \qquad \sigma_{i,n}^2 \to \begin{cases} \sigma^2, & i = n \\ 1 - a_{\mathsf{p}}^2, & \text{otherwise} \end{cases}, \\
&\mathbf{A}_n \to \rho \mathbf{I}_{N_{\mathsf{r}}}, \\
&\mathbf{D}_n \to \mathbf{B}_n^H \mathbf{B}_n + \sum_{i \neq n}^{N_{\mathsf{p}}} \frac{\mathbf{B}_{i,n}^H \mathbf{B}_{i,n}}{1 - \alpha_{\mathsf{p}}^2} + 2 \frac{\alpha_{\mathsf{p}}^2}{1 - \alpha_{\mathsf{p}}^2} \mathbf{B}_n^H \mathbf{B}_n - \frac{\alpha_{\mathsf{p}}}{1 - \alpha_{\mathsf{p}}^2} \sum_{i = n \pm 1} \left(x_i^* x_n \mathbf{B}_n^H \mathbf{B}_i + x_i x_n^* \mathbf{B}_i^H \mathbf{B}_n \right) \\
&\quad \to N_{\mathsf{r}} N_{\mathsf{p}} \frac{1 + \alpha_{\mathsf{p}}^2}{1 - \alpha_{\mathsf{p}}^2} \mathbf{I}_L, \\
&\mathbf{K}_n \to x_n \mathbf{B}_n^H, \\
&\mathbf{J}_{n,n} \to \mathbf{B}_n^H \frac{1 + \alpha_{\mathsf{p}}^2}{1 - \alpha_{\mathsf{p}}^2} - \frac{x_n^* \alpha_{\mathsf{p}}}{1 - \alpha_{\mathsf{p}}^2} \sum_{i = n \pm 1} x_i \mathbf{B}_i^H, \\
&\mathbf{J}_{i,n} \to \frac{\mathbf{B}_{i,n}^H - x_n x_i^* \alpha_{\mathsf{p}} \mathbf{B}_n^H}{1 - \alpha_{\mathsf{p}}^2}, i \neq n, \\
&\mathbf{J}_{i,n} \mathbf{J}_{i,n}^H \to N_{\mathsf{r}} \left(\frac{1 + |\beta_{i,n}|^2 + \omega_{i,n}^2}{\sigma_{i,n}^4} \right) \mathbf{I}_L \\
&\quad \to \frac{N_{\mathsf{r}} \left(1 + \alpha_{\mathsf{p}}^2 \right)}{(1 - \alpha_{\mathsf{p}}^2)^2} \mathbf{I}_L, i \neq n, \\
&\mathbf{G}_{i,n} \mathbf{G}_{i,n}^H \to \mathbf{J}_{i,n} \mathbf{J}_{i,n}^H + |\beta_{i \pm 1,n}|^2 \mathbf{J}_{i \pm 1,n} \mathbf{J}_{i \pm 1,n}^H + \frac{2 N_{\mathsf{r}} |\beta_{i \pm 1,n}|^2}{\sigma_{i,n}^2 \sigma_{i \pm 1,n}^2} \mathbf{I}_L \\
&\quad \to N_{\mathsf{r}} \frac{1 + \alpha_{\mathsf{p}}^4 + 4 \alpha_{\mathsf{p}}^2}{(1 - \alpha_{\mathsf{p}}^2)^2} \mathbf{I}_L, i \neq n.
\end{aligned}
\tag{5.50}
$$

Upon having these asymptotic values, we substitute these values into (5.49) to arrive at the residual interference power limit stated in the proposition, note that the computation of

$\mathbb{E}_{(\mathbf{x},\mathbf{B})} \left[\mathbf{B}_n \mathbf{D}_n^{-1} \left(\mathbf{G}_{i,n} \mathbf{G}_{j,n}^H x_i x_j^* \right) \mathbf{D}_n^{-1} \mathbf{B}_n^H \right], i \neq j$, is done similarly. This completes the proof.

Chapter 6

Resource Allocation, Trajectory Optimization, and Admission Control in UAV-based Wireless Networks

The content of this chapter was published in the following paper:

Minh Tri Nguyen and Long Bao Le, "Resource allocation, trajectory optimization, and admission control in UAV-based wireless networks," *IEEE Networking Letters*, vol. 3, no. 3, pp. 129–132, July 2021.

6.1 Abstract

In this letter, we study the resource allocation and trajectory optimization for multi-UAV based wireless networks. Our design maximizes the number of admitted users while satisfying their data transmission demands, which formulates a mixed-integer nonlinear problem. To tackle its difficulty, we first introduce soft admission variables and propose an iterative algorithm to solve this admission maximization problem. Each iteration comprises two steps, namely soft admission maximization and user removal. Our method guarantees that the number of admitted users increases over iterations.

Numerical results show that our algorithm outperforms the conventional approach based on block coordinate ascent and mixed-integer linear programming.

6.2 Introduction

Unmanned Aerial Vehicles (UAV) communications have emerged as an important solution that can meet requirements of various deployment scenarios thanks to controllable UAV trajectories [16]. Previous studies [35, 153] showed that by using multiple UAVs as flying base stations, the established wireless networks can provide better coverage compared to conventional fixed ground station deployments.

From the network perspective, it is desirable to admit as large number of users as possible in overloading situations while meeting their transmission requirements. UAV-based wireless networks with flexible UAV trajectories can increase the number of admitted users. In fact, admission control problems for UAV-based wireless networks have been investigated in several recent studies [35, 153]. Specifically, the works [153] and [35] studied the admission maximization problems in different network settings where the hovering locations of UAVs are optimized. The joint resource allocation and UAV deployment optimization in UAV-based wireless networks has been tackled by using the block coordinate ascent (BCA) approach where sub-problems in the form of Mixed Integer Linear Programming (MILP) are solved iteratively [35]. Since the objective function involves integer variables and is non-differentiable, the method can converge to an inefficient solution [53] and solving the underlying MILPs has high complexity [54].

In this letter, we propose a novel and efficient algorithm to tackle the admission maximization problem. First, we introduce the soft admission (SA) variables to replace the integer (hard) admission variables. Then, we develop an iterative algorithm to solve the admission control problem where two steps are performed in each iteration, namely soft admission maximization and user removal. In the soft admission maximization step, the allocation of bandwidth, power, and UAVs' trajectories are optimized until convergence. By imposing appropriate constraints on the soft admission variables, the number of admitted users increases over iterations. Our proposed algorithm has lower complexity than that based on BCA-MILP, since our method solves a series of convex optimization problems with continuous variables instead of solving MILP problems. We show the significant performance gains of the proposed algorithm compared to the conventional BCA-MILP based scheme by numerical studies.

6.3 System Models

6.3.1 Network Settings

We consider a UAV-based wireless network where there are N UAVs serving K ground users in downlink communications. The set of users is denoted as $\mathcal{K} = \{1, ..., K\}$, the cardinality of the user set is $|\mathcal{K}| = K$. Each user k demands to receive a specific amount of data D_k transmitted by the UAVs in the downlink direction. We assume that time is slotted and each time slot has an identical length of δ. The joint UAV trajectory and resource allocation optimization is performed over each service period of T time slots. We assume that UAV n flies at the fixed altitude h and its 2-D coordinate at slot t is denoted as $\mathbf{c}_n[t]$. The 2-D coordinate of ground user k is denoted as $\mathbf{u}_k$.

We assume that the total system bandwidth is B (Hz), which are shared by users for downlink communications in the orthogonal manner. The bandwidth to support the communication[1] between UAV n and user k at time slot t is denoted as $b_{n,k}[t]$. Then, we have the following constraint for bandwidth allocation:

$$\sum_{n=1}^{N} \sum_{k=1}^{K} b_{n,k}[t] \leq B, \forall t. \tag{6.1}$$

The power that UAV n uses at time slot t to transmit data to user k is denoted as $p_{n,k}[t]$(W). Let the maximum transmit power of each UAV be P_{max}. Then, we have the following transmit power constraint:

$$\sum_{k=1}^{K} p_{n,k}[t] \leq P_{\mathsf{max}}, \forall n, t. \tag{6.2}$$

The communication channels between UAVs and users are assumed to be dominated by Line of Sight (LoS) components. This was actually observed in various practical field tests [14] when UAVs flied sufficiently high. Then, the channel power gain between UAV n and user k at time t is assumed to be $\rho_0/(h^2 + \|\mathbf{c}_n[t] - \mathbf{u}_k\|^2)$, where ρ_0 is the channel power gain at the reference distance

[1] We assume that the Frequency Division Multiple Access (FDMA) is employed with continuous allocated bandwidths $b_{n,k}[t]$ as in [144].

of 1m from the UAV. The amount of data received by user k in time slot t can be computed as

$$d_k[t] = \delta \sum_{n=1}^{N} b_{n,k}[t] \log_2 \left(1 + \frac{\gamma}{b_{n,k}[t]} \frac{p_{n,k}[t]}{h^2 + \|\mathbf{c}_n[t] - \mathbf{u}_k\|^2}\right), \tag{6.3}$$

where $\gamma = \rho_0/\sigma^2$ is the normalized Signal to Noise Ratio (SNR) and σ^2 is the white noise power density (W/Hz).

6.3.2 Problem Formulation

We consider user admission design where each user k is admitted if the UAVs can transmit at least D_k bits to it during the service period. To facilitate the design, we denote s_k as the admission decision variable which is equal to 1 if $\sum_{t=1}^{T} d_k[t] \geq D_k$ and equal to 0, otherwise.

Our design aims to maximize the number of admitted users. Let $S(\mathcal{K}) = \sum_{k\in\mathcal{K}} s_k$. The admission maximization problem can be formulated as follows:

$$\mathcal{P}^{\mathsf{AM}}(\mathcal{K}): \quad \max_{\mathbf{\Theta},\{s_k\}} S(\mathcal{K}),$$

$$\text{s.t.} \quad \sum_{t=1}^{T} d_k[t] \geq s_k D_k, \forall k, \tag{6.4a}$$

$$\|\mathbf{c}_n[t] - \mathbf{c}_n[t-1]\| \leq \min\left(V_{\mathsf{max}}\delta, D_{\mathsf{max}}\right), \forall n, t, \tag{6.4b}$$

$$\|\mathbf{c}_n[t] - \mathbf{c}_m[t]\| \geq D_{\mathsf{O}}, \forall n \neq m, t, \tag{6.4c}$$

$$\mathbf{c}_n[1] = \mathbf{c}_n[T] = \mathbf{c}_{\mathsf{o}}, \forall n, \tag{6.4d}$$

$$s_k \in \{0, 1\}, \forall k, \tag{6.4e}$$

$$\text{constraints (6.1), (6.2),}$$

where $\mathbf{\Theta} = \{\{b_{n,k}[t]\}, \{p_{n,k}[t]\}, \{\mathbf{c}_n[t]\}\}$ denotes the set of optimization variables. The constraint (6.4b) captures the maximum distance that a UAV can travel in one time slot where V_{max} is the maximum speed of a UAV and D_{max} is the maximum displacement to ensure the LoS channel conditions stay approximately the same. The constraint (6.4c) is imposed to prevent collisions among UAVs. The constraint (6.4d) sets the initial and final positions of UAV, where $\mathbf{c}_{\mathsf{o}}$ is the coordinate of the launching station.

The problem $\mathcal{P}^{\mathsf{AM}}(\mathcal{K})$ contains non-convex constraints (6.4a) and (6.4c), and the optimization variables s_k are integer. Therefore, the problem $\mathcal{P}^{\mathsf{AM}}(\mathcal{K})$ is a Mixed-Integer Non Linear Programming (MINLP) problem, which is difficult to solve optimally.

6.4 Proposed Algorithm

We introduce the demand-aware and soft admission variables based on which we develop an efficient algorithm to solve the problem $\mathcal{P}^{\mathsf{AM}}(\mathcal{K})$.

6.4.1 Demand-Aware Transmission Data and Soft Admission Variables

Recall that users should be admitted if the amount of data they receive over the service period is at least equal to their data transmission demand. Therefore, we define the demand-aware transmission data of each user k, denoted as $\bar{D}_k$, as follows:

$$\bar{D}_k = \min\left(D_k, \sum_{t=1}^{T} d_k[t]\right). \tag{6.5}$$

Then, the soft admission (SA) decision variable $\bar{s}_k$ for user k and the sum of SA variables for the user set $\mathcal{K}$ are defined respectively as

$$\bar{s}_k = \frac{\bar{D}_k}{D_k}, \forall k, \tag{6.6a}$$

$$\bar{S}(\mathcal{K}) = \sum_{k \in \mathcal{K}} \bar{s}_k. \tag{6.6b}$$

Using these variables, we consider the following SA maximization problem:

$$\begin{aligned}
\mathcal{P}^{\mathsf{SAM}}(\mathcal{K}): \quad & \max_{\mathbf{\Theta},\{\bar{D}_k,\bar{s}_k\}} \bar{S}(\mathcal{K}), \\
\text{s.t.} \quad & \bar{D}_k \leq D_k, \forall\, k \in \mathcal{K}, && (6.7a) \\
& \sum_{t=1}^{T} d_k[t] \geq \bar{D}_k, \forall\, k \in \mathcal{K}, && (6.7b) \\
& (6.1), (6.2), (6.4b), (6.4c), (6.4d), (6.6a).
\end{aligned}$$

In fact, the demand-aware transmission data $\bar{D}_k$ and SA variable $\bar{s}_k$ enable us to tackle the integer constraints involving the admission control variables s_k. For a particular resource allocation solution and UAV trajectories $\mathbf{\Theta}$, the set of admitted users is denoted as $\mathcal{K}_{\mathsf{a}} = \{k : \bar{D}_k = D_k\}$.

Let the optimal value of $\mathcal{P}^{\mathsf{AM}}(\mathcal{K})$ be $S^*(\mathcal{K})$. Then, we have $S^*(\mathcal{K}) \geq |\mathcal{K}_{\mathsf{a}}|$. This is because the feasible set of $\mathcal{P}^{\mathsf{AM}}(\mathcal{K})$ contains the resource allocation and UAV trajectories that realize $\mathcal{K}_{\mathsf{a}}$. This relation provides connections between problem $\mathcal{P}^{\mathsf{AM}}(\mathcal{K})$ and problem $\mathcal{P}^{\mathsf{SAM}}(\mathcal{K})$. Recall that our design aims to increase the cardinality of $\mathcal{K}_{\mathsf{a}}$. In the following sections, we propose an algorithm to find an efficient solution of problem $\mathcal{P}^{\mathsf{AM}}(\mathcal{K})$ by iteratively solving problem $\mathcal{P}^{\mathsf{SAM}}(\mathcal{K})$. Specifically, there are two steps in each iteration of the proposed iterative algorithm. The first step is called soft admission maximization. The second step is called user removal step, where the user which has the largest data gap between its required transmission data and actual transmission data will be removed. We index the iterations of outer loop that runs these two steps by m, to distinguish from the iterations of the inner loop, indexed by i, that runs the soft admission maximization algorithm.

6.4.2 Step 1: Soft Admission Maximization

We develop an algorithm to solve problem $\mathcal{P}^{\mathsf{SAM}}(\mathcal{K})$ by using the combination of the BCA and successive convex approximation (SCA) methods.[2] Specifically, the BCA method is applied to optimize the objective function of $\mathcal{P}^{\mathsf{SAM}}(\mathcal{K})$ with respect to one set of variables given other sets of variables while the SCA is applied to approximate and convexify the trajectory control optimization sub-problem.

6.4.2.1 Optimization of Bandwidth and Power Allocation

The bandwidth and power allocation optimization sub-problem can be written as follows:

$$\begin{aligned} \mathcal{P}_{\mathsf{BP}}(\mathcal{K}): \quad & \max_{\left\{b_{n,k}[t], p_{n,k}[t], \bar{D}_k, \bar{s}_k\right\}} \sum_{k \in \mathcal{K}} \bar{s}_k, \\ \text{s.t.} \quad & (6.1), (6.2), (6.6\text{a}), (6.7\text{a}), (6.7\text{b}). \end{aligned}$$

[2]Note that the user set at outer iteration m is denoted as $\mathcal{K}^m$. However, in this section, we are only interested in solving problem $\mathcal{P}^{\mathsf{SAM}}(\mathcal{K})$ for a certain set of users $\mathcal{K}$. So the index m is omitted for brevity.

Problem $\mathcal{P}_{\mathsf{BP}}(\mathcal{K})$ is convex, so it can be solved optimally using standard solvers such as CVX.

6.4.2.2 Optimization of UAV Trajectories

Given the bandwidth and power allocation, the UAV trajectory optimization sub-problem can be stated as follows:

$$\begin{aligned}\mathcal{P}_{\mathsf{C}}(\mathcal{K}): \quad & \max_{\{\mathbf{c}_n[t],\bar{D}_k,\bar{s}_k\}} \sum_{k\in\mathcal{K}} \bar{s}_k, \\ \text{s.t.} \quad & (6.4\text{b}), (6.4\text{c}), (6.4\text{d}), (6.6\text{a}), (6.7\text{a}), (6.7\text{b}).\end{aligned}$$

The constraints (6.7b) and (6.4c) of this problem are non-convex. However, we can apply the SCA method to convexify and solve it efficiently. Specifically, let the set of UAV coordinates (from the previous iteration) be $\mathbf{c}_n^i[t]$ and $\mathbf{c}_m^i[t]$, constraint (6.4c) can be squared and then approximated by the following inequality.

$$2\left(\mathbf{c}_m^i[t]-\mathbf{c}_n^i[t]\right)^T\left(\mathbf{c}_m[t]-\mathbf{c}_n[t]\right)-\left\|\mathbf{c}_m^i[t]-\mathbf{c}_n^i[t]\right\|^2 \geq D_{\mathsf{O}}^2. \tag{6.10}$$

Applying the approximation technique from [205], we can approximate the logarithm terms in (6.3) as follows:

$$\begin{aligned}\log_2\left(1+\frac{\bar{\gamma}_{n,k}[t]}{h^2+\|\mathbf{c}_n[t]-\mathbf{u}_k\|^2}\right) \geq & \log_2\left(1+\frac{\bar{\gamma}_{n,k}[t]}{h^2+\|\mathbf{c}_n^i[t]-\mathbf{u}_k\|^2}\right) \\ & -\left(\|\mathbf{c}_n[t]-\mathbf{u}_k\|^2-\left\|\mathbf{c}_n^i[t]-\mathbf{u}_k\right\|^2\right)X_{n,k}^i[t],\end{aligned} \tag{6.11}$$

where $\bar{\gamma}_{n,k}[t]=\gamma p_{n,k}[t]/b_{n,k}[t]$, and

$$X_{n,k}^i[t]=\frac{\log_2(e)\bar{\gamma}_{n,k}[t]}{\left(h^2+\|\mathbf{c}_n^i[t]-\mathbf{u}_k\|^2\right)\left(\bar{\gamma}_{n,k}[t]+h^2+\|\mathbf{c}_n^i[t]-\mathbf{u}_k\|^2\right)}.$$

Using these approximations, the problem $\mathcal{P}_{\mathsf{C}}(\mathcal{K})$ can be solved by solving the following convex optimization problem.

$$\begin{aligned}
\bar{\mathcal{P}}_{\mathsf{C}}(\mathcal{K}): \quad & \max_{\{\mathbf{c}_n[t], \bar{D}_k, \bar{s}_k\}} \quad \sum_{k\in\mathcal{K}} \bar{s}_k, \\
\text{s.t.} \ & -\sum_{n=1}^{N}\sum_{t=1}^{T} \delta b_{n,k}[t] \Bigg[\log_2\left(1 + \frac{\bar{\gamma}_{n,k}[t]}{h^2 + \|\mathbf{c}_n^i[t] - \mathbf{u}_k\|^2}\right) \\
& \qquad - (\|\mathbf{c}_n[t] - \mathbf{u}_k\|^2 - \left\|\mathbf{c}_n^i[t] - \mathbf{u}_k\right\|^2) X_{n,k}^i[t] \Bigg] \geq \bar{D}_k, \qquad (6.12\text{a}) \\
& (6.4\text{b}), (6.4\text{c}), (6.4\text{d}), (6.6\text{a}), (6.7\text{a}).
\end{aligned}$$

Finally, problem $\mathcal{P}^{\mathsf{SAM}}(\mathcal{K})$ is solved by using an iterative algorithm where we solve problems $\mathcal{P}_{\mathsf{BP}}(\mathcal{K})$ and $\bar{\mathcal{P}}_{\mathsf{C}}(\mathcal{K})$ sequentially in each iteration.

6.4.3 Step 2: User Removal

Let the set of users at iteration m after solving problem $\mathcal{P}^{\mathsf{SAM}}(\mathcal{K}^m)$ be $\mathcal{K}^m$, we propose a user removal strategy where the user with the largest gap between its required transmission data and demand-aware transmission data will be removed, as follows:

$$k_{\mathsf{min}}^m = \underset{k\in\mathcal{K}^m}{\operatorname{argmax}} \ D_k - \bar{D}_k^*, \qquad (6.13)$$

where $\bar{D}_k^*$ is the demand-aware transmission data of user k expressed in (6.5) after solving problem $\mathcal{P}^{\mathsf{SAM}}(\mathcal{K}^m)$. In fact, this user removal strategy tends to remove the user who is unlikely to get admitted so that we can efficiently utilize the network resources for other users who are more likely to be admitted. Then, the set of users in the next iteration is $\mathcal{K}^{m+1} = \mathcal{K}^m \setminus \{k_{\mathsf{min}}\}$. Let $\mathcal{K}_{\mathsf{a}}^m$ be the set of admitted users after solving $\mathcal{P}^{\mathsf{SAM}}(\mathcal{K}^m)$. Our design aims to ensure that admitted users at iteration m will still be admitted at iteration $m+1$. To this end, we introduce the admitted condition constraint for users $k \in \mathcal{K}_{\mathsf{a}}^m$ to the soft admission maximization problem for iteration

$m+1$ as follows:

$$\begin{aligned}\mathcal{P}^{\mathsf{SAM}}(\mathcal{K}^{m+1}): \quad & \max_{\mathbf{\Theta},\{\bar{D}_k,\bar{s}_k\}} \bar{S}(\mathcal{K}^{m+1}), \\ \text{s.t.} \quad & \bar{s}_k = 1, \forall k \in \mathcal{K}_{\mathsf{a}}^m \qquad (6.14\text{a}) \\ & (6.1), (6.2), (6.4\text{b}), (6.4\text{c}), (6.4\text{d}), (6.6\text{a}),\end{aligned}$$

Proposition 6.1. *Let $\mathcal{K}_{\mathsf{a}}^{m+1}$ be the set of admitted users after solving $\mathcal{P}^{\mathsf{SAM}}(\mathcal{K}^{m+1})$, the following condition holds:*

$$|\mathcal{K}_{\mathsf{a}}^{m+1}| \geq |\mathcal{K}_{\mathsf{a}}^{m}|. \qquad (6.15)$$

Proof: First, we need to show that problem $\mathcal{P}^{\mathsf{SAM}}(\mathcal{K}^{m+1})$ with the new constraint (6.14a) is feasible. It is indeed the case provided that problem $\mathcal{P}^{\mathsf{SAM}}(\mathcal{K}^{m})$ with constraint (6.14a) is feasible, which is true for $m = 1$ since $\mathcal{K}_{\mathsf{a}}^0 = \phi$, i.e., initially there is no constraint for any admitted user. Then, it is straightforward to conclude (6.15) due to constraint (6.14a).

Our algorithm is described in Algorithm 6.1 in the following.

Algorithm 6.1. Admission Maximization

1: Initiate $\mathbf{\Theta}, m = 1, \mathcal{K}^1 = \mathcal{K}$
2: **while** 1 **do**
3: (*Soft admission maximization*) Solve problem $\mathcal{P}^{\mathsf{SAM}}(\mathcal{K}^m)$ by the algorithm in section III.B.
4: **if** $|\mathcal{K}_{\mathsf{a}}^m| = |\mathcal{K}^m|$ **then**
5: Break the loop.
6: **else**
7: (*User removal*) Let $\mathcal{K}^{m+1} = \mathcal{K}^m \setminus \{k_{\mathsf{min}}^m\}$, where k_{min}^m is defined in (6.13). Increase m by 1.
8: **end if**
9: **end while**
10: End of algorithm.

6.5 Numerical Results

We consider the simulation setting where users are randomly located in a circular network area with the radius of 2km. The UAVs is assumed to fly at 100m, the maximum power P_{max} is set at 20dBm, σ^2 is -174dBm/Hz, and $\rho_0 = 4 \times 10^{-5}$. The flight duration is 120s, which is divided into

120 time slots. User transmission demand is 45Mbits, the total bandwidth is $B = 1$MHz, and the total number of users is 20, unless stated otherwise.

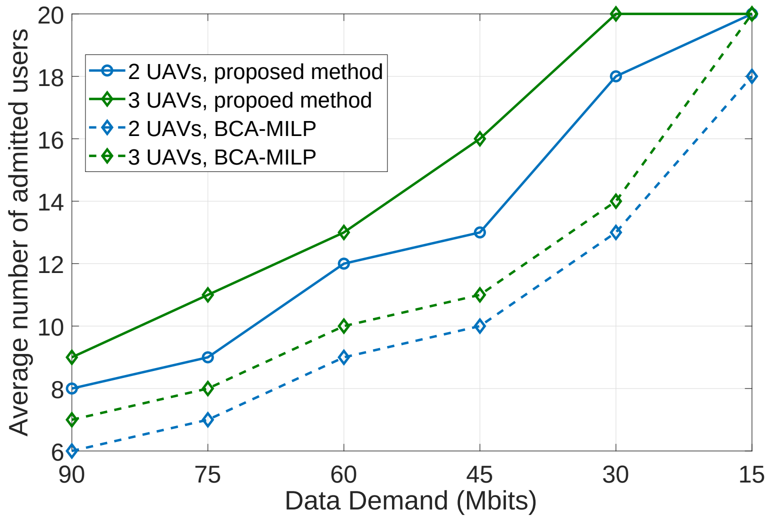

Figure 6.1: Number of served users versus data demand per user

For benchmarking purposes, we will numerically compare our proposed algorithm with a baseline. For this baseline, the problem $\mathcal{P}^{\mathsf{AM}}(\mathcal{K})$ is solved by applying the BCA method, where the sub-problems are MILPs. Specifically, in each iteration of this baseline, the bandwidth-power allocation, and trajectory optimization sub-problems with integer variables $\{s_k\}$ are solved by using the MOSEK solver. This baseline algorithm terminates when no more users can be admitted. This baseline is denoted as BCA-MILP in the following.

In Fig. 6.1, we show the number of admitted users versus varying user data demand. Two observations can be drawn from the figure. First, deploying more UAVs allows us to admit more users. However, when the data demands are low, deploying 2 UAVs is sufficient to admit all available users. Second, our proposed methods can admit significantly more users than that achieved by the BCA-MILP baseline. This confirms the efficacy of our proposed algorithm.

Fig. 6.2 presents the number of admitted users versus varying bandwidth. When there is more bandwidth available, the network can admit more users for both the proposed algorithm and the baseline. However, the performance gain of the proposed algorithm versus the baseline increases as the bandwidth grows, which implies that our approach utilizes radio resources more efficiently. This can be explained as follows. First, the SA maximization step in our algorithm optimizes a continuous objective function, so the algorithm can find better UAVs trajectories over iterations

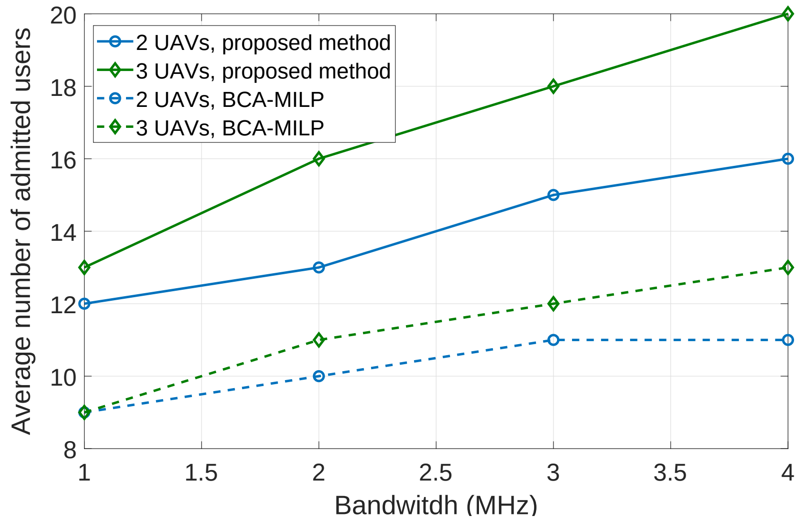

Figure 6.2: Number of served users versus total bandwidth

before convergence. This is not the case for the BCA-MILP in which convergence is reached after only a few iterations due to integer-valued objective function. Second, our developed user removal step efficiently removes poor users and thus their resources can be reserved and used more efficiently to serve better users.

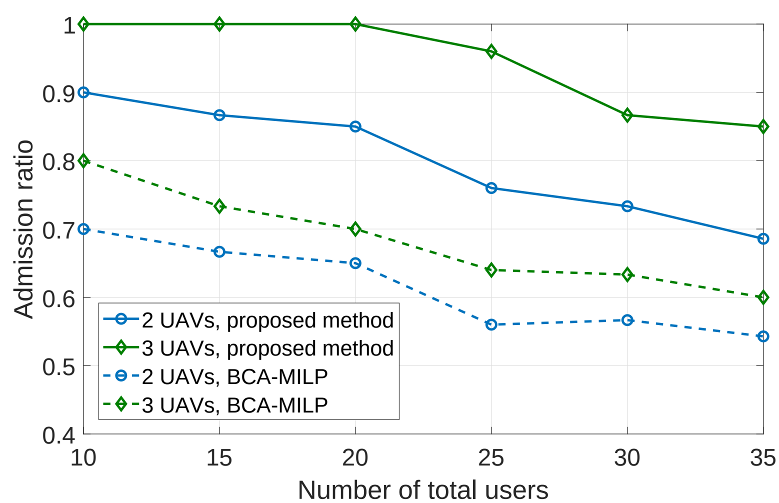

Figure 6.3: Coverage probability versus total number of users

Finally, we show the admission ratio with varying number of users in Fig. 6.3. It can be seen that the admission ratio decreases when there are more users. However, our proposed approach still achieves better performance than the BCA-MILP baseline.

6.6 Conclusion

In this letter, we have proposed an efficient algorithm to solve admission maximization problem by solving a series of soft admission maximization problems, where bandwidth, transmit powers, and UAVs' trajectories are optimized. Numerical results confirm the great performance gains of the proposed method compared to the conventional BCA-MILP approach.

Chapter 7

Multi-UAV Trajectory Control, Resource Allocation, and NOMA User Pairing for Uplink Energy Minimization

The content of this chapter is from the submitted version of the following article:

Minh Tri Nguyen and Long Bao Le, " Multi-UAV Trajectories Control, Resource Allocation, And NOMA User Pairing For Uplink Energy Minimization, " submitted to *IEEE Internet of Things Journal*, Dec., 2021.

7.1 Abstract

In this work, we study the joint optimization of multiple UAVs' trajectories, power allocation, user-UAV association, and user pairing for UAV-assisted wireless networks employing the non-orthogonal multiple access (NOMA) for uplink communications. The design aims to minimize the total energy consumption of ground users while guaranteeing to successfully transmit their required amount of data to the UAV-mounted base stations. The underlying problem is a mixed-integer

nonlinear program (MINLP), which is difficult to solve optimally. To tackle this problem, we derive the optimal power allocation as a function of other variables, which is used to transform the optimization problem into an equivalent form. We then propose an iterative algorithm to solve the resulting optimization problem by using the Block Coordinate Descent (BCD) method where three sub-problems are solved in each iteration and this process is repeated until convergence. Specifically, given the UAVs' trajectories and data rates, we solve the NOMA user pairing, and user-UAV association sub-problem optimally by exploiting its special structure. Then, we describe how to optimize the users' data rates and tackle the UAV trajectory optimization in the second and third sub-problems, respectively by using the successive convex approximation (SCA) method. Numerical results show that our proposed algorithm can provide efficient active-inactive schedules (by setting user's transmit powers to zero), and lower energy consumption compared to an existing baseline, and an OMA-based resource allocation and UAV-trajectory optimization strategy.

7.2 Introduction

Unmanned Aerial Vehicles (UAVs) have been emerging as one of the key components of future wireless networks thanks to their mobility, flexibility, and adaptive altitude [12]. In particular, the performance of UAV-based wireless networks in terms of coverage, throughput, and energy efficiency can be significantly enhanced by efficiently controlling UAVs' trajectories leveraging the potential Line-of-Sight (LoS) communications between UAVs and ground users [14]. In general, UAV communications can be employed to enhance the communications of existing terrestrial communications infrastructure and support various applications such as military, surveillance, monitoring, data collection for Internet of Thing (IoT) [15]. Therefore, UAV-based wireless networks are expected to play an important role in 5G and beyond-5G wireless systems [16].

From the connectivity viewpoint, the world has witnessed the rapidly increasing number of IoT connections with many emerging applications in recent years [3]. Design of energy-efficient IoT wireless networks is critical to elongate working durations of IoT devices and wireless networks [38]. There have been growing interests in leveraging UAV communications to enable energy-efficient operations (e.g., data collection, data dissemination) of IoT wireless networks [39–41]. In particular, efficient placement or trajectory control of UAVs and resource allocation can lead to reliable/LoS communications between IoT devices and UAVs enhancing their energy efficiency.

From the resource allocation perspective, Non-Orthogonal Multiple Access (NOMA), can significantly improve the spectral efficiency by allowing multiple users to communicate using the same time/frequency/space resources [8]. In the uplink NOMA, users with different channel conditions transmit their data simultaneously using the same frequency band and different transmit power levels. At the receiver, received signals are decoded in sequence by using successive interference cancellation (SIC) technique. Employment of NOMA in the UAV-based wireless networks allows to leverage the advantages of both NOMA and UAV communications to achieve desirable performance. In this direction, the works [41, 52, 141, 175] address different design problems in NOMA-enabled UAV-based wireless networks where UAVs' placement/trajectories are jointly optimized with other network functions. In particular, the work [41] minimizes the UAV's flight time for data collection where NOMA based user scheduling, transmit power allocation, and UAVs' locations are optimized. The authors of [52,141] investigate the resource allocation problems that aim to maximize the system throughput of UAV-based wireless networks in the uplink and downlink communications scenarios, respectively. Furthermore, maximization of the minimum achievable rate of ground users in the downlink NOMA communications is studied in [175] through joint optimization of UAV trajectory, transmit power, and user association.

Optimization of energy efficiency and power consumption in NOMA-enabled wireless networks have been studied in several existing works [55–57] where it has been shown that NOMA is indeed more energy efficient than the conventional Orthogonal Multiple-Access (OMA) in [10]. More recently, energy/power optimization for NOMA-enabled UAV-based wireless networks has been addressed in [29, 59, 142]. Specifically, the work [29] minimizes the total energy consumption of ground users by optimizing the NOMA user pairing and single UAV's trajectory for uplink communications using NOMA. The authors of [59] study the power minimization problem in the scenario where a single UAV assists a base station in serving multiple users while ensuring their required Quality of Service (QoS). An energy minimization problem is considered in [142] for the multi-UAV setting where each user communicates with all UAVs simultaneously using different channels with fixed bandwidth. This design may activate some non-LoS communications links, which reduces the achievable spectral efficiency. Moreover, all users are clustered into a single NOMA group, which considerably increases the complexity and decreases the reliability of the SIC process [176]. Nevertheless, most previous works either consider NOMA user pairing and placement of multiple static UAVs [50–52, 58–61] or joint NOMA user pairing and single-UAV trajectory optimization [29, 41, 62, 63] . However, joint optimization of NOMA user pairing and multi-UAV trajectories could result in much better performance for UAV-based networks, which has not been studied in the current literature.

In terms of problem formulation and solution approaches, the designs of NOMA-enabled UAV-based wireless networks usually involve solving Mixed-Integer Nonlinear Problems (MINLP) ([29,41,50,52,59,60,62,63,141,206], to name a few). In these papers, the underlying MINLPs are tackled by using different methods including non-iterative multi-step algorithms [29,41,50,52,59,60,206], and iterative Block Coordinate Descent (BCD) (for minimization problems) or Block Coordinate Ascent (BCA) for maximization problems [62, 63, 141]. In BCD or BCA algorithms, the variable set is decomposed into smaller subsets (e.g., power variables, UAV trajectory control variables) and optimization of one subset of variables given the values of other variables in the corresponding subproblem is performed sequentially in each iteration and this process is repeated until convergence. It is worth mentioning that the BCD-based approach is more numerically efficient when the value of the objective function is improved over iterations. This can be observed from numerical studies in [62, 63, 141] where throughput-related objective functions are considered. However, direct application of the BCD-based approach is not efficient in solving the energy/power optimization problem where the objective function contains only power optimization variables. This is because subproblems optimizing variables other than power variables are simply feasibility checking problems and solving feasibility checking problems does not improve the overall objective function over iterations. Therefore, further analysis and problem transformations are required before the BCD approach can be applied to solve power/energy minimization problems.

Two notable observations can be drawn from the above literature survey. First, to the best of our knowledge, joint optimization of NOMA user pairing and multi-UAV trajectories has not been studied in the literature. Second, using the BCD-based approach to solve energy minimization problems in NOMA-enabled UAV-based wireless networks is nontrivial because of the special structure of these underlying optimization problem as discussed above. Our current work aims to fill these gaps in the literature where we make the following key contributions.

- We formulate the total energy minimization problem where NOMA user pairing, transmit power allocation, user-UAV association, and multi-UAV trajectory control are jointly optimized. Our design ensures that users can successfully transmit their required amount of data to the UAVs in the uplink direction. We derive the optimal power allocation solution, which is expressed explicitly as a function of other optimization variables. Substituting this optimal power allocation into the objective function enables us to achieve an equivalent optimization problem for which we can employ the BCD method to solve the underlying problem.

- We develop an efficient algorithm, called Multi-UAV NOMA Energy Minimization (MUNE), to solve the considered problem by using the BCD approach. Specifically, we solve three smaller subproblems iteratively until convergence. The first problem optimizes user pairing and user-UAV association, given UAVs' trajectories, and data rates in each time slot, where we transform this subproblem into several maximum weighted matching problems (MWMP) whose solutions can be found in polynomial time [31]. The second subproblem optimizes the user data rate in each time slot while the third problem optimizes the UAVs' trajectories given the values of other optimization variables. We employ the SCA method to convexify and solve these two subproblems efficiently.
- To evaluate the performance of the proposed algorithm, we compare it with two other baselines. The first baseline is the Data Collection Optimization Algorithm (DCOA) which was developed in [29]. The second baseline is called Multi-UAV OMA Energy Minimization (MUOE) algorithm which employs the same design principles as for our proposed MUNE algorithm; however, the conventional orthogonal multiple access (OMA) instead of NOMA is used in MUNE. We show the convergence of the proposed MUNE, its typical UAVs' trajectories, and the superior performance of our algorithm compared to the two considered baselines via numerical studies. Moreover, we demonstrate the tradeoff between the UAV flight time and the total energy as well as the impacts of different parameters such as the numbers of users and UAVs on the total energy consumption.

The remaining of this paper is organized as follows. The system model and problem formulation are presented in Section 7.3. We describe our proposed algorithm in Section 7.4. Numerical results are presented in Section 7.5 followed by conclusion in Section 7.6.

For notations, we use bold normal letters to denote vectors and bold capitalized letters to denote matrices. If a variable $\mathbf{x}[t]$ has different values for different time slots t, we use $\{\mathbf{x}[t]\}$ to denote the set of all $\mathbf{x}[t], t = 1, ..., T$. As for the indices, we use semicolons (;) to separate indices that belong to different categories (i.e., users, UAVs, time slots) and commas (,) to separate indices that belong

Table 7.1: List of Notations

Notations	Explanation
N	Number of UAVs
K	Number of users
T	Number of time slots
δ	Length of one time slot
E_{all}	Total energy consumption of all users in the service period
B	Channel bandwidth assigned for each NOMA user pair
D_k	Data transmission demand of user k
h	Altitude of UAVs
μ	Channel power gain at reference distance
σ^2	Power of white Gaussian noise
$\mathbf{u}_k$	2-D coordinate of user k
$\mathbf{c}_n[t]$	2-D coordinate of UAV n in time slot t
$\mathbf{c}_{\mathsf{o}}$	2-D coordinate of UAV launching station
$\mathbf{D}_{\mathsf{safe}}$	Safe distance for UAVs
$\mathbf{V}_{\mathsf{max}}$	UAV's maximum speed
$p_k[t]$	Transmit power of user k in time slot t
P_{max}	Maximum user transmit power
$a_{k;n}[t]$	Association variable for UAV n and user k in time slot t
$x_{k,l}[t]$	User pairing variable for users k and l in time slot t
$\tau_{k;n}[t]$	Channel power gain for user k and UAV n in time slot t
$\tau_k[t]$	Channel power gain of user k in time slot t
$\lambda_k[t]$	Strong-weak role of user k in its pair in time slot t
$\mathsf{R}_k[t]$	Data rate of user k who is a strong user in time slot t
$\mathsf{r}_k[t]$	Data rate of user k who is a weak user in time slot t
$r_k[t]$	Target data rate of user k in time slot t
$\mathbf{P}[t]$	Collection of all user transmit powers in time slot t
$\mathbf{A}[t]$	Collection of user-UAV association variables in time slot t
$\mathbf{X}[t]$	Collection of user pairing variables in time slot t
$\mathbf{\Lambda}[t]$	Collection of strong-weak role variables in time slot t
$\mathbf{r}[t]$	Collection of target data rates of all users in time slot t

to the same category. The indicator function is denoted as $\mathbb{1}_{x>y}$ which takes value 1 when $x > y$ and takes value 0, otherwise. The base-2 logarithm and the natural logarithm of x are denoted as $\log(x)$ and $\ln(x)$, respectively. Summary of key notations used in the paper is given in Table 7.1.

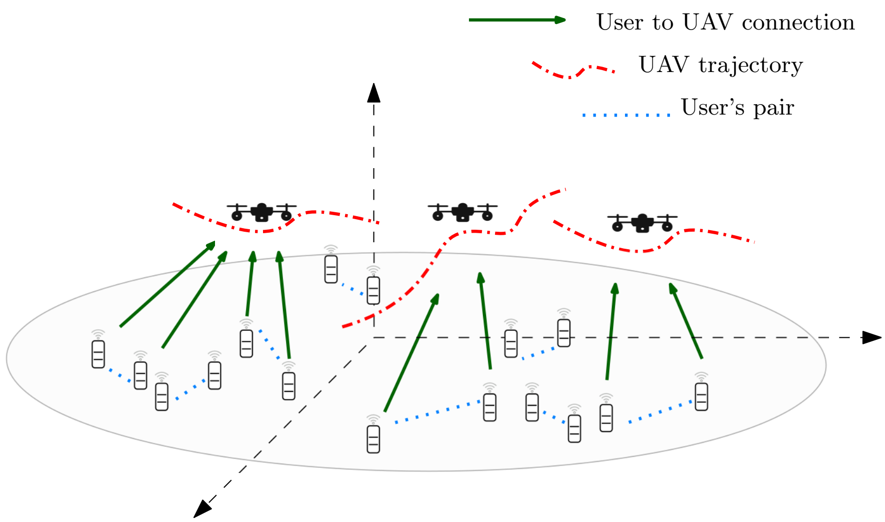

Figure 7.1: System model.

7.3 System Model and Problem Formulation

7.3.1 System Model

We consider uplink communications in an UAV-assisted wireless network with N flying UAVs and K ground users. The UAV flying duration is divided into T small time slots, each of which has an identical length of δ. We assume that UAV n flies at the fixed altitude h and its 2-D coordinate at time slot t is denoted as $\mathbf{c}_n[t]$. The 2-D coordinate of ground user k is denoted as $\mathbf{u}_k$. We assume that NOMA is employed to support the uplink communications where users are grouped into two-user pairs which transmit their data on orthogonal channels. Moreover, it is assumed that each user k requires to transmit an amount of data D_k to the UAVs by the end of the service period.[1] The considered UAV-assisted wireless network is illustrated in Fig. 7.1.

The Line of Sight (LoS) channel is assumed for the communication between users and UAVs. When the UAVs fly sufficiently high, this assumption aligns with the results observed in field tests [14]. Furthermore, the channel power gain between user k and UAV n at t, denoted as $\tau_{k;n}[t]$, can be expressed as follows:

$$\tau_{k;n}[t] = \frac{\mu}{\|\mathbf{c}_n[t] - \mathbf{u}_k\|^2 + h^2}, \tag{7.1}$$

[1]These data transmission demand constraints are typically needed in data collection scenarios for internet of things applications.

where μ is the channel power gain at the reference distance of 1m from the transmitter. Note that this channel model also aligns with the 3GPP standard for UAV communications [207].

7.3.2 User-UAV Association and NOMA User Pairing

Let $a_{k;n}[t]$ represent the association between user k and UAV n in time slot t where $a_{k;n}[t]$ is equal to 1 if user k is associated[2] with UAV n and equal to 0, otherwise. We assume that each user can only connect to one UAV but each UAV can connect to multiple users in any time slot. Therefore, we have the following constraints:

$$\sum_{n=1}^{N} a_{k;n}[t] = 1, \quad \forall k, t. \tag{7.2}$$

Using the association variables, the channel power gain of user k at t can be expressed as follows:

$$\tau_k[t] = \sum_{n=1}^{N} a_{k;n}[t]\tau_{k;n}[t], \quad \forall k, t. \tag{7.3}$$

Now, let $x_{k,l}[t]$ denote the user pairing decision variable which is equal to 1 if user k is paired with user l in time slot t and equal to 0, otherwise. We then have $x_{k,l} = 0$ if $k = l$, and $x_{k,l}[t] = x_{l,k}[t]$ for all k and l. In fact, there is a coupling between the user association and user pairing decision variables. Specifically, if users k and l are paired with each other in time slot t, we should have $a_{k;n}[t] = a_{l;n}[t] \;\; \forall n$, i.e., if users k and l are paired with each other, both users k and l must be associated with the same UAV. This coupling constraint can be expressed as follows:

$$x_{k,l}[t](a_{k;n}[t] - a_{l;n}[t]) = 0, \quad \forall (k, l), n, t. \tag{7.4}$$

7.3.3 NOMA Uplink Communications

We assume that users are paired and each user pair transmits data to the associated UAV in the uplink direction. The data received by the UAV is then decoded as follows. The message of the user in each pair with the better channel condition (strong user) is decoded first where the signal from the user with worse channel condition (weak user) is considered as noise. After the message

[2] In this paper, ‘connected’ and ‘associated’ are used interchangeably to describe the user-UAV association.

of the strong user is decoded and removed from the received signal, the message of the weak user is decoded. Specifically, if user k is the strong user in a particular pair, its achieved data rate in time slot t can be expressed as follows:

$$\mathsf{R}_k[t] = B\log\left(1+\frac{\tau_k[t]p_k[t]}{\sigma^2+\tau_k^{\mathsf{p}}[t]p_k^{\mathsf{p}}[t]}\right), \tag{7.5}$$

where B is the channel bandwidth assigned for the underlying user pair, σ^2 is the power of the Gaussian white noise, $\tau_k[t]$ and $p_k[t]$ are the power gain and transmit power of user k, respectively and $\tau_k^{\mathsf{p}}[t]$ and $p_k^{\mathsf{p}}[t]$ are the channel power gain and transmit power of its paired user, respectively which can be expressed as follows:

$$\tau_k^{\mathsf{p}}[t] = \sum_{l=1}^{K} x_{k,l}[t]\tau_l[t], \tag{7.6a}$$

$$p_k^{\mathsf{p}}[t] = \sum_{l=1}^{K} x_{k,l}[t]p_l[t]. \tag{7.6b}$$

If user k is the weak user in the considered pair in time slot t, its achieved data rate can be expressed as follows:

$$\mathsf{r}_k[t] = B\log\left(1+\frac{\tau_k[t]p_k[t]}{\sigma^2}\right). \tag{7.7}$$

7.3.4 Strong-Weak Relation for NOMA User Pairs

We need to capture the strong-weak relation between users in each pair and time slot. Specifically, we use $\lambda_k[t]$ to describe the strong-weak role of user k where it is equal to 1 if user k is the strong user and equal to 0 if it is the weak user in its associated pair and time slot t. Note that a user is strong or weak depending on its channel condition and the channel condition of its partner. In our design, the channel condition of a particular user depends on the coordinates of the associated UAV and the UAVs' coordinates are optimization variables. Therefore, it is necessary to define variables capturing the strong-weak roles of individual users. In fact, strong-weak variables play a crucial role in the problem formulation as will be detailed in the next section.

Alternatively, one could express the strong-weak variables by using indicator functions, i.e., $\lambda_k[t] = \mathbb{1}_{\tau_k[t]>\tau_k^{\mathsf{p}}[t]}$. Moreover, for the special network with a single UAV, one could simply determine the strong-weak channel conditions based on the distances from users to the UAV, without explicitly using $\lambda_k[t]$, as in [29, 41, 49, 62]. However, it is nontrivial to extend the approach in these works to the multi-UAV based networks, where the distances between users and their associated UAVs strongly depend on the user associations which are unknown in advance and need to be optimized.

Furthermore, there is also coupling between the strong-weak variables and the user-pairing optimization variables. Specifically, if user k is paired with user l, only one of them is the strong user. This coupling can be expressed in the following constraints:

$$x_{k,l}[t]\left(\lambda_k[t] + \lambda_l[t] - 1\right) = 0, \quad \forall (k,l), t. \tag{7.8}$$

Finally, the relationship between channel conditions and strong-weak variables can be stated as follows:

$$\tau_k[t] \geq \tau_k^{\mathsf{p}}[t], \quad \text{if} \quad \lambda_k[t] = 1, \tag{7.9a}$$

$$\tau_k[t] \leq \tau_k^{\mathsf{p}}[t], \quad \text{if} \quad \lambda_k[t] = 0. \tag{7.9b}$$

The inequalities (7.9a) and (7.9b) can be expressed by the following inequality:

$$\left(2\lambda_k[t] - 1\right)\left(\tau_k[t] - \tau_k^{\mathsf{p}}[t]\right) \geq 0, \quad \forall k, t. \tag{7.10}$$

The definition of strong-weak variables are convenient for the problem formulation; however, strong couplings between them and other variables, captured in (7.8) and (7.10) render the optimization problem difficult to solve. In addition, the values of strong-weak variables can be readily determined (as values of the indicator function $\mathbb{1}_{\tau_k[t] > \tau_k^{\mathsf{p}}[t]}$) when the UAV trajectories, user association, and user pairing variables are given. In the following, the strong-weak variables are occasionally omitted if they can be readily determined from the given values of other variables without causing any ambiguity.

7.3.5 Problem Formulation

Our design aims to minimize the energy consumption of all users by optimizing the user association ($\mathbf{A}[t]$), user pairing ($\mathbf{X}[t]$), the strong-weak variables ($\boldsymbol{\Lambda}[t]$), the power allocation ($\mathbf{P}[t]$), and the

UAV trajectories $\{\mathbf{c}_n[t]\}$. Additionally, we want to ensure that users be able to transmit their required amount of data to the UAVs within the service duration of T time slots. The considered optimization problem can be stated as follows:

$$\mathcal{P}_0 : \min_{\{\mathbf{A}[t],\mathbf{X}[t],\mathbf{\Lambda}[t],\mathbf{P}[t],\mathbf{c}_n[t]\}} E_{\mathsf{all}},$$

$$\text{s.t.} \sum_{t=1}^{T} \delta \left(\lambda_k[t]\mathsf{R}_k[t] + (1-\lambda_k[t])\,\mathsf{r}_k[t]\right) \geq D_k, \forall k, \tag{7.11a}$$

$$\mathbf{X}[t] = \mathbf{X}^T[t], \forall t, \tag{7.11b}$$

$$\sum_{l=1}^{K} x_{k,l}[t] = 1, \forall k, t, \tag{7.11c}$$

$$p_k[t] \leq P_{\mathsf{max}}, \forall k, t, \tag{7.11d}$$

$$\|\mathbf{c}_n[t] - \mathbf{c}_n[t-1]\| \leq \delta V_{\mathsf{max}}, \forall n, t, \tag{7.11e}$$

$$\|\mathbf{c}_n[t] - \mathbf{c}_m[t]\| \geq D_{\mathsf{safe}}, \forall t, \forall n \neq m, \tag{7.11f}$$

$$\mathbf{c}_n[1] = \mathbf{c}_n[T] = \mathbf{c}_{\mathsf{o}}, \forall n, \tag{7.11g}$$

$$\lambda_k \in \{0,1\}, a_{k;n} \in \{0,1\}, x_{k,l} \in \{0,1\}, \forall k, l, n, \tag{7.11h}$$

$$\text{constraints} \quad (7.2), (7.4), (7.8), (7.10),$$

where P_{max} denotes the maximum transmit power of each user, and the total energy can be expressed as

$$E_{\mathsf{all}} = \delta \sum_{t=1}^{T} \sum_{k=1}^{K} p_k[t]. \tag{7.12}$$

Constraints (7.11a) ensure that every user can transmit their required amount of data to the UAVs. Constraints (7.11b) and (7.11c) are imposed to make sure that the user pairing solution is valid. Constraints (7.11d) describe the maximum transmit powers of users. Constraints (7.11e) capture the maximum distance that a UAV can travel in one time slot, where V_{max} is the UAV's maximum speed. Constraints (7.11f) are imposed to avoid collision among UAVs, i.e., inter-distance between UAVs must be at least D_{safe} (meters). Constraints (7.11g) set the initial and final positions of UAVs, where $\mathbf{c}_{\mathsf{o}}$ is the coordinate of the launching station and constraints (7.11h) define different binary variables.

The formulated problem is a mixed-integer nonlinear program, which is nontrivial to solve. In the next section, we propose an algorithm to solve problem $\mathcal{P}_0$ efficiently.

7.4 Proposed Algorithms

7.4.1 Equivalent Problem Transformation

First, we introduce a set of auxiliary variables $\{\mathbf{r}[t]\}$, where $r_k[t]$ is the target data rate in time slot t for which user k transmits data to the UAVs to fulfill the data transmission demand. We can transform problem $\mathcal{P}_0$ into the following equivalent problem with additional variables $\{\mathbf{r}[t]\}$:

$$
\begin{aligned}
\mathcal{P}_1 : & \min_{\{\mathbf{A}[t],\mathbf{X}[t],\mathbf{\Lambda}[t],\mathbf{P}[t],\mathbf{c}_n[t],\mathbf{r}[t]\}} E_{\mathsf{all}}, \\
\text{s.t.} \ & \lambda_k[t]\mathsf{R}_k[t] + (1-\lambda_k[t])\mathsf{r}_k[t] \geq r_k[t], \forall k, t, && (7.13a)\\
& \sum_{k=1}^{K} \delta r_k[t] \geq D_k, \forall k, && (7.13b)\\
& (7.2), (7.4), (7.8), (7.10), \\
& (7.11b), (7.11c), (7.11d), (7.11e), (7.11f), (7.11g), (7.11h).
\end{aligned}
$$

The left hand side of (7.13a) describes the achievable data rate of user k, which is equal to the rate of a strong user or a weak user depending on the strong-weak role of this user. Constraints (7.13a) capture the fact that the target rate $r_k[t]$ is upper bounded by the achievable data rate. Moreover, (7.13b) describes the data transmission demand constraints expressed by using the target data rates. It can easily seen that problems $\mathcal{P}_0$ and $\mathcal{P}_1$ are equivalent [30] and the equality of (7.13a) holds at optimality. We will describe how to solve problem $\mathcal{P}_1$ in the following. Note that problem $\mathcal{P}_1$ is still a MINLP problem, which is difficult to solve as problem $\mathcal{P}_0$. However, we will show that the auxiliary variables $\{\mathbf{r}[t]\}$ help us transform problem $\mathcal{P}_1$ into more tractable problems. To this end, we provide an outline of our solution in section 7.4.2 and describe our proposed algorithm in the sections that follow.

7.4.2 Outline of Proposed Solution

For the considered optimization problem, we will show that the optimal power $\{\mathbf{P}^*[t]\}$ can be expressed explicitly in terms of other variables ($\{\mathbf{c}_n[t], \mathbf{X}[t], \mathbf{A}[t], \mathbf{r}[t]\}$). This key result will be stated in *Lemma 1* in section 7.4.3. In fact, the derivation of the optimum power $\{\mathbf{P}^*[t]\}$ with respect to other variables enables us to apply the BCD technique to solve problem $\mathcal{P}_1$ effectively.

We then propose to solve problem $\mathcal{P}_1$ by iteratively solving three following sub-problems. In the first subproblem, we assume that values of $\{\mathbf{c}_n[t], \mathbf{r}[t]\}$ are given and solve for the optimal power allocation where all other variables are the optimization variables. In the second subproblem, we optimize the data rate variables $\{\mathbf{r}[t]\}$ given $\{\mathbf{c}_n[t]\}$ and the values of other variables obtained from solving the first subproblem,. Finally, in the third subproblem, the UAVs' trajectories are optimized given the values of other variables. It can be shown that the total energy consumption is reduced over iterations, hence, the iterative process is guaranteed to converge.

7.4.3 Optimizations of Power and Integer Variables Given UAVs' Trajectories and Rates

Assuming that $\{\mathbf{c}_n[t], \mathbf{r}[t]\}$ are given, we develop an algorithm to find the optimal power $\{\mathbf{P}^*[t]\}$ with respect to $\{\mathbf{c}_n[t], \mathbf{r}[t]\}$, and other integer variables. Specifically, we solve for the optimal power and user association when the user pairing solution is known in 7.4.3.1. Then, the user pairing optimization is solved in section 7.4.3.2 by tackling the underlying maximum weighted graph matching problem. Then, the optimal user association is derived.

7.4.3.1 Optimization Problems as User Pairing Solution is Given

If the values of $\{\mathbf{c}_n[t], \mathbf{r}[t]\}$, and $\mathbf{X}[t]$ are given, the problem $\mathcal{P}_1$ is reduced to the following problem.

$$\begin{aligned}\mathcal{P}_{\mathsf{A,P}} : &\min_{\mathbf{A}[t]\mathbf{\Lambda}[t], \mathbf{P}[t]} E_{\mathsf{all}}, \\ &\text{s.t.} \;\; (7.2), (7.4), (7.8), (7.10), (7.11\text{d}), (7.11\text{h}), (7.13\text{a}).\end{aligned}$$

Furthermore, problem $\mathcal{P}_{\mathsf{A,P}}$ can be decomposed into several subproblems, denoted as $\tilde{\mathcal{P}}_{\mathsf{A,P}}(k, l; t)$ where subproblem $\tilde{\mathcal{P}}_{\mathsf{A,P}}(k, l; t)$ minimizes the total energy consumed by users k and l in time slot t, where the transmit power $p_k[t], p_l[t]$, the user association $\mathbf{a}_k[t], \mathbf{a}_l[t]$, and the strong-weak variables

$\lambda_k[t], \lambda_l[t]$ are optimized[3]. This subproblem can be expressed as follows:

$$\begin{aligned}
\tilde{\mathcal{P}}_{\mathsf{A,P}}(k,l;t): & \min_{\{\mathbf{a}_i[t],\lambda_i[t],p_i[t]\}_{i=k,l}} \delta(p_k[t]+p_l[t]), \\
\text{s.t. } & a_{k;n}[t] = a_{l;n}[t], && \text{(7.15a)} \\
& \lambda_k[t]+\lambda_l[t] = 1, && \text{(7.15b)} \\
& (2\lambda_k[t]-1)\left(\tau_k[t]-\tau_l[t]\right) \geq 0, && \text{(7.15c)} \\
& (7.2), (7.11\text{d}), (7.11\text{h}), (7.13\text{a}).
\end{aligned}$$

where (7.15a), (7.15b), and (7.15c) are deduced from (7.4), (7.8), and (7.10), respectively, given that $x_{k,l}[t]=1$.

Let $p_{k,l}[t]$ denote the sum power of two users k and l in the objective function of $\tilde{\mathcal{P}}_{\mathsf{A,P}}(k,l;t)$, then the total energy consumption can be expressed as follows:

$$E_{\mathsf{all}} = \frac{\delta}{2}\sum_{t=1}^{T}\sum_{k=1}^{K}\sum_{l=1}^{K} x_{k,l}[t]p_{k,l}[t]. \tag{7.16}$$

In the following, we find the optimal value of $p_{k,l}[t]$ for all t and all combinations of k and l. Specifically, we find the optimal power allocation with respect to the user association variables (i.e., if $\mathbf{a}_k[t]$ and $\mathbf{a}_l[t]$ are known). Note that when the user association solution is given, the channel conditions for k and l are determined by (7.3). Then, the values of strong-weak variables can also be readily determined by (7.15b) and (7.15c).[4] We substitute the optimal power allocation solution as a function of the user association variables into the objective function of $\tilde{\mathcal{P}}_{\mathsf{A,P}}(k,l;t)$ from which the optimal user association solutions with respect to every user pair (k,l) will be determined.

a) Finding Optimal Power Allocation Given User Association

Let us consider a particular pair of users k and l associated with UAV n. Assume that the channel of user k is stronger than that of user l (i.e., $\lambda_k[t]=1$ and $\lambda_l[t]=0$). Then, the problem

[3] Note that $\mathbf{a}_k[t] = [a_{k;1}[t],...,a_{k;N}[t]]$ denotes the user association vector corresponding to user k at t.

[4] Specifically, if users k and l are associated with UAV n in time slot t, we can compute their channel conditions according to (7.1). Then $\lambda_k[t]=1$ if $\tau_{k;n}[t] \geq \tau_{l;n}[t]$ and $\lambda_l[t]=0$, otherwise.

$\tilde{\mathcal{P}}_{\mathsf{A,P}}(k,l;t)$ can be deduced further into the following problem:

$$\begin{aligned}\tilde{\mathcal{P}}_{\mathsf{P}}(k,l;t;n) : \min_{\{p_i[t]\}_{i=k,l}} \ & \delta(p_k[t]+p_l[t]),\\ \text{s.t. } & (7.11\text{d}), (7.13\text{a}).\end{aligned}$$

We now state the optimal power allocation in the following lemma.

Lemma 7.1. *If the problem $\tilde{\mathcal{P}}_{\mathsf{P}}(k,l;t;n)$ is feasible, its optimal solution can be stated as follows:*

$$\begin{aligned} p_k^*[t] &= \sigma^2\tau_{k;n}^{-1}[t](\beta^{r_k[t]}-1)\beta^{r_l[t]},\\ p_l^*[t] &= \sigma^2\tau_{l;n}^{-1}[t](\beta^{r_l[t]}-1), \end{aligned} \tag{7.18}$$

where $\beta = 2^{1/B}$. Moreover, the problem is feasible if both $p_k^*[t]$ and $p_l^*[t]$ in (7.18) are no greater than P_{max}.

Proof. The power allocation solution can be derived by using the following steps. First, we equivalently transform constraints (7.13a) into linear constraints with respect to $p_l[t]$ and $p_k[t]$. The equivalent problem is linear; hence, it is straightforward to derive the minimum required transmit powers for each user. □

Note that the results for the downlink case, and when $r_k[t] = r_l[t]$, were stated or can be deduced implicitly in some previous works [10, 50, 56, 57]. The results in Lemma 7.1 allow us to explicitly express the optimal transmit powers of users k and l in terms of their channel conditions which further depend on the user association and distances from the users to their associated UAV. Therefore, hereafter we will use the right hand side of (7.18) instead of $p_k[t], p_l[t]$.

Let $p_{k,l;n}[t]$ be the optimal allocated power of users k and l assuming that they are paired and connected to UAV n in time slot t. Then, $p_{k,l;n}[t]$ can be expressed as follows:[5]

$$p_{k,l;n}[t] = \begin{cases} \sigma^2\left(\tau_{k;n}^{-1}[t](\beta^{r_k[t]}-1)\beta^{r_l[t]} + \tau_{l;n}^{-1}[t](\beta^{r_l[t]}-1)\right), \\ \qquad\qquad \text{if} \max(p_k^*[t], p_l^*[t]) \le P_{\mathsf{max}}, \\ \infty, \qquad\quad \text{otherwise}. \end{cases} \tag{7.19}$$

[5]We use the convention in [30] where the optimal value of a minimization problem is infinity if the problem is infeasible.

b) Finding Optimal User Association

The optimal value of the sum power of users k and l can be expressed with respect to the user association variables as follows:

$$p_{k,l}[t] = \sum_{n=1}^{N} a_{k;n}[t] p_{k,l;n}[t]. \tag{7.20}$$

Note that (7.20) is realized with the assumption that $x_{k,l}[t] = 1$, and hence $a_{k;n}[t] = a_{l;n}[t]$. The result in (7.20) allows us to find the optimal association for users k, l as stated in the following Lemma.

Lemma 7.2. *If $x_{k,l}[t] = 1$, the optimal association for users k and l at t can be found as follows:*

$$a^*_{k;n}[t] = a^*_{l;n}[t] = \begin{cases} 1, & \text{if } n = \underset{n}{\operatorname{argmin}}\, p_{k,l;n}[t] \\ 0, & \text{otherwise.} \end{cases} \tag{7.21}$$

Substituting the user association solution obtained from Lemma 7.2, we can find the optimal value of $p_{k,l}[t]$ from (7.20).

7.4.3.2 User Pairing Optimization Problem

Upon obtaining the optimal user association and the corresponding power allocation solution, the user pairing optimization problem can be expressed as follows:

$$\begin{aligned} \mathcal{P}_{\mathsf{X}} :& \min_{\mathbf{X}[t]} \frac{\delta}{2} \sum_{t=1}^{T} \sum_{k=1}^{K} \sum_{l=1}^{K} x_{k,l}[t] p_{k,l}[t], \\ \text{s.t. }& (7.11\text{b}), (7.11\text{c}), (7.11\text{h}). \end{aligned}$$

Similarly, problem $\mathcal{P}_{\mathsf{X}}$ can be further decomposed into several subproblems each of which optimizes the user pairing for one particular time slot t. These integer linear program subproblems in each time slot t is indeed the Maximum Weight Perfect Matching (MWPM) problem for a graph whose vertices are users, and the weight of the edge between users k and l is $p_{k,l}[t]$. This MWPM problem can be solved efficiently and optimally by using Edmon's algorithm [31].

In the following sections, we describe how to tackle the optimizations of other variables, given user association and user pairing solutions. We denote $(k,l)[t]$ as the users k and l to be paired in time slot t. Without loss of generality, it is the convention in the following sections that k is the strong user and l is the weak user.

7.4.4 Data Rate Optimization

From (7.12) and (7.19), the total energy consumption E_{all} can be expressed with respect to the data rates $\{\mathbf{r}[t]\}$ as follows:

$$E_{\mathsf{all}} = \delta\sigma^2 \sum_{t=1}^{T} \sum_{(k,l)[t]} \beta^{r_k[t]+r_l[t]}\tau_k^{-1}[t] + \beta^{r_l[t]} \left(\tau_l^{-1}[t] - \tau_k^{-1}[t]\right) - \delta\sigma^2 \sum_{t=1}^{T} \sum_{(k,l)[t]} \tau_l^{-1}[t]. \tag{7.23}$$

Note that the term in the second line is a constant, which does not depend on $\{\mathbf{r}[t]\}$. When UAV trajectory, user association, and user pairing solutions are given, the optimization of data rates can be stated as follows:

$$\mathcal{P}_{\mathsf{R}} : \min_{\{\mathbf{r}[t]\}} E_{\mathsf{all}},$$

$$\text{s.t.}\ \ \beta^{r_l[t]} - 1 \le \frac{P_{\mathsf{max}}}{\sigma^2}\tau_k[t], \forall (k,l)[t], \tag{7.24a}$$

$$\beta^{r_k[t]+r_l[t]} - \beta^{r_l[t]} \le \frac{P_{\mathsf{max}}}{\sigma^2}\tau_l[t], \forall (k,l)[t], \tag{7.24b}$$

$$(7.11b), (7.11c), (7.11d), (7.11e), (7.11f), (7.11h), (7.13b).$$

Since $\tau_l^{-1}[t] - \tau_k^{-1}[t] \ge 0$ for all user pairs $(k,l)[t]$, the objective function of problem $\mathcal{P}_{\mathsf{R}}$ is convex; however, problem $\mathcal{P}_{\mathsf{R}}$ is still non-convex due to the non-convexity of constraint (7.24b). However, it can be seen that (7.24b) is the difference of two convex functions; hence, we can approximate (7.24b) by the following constraint [30]:

$$\beta^{r_k[t]+r_l[t]} - \beta^{\bar{r}_l[t]}(1 + \ln(\beta)(r_l[t] - \bar{r}_l[t]))\tau_{l;n}^{-1}[t] \le \frac{P_{\mathsf{max}}}{\sigma^2}, \tag{7.25}$$

where we have replaced $\beta^{r_l[t]}$ by its first-order Taylor approximation at local point $\bar{r}_l[t]$. On the left hand side of (7.25), the first term is convex and the second term is linear with respect to the optimization variables $(r_k[t], r_l[t])$; hence, (7.25) is a convex constraint. Therefore, the Successive

Convex Approximation (SCA) technique can be applied to solve the problem $\mathcal{P}_{\mathsf{R}}$ iteratively where constraint (7.24b) is replaced by constraint (7.25) in each iteration of the iterative process.

7.4.5 UAV Trajectory Optimization

Using the results in (7.1), (7.12), and (7.19), the total energy E_{all} can also be expressed as a function of the UAVs' trajectories $\{\mathbf{c}_n[t]\}$ as follows:

$$\begin{aligned} E_{\mathsf{all}} = \delta\sigma^2 \sum_{t=1}^{T} \sum_{(k,l)[t]} \zeta_k[t] \|\mathbf{c}_{n_{(k,l)}}[t] - \mathbf{u}_k\|^2 + \zeta_l[t] \|\mathbf{c}_{n_{(k,l)}}[t] - \mathbf{u}_l\|^2 \\ + \delta\sigma^2 \sum_{t=1}^{T} \sum_{(k,l)[t]} (\zeta_k[t] + \zeta_l[t]) h^2, \end{aligned} \tag{7.26}$$

where $\zeta_k[t] = \mu^{-1}(\beta^{r_k[t]} - 1)\beta^{r_l[t]}$ and $\zeta_l[t] = \mu^{-1}(\beta^{r_l[t]} - 1)$; $\mathbf{c}_{n_{(k,l)}}[t]$ is the coordinate of the UAV serving user pair $(k,l)[t]$. Note that the second term does not depend on $\{\mathbf{c}_n[t]\}$.

The UAV trajectory optimization problem can be expressed as follows:

$$\begin{aligned} \mathcal{P}_{\mathsf{C}} : \min_{\{\mathbf{c}_n[t]\}} \; & E_{\mathsf{all}} \\ \text{s.t.} \; & \zeta_k[t] \left(\|\mathbf{c}_{n_{(k,l)}}[t] - \mathbf{u}_k\|^2 + h^2 \right) \le \frac{P_{\mathsf{max}}}{\sigma^2}, \forall (k,l)[t], & \text{(7.27a)} \\ & \zeta_l[t] \left(\|\mathbf{c}_{n_{(k,l)}}[t] - \mathbf{u}_l\|^2 + h^2 \right) \le \frac{P_{\mathsf{max}}}{\sigma^2}, \forall (k,l)[t], & \text{(7.27b)} \\ & (7.10), (7.11\text{e}), (7.11\text{g}), (7.11\text{f}). \end{aligned}$$

Even though problem $\mathcal{P}_{\mathsf{C}}$ is non-convex due to the non-convex constraint (7.11f), we can solve it by applying the SCA method. Specifically, we first square both sides of (7.11f) and then approximate the left hand side with its lower bound at the local point $\{\bar{\mathbf{c}}_n[t], \bar{\mathbf{c}}_m[t]\}$ by using the first-order Taylor expansion. We then can obtain the following approximated constraint:

$$2\,(\bar{\mathbf{c}}_m[t] - \bar{\mathbf{c}}_n[t])^T (\mathbf{c}_m[t] - \mathbf{c}_n[t]) - \|\bar{\mathbf{c}}_m[t] - \bar{\mathbf{c}}_n[t]\|^2 \ge D_{\mathsf{safe}}^2. \tag{7.28}$$

As constraints (7.11f) are approximated by (7.28), the resulting approximated problem of problem $\mathcal{P}_{\mathsf{C}}$ is convex with respect to the UAV trajectory variables. Therefore, the obtained convex problem can be solved optimally using standard solvers.

7.4.6 Proposed Algorithm

Our proposed iterative algorithm, named Multi-UAV NOMA Energy minimization (MUNE), is described in Algorithm 7.1. In this algorithm, ϵ is a small positive number that is set to balance between the desired accuracy and convergence time of this algorithm.

Algorithm 7.1. Multi-UAV NOMA Energy Minimization (MUNE)

Initiate values for UAV trajectories $\left\{\mathbf{c}_n^0[t], \mathbf{R}^0[t]\right\}$, set $i = 1$, $E_{\mathsf{all}}^0 = TKP_{\mathsf{max}}$.
while 1 **do**
  Given $\left\{\mathbf{c}_n^{i-1}[t], \mathbf{R}^{i-1}[t]\right\}$, solve problem $\tilde{\mathcal{P}}_{\mathsf{A,P}}(k, l; t)$ for all t and all possible user pairs (k, l), obtain optimal $\{p_{k,l}[t]\}$ from (7.20).
  From the obtained $\{p_{k,l}[t]\}$, solve problem $\mathcal{P}_{\mathsf{X}}$ for optimal user pairing variables $\left\{\mathbf{X}^i[t]\right\}$, and the corresponding user association variables $\left\{\mathbf{A}^i[t]\right\}$.
  Solve problem $\mathcal{P}_{\mathsf{R}}$ given the values of other variables iteratively until convergence, obtain the values of $\left\{\mathbf{R}^i[t]\right\}$.
  Solve problem $\mathcal{P}_{\mathsf{C}}$ given the values of other variables iteratively until convergence. Let $\{\mathbf{c}_n^i[t]\}$ and E_{all}^i denote the obtained UAVs' trajectories and the corresponding total energy consumption, respectively.
  if $E_{\mathsf{all}}^{i-1} - E_{\mathsf{all}}^i \leq \epsilon$ **then**
    Break the loop.
  else
    Let $i = i + 1$.
  end if
end while
End of algorithm.

7.4.7 Baseline Algorithms

We now introduce two baseline algorithms whose performances will be compared with that achieved by our proposed algorithm in the next section.

The first baseline algorithm, called Data Collection Optimization Algorithm (DCOA) was developed in [29], in which the Generalized Benders Decomposition [32] is used to solve the joint NOMA user pairing and power allocation optimization problem. Then, the UAV trajectory is optimized to maximize the total transmitted data from all users. The key idea is that when the total transmitted data exceeds the required amount of transmitted data, the energy consumption can be reduced by solving the power minimization problem in the next iteration. The DCOA can only be applied to the single UAV setting.

To demonstrate the importance of non-orthogonal access to the achievable performance, we also present the second baseline algorithm, called Multi-UAV OMA Energy Minimization (MUOE), whose details are given in Appendix 7.A, where the orthogonal multiple access (OMA) strategy is used instead of NOMA. The MUOE algorithm can be applied to single and multi-UAV settings. In this OMA based strategy, each user is connected to the closest UAV and they have an assigned bandwidth of $B/2$ in each time slot.

7.5 Numerical Results

We consider a circular network area with radius of 1000m in which users are placed randomly and uniformly. We assume that UAVs fly at the fixed altitude of $h = 100$m and all users require the same amount of data to be collected $D_k = 6$Mbits $\forall k$, unless stated otherwise. The bandwidth allocated for each user pair is 100kHz, the noise power is set to -105dBm, and μ is set equal to 6.5×10^{-4}. The number of time slots is $T = 60$, unless stated otherwise and each time slot has the length of $\delta = 1$s. The maximum transmit power is $P_{\mathsf{max}} = 0.1$W and the value of ϵ in Algorithm 1 controlling the numerical accuracy is set at 10^{-2}.

The UAV station is located at the center of the network area, $\mathbf{c}_{\mathsf{o}} = (0, 0)$. Initially, we let $r_k[t] = D_k/T$ for all user k, i.e., the initial data rates in each time slot are identical for all users. Note that we do not set the initial values for user pairing, user association, and user transmit powers, as they are to be optimized in the first iteration by Algorithm 1. For the UAVs' initial trajectories, we let UAV n start at $\mathbf{c}_{\mathsf{o}} = (0, 0)$ and fly in counter clockwise direction along a circular trajectory with radius of $r_{\mathsf{o}} = 300$m and center at $(r_{\mathsf{o}} \cos \frac{n2\pi}{N}, r_{\mathsf{o}} \sin \frac{n2\pi}{N})$. Specifically, the initial location of UAV n in time slot t can be expressed as

$$\mathbf{c}_n^0[t] = \left(r_{\mathsf{o}} \left(\cos \frac{n2\pi}{N} + \cos \frac{t2\pi}{T} \right), r_{\mathsf{o}} \left(\sin \frac{n2\pi}{N} + \sin \frac{t2\pi}{T} \right) \right).$$

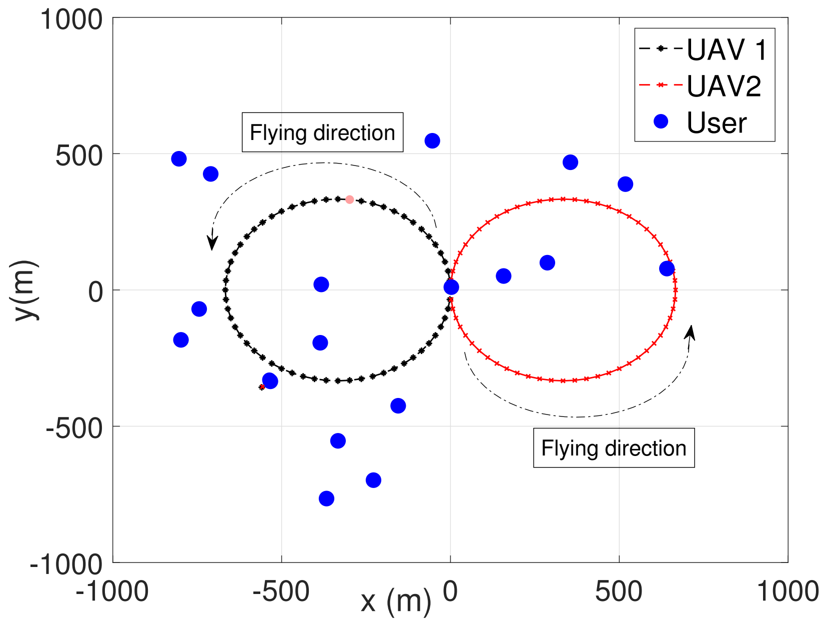

Figure 7.2: User's locations and UAV's initial trajectories.

We depict the considered users' locations and the initial trajectories of UAVs for the 2-UAV setting in Fig. 7.2 where the flying directions of each UAV and locations of 18 users are also shown.

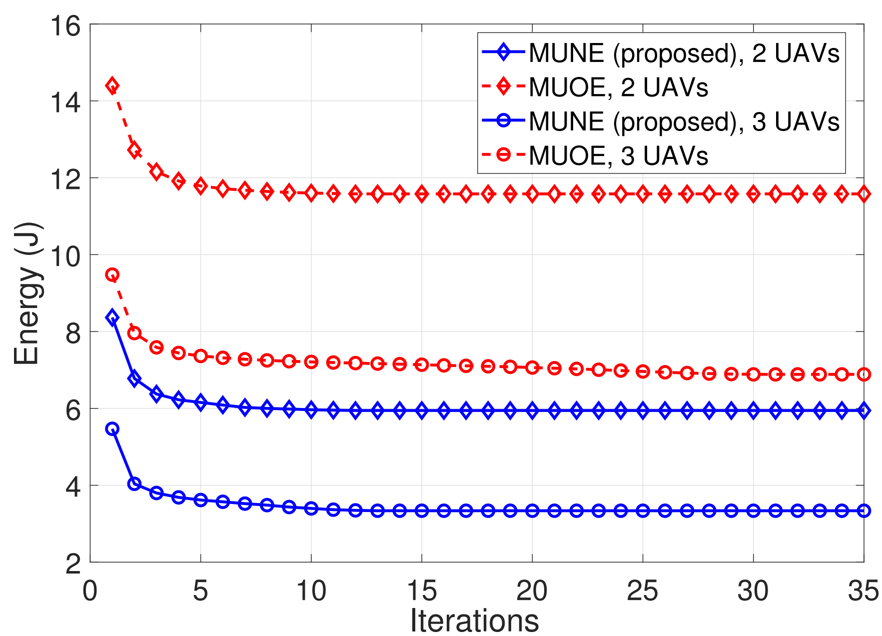

Figure 7.3: Convergence of different algorithms with different numbers of UAVs.

In Fig. 7.3, we show the convergence of the MUNE and MUOE algorithms in the scenarios with 2 and 3 UAVs. It can be seen from this figure that both algorithms converge pretty fast. Moreover, the proposed MUNE algorithm achieve better performances than that of the MUOE algorithm in both scenarios. Moreover, it takes around 5 iterations for both algorithms to converge in the case of 2 UAVs, and around 10 iterations in the case of 3 UAVs. This can be explained as follows. Larger number of UAVs in the network increases the number of variables and complexity of the optimization problems. Nevertheless, the numbers of iterations required to reach the convergence of both algorithms are sufficiently small.

We present numerical results for single-UAV and multiple-UAV settings in the following.

7.5.0.1 Numerical Results for Single-UAV Setting

We show the performances achieved by our proposed MUNE algorithm, the MUOE algorithm, and the DCOA algorithm from [29] for the network setting with one UAV and varying number of users. Specifically, in Fig. 7.4, we show the total energy consumption of all users as these algorithms are applied. This figure shows that the proposed MUNE algorithm achieves the lowest energy consumption among the three algorithms. Moreover, the gaps between the total energy consumption due to the proposed algorithm and the two baselines increases as the number of users increases.

As for the two baselines, the MUOE algorithm still outperforms the DCOA from the energy consumption viewpoint. This can be explained by carefully analyzing the DCOA algorithm in [29] as follows. Specifically, the DCOA algorithm first attempts to reach a feasible solution by finding the user pairing and power allocation solutions with an initial UAV trajectory. Then, this algorithm employs an iterative procedure consisting of two steps in each iteration. In first step, it determines the UAV trajectory that increases the amount of transmitted data, then it minimizes the energy consumption with the newly obtained trajectories in the second step. Hence, the considered objective function, which is the energy consumption, is not directly optimized (in the first step), which could result in an in-efficient UAV trajectory, and hence, poor performance. For the MUOE algorithm, the objective function, after the optimal transmit power expressed as a function of other variables in (7.30) is substituted into it, is optimized directly. This optimization, therefore, could result in a better solution compared to that achieved by the DCOA algorithm.

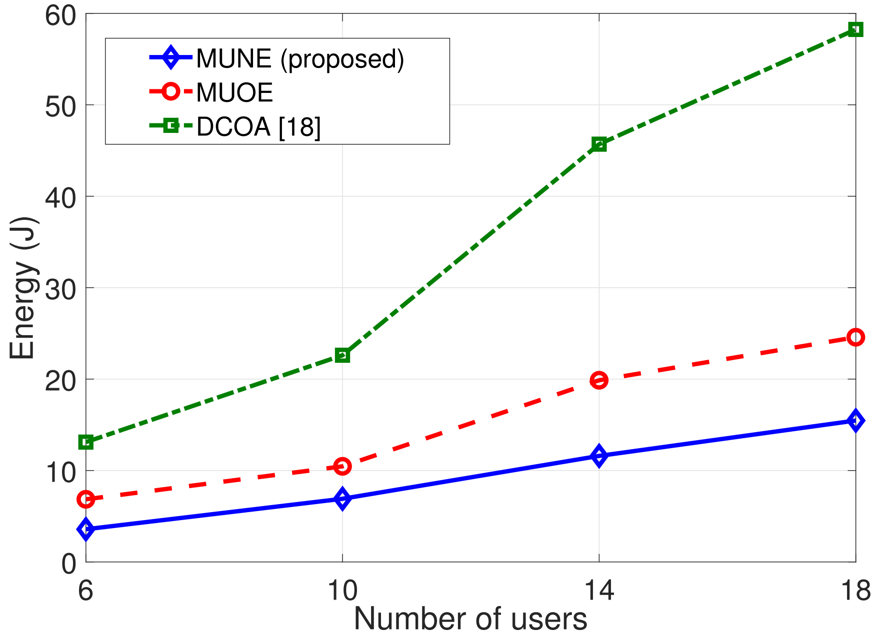

Figure 7.4: Total energy consumption versus number of users for single-UAV setting.

7.5.0.2 Numerical Results for Multi-UAV Settings

We now present numerical results for multi-UAV settings. Note that the DCOA algorithm cannot be applied to multi-UAV settings; therefore, we only show the performance achieved by the proposed MUNE and MUOE algorithms.

We first study a particular network scenario for which users' locations and UAVs' initial trajectories are shown in Fig. 7.2. In Fig. 7.5, we show the UAVs' trajectories obtained by the MUNE and MUOE algorithms at convergence. Several interesting observations can be drawn from this figure. First, the trajectories of UAV 1 achieved by both algorithms seem to follow a convex boundary established by users located at the network edge where these edge users are closer to the initial trajectory of UAV 1 than that of UAV 2. Moreover, the trajectories of UAV 1 due to both algorithms are quite close to each other. However, there is a clear difference in the trajectories of UAV 2 obtained by the two algorithms. The trajectory obtained by the MUNE algorithm also follows the convex boundary of the edge users that are closer to the initial trajectory of UAV 2. However, the trajectory obtained by the MUOE algorithm squeezes tightly to almost a curve. This can be explained by carefully studying the users' locations. In particular, in the few time slots of the flight right after departure ($t = 0$ to $t = 10$), UAV 2 has to fly down to serve users on the bottom left

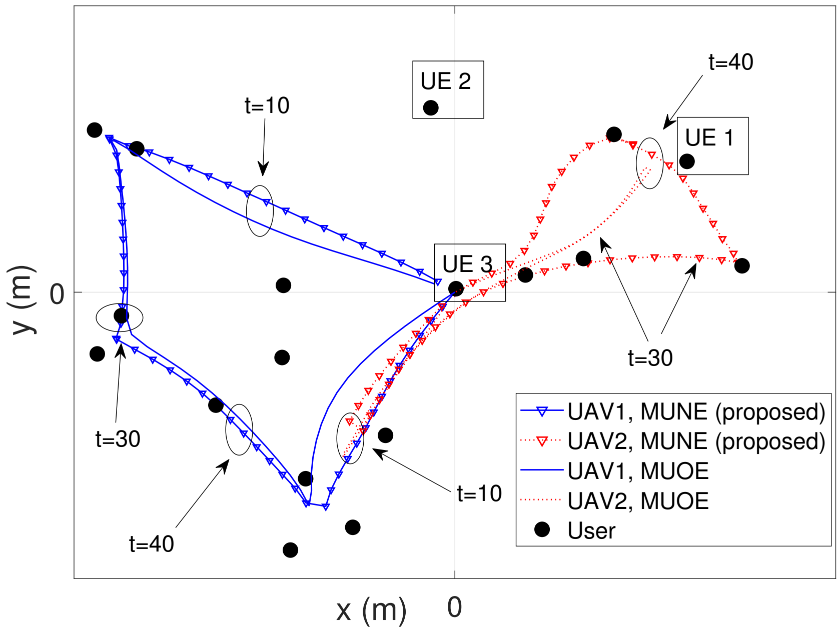

Figure 7.5: UAVs' trajectories due to different algorithms.

side of the network area. Moreover, in the second half on the flight ($t \geq 30$), this UAV has to serve users on the top right of the network area, and user 2 indicated in the figure. In order to serve a set of spatially diverged users, UAV 2 has to stay around certain desired locations that could lead to favorable channel conditions for its served users due to the nature of the OMA scheme. Specifically, OMA assigns each user a non-zero amount of bandwidth; hence, the assigned bandwidth could be wasted if the corresponding user does not transmit data. On the other hand, the NOMA scheme is more flexible and efficient in bandwidth utilization, since the total bandwidth assigned for a user pair can be used efficiently by both users or either one of the two paired users.

We now investigate the resource allocation solutions due to MUNE and MUOE by studying the transmit powers over time of three typical users indicated in Fig. 7.5: *i)* (edge) user 1 that lies close to the initial trajectory of one UAV and far from the initial trajectory of the other UAV, *ii)* (edge) user 2 who is far away from the initial trajectories of both UAVs, and *iii)* (center) user 3. We plot the transmit powers over time of these three users in Figure 7.6 and we also indicate their roles (strong or weak, or $\lambda_k[t] = 1$ or $\lambda_k[t] = 0$, respectively) in this figure. Note that when $p_k[t] = 0$, it does not matter if user k is assigned as a strong or weak user[6]. Therefore, if $p_k[t] = 0$, we assume that user k is a weak user for convenience.

[6]It can be verified easily by looking at the optimal power formula (7.18).

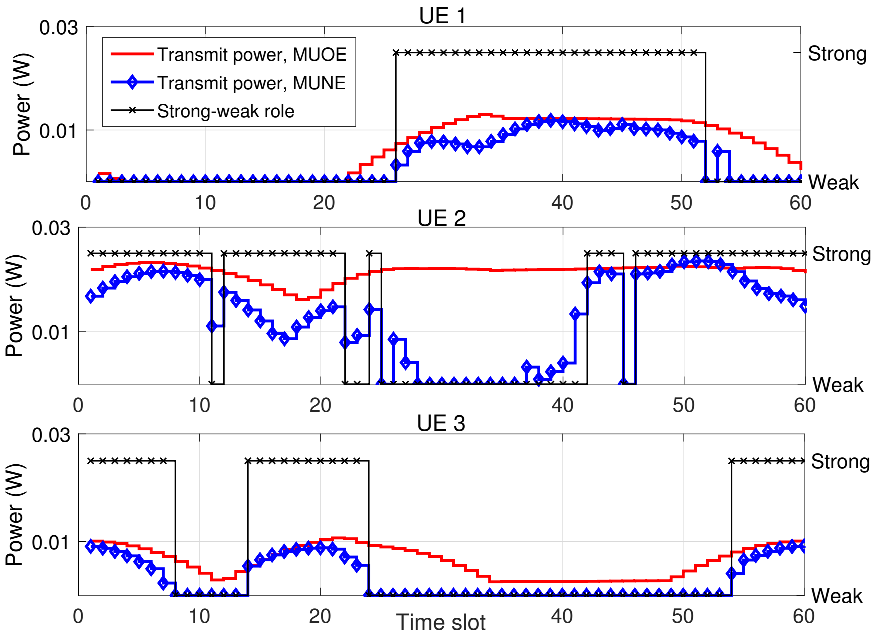

Figure 7.6: Users' transmit powers over time.

Several interesting observations can be drawn from the figure. First, the transmit powers of users in the NOMA case are usually smaller compared to the corresponding powers due to the OMA case. Second, NOMA allows users to be inactive more frequently compared to OMA (e.g., see the transmit powers of users 2, 3). For instance, when both UAVs are far away from user 2 (from $t = 20$ to $t = 40$), NOMA enables the user to be inactive while OMA mostly lets the user transmit with pretty high power so that user 2 can successfully transmit the required amount of data to the UAVs).

We now study the total energy due to MUNE and MUOE as different key system parameters vary. Specifically, Fig. 7.7 and Fig. 7.8 show the total energy as the number of users and the flight time (δT) vary, respectively for network settings with 2, 3 UAVs. It can be seen from Fig. 7.7 that less energy is required with more UAVs deployed in the network for both algorithms. This can be explained as follows. Each UAV tends to serve a smaller number of users in each time slot when there are more UAVs in the network. Hence, each UAV can establish a trajectory to serve a subset of users more efficiently with a larger number of UAVs. Fig. 7.7 again confirms that the MUNE algorithm outperforms the MUOE algorithm.

In Fig. 7.8, we plot the total energy versus the flight time by varying T from $T = 180$ to $T = 60$. At first, it is a bit surprising that longer flight time results in smaller energy consumption.

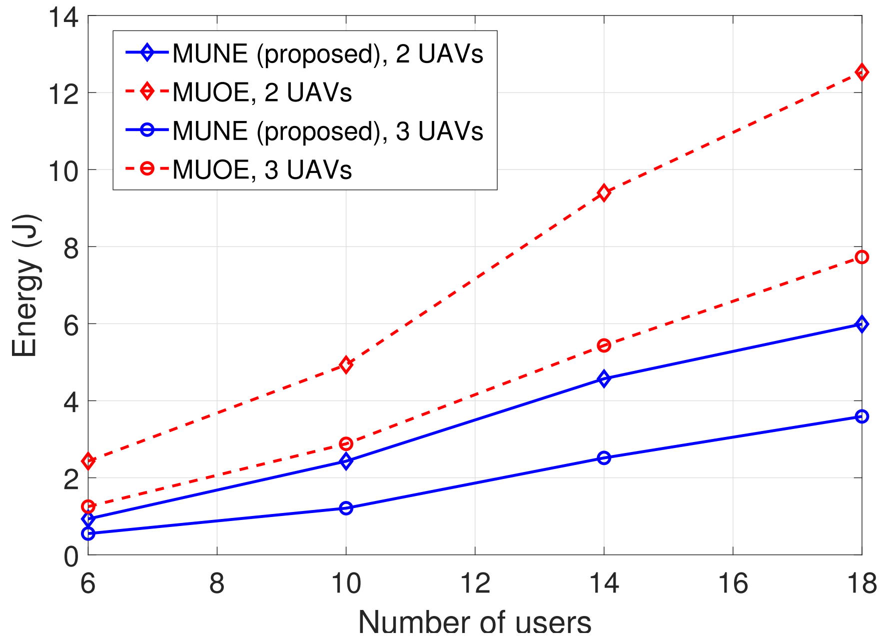

Figure 7.7: Total energy versus number of users.

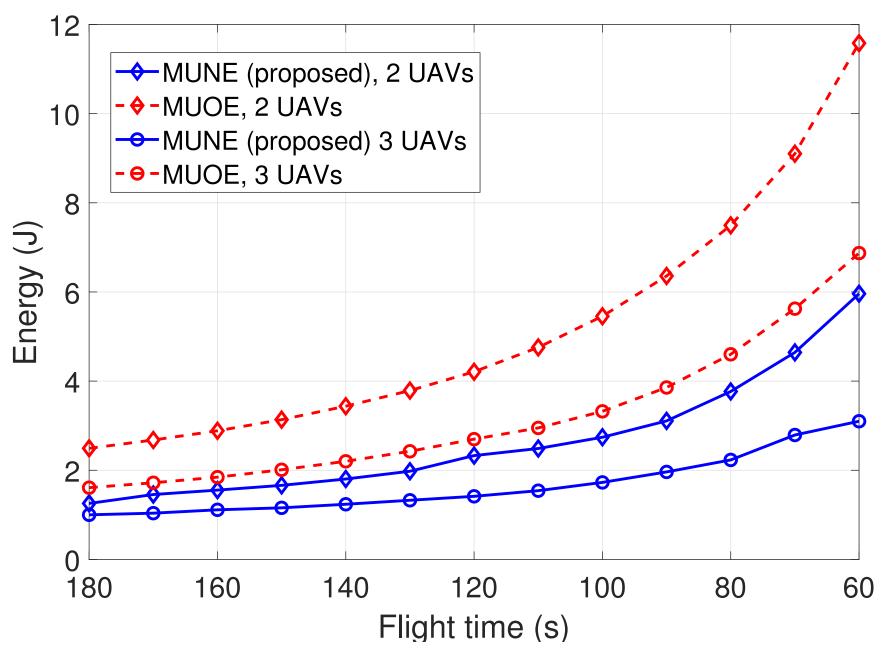

Figure 7.8: Total energy versus flight time.

However, the result in Fig. 7.8 can be explained by referring to the results in Fig. 7.6. In fact, both MUNE and MUOE algorithms allow a user to stay inactive when there is no UAV sufficiently close to it. Nevertheless, the proposed MUNE algorithm tends to provide more 'active-inactive' cycles for individual users compared to the MUOE algorithm, as can be observed in Fig. 7.6. Furthermore, the results in Fig. 7.8 shows that the MUNE algorithm outperforms the MUOE algorithm. Lastly,

Fig. 7.8 shows us that there is a tradeoff between the total energy consumption and flight time to fulfill the demands of data collection tasks for all users. Specifically, one can decrease the flight time at the cost of higher energy consumption or one can reduce the energy consumption if the time required for the data collection can be stretched.

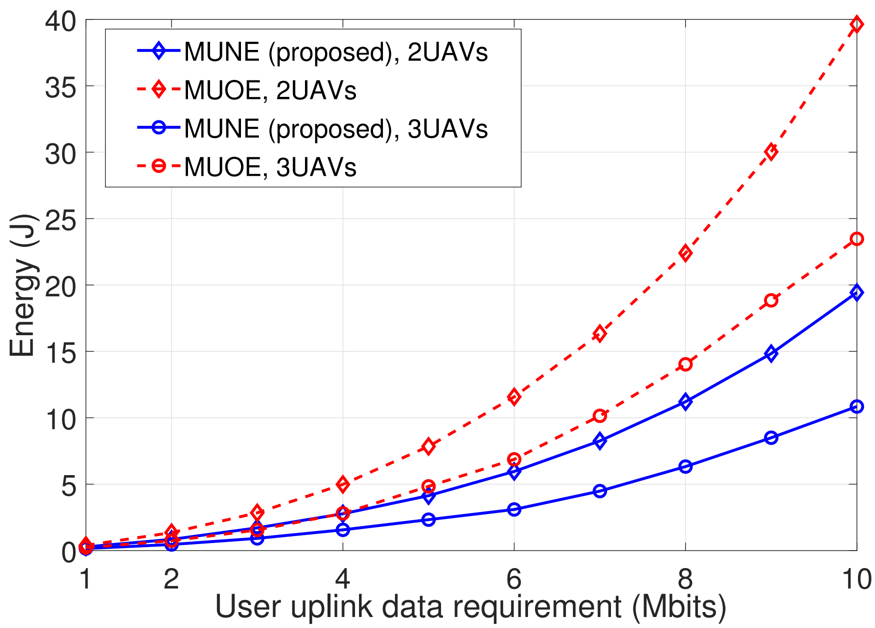

Figure 7.9: Total energy versus user demand.

Fig. 7.9 presents the variations of total energy with required amount of transmission data D_k of each user for network settings with 2 or 3 UAVs, and $T = 60$. It can be seen from this figure that the energy consumption increases rapidly when the required amount of transmission data increases. This can be explained by noticing the logarithmic form of the achievable data rate with respect to the transmit power. However, this figure shows that as the required amount of transmission data increases, the increasing rate of the energy consumption due to the MUNE algorithm is much lower than that due to the MUOE algorithm. This again confirms the superiority of our proposed algorithm leveraging NOMA compared to the MUOE counterpart.

Finally, we plot the energy consumption versus the number of UAVs, which varies from 2 to 8 UAVs in Fig. 7.10. It is expected that the energy consumption decreases when the number of UAVs increases. However, it is interesting to observe that the difference in energy consumption between the MUNE and MUOE algorithms decreases as the number of UAVs becomes larger. This implies that the gain due to NOMA over OMA is more significant in denser networks where each UAV must serve a large number of users on average. The results in this figure suggest that for network

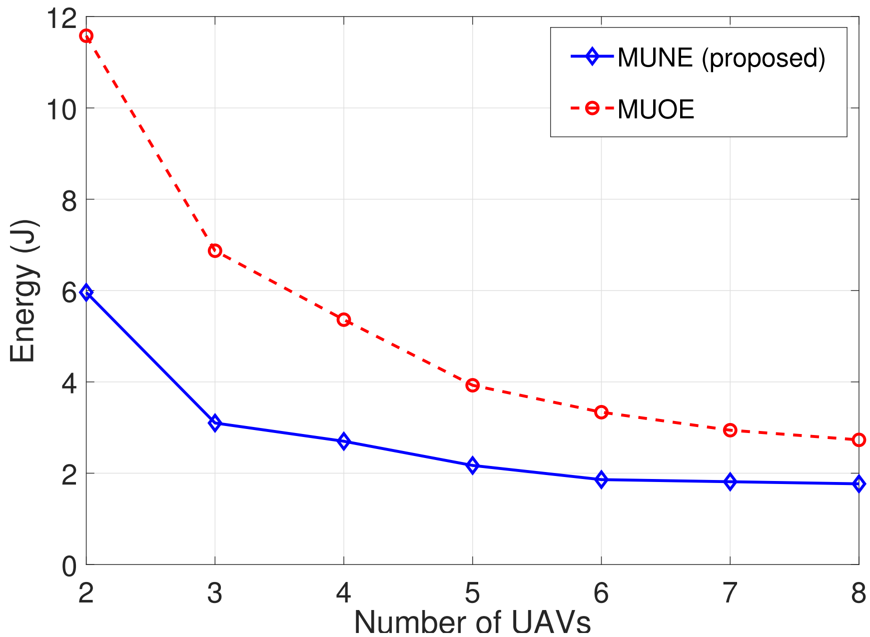

Figure 7.10: Total energy versus the number of UAVs.

settings in which the number of users per UAV is sufficiently high (e.g., more than 10 users per UAV), employment of NOMA instead of OMA for data collection tasks in multi-UAV based wireless networks is very rewarding.

7.6 Conclusion

In this paper, we have tackled the energy minimization problem for the wireless networks employing multiple UAVs and NOMA where we optimize the user's transmit power, NOMA user pairing, user-UAV association, and multi-UAV trajectories. To solve the underlying MINLP problem, we first introduced a set of auxiliary variables, namely users' data rates, then we have derived the optimal transmit powers in terms of other variables which are substituted into the objective function to obtain an equivalent problem. The BCD method was employed to solve the resulting problem where each set of variables (UAV trajectories, users' data rates, and integer (strong-weak and user association) variables) is optimized while the other sets of variables are given in each iteration of the algorithm. We showed that the user pairing problem can be transformed into maximum weighted graph matching problem which can be solved optimally in polynomial complexity. Moreover, the SCA method was employed to tackle the data rate and UAV trajectory optimization problems. Numerical studies showed that the proposed MUNE algorithm outperforms the baseline algorithms in terms of energy consumption because MUNE provides more efficient active-inactive schedules for users over the flight period compared to the MUOE algorithm. Furthermore, there is a tradeoff between the flight time and the energy consumption, i.e., longer the flight time leads to the lower energy consumption and vice versa.

Appendices

7.A Multi-UAV OMA Energy Minimization Algorithm (MUOE)

In this Appendix, we present the baseline algorithm where OMA instead of NOMA is employed. Let $p_k[t]$ be the transmit power that user k uses to transmit data to its associated UAV in time slot t. The optimization problem for this OMA-based strategy can be formulated as follows:

$$
\begin{aligned}
\mathcal{P}_0^{\mathsf{OMA}}: &\min_{\{\mathbf{P}[t], \mathbf{c}_n[t]\}} \delta \sum_{t=1}^{T} \sum_{k=1}^{K} p_k[t], \\
\text{s.t.} \quad & \delta \sum_{t=1}^{T} \frac{B}{2} \log \left(1 + \frac{\tau_k[t] p_k[t]}{\sigma^2/2} \right) \geq D_k, \forall k, t, && (7.29a) \\
& p_k[t] \leq P_{\mathsf{max}}, \forall k, t, && (7.29b) \\
& \text{constraints} \quad (7.11e), (7.11f), (7.11g).
\end{aligned}
$$

It can be verified that problem $\mathcal{P}_0^{\mathsf{OMA}}$ is non-convex. Moreover, the appearance of the transmit power variables in the objective function prevents us from applying the BCD method to solve the problem. We employ a similar method, which was used to develop our NOMA-based algorithm, to tackle problem $\mathcal{P}_0^{\mathsf{OMA}}$. Specifically, we first introduce the auxiliary variables $\{\mathbf{r}[t]\}$ where $r_k[t]$ is the data rate that user k transmits data to its associated UAV in time slot t. Let $\{\mathbf{P}^*[t]\}$ be the optimal power allocation of $\mathcal{P}_0^{\mathsf{OMA}}$, then

$$
p_k^*[t] = \frac{\sigma^2}{2} \tau_k^{-1}[t] \left(2^{2 r_k[t]/B} - 1 \right). \tag{7.30}
$$

The derivation of (7.30) is similar to one of NOMA in Lemma 7.1, and is omitted here. Substituting the right hand side of (7.30) into the objective function of $\mathcal{P}_0^{\mathsf{OMA}}$, we can obtain an equivalent optimization problem of $\mathcal{P}_0^{\mathsf{OMA}}$, which can be solved by using the BCD approach. Specifically, $\{\mathbf{r}[t]\}$ and $\{\mathbf{c}_n[t]\}$ are optimized iteratively until convergence. The optimization problem when one optimizes $\{\mathbf{r}[t]\}$ given $\{\mathbf{c}_n[t]\}$ can be expressed in the following.

$$\begin{aligned} \mathcal{P}_{\mathsf{R}}^{\mathsf{OMA}} : &\min_{\{\mathbf{r}[t]\}} \delta \frac{\sigma^2}{2} \sum_{t=1}^{T} \sum_{k=1}^{K} \tau_k^{-1}[t] \left(2^{2r_k[t]/B} - 1\right), \\ \text{s.t.} \;\; &\delta \sum_{t=1}^{T} r_k[t] \geq D_k, \forall k, && (7.31a) \\ &\frac{\sigma^2}{2} \tau_k^{-1}[t] \left(2^{2r_k[t]/B} - 1\right) \leq P_{\mathsf{max}}, \forall k, t. && (7.31b) \end{aligned}$$

Problem $\mathcal{P}_{\mathsf{R}}^{\mathsf{OMA}}$ has convex objective function and convex constraints. Hence it can be solved efficiently by using the CVX solver.

Let $\mathbf{c}_{(k)}[t]$ be the coordinate of the UAV serving user k in time slot t. Note that $\tau_k^{-1}[t] = \mu^{-1}\left(\|\mathbf{c}_{(k)}[t] - \mathbf{u}_k\|^2 + h^2\right)$, the UAV trajectory optimization problem, given $\{\mathbf{r}[t]\}$, can be expressed as follows:

$$\begin{aligned} \mathcal{P}_{\mathsf{C}}^{\mathsf{OMA}} : &\min_{\{\mathbf{c}_n[t]\}} \delta \sum_{t=1}^{T} \sum_{k=1}^{K} \eta_k[t] \left(\|\mathbf{c}_{(k)}[t] - \mathbf{u}_k\|^2 + h^2\right), \\ \text{s.t.} \;\; &\eta_k[t] \left(\|\mathbf{c}_{(k)}[t] - \mathbf{u}_k\|^2 + h^2\right) \leq P_{\mathsf{max}}, \forall k, t, && (7.32a) \\ &\text{constraints} \quad (7.11\text{e}), (7.11\text{f}), (7.11\text{g}), \end{aligned}$$

where $\eta_k[t] = \frac{\sigma^2}{2\mu}\left(2^{2r_k[t]/B} - 1\right)$.

It can be verified that problem $\mathcal{P}_{\mathsf{C}}^{\mathsf{OMA}}$ is still non-convex. However, it can be solved by using the SCA technique where constraint (7.11f) is approximated by constraint (7.28) as in the development of our MUNE algorithm.

In summary, we can solve problem $\mathcal{P}_0^{\mathsf{OMA}}$ by using the BCD technique to tackle the transformed problem where problems $\mathcal{P}_{\mathsf{R}}^{\mathsf{OMA}}$ and $\mathcal{P}_{\mathsf{C}}^{\mathsf{OMA}}$ are solved iteratively until convergence. This iterative algorithm is refereed to as the MUOE algorithm.

Chapter 8

Conclusions and Further Research Directions

In this chapter, we summarize our research contributions and discuss some potential directions for further research.

8.1 Major Research Contributions

The research performed in this dissertation results in three set of contributions. The first set of contributions are related to publications in [25, 48, 208] in which we investigate the general interference scenario where the interfering source and interfered receiver are un-synchronized and occupy overlapping channels of different bandwidths. Specifically, in the preliminary work [48], we develop the cancellation technique for the first and higher orders of adjacent-band interference components caused by the overlapping frequency bands and the non-linearity of the amplifier from the transmitter's side. In the second work [25], we propose a joint interference cancellation, fast fading channel estimation, and symbol detection design for the same interference scenario. However, while the first work assumes the knowledge of desired channel information, our second work only assumes the knowledge of the statistical characteristics of the desired channel, which makes the interference cancellation task much more challenging. Finally, the third work [208] provides an enhanced iterative interference cancellation framework, extensive analysis, and numerical studies that help gain more insights into the achievable performances in terms of the asymptotic behaviors, error rate, and throughput. Noticeable results obtained from this line of works can be summarized as follows: *first*, the proposed interference cancellation framework can reduce the interference power level close to the noise floor for a large range of interference power; *second*, the proposed symbol detection can achieve about 3dB SNR gain for the same error rate compared to an existing technique; *finally*, our numerical studies suggest that the pilot density as low as 10% can yield the maximum throughput for the considered frame structure.

The second set of contributions correspond to publications [209–211] in which we study resource allocation problems in UAV-based wireless networks. Particularly, in the work [209], we study the relationship between the UAV flight time and downlink throughput for single and double UAV settings. Our analysis suggests that there is a unique value of the UAV flight time achieving the optimal downlink throughout in the single UAV case. The same result is also verified numerically for the double UAV case. Further, we propose a consistent service design framework for multi-UAV based wireless networks in [210] where users are prioritized to be served based on their waiting time and data transmission demands. The framework does not require UAVs to have identical starting and ending positions as considered in many existing works, hence, our design provides more flexibility and eases the practical implementation. Finally, in [211], we study the admission maximization problem for UAV downlink communications where the multi-UAVs' trajectories and resource allocation are optimized. We show that our proposed algorithm outperforms the conventional scheme based on the BCA-MILP methods. Specifically, our numerical studies show that the proposed algorithm can admit up to 40% more users on the average compared to the baseline.

In the final set of contributions whose corresponding works are published in [50, 212], we study the joint resource allocation and NOMA user pairing problems in UAV-based wireless networks. In particular, in [50], we derive the optimal power allocation and UAV's position to maximize the downlink sum rate for the two-user case and propose a heuristic algorithm to maximize the minimum total rate of different user pairs when there are more than two users in the network. In the second work [212], we study the joint optimization of multiple UAVs' trajectories, transmit power allocation, user-UAV association, and user pairing to minimize the total energy consumption of ground users. Specifically, we first derive the optimal power allocation as a function of other variables, which enables us to apply the BCD method to solve the underlying problem efficiently in a three-step iterative algorithm. The numerical results show that our proposed algorithm can provide efficient active-inactive schedules and significantly lower energy consumption (from 45% to 65% of energy saving) compared to baseline schemes.

8.2 Further Research Directions

We now discuss potential research directions for further research following the studies in this dissertation.

8.2.1 Interference Management and Cancellations

For the research conducted in this dissertation, we have considered the interference cancellation for communications on overlapping channels, which is more general than the FD communications scenario. However, there are still several open questions and problems which need further studies for this general interference scenario. *First*, can the proposed algorithm in this dissertation be applied for the case where the desired signal's bandwidth is multiple times larger than that of the interfering signal? *Second*, how can we design an interference cancellation, channel estimation, and symbol detection framework if the superimposed pilot is used instead of the interleaved pilot block structure? *Third*, how can we efficiently perform interference cancellation in the multi-carrier communications system? *Fourth*, should the interleaved pilot structure in the time/frequency domain be used instead of interleaved pilots in the time domain only for the multi-carrier communication system? Addressing these questions and open issues will provide further insights and open up new applications, e.g., for FD communications and mixed numerology OFDM based wireless systems.

Furthermore, it has been shown that the performance of OFDM is limited in time-varying channels with high Doppler spread. Among new modulation techniques that has been studied recently, Orthogonal Time Frequency Space (OTFS) communication is one of the most promising candidates due to its robustness against channel time-variations [213–215]. Studying interference cancellation for concurrent OTFS communications can further boost the performance of future wireless systems so that they can support different applications with different QoS in high Doppler spread scenarios.

8.2.2 Advanced NOMA Communication Schemes

While various studies have showed promising advantages of NOMA compared to the conventional OMA communications, the complexity of NOMA communications, resource allocation, and receiver hardware may hinder the practical deployment of NOMA. Thus, more research is required to address the aforementioned limitations of NOMA. There are also several directions to extend the applications of NOMA such as grant-free NOMA [167, 216] and NOMA for generally concurrent communications on overlapping channels.

Thanks to its non-orthogonality nature, NOMA can be a very good candidate for grant-free communication protocols where users can randomly select their resource blocks for data transmission. In certain network settings, the decoding process may require to solve blind multi-user detection problems [217]. Furthermore, recent works [218, 219] show that many grant-free NOMA schemes can outperform OFDMA in practically relevant scenarios. We refer the interest reader to [216, 218] and reference therein for more comprehensive reviews of the state-of-the-art grant-free NOMA communications.

In fact, NOMA can be applied for generally overlapping communications with different bandwidths. Though it is challenging to devise efficient interference cancellation strategies with high performance in these general scenarios due to their complicated interference characteristics, the developed solutions would have great values in future generation wireless networks. This is because useable spectrum has been exploited and reused exhaustively causing severe and complicated interference to manage in recent years and communication signals using overlapping spectrum generated by different applications tend to have diverse QoS requirements.

8.2.3 Decentralized and Machine Learning Approaches for Resource Allocation in UWNs

While various design optimizations in UWNs can be performed for each service period, development and deployment of efficient algorithms for these optimization tasks can be quite challenging and may not be efficient in practice. This is because such an optimization algorithm cannot account for factors occurring during the considered service period. To this end, online optimization algorithms are more desirable because they can better adapt to system dynamics. Several techniques can be employed to achieve this design target. In particular, decentralized optimization methods can be applied to engineer the UWNs in which individual UAVs can make their own decisions by using local network information and in collaboration with other UAVs in the network. Moreover, reinforcement learning techniques could be employed to optimize network operations so as to optimize the long-term performance.

8.3 List of Publications

8.3.1 Journals

[J1]. **Minh Tri Nguyen** and Long Bao Le, "Interference cancellation, channel estimation, and symbol detection for communications on overlapping channels," *IEEE Access*, vol. 8, pp. 89822–89838, 2020.

[J2]. **Minh Tri Nguyen** and Long Bao Le, "Resource allocation, trajectory optimization, and admission control in UAV-based wireless networks," *IEEE Networking Letters*, vol. 3, no. 3, pp. 129d–132, 2021.

[J3]. **Minh Tri Nguyen** and Long Bao Le, "Multi-UAV trajectory control, resource allocation, and NOMA user pairing for uplink energy minimization," *submitted to IEEE Internet of Things Journal*, Dec. 2021.

8.3.2 Conferences

[C1]. **Minh Tri Nguyen** and Long Bao Le, "Multi-UAV trajectory, resource allocation design for UAV-based wireless networks with dynamic data demand for consecutive service periods", in *Proceeding of the 30th Biennial Symposium on Communications (BSC)*. Springer, 2021, to be published.

[C2]. **Minh Tri Nguyen** and Long Bao Le, "Flight Scheduling and Trajectory Control in UAV-Based Wireless Networks", in *Proceeding of the IEEE Wireless Communications and Networking Conference (WCNC)*, 2020, pp. 1–6.

[C3]. **Minh Tri Nguyen** and Long Bao Le, “NOMA user pairing and UAV placement in UAV-based wireless networks”, in *Proceeding of the IEEE International Conference on Communications (ICC)*, 2019, pp. 1–6.

[C4]. **Minh Tri Nguyen** and Long Bao Le, “Channel estimation and symbol detection for communications on overlapping channels”, in *IEEE Globecom Workshops (GC Wkshps)*, 2018, pp. 1–6.

[C5]. **Minh Tri Nguyen** and Long Bao Le, “Adjacent channel interference cancellation for robust spectrum sharing in satellite communications systems”, in *Proceeding of the IEEE 28th Annual International Symposium on Personal, Indoor, and Mobile Radio Communications (PIMRC)*, 2017, pp. 1–5.

[C6]. Dai Nguyen, **Minh Tri Nguyen** and Long Bao Le, “Cognitive Radio Based Resource Allocation for Sum Rate Maximization in Dual Satellite Systems”, in *Proceeding of the IEEE 86th Vehicular Technology Conference (VTC-Fall)*, 2017, pp. 1–5.

References

[1] Ericsson., "Ericsson mobility report," Available at https://www.ericsson.com/assets/local/reports-papers/mobility-report/documents/2019/ericsson-mobility-report-june-2019.pdf (accessed Nov. 2021), June 2019.

[2] Statista, "Internet of Things (IoT) connected devices installed base worldwide from 2015 to 2025," Available at https://www.statista.com/statistics/471264/iot-number-of-connected-devices-worldwide/ (accessed Nov. 2021), Nov. 2016.

[3] Cisco, "Annual internet report," Available at https://www.cisco.com/c/en/us/solutions/collateral/executive-perspectives/annual-internet-report/white-paper-c11-741490.pdf (accessed Nov. 2021), Mar. 2020.

[4] 3GPP, "5G; NR; base station (BS) radio transmission and reception (3GPP TS 38.104 version 16.5.0 release 16)," Available at https://www.etsi.org/deliver/etsi_ts/138100_138199/138104/16.05.00_60/ts_138104v160500p.pdf (accessed Nov. 2021), Nov. 2020.

[5] ——, "LTE; evolved universal terrestrial radio access (E-UTRA); user equipment (UE) radio transmission and reception (3GPP TS 36.101 version 14.3.0 release 14)," Available at https://www.etsi.org/deliver/etsi_ts/136100_136199/136101/14.03.00_60/ts_136101v140300p.pdf (accessed Nov. 2021), Apr. 2017.

[6] D. Bharadia, E. McMilin, and S. Katti, "Full duplex radios," in *Proc. ACM SIGCOMM*, vol. 43, no. 4, 2013, pp. 375–386.

[7] A. Yazar, S. Dogan-Tusha, and H. Arslan, "6G vision: An ultra-flexible perspective," *ITU J. Future Evol. Technol.*, vol. 1, no. 1, pp. 1–20, Dec. 2020.

[8] Y. Saito, Y. Kishiyama, A. Benjebbour, T. Nakamura, A. Li, and K. Higuchi, "Non-orthogonal multiple access (noma) for cellular future radio access," in *Proc. IEEE Veh. Technol. Conf. (VTC Spring)*. IEEE, June 2013, pp. 1–5.

[9] M. Vaezi and H. V. Poor, "NOMA: An information-theoretic perspective," in *Multiple access techniques for 5G wireless networks and beyond*. Springer, 2019, pp. 167–193.

[10] Z. Chen, Z. Ding, X. Dai, and R. Zhang, "An optimization perspective of the superiority of NOMA compared to conventional OMA," *IEEE Trans. Signal Process.*, vol. 65, no. 19, pp. 5191–5202, Oct. 2017.

[11] S. R. Islam, N. Avazov, O. A. Dobre, and K.-S. Kwak, "Power-domain non-orthogonal multiple access (NOMA) in 5G systems: Potentials and challenges," *IEEE Commun. Surveys Tut.*, vol. 19, no. 2, pp. 721–742, Second Quarter 2017.

[12] A. Fotouhi, H. Qiang, M. Ding, M. Hassan, L. G. Giordano, A. Garcia-Rodriguez, and J. Yuan, "Survey on UAV cellular communications: Practical aspects, standardization advancements, regulation, and security challenges," *IEEE Commun. Surveys Tut.*, vol. 21, no. 4, pp. 3417–3442, Fourth Quarter 2019.

[13] G. K. Kurt, M. G. Khoshkholgh, S. Alfattani, A. Ibrahim, T. S. Darwish, M. S. Alam, H. Yanikomeroglu, and A. Yongacoglu, "A vision and framework for the high altitude platform station (HAPS) networks of the future," *IEEE Commun. Surveys Tut.*, vol. 23, no. 2, pp. 729–779, Secondquarter 2021.

[14] Qualcomm Technologies, "LTE unmanned aircraft systems," Available at https://www.qualcomm.com/media/documents/files/lte-unmanned-aircraft-systems-trial-report.pdf (accessed Mar. 2021), May 2017.

[15] N. H. Motlagh, T. Taleb, and O. Arouk, "Low-altitude unmanned aerial vehicles-based internet of things services: Comprehensive survey and future perspectives," *IEEE Internet Things J.*, vol. 3, no. 6, pp. 899–922, Dec. 2016.

[16] S. Sekander, H. Tabassum, and E. Hossain, "Multi-tier drone architecture for 5G/B5G cellular networks: Challenges, trends, and prospects," *IEEE Commun. Mag.*, vol. 56, no. 3, pp. 96–103, Mar. 2018.

[17] FCC, "Technical analysis of Ligado interference impact on Iridium user links," Available at https://ecfsapi.fcc.gov/file/10902228186199/TechDescriptionofLigadoInterferenceImpact9.1.16-PUBLIC.pdf(accessed May 2020), Sept. 2016.

[18] ERC, "Assessment of interference from unwanted emissions of NGSO MSS satellite transmitters operating in the space-to-earth direction in the band 1621.35 - 1626.5 MHz to GSO MSS satellite receivers operating in the earth-to-space direction in the band 1626.5 - 1660.5 MHz," Available at https://www.ecodocdb.dk/download/148a1dcc-7c7a/REP091.PDF(accessed May 2020), June 2000.

[19] H. Q. Ngo, H. A. Suraweera, M. Matthaiou, and E. G. Larsson, "Multipair full-duplex relaying with massive arrays and linear processing," *IEEE J. Sel. Areas Commun.*, vol. 32, no. 9, pp. 1721–1737, Sept. 2014.

[20] X. Huang, K. Yang, F. Wu, and S. Leng, "Power control for full-duplex relay-enhanced cellular networks with QoS guarantees," *IEEE Access*, vol. 5, pp. 4859–4869, Mar. 2017.

[21] H. S. Wang and P.-C. Chang, "On verifying the first-order Markovian assumption for a Rayleigh fading channel model," *IEEE Trans. Veh. Technol.*, vol. 45, no. 2, pp. 353–357, May 1996.

[22] C. C. Tan and N. C. Beaulieu, "On first-order Markov modeling for the Rayleigh fading channel," *IEEE Trans. Commun.*, vol. 48, no. 12, pp. 2032–2040, Dec. 2000.

[23] L. Tong, B. M. Sadler, and M. Dong, "Pilot-assisted wireless transmissions: General model, design criteria, and signal processing," *IEEE Signal Process. Mag.*, vol. 21, no. 6, pp. 12–25, June 2004.

[24] A. T. Asyhari and S. ten Brink, "Orthogonal or superimposed pilots? A rate-efficient channel estimation strategy for stationary MIMO fading channels," *IEEE Trans. Wireless Commun.*, vol. 16, no. 5, pp. 2776–2789, May 2017.

[25] M. T. Nguyen and L. B. Le, "Channel estimation and symbol detection for communications on overlapping channels," in *Proc. IEEE Globecom Workshops*, 2018, pp. 1–6.

[26] D. Tse and P. Viswanath, *Fundamentals of wireless communication*. Cambridge university press, 2005.

[27] N. Sun and J. Wu, "Maximizing spectral efficiency for high mobility systems with imperfect channel state information," *IEEE Trans. Wireless Commun.*, vol. 13, no. 3, pp. 1462–1470, Mar. 2014.

[28] M. A. Mahamadu, J. Wu, Z. Ma, W. Zhou, Y. Tang, and P. Fan, "Fundamental tradeoff between Doppler diversity and channel estimation errors in SIMO high mobility communication systems," *IEEE Access*, vol. 6, pp. 21 867–21 878, Apr. 2018.

[29] J. Zhao, Y. Wang, Z. Fei, X. Wang, and Z. Miao, "NOMA-aided UAV data collection system: Trajectory optimization and communication design," *IEEE Access*, vol. 8, pp. 155 843–155 858, Sept. 2020.

[30] S. Boyd and L. Vandenberghe, *Convex optimization*. Cambridge university press, 2004.

[31] J. Edmonds, "Paths, trees, and flowers," *Canadian J. Math.*, vol. 17, pp. 449–467, 1965.

[32] A. M. Geoffrion, "Generalized Benders decomposition," *J. Optim. Theory Applicat.*, vol. 10, no. 4, pp. 237–260, 1972.

[33] 3GPP, "Technical specification group radio access network; study on enhanced LTE support for aerial vehicles (release 15), rep. 36.777," Available at https://www.3gpp.org/ftp/Specs/archive/36_series/36.777/ (accessed Dec. 2021), Dec. 2017.

[34] M. Mozaffari, W. Saad, M. Bennis, Y.-H. Nam, and M. Debbah, "A tutorial on UAVs for wireless networks: Applications, challenges, and open problems," *IEEE Commun. Surveys Tut.*, vol. 21, no. 3, pp. 2334–2360, Third Quarter 2019.

[35] M. Alzenad, A. El-Keyi, and H. Yanikomeroglu, "3-D placement of an unmanned aerial vehicle base station for maximum coverage of users with different QoS requirements," *IEEE Wireless Commun. Lett.*, vol. 7, no. 1, pp. 38–41, Feb. 2018.

[36] M. Mozaffari, W. Saad, M. Bennis, and M. Debbah, "Mobile unmanned aerial vehicles (UAV s) for energy-efficient internet of things communications," *IEEE Trans. Wireless Commun.*, vol. 16, no. 11, pp. 7574–7589, Nov. 2017.

[37] H. Huang, C. Huang, and D. Ma, "A method for deploying the minimal number of UAV base stations in cellular networks," *IEEE/CAA J. Automatica Sinica*, vol. 7, no. 2, pp. 559–567, Mar. 2020.

[38] N. C. Luong, D. T. Hoang, P. Wang, D. Niyato, D. I. Kim, and Z. Han, "Data collection and wireless communication in internet of things (IoT) using economic analysis and pricing models: A survey," *IEEE Commun. Surveys Tuts.*, vol. 18, no. 4, pp. 2546–2590, Fourth Quarter 2016.

[39] C. Zhan, Y. Zeng, and R. Zhang, "Energy-efficient data collection in UAV enabled wireless sensor network," *IEEE Wireless Commun. Lett*, vol. 7, no. 3, pp. 328–331, June 2018.

[40] J. Gong, T.-H. Chang, C. Shen, and X. Chen, "Flight time minimization of UAV for data collection over wireless sensor networks," *IEEE J. Sel. Areas Commun.*, vol. 36, no. 9, pp. 1942–1954, Sept. 2018.

[41] W. Wang, N. Zhao, L. Chen, X. Liu, Y. Chen, and D. Niyato, "UAV-assisted time-efficient data collection via uplink NOMA," *IEEE Trans. Commun.*, vol. 69, no. 11, pp. 7851–7863, Nov. 2021.

[42] B. Debaillie, D.-J. van den Broek, C. Lavin, B. van Liempd, E. A. Klumperink, C. Palacios, J. Craninckx, B. Nauta, and A. Pärssinen, "Analog/RF solutions enabling compact full-duplex radios," *IEEE J. Sel. Areas Commun.*, vol. 32, no. 9, pp. 1662–1673, Sept. 2014.

[43] A. Sabharwal, P. Schniter, D. Guo, D. W. Bliss, S. Rangarajan, and R. Wichman, "In-band full-duplex wireless: Challenges and opportunities," *IEEE J. Sel. Areas Commun.*, vol. 32, no. 9, pp. 1637–1652, Sept. 2014.

[44] K. E. Kolodziej, B. T. Perry, and J. S. Herd, "In-band full-duplex technology: Techniques and systems survey," *IEEE Trans. Microw. Theory Techn.*, vol. 67, no. 7, pp. 3025–3041, July 2019.

[45] K. Schwarzenbarth, J. Grotz, and B. Ottersten, "MMSE based interference processing for satellite broadcast reception," in *Proc. IEEE 65th Veh. Technol. Conf. (VTC-Spring)*, Apr. 2007, pp. 1345–1349.

[46] K. Pedersen, G. Pocovi, J. Steiner, and A. Maeder, "Agile 5G scheduler for improved E2E performance and flexibility for different network implementations," *IEEE Commun. Mag.*, vol. 56, no. 3, pp. 210–217, Mar. 2018.

[47] X. Zhang, L. Zhang, P. Xiao, D. Ma, J. Wei, and Y. Xin, "Mixed numerologies interference analysis and inter-numerology interference cancellation for windowed OFDM systems," *IEEE Trans. Veh. Technol.*, vol. 67, no. 8, pp. 7047–7061, Aug. 2018.

[48] M. T. Nguyen and L. B. Le, "Adjacent channel interference cancellation for robust spectrum sharing in satellite communications systems," in *Proc. IEEE 28th Annu. Int. Symp. Pers., Indoor, Mobile Radio Commun. (PIMRC)*, Oct. 2017, pp. 1–5.

[49] Y. Liu, Z. Qin, Y. Cai, Y. Gao, G. Y. Li, and A. Nallanathan, "UAV communications based on non-orthogonal multiple access," *IEEE Wireless Commun.*, vol. 26, no. 1, pp. 52–57, Feb. 2019.

[50] M. T. Nguyen and L. B. Le, "NOMA user pairing and UAV placement in UAV-based wireless networks," in *Proc. Int. Conf. Commun. (ICC)*. IEEE, 2019, pp. 1–6.

[51] J. Lu, Y. Wang, T. Liu, Z. Zhuang, X. Zhou, F. Shu, and Z. Han, "UAV-enabled uplink non-orthogonal multiple access system: Joint deployment and power control," *IEEE Trans. Veh. Technol.*, vol. 69, no. 9, pp. 10 090–10 102, Sept. 2020.

[52] R. Duan, J. Wang, C. Jiang, H. Yao, Y. Ren, and Y. Qian, "Resource allocation for multi-UAV aided IoT NOMA uplink transmission systems," *IEEE Internet Things J.*, vol. 6, no. 4, pp. 7025–7037, Aug. 2019.

[53] P. Tseng, "Convergence of a block coordinate descent method for nondifferentiable minimization," *J. Optim. Theory Appl.*, vol. 109, no. 3, pp. 475–494, June 2001.

[54] J. T. Linderoth and A. Lodi, "MILP software," *Wiley encyclopedia of operations research and management science*, vol. 5, pp. 3239–3248, 2010.

[55] L. Lei, D. Yuan, and P. Värbrand, "On power minimization for non-orthogonal multiple access (NOMA)," *IEEE Commun. Lett.*, vol. 20, no. 12, pp. 2458–2461, Dec. 2016.

[56] X. Li, C. Li, and Y. Jin, "Dynamic resource allocation for transmit power minimization in OFDM-based NOMA systems," *IEEE Commun. Lett.*, vol. 20, no. 12, pp. 2558–2561, Dec. 2016.

[57] M. Zeng, A. Yadav, O. A. Dobre, and H. V. Poor, "Energy-efficient joint user-RB association and power allocation for uplink hybrid NOMA-OMA," *IEEE Internet Things J.*, vol. 6, no. 3, pp. 5119–5131, June 2019.

[58] J. Wang, M. Liu, J. Sun, G. Gui, H. Gacanin, H. Sari, and F. Adachi, "Multiple unmanned aerial vehicles deployment and user pairing for non-orthogonal multiple access schemes," *IEEE Internet Things J.*, vol. 8, no. 3, Feb. 2021.

[59] W. Shi, Y. Sun, M. Liu, H. Xu, G. Gui, T. Ohtsuki, B. Adebisi, H. Gacanin, and F. Adachi, "Joint UL/DL resource allocation for UAV-aided full-duplex NOMA communications," *IEEE Trans. Commun.*, vol. 69, no. 12, pp. 8474–8487, Dec. 2021.

[60] W. Chen, S. Zhao, R. Zhang, Y. Chen, and L. Yang, "UAV-assisted data collection with nonorthogonal multiple access," *IEEE Internet Things J.*, vol. 8, no. 1, pp. 501–511, Jan. 2021.

[61] X. Liu, J. Wang, N. Zhao, Y. Chen, S. Zhang, Z. Ding, and F. R. Yu, "Placement and power allocation for NOMA-UAV networks," *IEEE Wireless Commun. Lett*, vol. 8, no. 3, pp. 965–968, June 2019.

[62] X. Mu, Y. Liu, L. Guo, J. Lin, and Z. Ding, "Energy-constrained UAV data collection systems: NOMA and OMA," *IEEE Trans. Veh. Technol.*, vol. 70, no. 7, pp. 6898–6912, July 2021.

[63] N. Zhao, X. Pang, Z. Li, Y. Chen, F. Li, Z. Ding, and M.-S. Alouini, "Joint trajectory and precoding optimization for UAV-assisted NOMA networks," *IEEE Trans. Commun.*, vol. 67, no. 5, pp. 3723–3735, May 2019.

[64] E. Everett, A. Sahai, and A. Sabharwal, "Passive self-interference suppression for full-duplex infrastructure nodes," *IEEE Trans. Wireless Commun.*, vol. 13, no. 2, pp. 680–694, Feb. 2014.

[65] Q. Xu, M. Biedka, and Y. E. Wang, "Indented antenna arrays for high isolation: The growing interest in simultaneous-transmit-and-receive-based full-duplex communication systems," *IEEE Antennas Propag. Mag.*, vol. 60, no. 1, pp. 72–80, Feb. 2018.

[66] E. A. Etellisi, M. A. Elmansouri, and D. Filipovic, "Broadband full-duplex monostatic circular-antenna arrays: Circular arrays reaching simultaneous transmit and receive operation," *IEEE Antennas Propag. Mag.*, vol. 60, no. 5, pp. 62–77, Oct. 2018.

[67] R. Lian, T.-Y. Shih, Y. Yin, and N. Behdad, "A high-isolation, ultra-wideband simultaneous transmit and receive antenna with monopole-like radiation characteristics," *IEEE Trans. Antennas Propag.*, vol. 66, no. 2, pp. 1002–1007, Feb. 2017.

[68] J. Ha, M. A. Elmansouri, P. V. Prasannakumar, and D. S. Filipovic, "Monostatic co-polarized full-duplex antenna with left-or right-hand circular polarization," *IEEE Trans. Antennas Propag.*, vol. 65, no. 10, pp. 5103–5111, Oct. 2017.

[69] S. N. Venkatasubramanian, L. Li, A. Lehtovuori, C. Icheln, and K. Haneda, "Impact of using resistive elements for wideband isolation improvement," *IEEE Trans. Antennas Propag.*, vol. 65, no. 1, pp. 52–62, Jan. 2017.

[70] J. Wu, M. Li, and N. Behdad, "A wideband, unidirectional circularly polarized antenna for full-duplex applications," *IEEE Trans. Antennas Propag.*, vol. 66, no. 3, pp. 1559–1563, Mar. 2018.

[71] P. V. Prasannakumar, M. A. Elmansouri, and D. S. Filipovic, "Wideband decoupling techniques for dual-polarized bi-static simultaneous transmit and receive antenna subsystem," *IEEE Trans. Antennas Propag.*, vol. 65, no. 10, pp. 4991–5001, Oct. 2017.

[72] M. Heino, S. N. Venkatasubramanian, C. Icheln, and K. Haneda, "Design of wavetraps for isolation improvement in compact in-band full-duplex relay antennas," *IEEE Trans. Antennas Propag.*, vol. 64, no. 3, pp. 1061–1070, Mar. 2016.

[73] H. Xu, H. Zhou, S. Gao, H. Wang, and Y. Cheng, "Multimode decoupling technique with independent tuning characteristic for mobile terminals," *IEEE Trans. Antennas Propag.*, vol. 65, no. 12, pp. 6739–6751, Dec. 2017.

[74] T. Snow, C. Fulton, and W. J. Chappell, "Transmit-receive duplexing using digital beamforming system to cancel self-interference," *IEEE Trans. Microw. Theory Techn.*, vol. 59, no. 12, pp. 3494–3503, Dec. 2011.

[75] E. Everett, C. Shepard, L. Zhong, and A. Sabharwal, "Softnull: Many-antenna full-duplex wireless via digital beamforming," *IEEE Trans. Wireless Commun.*, vol. 15, no. 12, pp. 8077–8092, Dec. 2016.

[76] E. Aryafar, M. A. Khojastepour, K. Sundaresan, S. Rangarajan, and M. Chiang, "MIDU: Enabling MIMO full duplex," in *Proc. ACM Int. Conf. MobiCom Netw.,*, Aug. 2012, pp. 257–268.

[77] M. Duarte, C. Dick, and A. Sabharwal, "Experiment-driven characterization of full-duplex wireless systems," *IEEE Trans. Wireless Commun.*, vol. 11, no. 12, pp. 4296–4307, Dec. 2012.

[78] S. B. Venkatakrishnan, E. A. Alwan, and J. L. Volakis, "Wideband RF self-interference cancellation circuit for phased array simultaneous transmit and receive systems," *IEEE Access*, vol. 6, pp. 3425–3432, 2018.

[79] D.-J. van den Broek, E. A. Klumperink, and B. Nauta, "An in-band full-duplex radio receiver with a passive vector modulator downmixer for self-interference cancellation," *IEEE J. Solid-State Circuits*, vol. 50, no. 12, pp. 3003–3014, Dec. 2015.

[80] Y. Liu, X. Quan, W. Pan, and Y. Tang, "Digitally assisted analog interference cancellation for in-band full-duplex radios," *IEEE Commun. Lett.*, vol. 21, no. 5, pp. 1079–1082, May 2017.

[81] D. Korpi, L. Anttila, V. Syrjälä, and M. Valkama, "Widely linear digital self-interference cancellation in direct-conversion full-duplex transceiver," *IEEE J. Sel. Areas Commun.*, vol. 32, no. 9, pp. 1674–1687, Sept. 2014.

[82] E. Ahmed and A. M. Eltawil, "All-digital self-interference cancellation technique for full-duplex systems," *IEEE Trans. Wireless Commun.*, vol. 14, no. 7, pp. 3519–3532, July 2015.

[83] K. Komatsu, Y. Miyaji, and H. Uehara, "Frequency-domain Hammerstein self-interference canceller for in-band full-duplex OFDM systems," in *Proc. IEEE Wireless Commun. Netw. Conf. (WCNC)*, Mar. 2017, pp. 1–6.

[84] F. H. Gregorio, G. J. González, J. Cousseau, T. Riihonen, and R. Wichman, "Predistortion for power amplifier linearization in full-duplex transceivers without extra RF chain," in *Proc. IEEE Int. Conf. Acoust. Speech Signal Process. (ICASSP)*. IEEE, Mar. 2017, pp. 6563–6567.

[85] J. I. Choi, M. Jain, K. Srinivasan, P. Levis, and S. Katti, "Achieving single channel, full duplex wireless communication," in *Proc. Int. Conf. Mobile Comput. Netw.*, 2010, pp. 1–12.

[86] M. Duarte, A. Sabharwal, V. Aggarwal, R. Jana, K. Ramakrishnan, C. W. Rice, and N. Shankaranarayanan, "Design and characterization of a full-duplex multiantenna system for WiFi networks," *IEEE Trans. Veh. Technol.*, vol. 63, no. 3, pp. 1160–1177, Mar. 2014.

[87] M. Chung, M. S. Sim, J. Kim, D. K. Kim, and C.-B. Chae, "Prototyping real-time full duplex radios," *IEEE Commun. Mag.*, vol. 53, no. 9, pp. 56–63, Sept. 2015.

[88] M. Heino, D. Korpi, T. Huusari, E. Antonio-Rodriguez, S. Venkatasubramanian, T. Riihonen, L. Anttila, C. Icheln, K. Haneda, R. Wichman *et al.*, "Recent advances in antenna design and interference cancellation algorithms for in-band full duplex relays," *IEEE Commun. Mag.*, vol. 53, no. 5, pp. 91–101, May 2015.

[89] D. Korpi, M. Heino, C. Icheln, K. Haneda, and M. Valkama, "Compact inband full-duplex relays with beyond 100 dB self-interference suppression: Enabling techniques and field measurements," *IEEE Trans. Antennas Propag.*, vol. 65, no. 2, pp. 960–965, Feb. 2017.

[90] S. Doğan Tusha, A. Tusha, E. Başar, S. Althunibat, K. Qaraqe, and H. Arslan, "Inter-numerology interference in OFDM-IM systems," *IET Commun. 15*, pp. 1941–1949, 2021.

[91] A. B. Kihero, M. S. J. Solaija, and H. Arslan, "Inter-numerology interference for beyond 5G," *IEEE Access*, vol. 7, pp. 146 512–146 523, 2019.

[92] P. Sadeghi, R. A. Kennedy, P. B. Rapajic, and R. Shams, "Finite-state Markov modeling of fading channels-a survey of principles and applications," *IEEE Signal Process. Mag.*, vol. 25, no. 5, pp. 57–80, Sept. 2008.

[93] Y. Liu, Z. Tan, H. Hu, L. J. Cimini, and G. Y. Li, "Channel estimation for OFDM," *IEEE Commun. Surveys Tut.*, vol. 16, no. 4, pp. 1891–1908, Fourth Quarter 2014.

[94] M. K. Ozdemir and H. Arslan, "Channel estimation for wireless OFDM systems," *IEEE Commun. Surveys Tut.*, vol. 9, no. 2, pp. 18–48, Second Quarter 2007.

[95] H. Mai, Y. V. Zakharov, and A. G. Burr, "Iterative channel estimation based on B-splines for fast flat fading channels," *IEEE Trans. Wireless Commun.*, vol. 6, no. 4, pp. 1224–1229, Apr. 2007.

[96] T. Wang, L. Shi, S. Zhang, and H. Wang, "Gaussian mixture message passing for blind known interference cancellation," *IEEE Trans. Wireless Commun.*, vol. 18, no. 9, pp. 4268–4282, Sept. 2019.

[97] A. Mishra, R. Gayathri, and A. K. Jagannatham, "Random parameter EM-based Kalman filter (REKF) for joint symbol detection and channel estimation in fast fading STTC MIMO systems," *IEEE Signal Process. Lett.*, vol. 21, no. 6, pp. 766–770, June 2014.

[98] E. P. Simon and M. A. Khalighi, "Iterative soft-Kalman channel estimation for fast time-varying MIMO-OFDM channels," *IEEE Wireless Commun. Lett.*, vol. 2, no. 6, pp. 599–602, Dec. 2013.

[99] H. Niu, M. Shen, J. A. Ritcey, and H. Liu, "A factor graph approach to iterative channel estimation and LDPC decoding over fading channels," *IEEE Trans. Wireless Commun.*, vol. 4, no. 4, pp. 1345–1350, July 2005.

[100] K. Kwak, S. Lee, H. Min, S. Choi, and D. Hong, "New OFDM channel estimation with dual-ICI cancellation in highly mobile channel," *IEEE Trans. Wireless Commun.*, vol. 9, no. 10, pp. 3155–3165, Oct. 2010.

[101] Y. Zhu, D. Guo, and M. L. Honig, "A message-passing approach for joint channel estimation, interference mitigation, and decoding," *IEEE Trans. Wireless Commun.*, vol. 8, no. 12, Dec. 2009.

[102] X. Ma, G. B. Giannakis, and S. Ohno, "Optimal training for block transmissions over doubly selective wireless fading channels," *IEEE Trans. Signal Process.*, vol. 51, no. 5, pp. 1351–1366, May 2003.

[103] S. Zhang, S.-C. Liew, and H. Wang, "Blind known interference cancellation," *IEEE J. Sel. Areas Commun.*, vol. 31, no. 8, pp. 1572–1582, Aug. 2013.

[104] C. Shin, R. W. Heath, and E. J. Powers, "Blind channel estimation for MIMO-OFDM systems," *IEEE Trans. Veh. Technol.*, vol. 56, no. 2, pp. 670–685, Mar. 2007.

[105] F. Gao and A. Nallanathan, "Blind channel estimation for MIMO OFDM systems via nonredundant linear precoding," *IEEE Trans. Signal Process.*, vol. 55, no. 2, pp. 784–789, Jan. 2007.

[106] F. Wan, W.-P. Zhu, and M. Swamy, "Semiblind sparse channel estimation for MIMO-OFDM systems," *IEEE Trans. Veh. Technol.*, vol. 60, no. 6, pp. 2569–2582, July 2011.

[107] O. Simeone, Y. Bar-Ness, and U. Spagnolini, "Pilot-based channel estimation for OFDM systems by tracking the delay-subspace," *IEEE Trans. Wireless Commun.*, vol. 3, no. 1, pp. 315–325, Jan. 2004.

[108] S. Kalyani and K. Giridhar, "Mitigation of error propagation in decision directed OFDM channel tracking using generalized M estimators," *IEEE Trans. Signal Process.*, vol. 55, no. 5, pp. 1659–1672, May 2007.

[109] M. Raghavendra, E. Lior, S. Bhashyam, and K. Giridhar, "Parametric channel estimation for pseudo-random tile-allocation in uplink OFDMA," *IEEE Trans. Signal Process.*, vol. 55, no. 11, pp. 5370–5381, Nov. 2007.

[110] Y. Liu and S. Sezginer, "Two iterative channel estimation algorithms in single-input multiple-output (SIMO) LTE systems," *Trans. Emerging Telecommun. Technol.*, vol. 24, no. 1, pp. 59–68, Jan. 2013.

[111] T. Wo, P. A. Hoeher, and Z. Shi, "Graph-based soft channel estimation for fast fading channels," *IEEE Trans. Wireless Commun.*, vol. 11, no. 12, pp. 4243–4251, Dec. 2012.

[112] Z. J. Wang, Z. Han, and K. R. Liu, "A MIMO-OFDM channel estimation approach using time of arrivals," *IEEE Trans. Wireless Commun.*, vol. 4, no. 3, pp. 1207–1213, May 2005.

[113] W.-S. Hou and B.-S. Chen, "ICI cancellation for OFDM communication systems in time-varying multipath fading channels," *IEEE Trans. Wireless Commun.*, vol. 4, no. 5, pp. 2100–2110, Sept. 2005.

[114] Y. Zhao and S.-G. Haggman, "Intercarrier interference self-cancellation scheme for OFDM mobile communication systems," *IEEE Trans. Commun.*, vol. 49, no. 7, pp. 1185–1191, July 2001.

[115] S. U. Hwang, J. H. Lee, and J. Seo, "Low complexity iterative ICI cancellation and equalization for OFDM systems over doubly selective channels," *IEEE Trans. Broadcast.*, vol. 55, no. 1, pp. 132–139, Mar. 2009.

[116] N. Aboutorab, W. Hardjawana, and B. Vucetic, "A new iterative Doppler-assisted channel estimation joint with parallel ICI cancellation for high-mobility MIMO-OFDM systems," *IEEE Trans. Veh. Technol.*, vol. 61, no. 4, pp. 1577–1589, May 2012.

[117] S. Tomasin, A. Gorokhov, H. Yang, and J.-P. Linnartz, "Iterative interference cancellation and channel estimation for mobile OFDM," *IEEE Trans. Wireless Commun.*, vol. 4, no. 1, pp. 238–245, Jan. 2005.

[118] H. Shakhatreh, A. H. Sawalmeh, A. Al-Fuqaha, Z. Dou, E. Almaita, I. Khalil, N. S. Othman, A. Khreishah, and M. Guizani, "Unmanned aerial vehicles (UAVs): A survey on civil applications and key research challenges," *IEEE Access*, vol. 7, pp. 48 572–48 634, 2019.

[119] H. Kim, L. Mokdad, and J. Ben-Othman, "Designing UAV surveillance frameworks for smart city and extensive ocean with differential perspectives," *IEEE Commun. Mag.*, vol. 56, no. 4, pp. 98–104, Apr. 2018.

[120] R. Shakeri, M. A. Al-Garadi, A. Badawy, A. Mohamed, T. Khattab, A. K. Al-Ali, K. A. Harras, and M. Guizani, "Design challenges of multi-UAV systems in cyber-physical applications: A comprehensive survey and future directions," *IEEE Commun. Surveys Tut.*, vol. 21, no. 4, pp. 3340–3385, Fourth Quarter 2019.

[121] B. Li, Z. Fei, and Y. Zhang, "UAV communications for 5G and beyond: Recent advances and future trends," *IEEE Internet Things J.*, vol. 6, no. 2, pp. 2241–2263, Apr. 2018.

[122] R. Amorim, H. Nguyen, P. Mogensen, I. Z. Kovács, J. Wigard, and T. B. Sørensen, "Radio channel modeling for UAV communication over cellular networks," *IEEE Wireless Commun. Lett.*, vol. 6, no. 4, pp. 514–517, Aug. 2017.

[123] A. A. Khuwaja, Y. Chen, N. Zhao, M.-S. Alouini, and P. Dobbins, "A survey of channel modeling for UAV communications," *IEEE Commun. Surveys Tut.*, vol. 20, no. 4, pp. 2804–2821, Fourth Quarter 2018.

[124] V. V. Chetlur and H. S. Dhillon, "Downlink coverage analysis for a finite 3-D wireless network of unmanned aerial vehicles," *IEEE Trans. Commun.*, vol. 65, no. 10, pp. 4543–4558, Oct. 2017.

[125] M. M. Azari, F. Rosas, K.-C. Chen, and S. Pollin, "Ultra reliable UAV communication using altitude and cooperation diversity," *IEEE Trans. Commun.*, vol. 66, no. 1, pp. 330–344, Jan. 2018.

[126] A. A. Khuwaja, Y. Chen, and G. Zheng, "Effect of user mobility and channel fading on the outage performance of UAV communications," *IEEE Wireless Commun. Lett.*, vol. 9, no. 3, pp. 367–370, Mar. 2020.

[127] G. Fontanesi, A. Zhu, and H. Ahmadi, "Outage analysis for millimeter-wave fronthaul link of UAV-aided wireless networks," *IEEE Access*, vol. 8, pp. 111 693–111 706, 2020.

[128] I. Y. Abualhaol and M. M. Matalgah, "Outage probability analysis in a cooperative UAVs network over Nakagami-m fading channels," in *Proc. IEEE Veh. Technol. Conf.* IEEE, Sept. 2006, pp. 1–4.

[129] Y. H. Kim, I. A. Chowdhury, and I. Song, "Design and analysis of UAV-assisted relaying with simultaneous wireless information and power transfer," *IEEE Access*, vol. 8, pp. 27 874–27 886, 2020.

[130] J. Zhao, J. Liu, J. Jiang, and F. Gao, "Efficient deployment with geometric analysis for mmWave UAV communications," *IEEE Wireless Commun. Lett.*, vol. 9, no. 7, pp. 1115–1119, July 2020.

[131] B. Ji, Y. Li, B. Zhou, C. Li, K. Song, and H. Wen, "Performance analysis of UAV relay assisted IoT communication network enhanced with energy harvesting," *IEEE Access*, vol. 7, pp. 38 738–38 747, 2019.

[132] B. Ji, Y. Li, D. Cao, C. Li, S. Mumtaz, and D. Wang, "Secrecy performance analysis of UAV assisted relay transmission for cognitive network with energy harvesting," *IEEE Trans. Veh. Technol.*, vol. 69, no. 7, pp. 7404–7415, July 2020.

[133] W. Tang, H. Zhang, and Y. He, "Tractable modelling and performance analysis of UAV networks with 3D blockage effects," *IEEE Wireless Commun. Lett.*, vol. 9, no. 12, pp. 2064–2067, Dec. 2020.

[134] M. Banagar, H. S. Dhillon, and A. F. Molisch, "Impact of UAV wobbling on the air-to-ground wireless channel," *IEEE Trans. Veh. Technol.*, vol. 69, no. 11, pp. 14 025–14 030, Nov. 2020.

[135] S. K. Singh, K. Agrawal, K. Singh, and C.-P. Li, "Outage probability and throughput analysis of UAV-assisted rate-splitting multiple access," *IEEE Wireless Commun. Lett.*, vol. 10, no. 11, pp. 2528–2532, Nov. 2021.

[136] J. Liu, M. Sheng, R. Lyu, and J. Li, "Performance analysis and optimization of UAV integrated terrestrial cellular network," *IEEE Internet Things J.*, vol. 6, no. 2, pp. 1841–1855, Apr. 2019.

[137] B. Li, X. Guo, R. Zhang, X. Du, and M. Guizani, "Performance analysis and optimization for the MAC protocol in UAV-based IoT network," *IEEE Trans. Veh. Technol.*, vol. 69, no. 8, pp. 8925–8937, Aug. 2020.

[138] X. Wang and M. C. Gursoy, "Coverage analysis for energy-harvesting UAV-assisted mmWave cellular networks," *IEEE J. Sel. Areas Commun.*, vol. 37, no. 12, pp. 2832–2850, Dec. 2019.

[139] X. Li, Q. Wang, H. Peng, H. Zhang, D.-T. Do, K. M. Rabie, R. Kharel, and C. C. Cavalcante, "A unified framework for HS-UAV NOMA networks: Performance analysis and location optimization," *IEEE Access*, vol. 8, pp. 13 329–13 340, 2020.

[140] J. Ji, K. Zhu, D. Niyato, and R. Wang, "Probabilistic cache placement in UAV-assisted networks with D2D connections: performance analysis and trajectory optimization," *IEEE Trans. Commun.*, vol. 68, no. 10, pp. 6331–6345, Oct. 2020.

[141] R. Zhang, X. Pang, J. Tang, Y. Chen, N. Zhao, and X. Wang, "Joint location and transmit power optimization for NOMA-UAV networks via updating decoding order," *IEEE Wireless Commun. Lett*, vol. 10, no. 1, pp. 136–140, Jan. 2021.

[142] X. Zhang, J. Zhang, J. Xiong, L. Zhou, and J. Wei, "Energy-efficient multi-UAV-enabled multiaccess edge computing incorporating NOMA," *IEEE Internet Things J.*, vol. 7, no. 6, pp. 5613–5627, June 2020.

[143] C. Zhan and H. Lai, "Energy minimization in Internet-of-Things system based on rotary-wing UAV," *IEEE Wireless Commun. Lett*, vol. 8, no. 5, pp. 1341–1344, Oct. 2019.

[144] Q. Wu, Y. Zeng, and R. Zhang, "Joint trajectory and communication design for multi-UAV enabled wireless networks," *IEEE Trans. Wireless Commun*, vol. 17, no. 3, pp. 2109–2121, Mar. 2018.

[145] J. Park, H. Lee, S. Eom, and I. Lee, "UAV-aided wireless powered communication networks: Trajectory optimization and resource allocation for minimum throughput maximization," *IEEE Access*, vol. 7, pp. 134 978–134 991, 2019.

[146] L. Xie, J. Xu, and Y. Zeng, "Common throughput maximization for UAV-enabled interference channel with wireless powered communications," *IEEE Trans. Commun.*, vol. 68, no. 5, pp. 3197–3212, May 2020.

[147] Q. Wu and R. Zhang, "Common throughput maximization in UAV-enabled OFDMA systems with delay consideration," *IEEE Trans. Commun.*, vol. 66, no. 12, pp. 6614–6627, Dec. 2018.

[148] M. Mozaffari, W. Saad, M. Bennis, and M. Debbah, "Wireless communication using unmanned aerial vehicles (UAVs): Optimal transport theory for hover time optimization," *IEEE Trans. Wireless Commun*, vol. 16, no. 12, pp. 8052–8066, Dec. 2017.

[149] Y. Zeng, X. Xu, and R. Zhang, "Trajectory design for completion time minimization in UAV-enabled multicasting," *IEEE Trans. Wireless Commun.*, vol. 17, no. 4, pp. 2233–2246, Apr. 2018.

[150] C. Zhan and Y. Zeng, "Completion time minimization for multi-UAV-enabled data collection," *IEEE Trans. Wireless Commun.*, vol. 18, no. 10, pp. 4859–4872, Oct. 2019.

[151] M. Mozaffari, W. Saad, M. Bennis, and M. Debbah, "Efficient deployment of multiple unmanned aerial vehicles for optimal wireless coverage," *IEEE Commun. Lett.*, vol. 20, no. 8, pp. 1647–1650, Aug. 2016.

[152] X. Zhang and L. Duan, "Fast deployment of UAV networks for optimal wireless coverage," *IEEE Trans. Mobile Comput.*, vol. 18, no. 3, pp. 588–601, Mar. 2019.

[153] D. Zhai and R. Zhang, "Joint admission control and resource allocation for multi-carrier uplink NOMA networks," *IEEE Wireless Commun. Lett.*, vol. 7, no. 6, pp. 922–925, Dec. 2018.

[154] T. Shafique, H. Tabassum, and E. Hossain, "End-to-end energy-efficiency and reliability of UAV-assisted wireless data ferrying," *IEEE Trans. Commun.*, vol. 68, no. 3, pp. 1822–1837, Mar. 2020.

[155] M. Li, N. Cheng, J. Gao, Y. Wang, L. Zhao, and X. Shen, "Energy-efficient UAV-assisted mobile edge computing: Resource allocation and trajectory optimization," *IEEE Trans. Veh. Technol.*, vol. 69, no. 3, pp. 3424–3438, Mar. 2020.

[156] Y. Cai, Z. Wei, R. Li, D. W. K. Ng, and J. Yuan, "Joint trajectory and resource allocation design for energy-efficient secure UAV communication systems," *IEEE Trans. Commun.*, vol. 68, no. 7, pp. 4536–4553, July 2020.

[157] M. Hua, Y. Wang, Q. Wu, H. Dai, Y. Huang, and L. Yang, "Energy-efficient cooperative secure transmission in multi-UAV-enabled wireless networks," *IEEE Trans. Veh. Technol.*, vol. 68, no. 8, pp. 7761–7775, Aug. 2019.

[158] J. Baek, S. I. Han, and Y. Han, "Energy-efficient UAV routing for wireless sensor networks," *IEEE Trans. Veh. Technol.*, vol. 69, no. 2, pp. 1741–1750, Feb. 2020.

[159] T. Bai, J. Wang, Y. Ren, and L. Hanzo, "Energy-efficient computation offloading for secure UAV-edge-computing systems," *IEEE Trans. Veh. Technol.*, vol. 68, no. 6, pp. 6074–6087, June 2019.

[160] Z. Wang, R. Liu, Q. Liu, J. S. Thompson, and M. Kadoch, "Energy-efficient data collection and device positioning in UAV-assisted IoT," *IEEE Internet Things J.*, vol. 7, no. 2, pp. 1122–1139, Feb. 2020.

[161] X. Li, H.-H. Chen, Y. Qian, B. Rong, and M. R. Soleymani, "Welch bound analysis on generic code division multiple access codes with interference free windows," *IEEE Trans. Wireless Commun.*, vol. 8, no. 4, pp. 1603–1607, Apr. 2009.

[162] B. Makki, K. Chitti, A. Behravan, and M.-S. Alouini, "A survey of NOMA: Current status and open research challenges," *IEEE Open J. Commun. Soc.*, vol. 1, pp. 179–189, Jan. 2020.

[163] L. Dai, B. Wang, Y. Yuan, S. Han, I. Chih-Lin, and Z. Wang, "Non-orthogonal multiple access for 5G: solutions, challenges, opportunities, and future research trends," *IEEE Commun. Mag.*, vol. 53, no. 9, pp. 74–81, Sept. 2015.

[164] F. Wei and W. Chen, "Low complexity iterative receiver design for sparse code multiple access," *IEEE Trans. Commun.*, vol. 65, no. 2, pp. 621–634, Feb. 2017.

[165] Qualcomm Technologies, "Resource spread multiple access, 3GPP document r1-164688," May 2016.

[166] LG Electronics, "Transmitter side signal processing schemes for NCMA, 3GPP R1-1808499, RAN194," Aug. 2018.

[167] I. Budhiraja, N. Kumar, S. Tyagi, S. Tanwar, Z. Han, D. Y. Suh, and M. J. Piran, "A systematic review on NOMA variants for 5G and beyond," *IEEE Access*, vol. 9, pp. 85 573–85 644, 2021.

[168] M. Zeng, A. Yadav, O. A. Dobre, G. I. Tsiropoulos, and H. V. Poor, "Capacity comparison between MIMO-NOMA and MIMO-OMA with multiple users in a cluster," *IEEE J. Sel. Areas Commun.*, vol. 35, no. 10, pp. 2413–2424, Oct. 2017.

[169] Z. Ding, Y. Liu, J. Choi, Q. Sun, M. Elkashlan, I. Chih-Lin, and H. V. Poor, "Application of non-orthogonal multiple access in LTE and 5G networks," *IEEE Commun. Mag.*, vol. 55, no. 2, pp. 185–191, Feb. 2017.

[170] M. S. Ali, H. Tabassum, and E. Hossain, "Dynamic user clustering and power allocation for uplink and downlink non-orthogonal multiple access (NOMA) systems," *IEEE Access*, vol. 4, pp. 6325–6343, 2016.

[171] L. Zhu, J. Zhang, Z. Xiao, X. Cao, and D. O. Wu, "Optimal user pairing for downlink non-orthogonal multiple access (NOMA)," *IEEE Wireless Commun. Lett.*, vol. 8, no. 2, pp. 328–331, Apr. 2019.

[172] W. Liang, Z. Ding, Y. Li, and L. Song, "User pairing for downlink non-orthogonal multiple access networks using matching algorithm," *IEEE Trans. Commun.*, vol. 65, no. 12, pp. 5319–5332, Dec. 2017.

[173] D. Zhai, R. Zhang, L. Cai, B. Li, and Y. Jiang, "Energy-efficient user scheduling and power allocation for NOMA-based wireless networks with massive IoT devices," *IEEE Internet Things J.*, vol. 5, no. 3, pp. 1857–1868, June 2018.

[174] Z. Yang, Z. Ding, P. Fan, and N. Al-Dhahir, "A general power allocation scheme to guarantee quality of service in downlink and uplink NOMA systems," *IEEE Trans. Wireless Commun.*, vol. 15, no. 11, pp. 7244–7257, Nov. 2016.

[175] F. Cui, Y. Cai, Z. Qin, M. Zhao, and G. Y. Li, "Multiple access for mobile-UAV enabled networks: Joint trajectory design and resource allocation," *IEEE Trans. Commun.*, vol. 67, no. 7, pp. 4980–4994, July 2019.

[176] Y. Liu, Z. Qin, M. Elkashlan, Z. Ding, A. Nallanathan, and L. Hanzo, "Non-orthogonal multiple access for 5G and beyond," *Proc. IEEE*, vol. 105, no. 12, pp. 2347–2381, 2017.

[177] Y. Nesterov and A. Nemirovskii, *Interior-point polynomial algorithms in convex programming.* Society for Industrial and Applied Mathematics, 1994.

[178] A. Ben-Tal and A. Nemirovski, *Lectures on modern convex optimization: analysis, algorithms, and engineering applications.* Society for Industrial and Applied Mathematics, 2001.

[179] J. Nocedal and S. Wright, *Numerical optimization.* Springer Science & Business Media, 2006.

[180] CVX Research, Inc., "CVX: Matlab software for disciplined convex programming, version 2.1," Available at http://cvxr.com/cvx, Dec. 2018.

[181] MOSEK ApS, *The MOSEK optimization toolbox for MATLAB manual. Version 9.0.*, 2019. [Online]. Available: http://docs.mosek.com/9.0/toolbox/index.html

[182] M. Razaviyayn, "Successive convex approximation: Analysis and applications," Ph.D. dissertation, University of Minnesota, 2014.

[183] M. Blondel, K. Seki, and K. Uehara, "Block coordinate descent algorithms for large-scale sparse multiclass classification," *Machine learning*, vol. 93, no. 1, pp. 31–52, 2013.

[184] Z. Ding, F. Adachi, and H. V. Poor, “The application of MIMO to non-orthogonal multiple access,” *IEEE Trans. Wireless Commun.*, vol. 15, no. 1, pp. 537–552, Jan. 2016.

[185] A. Al-Hourani, S. Kandeepan, and A. Jamalipour, “Modeling air-to-ground path loss for low altitude platforms in urban environments,” in *Proc. IEEE Glob. Telecommun. Conf. (GLOBECOM).* IEEE, Dec. 2014, pp. 2898–2904.

[186] G. Naik, J. Liu, and J.-M. J. Park, “Coexistence of wireless technologies in the 5 GHz bands: A survey of existing solutions and a roadmap for future research,” *IEEE Commun. Surveys Tuts.*, vol. 20, no. 3, pp. 1777–1798, Third Quarter 2018.

[187] N. Lee and R. W. Heath Jr, “Advanced interference management technique: Potentials and limitations,” *IEEE Wireless Commun.*, vol. 23, no. 3, pp. 30–38, June 2016.

[188] Samsung Electronics Co. Ltd., “5G vision,” Available at https://images.samsung.com/is/content/samsung/p5/global/business/networks/insights/white-paper/5g-vision/global-networks-insight-samsung-5g-vision-2.pdf (accessed Nov. 2021), Aug. 2015.

[189] Ericsson., “5G systems: Enabling the transportation of industry and society,” Available at https://www.ericsson.com/49daeb/assets/local/reports-papers/white-papers/wp-5g-systems.pdf (accessed May 2020), Jan. 2017.

[190] S. A. A. Shah, E. Ahmed, M. Imran, and S. Zeadally, “5G for vehicular communications,” *IEEE Commun. Mag.*, vol. 56, no. 1, pp. 111–117, Jan. 2018.

[191] 3GPP, “Requirements for further advancements for evolved universal terrestrial radio access (E-UTRA) (LTE-Advanced),” Available at https://www.3gpp.org/DynaReport/36913.htm, July 2018.

[192] J. Wu and P. Fan, “A survey on high mobility wireless communications: Challenges, opportunities and solutions,” *IEEE Access*, vol. 4, pp. 450–476, 2016.

[193] G. Noh, J. Kim, H. Chung, and I. Kim, “Realizing multi-Gbps vehicular communication: Design, implementation, and validation,” *IEEE Access*, vol. 7, pp. 19 435–19 446, 2019.

[194] Y. Cai, Z. Qin, F. Cui, G. Y. Li, and J. A. McCann, “Modulation and multiple access for 5G networks,” *IEEE Commun. Surveys Tuts.*, vol. 20, no. 1, pp. 629–646, First Quarter 2018.

[195] V. Syrjala, M. Valkama, L. Anttila, T. Riihonen, and D. Korpi, “Analysis of oscillator phase-noise effects on self-interference cancellation in full-duplex OFDM radio transceivers,” *IEEE Trans. Wireless Commun.*, vol. 13, no. 6, pp. 2977–2990, June 2014.

[196] G. E. Bottomley and S. Chennakeshu, “Unification of MLSE receivers and extension to time-varying channels,” *IEEE Trans. Commun.*, vol. 46, no. 4, pp. 464–472, Apr. 1998.

[197] H. A. U. Mustafa, M. A. Imran, M. Z. Shakir, A. Imran, and R. Tafazolli, “Separation framework: An enabler for cooperative and D2D communication for future 5G networks,” *IEEE Commun. Surveys Tuts.*, vol. 18, no. 1, pp. 419–445, First Quarter 2016.

[198] J. Hu, Y. Cai, and N. Yang, “Secure transmission design with feedback compression for the internet of things,” *IEEE Trans. Signal Process.*, vol. 66, no. 6, pp. 1580–1593, Mar. 2018.

[199] Q. Fenzhong and Y. Liuqing, "On the estimation of doubly-selective fading channels," *IEEE Trans. Wireless Commun.*, vol. 9, no. 4, pp. 1261–1265, Apr. 2010.

[200] T. Zemen and A. F. Molisch, "Adaptive reduced-rank estimation of nonstationary time-variant channels using subspace selection," *IEEE Trans. Veh. Technol.*, vol. 61, no. 9, pp. 4042–4056, Sept. 2012.

[201] C. Xu, J. Zhang, T. Bai, P. Botsinis, R. G. Maunder, R. Zhang, and L. Hanzo, "Adaptive coherent/non-coherent single/multiple-antenna aided channel coded ground-to-air aeronautical communication," *IEEE Trans. Commun.*, vol. 67, no. 2, pp. 1099–1116, Feb. 2019.

[202] A. Yeredor, "The joint MAP-ML criterion and its relation to ML and to extended least-squares," *IEEE Trans. Signal Process.*, vol. 48, no. 12, pp. 3484–3492, Dec. 2000.

[203] Q. Shi, N. Wu, X. Ma, and H. Wang, "Frequency-domain joint channel estimation and decoding for faster-than-Nyquist signaling," *IEEE Trans. Commun.*, vol. 66, no. 2, pp. 781–795, Feb. 2018.

[204] R. G. Gallager, *Stochastic processes: theory for applications.* Cambridge University Press, 2013.

[205] Y. Guo, S. Yin, and J. Hao, "Resource allocation and 3-D trajectory design in wireless networks assisted by rechargeable UAV," *IEEE Wireless Commun. Lett.*, vol. 8, no. 3, pp. 781–784, 2019.

[206] H. Zhang, J. Zhang, and K. Long, "Energy efficiency optimization for NOMA UAV network with imperfect CSI," *IEEE J. Sel. Areas Commun.*, vol. 38, no. 12, pp. 2798–2809, Dec. 2020.

[207] 3GPP-TR-36.777, "Study on enhanced LTE support for aerial vehicles," Available at http://www.3gpp.org/dynareport/36777.htm (accessed Sept. 2021), 2017.

[208] M. T. Nguyen and L. B. Le, "Interference cancellation, channel estimation, and symbol detection for communications on overlapping channels," *IEEE Access*, vol. 8, pp. 89 822–89 838, 2020.

[209] ——, "Flight scheduling and trajectory control in UAV-based wireless networks," in *Proc. IEEE Wireless Commun. Netw. Conf. (WCNC).* IEEE, 2020, pp. 1–6.

[210] ——, "Multi-UAV trajectory, resource allocation design for UAV-based wireless networks with dynamic data demand for consecutive service periods," in *Proc. 30th Biennial Symp. Commun. (BSC 2021).* Springer.

[211] ——, "Resource allocation, trajectory optimization, and admission control in UAV-based wireless networks," *IEEE Netw. Lett.*, vol. 3, no. 3, pp. 129–132, 2021.

[212] ——, "Multi-UAV trajectories control, resource allocation, and NOMA user pairing for uplink energy minimization," *Submitted to IEEE Internet Things J.*, Dec. 2021.

[213] R. Hadani, S. Rakib, M. Tsatsanis, A. Monk, A. J. Goldsmith, A. F. Molisch, and R. Calderbank, "Orthogonal time frequency space modulation," in *Proc. IEEE Wireless Commun. Netw. Conf. (WCNC).* IEEE, 2017, pp. 1–6.

[214] P. Raviteja, K. T. Phan, Y. Hong, and E. Viterbo, "Interference cancellation and iterative detection for orthogonal time frequency space modulation," *IEEE Trans. Wireless Commun.*, vol. 17, no. 10, pp. 6501–6515, Oct. 2018.

[215] G. Surabhi, R. M. Augustine, and A. Chockalingam, "On the diversity of uncoded otfs modulation in doubly-dispersive channels," *IEEE Trans. Wireless Commun.*, vol. 18, no. 6, pp. 3049–3063, June 2019.

[216] A. C. Cirik, N. M. Balasubramanya, L. Lampe, G. Vos, and S. Bennett, "Toward the standardization of grant-free operation and the associated NOMA strategies in 3GPP," *IEEE Commun. Stand. Mag.*, vol. 3, no. 4, pp. 60–66, Dec. 2019.

[217] A. C. Cirik, N. M. Balasubramanya, and L. Lampe, "Multi-user detection using ADMM-based compressive sensing for uplink grant-free NOMA," *IEEE Wireless Commun. Lett.*, vol. 7, no. 1, pp. 46–49, Feb. 2017.

[218] Z. Wu, K. Lu, C. Jiang, and X. Shao, "Comprehensive study and comparison on 5G NOMA schemes," *IEEE Access*, vol. 6, pp. 18 511–18 519, 2018.

[219] R. Abbas, M. Shirvanimoghaddam, Y. Li, and B. Vucetic, "A novel analytical framework for massive grant-free NOMA," *IEEE Trans. Commun.*, vol. 67, no. 3, pp. 2436–2449, Mar. 2018.